University of Alberta

Library Release Form

Name of Author: Dũng Ngọc Đào

Title of Thesis: Designs of Space-Time Codes for Multiple-Antenna Wireless Communication Systems

Degree: Doctor of Philosophy

Year this Degree Granted: 2007

. . . . . .

Dũng Ngọc Đào (signed, December 20, 2006)

University of Alberta

DESIGNS OF SPACE-TIME CODES FOR MULTIPLE-ANTENNA WIRELESS COMMUNICATION SYSTEMS

by

Dũng Ngọc Đào

A thesis submitted to the Faculty of Graduate Studies and Research
in partial fulfillment of the requirements for the degree of

Doctor of Philosophy

Department of Electrical and Computer Engineering

Edmonton, Alberta
Spring 2007

University of Alberta

Faculty of Graduate Studies and Research

The undersigned certify that they have read, and recommend to the Faculty of Graduate Studies and Research for acceptance, a thesis entitled **Designs of Space-Time Codes for Multiple-Antenna Wireless Communication Systems** submitted by **Dũng Ngọc Đào** in partial fulfillment of the requirements for the degree of **Doctor of Philosophy**.

. . . . . .

Professor Chintha Tellambura (Supervisor, signed, Dec. 19, 2006)

. . . . . .

Professor Robert Schober
(Professor Scott Dick, Chair, initialed on behalf, Dec. 14, 2006)

. . . . . .

Professor Witold Krzymien (signed, Dec. 13, 2006)

. . . . . .

Professor Mike MacGregor (signed, Dec. 13, 2006)

. . . . . .

Professor Alan Lynch (signed, Dec. 13, 2006)

. . . . . .

Professor Masoud Ardakani (signed, Dec. 13, 2006)

Date: December 19, 2006

To my mother, ***Nguyễn Thị Tiếp****,*

my wife, ***Tạ Ly Hương****,*

and my daughter, ***Đào Dạ Thảo****.*

Abstract

Space-time coding is an effective approach to improve the reliability of data transmission as well as the data rates over multiple-input multiple-output (MIMO) fading wireless channels. In this thesis, space-time code designs are investigated with a view to address practical concerns such as decoding complexity and channel impairments.

We study low-decoding complexity space-time block codes (STBC), a popular subclass of space-time codes, for quasi-static frequency-flat fading MIMO channels. Therefore, the space-time code matrices are designed to allow the separation of transmitted symbols into groups for decoding; we call these codes multi-group decodable STBC. A new multi-group decodable STBC, called orthogonality-embedded space-time (OEST) codes, is then proposed. The equivalent channel, general decoder, and maximum mutual information of OEST codes are presented. The following contributions, based on OEST codes, are made:

- It is shown that OEST codes subsume existing orthogonal, quasi-orthogonal, and circulant STBC. Therefore, the results of OEST codes can be readily applied to these codes.

- New STBC, called semi-orthogonal algebraic space-time (SAST) codes, are derived from OEST codes. SAST codes are rate-one, full-diversity, four-group decodable, delay-optimal for even number of antennas. SAST codes nearly achieve the capacity of multiple-input single-output channels.

- The framework of OEST codes is applied to the existing single-symbol decodable codes, like minimum decoding complexity quasi-orthogonal STBC (MDC-QSTBC) and coordinate-interleaved orthogonal designs, and 4-group quasi-orthogonal STBC. Several open problems of these codes are solved, including equivalent channel, general decoder, symbol error rate performance analysis, and optimal signal rotations.

Additionally, MDC-QSTBC are shown to achieve full diversity using antenna selection with limited feedback.

We also consider the designs of space-time codes for MIMO systems, using orthogonal frequency division multiplexing (OFDM) for frequency-selective fading channels. The resulting codes are called space-frequency codes. The OFDM system performance is heavily affected by inter-carrier interference, which is caused by frequency offset between the carrier oscillators of the transmitter and receiver. We analytically quantify the performance loss of space-frequency codes due to frequency offset. A new class space-frequency codes, called inter-carrier interference self-cancellation space-frequency (ISC-SF) codes, is proposed to effectively mitigate the effect of frequency offset.

Acknowledgements

First of all, I would like to thank my supervisor, Professor Chintha Tellambura, not only for his academic guidance but also for numerous supports outside the academic activities throughout the years I worked with him. He has provided me with all the freedom and opportunities to carry out my Ph.D. research and to develop my long-term profession.

My sincere thanks extend to all committee members, Professor Witold Krzymien, Professor Mike MacGregor, Professor Alan Lynch, Professor Masoud Ardakani, and Professor Robert Schober for their critical comments and constructive suggestions on the methodology and topics of the research. I particularly admired the well-prepared lectures and insightful views of Professor Witold Krzymien on wireless communication systems.

I am pleased to acknowledge Ms. Sandra Abello for the administrative support. Thanks are due to lab-mates and friends at University of Alberta, who made my stay in Edmonton during the PhD program enjoyable. I greatly appreciate the longtime friendship and valuable support of Professor Ha Hoang Nguyen and Dr. Huy Vu Gia, University of Saskatchewan.

My special thanks should go to The National Sciences and Engineering Research Council Canada (NSERC) and Alberta Informatics Circle of Research Excellence (iCORE) for financial supports through the research assistantship of my supervisor.

I am deeply indebted to my beloved parents, my brother and my wife for their love, sharing, and encouragement.

Finally, I would like to dedicate my achievements to my mother, who does everything that she can for her sons.

Contents

List of Figures

List of Tables

List of Abbreviations

3G	third generation
4G	fourth generation
ABBA	a construction of quasi-orthogonal space-time block code
APSK	amplitude phase shift keying
BER	bit error rate
BLAST	Bell laboratories layered space time
CIOD	coordinate-interleaved orthogonal designs
CDMA	code division multiple access
CP	cyclic prefix
D-BLAST	diagonal Bell laboratories layered space time
DAST	diagonal algebraic space-time
DST	diagonal space-time
DFT	discrete Fourier transform
FER	frame error rate
GRV	Gaussian random variable
H-BLAST	horizontal Bell laboratories layered space time
HEX	hexagonal
i.i.d	independent and identically distributed
IDFT	inverse discrete Fourier transform
ISC-SF	inter-carrier interference self-cancellation space-frequency
ST-LCP	space-time linear complex field precoding
LTAST	linear threaded algebraic space-time
MDC	minimum decoding complexity
MIMO	multiple-input multiple-output

MISO	multiple-input single-output
(M, N)	MIMO system with M transmit and N receive antennas
OEST	orthogonality-embedded space-time
OFDM	orthogonal frequency division multiplexing
OSTBC	orthogonal space-time block code/codes/coding
pcu	per channel use
PAPR	peak-to-average power ratio
PCC	polynomial cancellation coding
PEP	pair-wise error probability
PSK	phase shift keying
QAM	quadrature amplitude modulation
QAM-R	quadrature amplitude modulation using rectangular constellations
QAM-S	quadrature amplitude modulation using square constellations
QAM-SR	quadrature amplitude modulation using square-rotated constellations
QoS	quality of service
QSTBC	quasi-orthogonal space-time block code/codes/coding
SAST	semi-orthogonal algebraic space-time
SER	symbol error rate
SISO	single-input single-output
SNR	signal-to-noise ratio
SPEP	symbol pair-wise error probability
STBC	space-time block code/codes/coding
TAST	threaded algebraic space-time
TRI	lattice of equilateral triangular
WLAN	wireless local area networks
WMAN	wireless metropolitan area networks
V-BLAST	vertical Bell laboratories layered space time
ZF-DFE	zero-forcing decision feedback equalization

List of Symbols

$\equiv$	equivalent
$\otimes$	Kronecker product
$\mathbb{C}$	complex number field
$\mathcal{CN}(m, \sigma^2)$	mean-m and variance-σ^2 circularly complex Gaussian random variable
$d_{\min}$	minimum Euclidean distance of signal constellation
$\det(X)$	determinant of matrix X
$\mathrm{diag}(\boldsymbol{x})$	diagonal matrix with elements of vector $\boldsymbol{x}$ on the main diagonal
$\mathbb{E}[\cdot]$	statistical average
$\boldsymbol{I}_m$	$m \times m$ identity matrix
$\Im(X)$	imaginary part of X
$\mathrm{lcm}(a, b)$	least common multiple of integers a and b
$\min(x)$	minimum value of variable x
$\mathbf{0}_m$	$m \times m$ all-zero matrix
$\mathbf{0}_{m\times n}$	$m \times n$ all-zero matrix
$\mathrm{rank}(X)$	rank of matrix X
$\Re(X)$	real part of matrix X
$\mathrm{trace}(X)$	trace of matrix X
$[x_{ij}]$	matrix X with element x_{ij} at row i column j
X^*	conjugation of matrix X
$X^\dagger$	conjugate transpose of matrix X
$\|X\|_{\mathsf{F}}$	Frobenius norm of matrix X
X^{T}	transpose of matrix X

Chapter 1

Introduction

1.1 MIMO Systems for Future Wireless Communications

Future wireless communication networks must accommodate a large number of subscribers and variety of services with different levels of predefined quality of service (QoS) [1, 2]. Currently, users select communication services, such as voice and data services, with data rate up to 2 Mb/s via third generation (3G) land mobile communication networks [3]. Additionally, wireless local area networks (WLAN) offer data rates up to 100 Mb/s [4]. However, the throughput of wireless networks at the access points (base stations) is expected to grow tremendously, in the order of Gbit/s [4, 5].

There are several technical challenges for reaching high data rates for future wireless networks. First, signal fading inherent in mobile wireless channels limits the maximum data rates [6]. Second, the radio spectrum available for land mobile communications is limited [6]. Third, the transmit radio power is limited because the radio emissions need to be controlled for health reasons and for reduction of the interference to other radio channels of the same or different wireless systems [6]. Additionally, handheld mobile units or data terminals have limited-capacity batteries.

These three challenges may be overcome by MIMO (multiple-input multiple-output) technology, where multiple antennas are used at *both* transmitter and receiver [7–9]. Throughout this thesis, the notation (M, N) denotes a MIMO system with M transmit and N receive antennas. The capacity studies by Telatar [8, 10] and Foschini [9, 11] show that a much higher capacity (i.e. data rates) can be extracted from MIMO systems than from single-input single-output (SISO) systems. Following these initial studies, various MIMO

systems have been proposed. For example, a popular spatial multiplexing architecture is called BLAST (Bell laboratories layered space time) [9, 12, 13]. Depending on how the data streams are distributed over multiple transmit antennas, one obtains V-BLAST (vertical BLAST), D-BLAST (diagonal BLAST) and H-BLAST (horizontal BLAST) [14]. By using such MIMO systems, one can overcome the capacity limitation of SISO systems without spectral expansion or power increase.

In order to increase the reliability of data transmission against fading, space-time coding has been proposed by exploiting the rich diversity of MIMO channels [15, 16]. A space-time code spreads input modulation symbols across multiple antennas (space dimension) and multiple time slots (time dimension). A space-time code design has been suggested by Guey $et\,al.$ [17, 18]. However, the design criteria of Tarokh $et\,al.$ [15, 16] are more systematic and applicable for different channel models, such as Rayleigh and Rician fading channels [16]. Thus, these designs of space-time codes exploit fading inherent in wireless channels to improve communication reliability.

To achieve full spatial multiplexing (i.e., the number of transmit symbols per channel use (pcu) equals to the number of transmit antennas), the number of receive antennas should be at least equal to the number of transmit antennas [9, 12, 13]. However, in practice, due to size and/or cost constraints, the number of antennas at the mobile handset is likely not more than that at the base station [19]. From information theory and efficient signal detection viewpoints, the maximum data rate should not exceed minimum values of M and N [9, 12, 20]. Thus, the non-full-rate MIMO mobile wireless systems are more prevalent. However, with lower rates, more stringent mathematical structures can be embedded into the space-time code matrices, helping to reduce the decoding-complexity at the receiver.

The current developments of wireless systems have been integrating MIMO into standards. For example, the IEEE 802.11n standard for WLAN applications [21–23] recommends the use of multiple antennas (up to 4) at the transmitter and receiver to provide a data rate of 100 Mbit/s or higher. The IEEE 802.16e-2005 standard [24, 25] for fixed and mobile wireless wide-area broadband access also integrate the Alamouti space-time block coding [26] and MIMO spatial multiplexing configurations (2, 2), (3, 2), and (4, 2). The MIMO architectures are also studied for beyond 3G mobile wireless systems [27].

In conclusion, the applications of MIMO systems can solve the three challenges of wire-

less communications. In the next section, we will review the design principle of space-time codes. In particular, a special class of space-time codes, space-time block codes (STBC), will be discussed in more detail.

1.2 MIMO Channel Models

We consider a MIMO system over a quasi-static Rayleigh fading channel [8–10,16], i.e. the channel gains are constant during the duration of a codeword, and can vary from codeword to codeword. The transmitter and receiver are equipped with M transmit and N receive antennas. The channel gain $h_{mn}(m = 1, 2, ..., M; n = 1, 2, ..., N)$ between the (m, n)-th transmit-receive antenna pair is assumed $\mathcal{CN}(0, 1)$, which is consistent with the Rayleigh fading assumption. This is the most common channel model used for space-time code designs. We assume no spatial correlation at either the transmit or receive array. The receiver, but not the transmitter, completely knows the channel gains.

The above-mentioned channel model is ideal and is only applicable when there is a rich scattering environment around the receive antennas. There exist several more realistic MIMO channel models to analyze the performance of space-time codes (see e.g. [28–31]). These channel models incorporate the correlation among transmit and/or receive antenna arrays; the channel gains may also have distributions that are different from the Rayleigh distribution [32]. Nevertheless, the MIMO channel model with uncorrelated Rayleigh fading is the most widely used model in the literature and will be used throughout the thesis.

1.3 Space-Time Code Design Criteria

We examine the design criteria of space-time codes using the channel model described in Section 1.2. The block diagram of a communication system over MIMO channels is sketched in Fig. 1.1.

The space-time encoder parses data symbols into space-time codewords $C = [c_{tm}]$ of size $T \times M$, where c_{tm} is the symbol transmitted from antenna m at time t ($1 \leq t \leq T$). The average energy of a codeword is constrained such that

$$\sum_{m=1}^{M} \sum_{t=1}^{T} \mathbb{E}[|c_{tm}|^2] = T. \tag{1.1}$$

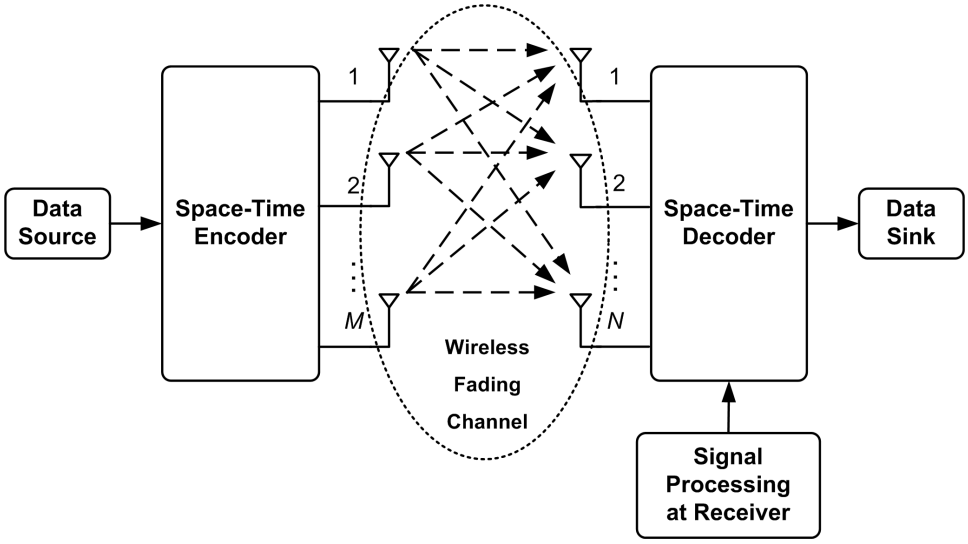

Figure 1.1: Multiple-input multiple-output (MIMO) system model.

The baseband received signal y_{tn} at the receive antenna n and at time slot t is the superposition of the signals transmitted from M transmit antennas:

$$y_{tn} = \sqrt{\rho} \sum_{m=1}^{M} c_{tm} h_{mn} + w_{tn} \tag{1.2}$$

where w_{tn} is independently, identically distributed (i.i.d.) additive white noise with distribution $\sim \mathcal{CN}(0, 1)$.

The received signals y_{tn} can be arranged in a matrix Y of size $T \times N$. Thus, the transmit-receive signal relation can be represented compactly as

$$Y = \sqrt{\rho} C H + W \tag{1.3}$$

where $H = [h_{mn}]$, $W = [w_{tk}]$ of size $T \times N$. The transmit power is scaled by ρ so that the average signal-to-noise ratio (SNR) at each receive antenna is ρ, independent of the number of transmit antennas.

The upper-bound of pair-wise error probability (PEP) derived by Tarokh $et\,al.$ [16] is as follows:

$$P(C \to \hat{C}) \leq \left(\prod_{i=1}^{\Gamma} \lambda_i \right)^{-N} \left(\frac{\rho}{4} \right)^{-\Gamma N} \tag{1.4}$$

where C and $\hat{C}$ are the transmitted and erroneous codewords, Γ is the minimum rank of a matrix Δ_C ($\Delta_C = C - \hat{C}$) for all $C \neq \hat{C}$, $\lambda_1, \lambda_2, , ..., \lambda_\Gamma$ are non-zero eigenvalues of a product matrix $P_C = \Delta_C^\dagger \Delta_C$.

Definition 1.1. *The diversity gain or diversity order G_d and coding gain G_c of a space-time code are defined as follows:*

$$G_d = \Gamma N \tag{1.5}$$

$$G_c = \min_{C \neq \hat{C}} \left(\prod_{i=1}^{\Gamma} \lambda_i \right)^{1/\Gamma} \tag{1.6}$$

The space-time code design criteria can be stated as follows [16]:

- *The rank criterion*: The minimum rank of Δ_C of all pairs of distinct codewords should be maximized. If the minimum rank of Δ_C is Γ, then diversity order of ΓN is achieved.

- *The determinant criterion*: The coding gain G_c taken over all pairs of distinct codewords must be as large as possible.

Since the $\mathrm{rank}\, \Delta_C = \mathrm{rank}\, P_C$, if Δ_C of a space-time code is of full rank M for all pairs of distinct codewords, then so is the P_C and the diversity order is maximized, i.e. $G_d = MN$.

Definition 1.2. *A space-time code is said to achieve full-diversity if its diversity order is MN.*

In the case of full-diversity codes, the coding gain follows

$$G_c = \min_{C \neq \hat{C}} \left[\det(\Delta_C^{\dagger} \Delta_C) \right]^{1/M}. \tag{1.7}$$

The diversity order tells us how fast the error rate decays with SNR on a log-log scale, while the coding gain reflects the SNR saving to achieve the same error rate performance. The larger the diversity order, the faster error rate reduces; and the larger the coding gain, the better the SNR saving. We illustrate the diversity order and coding gain of several systems in Fig. 1.2, where the values of the error rate and SNR are in log scale. For example, the (2, 2) MIMO system has a diversity order of 4, which is higher than the diversity-one of the SISO system. Thus, the error rate curve of the former is steeper than that of the latter. For the two (2, 2) systems, the better-designed system will save some SNR compared with the worse-designed system.

Note that the coding gain is an asymptotic performance metric since it is defined for the worst-case PEP basis and at high SNR. The actual performance of a space-time code

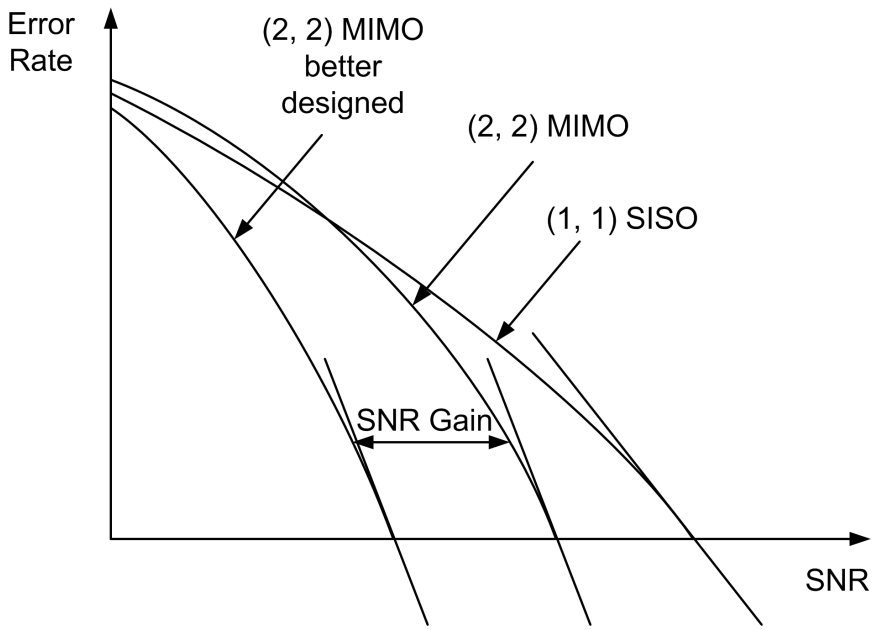

Figure 1.2: Illustration of the diversity order and SNR gain of space-time systems.

depends on the whole PEP spectrum of all codewords. Simulations are therefore required to compare the SNR gain of different space-time codes.

Instead of the above rank-determinant criteria, Hassibi and Hochwald [33] proposed an information-theoretic criterion, whereby the mutual information between the transmitter and the receiver is maximized. While space-time codes can be constructed for any number of transmit or receive antennas using mutual information criterion, full diversity is not necessarily guaranteed. Moreover, while the rank-determinant approach can be applied to design a wide range of space-time codes, the search for good codes using mutual information criterion becomes highly complicated for a large number of antennas or large delay.

Though the upper bound on PEP is given in (1.4), the exact PEP of space-time codes can be evaluated analytically [34–37]. Thus, the union bound on PEP can be evaluated [37]. Let Ω be the size of the codebook. The union bound on PEP is given below:

$$P_{UB} = \frac{2}{\Omega} \sum_{i=1}^{\Omega-1} \sum_{j=i+1}^{\Omega} P(C_i \rightarrow \hat{C}_j). \tag{1.8}$$

A design criterion optimizing the union bound is proposed for several space-time codes (e.g. in [38, 39]). This approach improves the error performance of the space-time codes.

Tarokh $et\,al.$ provided space-time trellis codes (STTC) and space-time block codes (STBC) [16, 40]. There are also several types of space-time codes designed from error

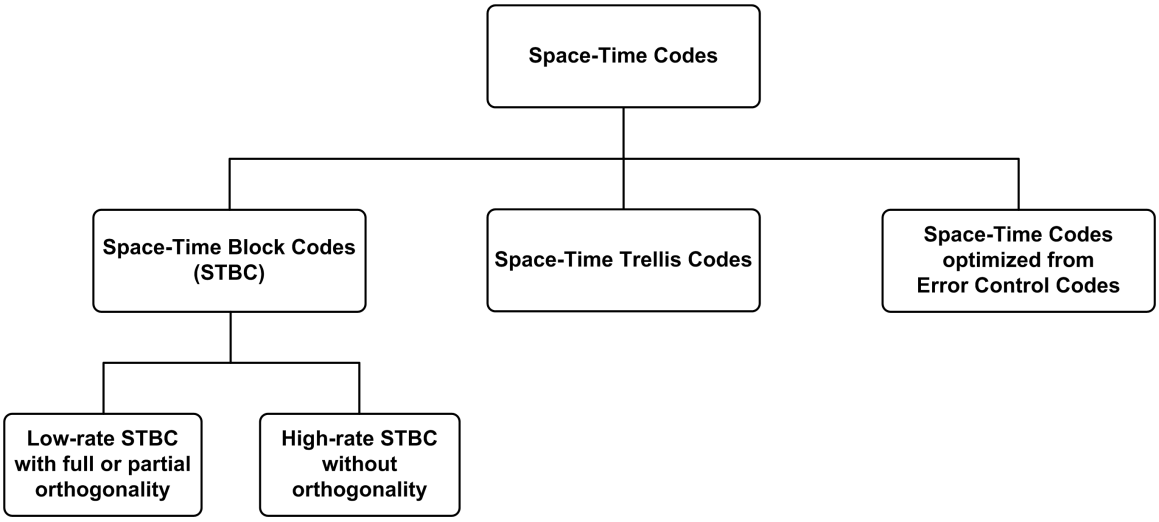

Figure 1.3: Classification of space-time codes.

control codes [41–43]. In Fig. 1.3 space-time codes are classified. In the first group of the STBC branch, low-rate STBC with orthogonality, includes OSTBC and QSTBC [40, 44–48]. The other existing STBC (for example, [49–54]) belong to the high-rate non-orthogonal group. In this thesis, we focus on STBC and their design criteria based on either rank-determinant or union bound performance.

1.4 Space-Time Block Codes

Space-time block codes, which are an important class of space-time codes, have been studied extensively recently. They are expected to play a prominent role in both third generation and beyond wireless standards [55–57]. We consider linear STBC, in which, the space-time code matrix is linear with respect to the data symbols and their conjugates. In the following, we use the notation STBC to imply linear STBC where no confusion may arise.

In the STBC encoder, a block of K data symbols $(s_1, s_2, ..., s_K)$ is mapped into the space-time code matrix of size $T \times M$. The space-time code matrix has the following general form [33, 40]:

$$X = \sum_{k=1}^{K} (A_k s_k + B_k s_k^*) \tag{1.9}$$

where A_k and B_k, $(k = 1, 2, ..., K)$ are (possibly complex-valued) fixed matrices of the same size $T \times M$.

To compare the coding efficiency of different coding schemes, including the coding for SISO channels, the code rate of space-time codes, in symbols per channel use (pcu) is defined as follows [16, 58].

Definition 1.3. *The code rate of a space-time code in symbols per channel use is the ratio of number of data symbols transmitted in the space-time code matrix and the number of channel uses T. Thus, the code rate is given by*

$$R = K/T. \tag{1.10}$$

For example, the Alamouti code $X = \begin{bmatrix} s_1 & s_2 \\ -s_2^* & s_1^* \end{bmatrix}$ has a rate of $R = 1$ [26].

1.4.1 Design Parameters and Fundamental Limits

There are several design parameters to be considered for STBC:

1. number of transmit antennas (M);
2. code matrix length (T) and also the number of channel uses per code matrix;
3. number of receive antennas (N);
4. diversity gain (or diversity order) (G_d);
5. coding gain (G_c);
6. code rate (R);
7. maximum mutual information (I).

There are some fundamental limits on the parameter designs as follows [20].

- The maximum diversity order is $G_{d,\max} = MN$.
- To achieve the maximum diversity order, the minimum encoding delay is $T_{\min} = M$. This limit comes from the *rank criterion*; the rank of the matrix of order $M \times T$ can not be more than the minimum of M and T. If full diversity is required, then the necessary condition is $M \leq T$.

- The maximum code rate ($R_{\max} = M$). With M transmit antennas, we cannot transmit more than M independent symbols in a time epoch.

Definition 1.4. *A space-time code for an (M, N) system is said to be full-rate if its code rate is equal to M symbols pcu.*

The code length T is proportional to the memory length and encoding/decoding delay. Therefore, given a diversity order, the code length T is subject to be minimized.

Definition 1.5. *A space-time code is said to be delay-optimal if the encoding delay T is equal to M.*

Some of these parameters can be combined for optimized code design. For example, STBC can be designed with full-diversity $G_d = MN$ and optimal delay $T = M$ [49–51, 59]. On the other hand, linear dispersion codes in [33] are designed to maximize I, with respect to M, N, and T. We next briefly review several classes of STBC designed with the rank-determinant criteria.

1.4.2 Orthogonal and Quasi-Orthogonal STBC

The Alamouti code, one of the most well-known STBC, is designed for two transmit antennas [26]. The code is successfully integrated in 3G standards [55]. It has been generalized as orthogonal STBC (OSTBC) by Tarokh $et\,al.$ [40] using the results of orthogonal matrix theory developed by Hurwitz and Radon [60].

Orthogonal design results in a decoupling of symbol detection, enabling minimal maximum likelihood detection complexity. However, orthogonal designs entail low code rates [44, 45]; a code rate of one symbol pcu with complex constellations is available for two transmit antennas only, and the code rate approaches 1/2 for a large number of transmit antennas [44, 45]. The code rate may be improved by quasi-orthogonal STBC (QSTBC) [46–48], which achieve full diversity by signal constellation rotations (see [61] and references therein), but require joint maximum likelihood detection[1] of pairs of symbols. Moreover, QSTBC also have low code rates because they are based on OSTBC.

The channel decoupling property of OSTBC implies that maximum likelihood detection of a vector of input symbols is equivalent to solving a set of scalar detection problems, one

[1] We use the terms detection and decoding synonymously.

for each input symbol; that is, the MIMO channel is decoupled into several equivalent SISO channels. The maximum likelihood receiver then has the lowest complexity. The transmit-receive signals in (1.3) can be written equivalently for OSTBC [59, 62] as

$$\bar{y} = \|H\|_{\mathsf{F}} s_k + \bar{w}. \tag{1.11}$$

Since all the transmitted symbols experience the same Frobenious norm $\|H\|_{\mathsf{F}}$ [63] of the channel matrix, this quantity $\|H\|_{\mathsf{F}}$ can be considered as the equivalent channel of OSTBC. The decoding of QSTBC is also decoupled into the detection of groups of two symbols [46–48]. However, it is not known what the equivalent channels of QSTBC are.

1.4.3 Non-orthogonal STBC

Alternatively, the orthogonality requirement can be sacrificed for increasing the code rate; an example is full-diversity diagonal space-time (DST) codes [49–51]. Rate-one codes can thus be constructed for any number of transmit antennas. Optimal DST codes yield better coding gains compared with OSTBC for more than two transmit antennas. Moreover, higher rate codes, namely threaded algebraic space-time (TAST) codes (up to full-rate) can be derived from DST codes, for example, in [58]. However, DST and TAST codes exhibit high peak-to-average-power ratio (PAPR) and high complexity maximum likelihood detection because all the transmitted symbols must be jointly detected. PAPR can, however, be reduced by linear TAST (LTAST) codes [20]. Rate-one LTAST codes have a circulant structure [64] and the same PAPR as the input constellation. TAST and LTAST codes are both delay optimal in the sense that the number of channel uses per space-time codeword equals to the number of transmit antennas, i.e., the space-time codewords are square matrices [40]. However, LTAST codes incur the same high complexity maximum likelihood detection as TAST codes.

Using the cyclotomic number theory, the authors in [53, 54] derive the optimal coding gain for diagonal algebraic space-time (DAST) codes and TAST codes. The high rate STBC are also constructed using division algebras [52, 65]. These codes also have high maximum likelihood decoding complexity as TAST codes.

1.5 Designs of Space-Time Codes for Frequency-Selective Fading Channels

As mentioned before, the first space-time codes proposed by Tarokh $et\,al.$ [16] for coherent systems over MIMO quasi-static flat fading channels (i.e., frequency non-selective fading) achieve the maximum diversity order $d = MN$, where M and N are the number of transmit and receive antennas. In frequency-selective fading channels, the maximum achievable diversity order is $d = L_pMN$ where L_p is the number of paths of the frequency-selective fading channel [66, 67]. The achievable diversity order of frequency-selective fading is therefore higher than that of frequency-flat channels. Therefore, space-time code design for MIMO frequency-selective fading channels has received much attention.

Orthogonal frequency division multiplexing (OFDM) is robust to frequency selective fading [68–70]. OFDM converts the wideband frequency-selective channel into parallel narrowband frequency-flat channels, which allow simple receiver designs. Therefore, OFDM is widely used in WLAN as well as wireless metropolitan area networks (WMAN) [6, 71, 72]. It is expected that OFDM will be the technology of choice for future 4th-generation (4G) wireless systems [24, 57, 73–75].

The simplified model of MIMO-OFDM systems employing space-time coding is illustated in Fig. 1.4. Since with OFDM, the frequency-selective channel is converted to parallel subchannels, the frequency diversity can be obtained only if the data are spread over multiple subchannels. Therefore, when the space-time codes designed for frequency-flat fading channels are transmitted over MIMO-OFDM, the maximum diversity order L_pMN may not be achievable.

To achieve the full potential diversity order of frequency-selective fading channels, in general, space-time codes can be designed in the time domain [76] or in the frequency domain using OFDM and the resulting codes are called space-frequency codes [66], [67], [77]. Coding for MIMO-OFDM to achieve high diversity order has received much attention after the initial papers [66] and [67]. The authors in [42] design space-frequency codes (and also space-time codes) using algebraic theory for frequency-selective fading channels [78]. Reference [79] introduces a full-diversity full-rate space-frequency code design, which is developed using complex field coding [80]. The authors in [81] propose a con-

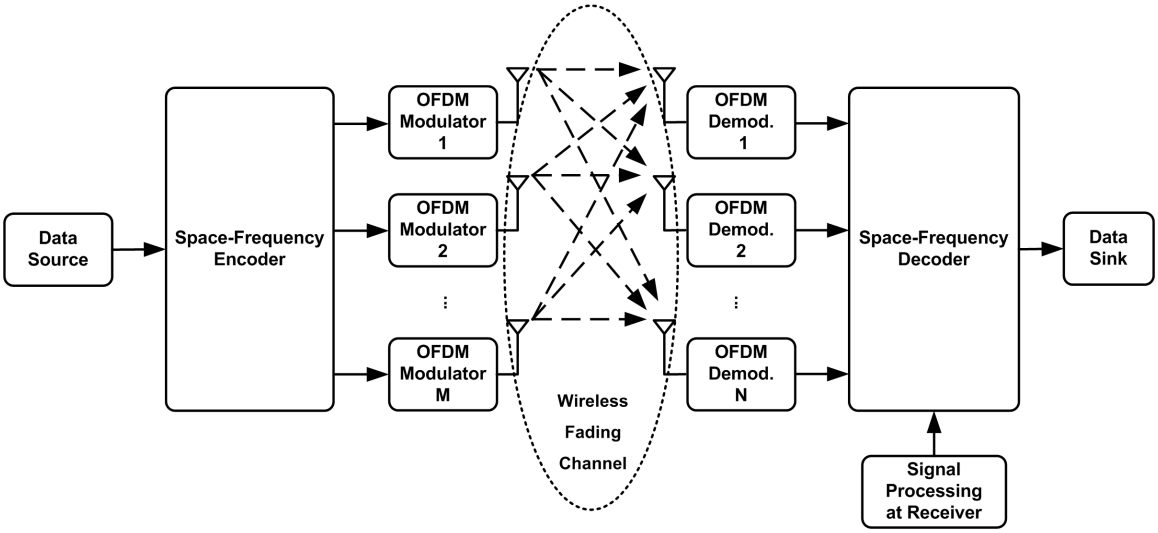

Figure 1.4: Simplified diagram of MIMO-OFDM systems.

catenation scheme with Alamouti code [82] as the inner and a trellis code as the outer. Su $et\,al.$ [83] derive space-frequency code criteria, showing an explicit relation between the space-frequency code matrix and the characteristic parameters of frequency-selective fading channels, such as the path delays and power delay profile. The authors in [83] introduce a class of space-frequency codes formed by repetition space-time codes. They also show that when any full diversity space-time code is used in MIMO-OFDM as a space-frequency code, it achieves at least the diversity order that has been designed in the time domain. Thus, many space-time codes are usable as space-frequency codes.

The design criteria of space-frequency codes are similar to those of space-time codes described in Section 1.3 [83]. These criteria will be revisited in Chapter VI when we investigate the performance of space-frequency codes in the presence of inter-carrier interference.

1.6 Problem Formulation

1.6.1 Designs of STBC for flat fading MIMO channels

Since several STBC are well-known in the literature, it is worthwhile to summarize their properties. Table 1.1 compares existing space-time code designs [OSTBC, QSTBC and rate-one TAST/LTAST codes (or DST codes)]. By emphasizing the complexity (i.e. the number of real or complex symbols to be jointly maximum likelihood detected), we can

Table 1.1: Comparisons of Several STBC

Code	M	G_d	R	maximum likelihood real-symbol decoding
OSTBC	4	$4N$	0.75	2 symbol
QSTBC	4	$4N$	1	4 symbols
LTAST	4	$4N$	1	8 symbols
OSTBC	8	$8N$	0.625	2 symbol
QSTBC	8	$8N$	0.75	4 symbols
LTAST	8	$8N$	1	16 symbols

draw the following observations:

1. Low-rate OSTBC and QSTBC: Current designs of OSTBC and QSTBC have low (maximum likelihood) decoding complexity, but they are subject to the limitation of rates less than 1 symbol pcu; the rate 1 symbol pcu exists for OSTBC with 2 transmit antennas and QSTBC with 4 transmit antennas only.

2. High-complexity, full-rate STBC: Full-rate codes such as TAST codes can achieve full-diversity, but the decoding complexity is high since all of the transmitted symbols in a code matrix must be jointly decoded in order to achieve full diversity.

In practical mobile wireless systems, the number of antennas at the mobile units may be smaller than that at the base stations; the maximum symbol rate in this case should be equal to the number of receive antennas. Thus, full-rate STBC may not be needed.

Consequently, designs of full-diversity, non-full-rate STBC with low maximum likelihood decoding complexity are important; the design of such STBC is *one of the main challenges in this thesis*.

An important property influencing the decoding complexity is the orthogonality. In other areas of communications, e.g. CDMA (code division multiple access), orthogonal sequences are used to separate users' data at the receiver [84]. In the designs of STBC, the orthogonality among linear dispersion matrices of transmitted symbols will determine the decoding complexity.

1.6.2 Designs of Space-Frequency Codes for MIMO-OFDM Systems

Since the space-frequency codes use OFDM, their performance can be affected by underlying impairments, such as frequency offset, phase noise and time-varying channels. A residual frequency offset exists due to carrier synchronization mismatch and Doppler shift [85]. Residual frequency offset destroys subcarrier orthogonality, which generates inter-carrier interference and the bit error rate (BER) increases consequently. The effect of such impairments on the conventional (i.e. single input single output (SISO)) OFDM has been widely investigated. For example, in [86], BER is calculated for uncoded SISO-OFDM systems with several modulation schemes. The authors in [87], [88] provide BER expressions of MIMO-OFDM employing Alamouti's scheme [82]. The authors in [89] analyze the space-frequency code performance in different propagation environments, such as Rayleigh and Rician fading channels, and with spatial correlation at the transmitter and/or receiver. However, the impact of inter-carrier interference due to frequency offset on the pairwise error probability (PEP) performance of general space-frequency codes have not been investigated. Additionally, the design criteria of space-frequency codes when inter-carrier interference exists are unknown. These problems will be addressed in this thesis.

1.7 Contributions of Thesis

The main contributions of this thesis are broadly twofold. First, we characterize the necessary and sufficient conditions to obtain low-complexity STBC for frequency-flat fading channels. The low complexity is achieved by separating the transmitted symbols into subgroups for maximum likelihood detection. The codes with such properties are called multi-group decodable STBC. We propose a new multi-group decodable STBC called orthogonality-embedded space-time (OEST) codes. Second, we analyze the performance of space-frequency codes for MIMO-OFDM systems in the presence of frequency offset and propose a new class of space-frequency codes to combat effectively frequency offset. The detailed contributions are summarized in the following.

In Chapter II, the necessary and sufficient conditions for low-decoding complexity STBC are presented. A new framework to design STBC called OEST codes is proposed. OEST codes subsume existing STBC such as OSTBC, QSTBC, circulant STBC as spe-

cial cases. Several properties of OEST codes will also be derived. We derive a subclass of OEST called semi-orthogonal algebraic space-time (SAST) codes, which are identified with many desirable features: near capacity achieving, low decoding complexity, and better performance than several codes of the same rate.

Chapter III treats several open problems of QSTBC, a special class of OEST codes, originally proposed by Tirkkonen *et al.* [47]. This code has been named ABBA because of its structure. We will show how to obtain maximum likelihood single-complex symbol decoding for ABBA code, which is the minimum decoding complexity level that can be achieved by any non-orthogonal STBC. For ABBA codes, we also systematically solve the open problems, including performance analysis, optimal signal rotation, capacity calculation, channel state information feedback, and antenna selection with limited feedback.

Chapter IV proposes a new encoding method so that the OEST codes even have lower decoding complexity. SAST codes, a special case of OEST codes, are analyzed in detail. Initially, SAST codes allow the decoding of transmitted symbols into two groups. A new decoder is derived, enabling the decoding of the transmitted symbols into four groups and resulting in a great complexity reduction. The exact PEP and optimal signal transformation of SAST codes are derived.

Chapter V extends the results developed for OEST codes to solve open issues of other STBC, including coordinate-interleaved orthogonal designs (CIOD) [90–92] and QSTBC with four-group decoding [93]. New decoders, performance analysis and optimal signal designs are presented for these two codes.

Chapter VI contributes a performance analysis of space-frequency codes in the presence of frequency offset. Additionally, inter-carrier interference caused by a time-varying channel and phase noise is also considered. More importantly, we propose a new space-frequency coding scheme, called inter-carrier interference self-cancellation space-frequency codes, to combat even high values of frequency offset, up to 10%.

In Chapter VII, we summarize the contributions of the dissertation. Open research topics that can be developed from this thesis are identified.

Chapter 2

Multi-Group Decodable Space-Time Block Codes

Since low decoding complexity STBC are desirable for practical applications, the code matrix structure should allow the separation of the transmitted symbols into sub-groups for maximum likelihood decoding, resulting in multi-group decodable STBC. Here we emphasize maximum likelihood decoding as it is a sufficient condition to realize full-diversity. Suboptimal detectors, such as zero-forcing decision feedback equalization [94], may not achieve full diversity. In this chapter, we first derive the necessary and sufficient conditions so that the separation of transmitted symbols for maximum likelihood decoding is possible. Second, we propose a new class of STBC called orthogonality-embedded space-time (OEST) codes that are multi-group decodable.

2.1 Algebraic Constraints of Multi-Group Decodable STBC

2.1.1 System Model

We use the MIMO quasi-static frequency-flat fading channel model described in Section 1.2. Other notations of STBC given in Chapter I will be utilized in this and other chapters. However, for the reader's convenience, several basic equations are repeated.

There are M transmit and N receive antennas. In the space-time encoder, the data symbols are parsed into a $T \times M$ code matrix[1] X of an space-time code $\mathcal{X}$ as follows:

$$X = \left[c_{tm}\right]_{t=1,\ldots,T;m=1,\ldots,M} \tag{2.1}$$

[1]We use the term "codeword" and "code matrix" interchangeably.

where c_{tm} is the symbol transmitted from antenna m at time t ($1 \leq t \leq T$). The average energy of code matrices is constrained such that

$$\mathcal{E}_{\mathcal{X}} = \mathbb{E}[\mathrm{trace}(X^{\dagger}X)] = \mathbb{E}[\|X\|_{\mathsf{F}}^2] = \sum_{m=1}^{M}\sum_{t=1}^{T}\mathbb{E}[|c_{tm}|^2] = T \tag{2.2}$$

where $\mathrm{trace}(X)$ denotes the trace of matrix X [95].

The received signals y_{tn} of the nth antenna at time t can be arranged in a matrix Y of size $T \times N$. Thus, one can represent the transmit-receive signal relation as

$$Y = \sqrt{\rho}XH + W \tag{2.3}$$

where $H = [h_{mn}]$, and $W = [w_{tn}]$ of size $T \times N$, and w_{tn} are independently, identically distributed (i.i.d.) $\mathcal{CN}(0,1)$. The transmit power is scaled by ρ so that the average signal-to-noise ratio (SNR) at each receive antenna is ρ, independent of the number of transmit antennas. However, ρ is sometimes omitted for notational brevity.

The mapping of a block of K data symbols $(s_1, s_2, \cdots, s_K)$ into a $T \times M$ code matrix can be represented in a general dispersion form [33, 40] as follows:

$$X = \sum_{k=1}^{K}(a_k A_k + b_k B_k) \tag{2.4}$$

where A_k and B_k, ($k = 1, 2, \cdots, K$) are $T \times M$ complex-valued constant matrices; they are commonly called dispersion matrices. The real and imaginary parts of the symbol s_k are a_k and b_k.

In (2.4), there are totally $2K$ variables a_i and b_i. We replace variables a_i and b_i (and their dispersion matrices A_k and B_k) by the same symbolic variable c_l (and dispersion matrix C_l). Then (2.4) becomes

$$X = \sum_{l=1}^{L} c_l C_l. \tag{2.5}$$

The benefit of the expression (2.5) will be clearer when we derive the algebraic constraints of multi-group decodable STBC. Note that L in (2.5) is not necessarily an even number.

Denote the transmitted data vector $\boldsymbol{c} = \begin{bmatrix} c_1 & c_2 & \dots c_L \end{bmatrix}^{\mathsf{T}}$. The maximum likelihood decoding of STBC is to find the solution $\hat{\boldsymbol{c}}$ of the following metric:

$$\hat{\boldsymbol{c}} = \arg\min_{\boldsymbol{c}} \|Y - \sqrt{\rho}XH\|_{\mathsf{F}}^2 . \tag{2.6}$$

2.1.2 Algebraic Constraints of Multi-Group Decodable STBC

The concept of QSTBC [46–48] is to relax the orthogonality constraints of OSTBC to achieve higher data rates. In the code matrices of QSTBC [46–48], the columns are non-orthogonal in pairs; the maximum likelihood detection of QSTBC can be made in pairs of symbols. To obtain a higher data rate of one symbol for any number of antennas, in [96–100] the orthogonality is further relaxed so that the columns of code matrices can be divided into two groups, and the columns of one group are orthogonal to the columns of the other group. The maximum likelihood detection of transmitted symbols are decoupled into two groups. A rule of thumb can be drawn from the STBC in [46–48, 96–100]: The number of columns of a group (that is orthogonal to the other groups of columns) equals the number of symbols to be jointly detected.

In fact, the orthogonality of columns of code matrices is not the fundamental condition to obtain multi-group decodable STBC, as we will show later. We provide a definition of multi-group decodable STBC to unify the notation in this thesis as follows.

Definition 2.1. *A STBC is said to be Γ-group decodable STBC if the maximum likelihood decoding metric* (2.6) *can be decoupled into a linear sum of Γ independent submetrics, where each submetric consists of the symbols from only one group. The Γ-group decodable STBC is denoted by Γ-group STBC for short.*

It is worthwhile to emphasize the following points from Definition 2.1:

1. The numbers of symbols in groups are not necessarily the same.

2. Since there are no restrictions on the dispersion matrices of the real or imaginary parts of a complex symbol, they may belong to different groups. That is, the real and imaginary parts of a complex symbol can be decoded independently. Such decoding is possible for quadrature amplitude modulation (QAM) signals, as we will show later.

3. There is no orthogonality constraint on the columns of Γ-group STBC even though there are some degree of orthogonality imposed in the code matrices of some existing Γ-group STBC [46–48, 96, 97, 99, 100]. We will show an example of Γ-group STBC, in which the columns of code matrices are not orthogonal at all.

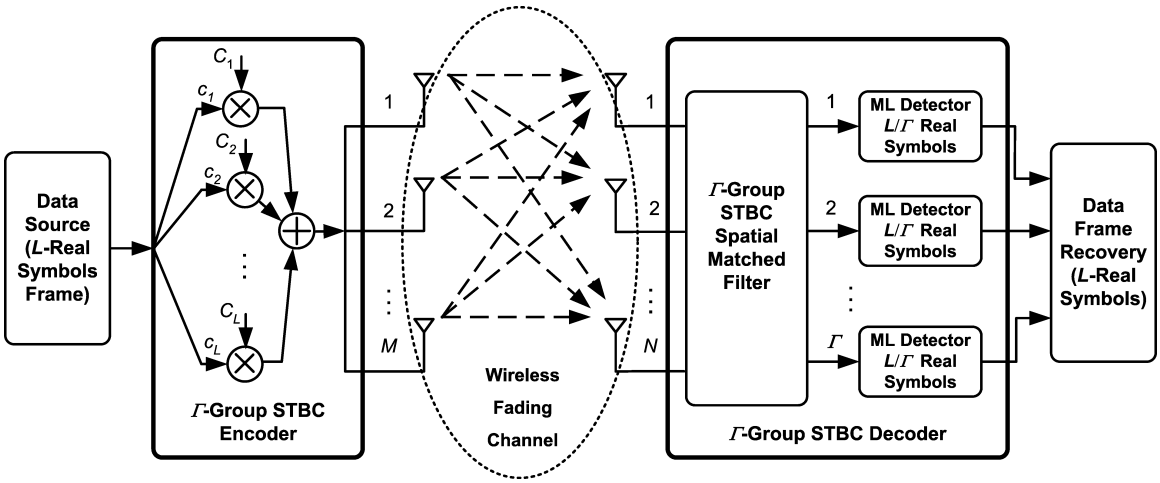

Figure 2.1: Block diagram of MIMO systems using multi-group decodable STBC.

The block diagram of MIMO systems with multi-group STBC is illustrated in Fig. 2.1. The data frame of L-real symbols is encoded using multi-group STBC encoder, which performs the multiplications and additions. At the receiver, the data symbols are separated into groups by spatial matched filters. Each group of real symbols is maximum-likelihood detected so that the whole data frame can be recovered. Thus, the question is how to design the spatial matched filters to separate the data symbols. This question can be addressed by exploiting the properties of the space-time encoder, i.e. the dispersion matrices. Thus, we must first find the properties of the dispersion matrices of multi-group STBC.

In the most general case, we assume that there are Γ groups; each group is denoted by $\Psi_i (i = 1, 2, \ldots, \Gamma)$ and has L_i symbols. Thus, $L = \sum_{i=1}^{\Gamma} L_i$. Let Θ_i be the set of indexes of symbols in the group Ψ_i.

Yuen *et al.* [98, Theorem 1] have shown a sufficient condition for a STBC be multi-group decodable. In fact, this condition is also the necessary condition. We will state these results in the following theorem.

Theorem 2.2. *The necessary and sufficient conditions for a STBC to be Γ-group decodable are*

$$C_p^{\dagger} C_q + C_q^{\dagger} C_p = \mathbf{0} \quad \forall p \in \Theta_i, \forall q \in \Theta_j, i \neq j. \tag{2.7}$$

Theorem 2.2 covers [92, Theorem 9] (single-symbol decodable STBC) and can be shown similarly below.

Proof. Let $\boldsymbol{y}_n$ and $\boldsymbol{h}_n$ be the nth column of Y and H, respectively. The maximum likelihood metric (2.6) is rewritten as

$$\begin{aligned}\|Y - XH\|_{\mathsf{F}}^2 &= \sum_{n=1}^{N} \|\boldsymbol{y}_n - X\boldsymbol{h}_n\|_{\mathsf{F}}^2 \\ &= \sum_{n=1}^{N} \left[\boldsymbol{h}_n^\dagger C^\dagger C \boldsymbol{h}_n - 2\Re(\boldsymbol{y}_n^\dagger C \boldsymbol{h}_n)\right] + \|Y\|_{\mathsf{F}}^2. \end{aligned} \tag{2.8}$$

In (2.8), $\|Y\|_{\mathsf{F}}^2$ is a constant with respect to the code matrix C, it can be therefore discarded. The term $\Re(\boldsymbol{y}_n^\dagger C \boldsymbol{h}_n)$ is linear in real variables c_i. Thus, we just need to consider the product $C^\dagger C$, which consists of cross products of variables c_i:

$$\begin{aligned} C^\dagger C &= \left(\sum_{p=1}^{L} c_p C_p^\dagger\right)\left(\sum_{q=1}^{L} c_q C_q\right) \\ &= \sum_{l=1}^{L} c_l^2 C_l^\dagger C_l + \sum_{p,q=1,p\neq q}^{L} c_p c_q \left(C_p^\dagger C_q + C_q^\dagger C_p\right). \end{aligned} \tag{2.9}$$

Now we show the necessary condition of Theorem 2.2. If C_i satisfies the condition (2.7), then

$$C^\dagger C = \sum_{i=1}^{\Gamma} f(\Psi_i) \tag{2.10}$$

where

$$f(\Psi_i) = \sum_{m,n\in\Theta_i} c_m c_n C_m^\dagger C_n. \tag{2.11}$$

Hence, the maximum likelihood metric (2.8) can be decomposed into a linear sum of Γ submetrics, each submetric involves only the symbols of one group. Thus, to minimize the metric in (2.8), one can minimize Γ individual submetrics. In other words, the decoding of L symbols can be decoupled into Γ independent groups.

We next prove the sufficient condition. The assumption is that the maximum likelihood decoding metric is a linear sum of Γ independent submetrics, each submetric consists of variables from only one group. From (2.9) we cannot decompose further the sum that involves the cross-products of variables c_p and c_q. Thus, the maximum likelihood metric is a linear sum of independent submetrics only if that (2.7) holds. That concludes the proof. □

Using Theorem 2.2, we can identify whether a STBC is multi-group decodable or not. For example, let us examine a 2-by-2 circulant STBC [20, 101] with the code matrix $X = \begin{bmatrix} x_1 & x_2 \\ x_2 & x_1 \end{bmatrix}$. Let $x_1 = a_1 + \mathrm{j}\, b_1, x_2 = a_2 + \mathrm{j}\, b_2$. It is not hard to verify that the dispersion matrices of symbols (a_1, a_2) and symbols (b_1, b_2) satisfy Theorem 2.2. Thus, this 2×2 circulant STBC is a 2-group STBC; it is also a rate-one single complex-symbol decodable STBC for 2 transmit antennas, which is similar to the Alamouti code. However, the Alamouti code performs better than this 2×2 circulant STBC since OSTBC are optimal in terms of SNR [102] [26]. The other higher order circulant STBC can also be shown to be 2-group STBC, but this fact is not recognized in [20, 101]. Interestingly, circulant STBC are an example of 2-group STBC, in which the columns of the code matrix are not orthogonal at all. In the next sections, we develop two new classes of rate-one 4-group STBC, which have lower decoding complexity than the two-group decodable circulant STBC.

There are several existing multi-group decodable STBC, for example OSTBC [26, 40, 44], QSTBC [46–48], and circulant STBC [20, 101]. They have different code constructions, degrees of column orthogonality, different code rates, and decoding complexity. However, we will show that there is a mother code, called orthogonality-embedded space-time (OEST) codes, of OSTBC, QSTBC, and circulant STBC.

The OEST code construction utilizes the generalized complex or real orthogonal designs of the form $\sum (s_k A_k + s_k^* B_k)$, where A_k and B_k are the linear dispersion matrices of an underlying OSTBC and s_k are transmitted symbols, with two modifications: (1) Each transmitted symbol s_k is replaced by a circulant matrix C_k, in which a block of transmitted symbols is encoded; (2) The regular scalar-matrix product is replaced by the Kronecker product [63, 95]. Therefore, it is of interest to review important properties of OSTBC and circulant STBC to be used later. We will present the results of OEST codes with generalized complex orthogonal designs; however, these results can be easily extended to generalized real orthogonal designs. Therefore, only the properties of OSTBC from generalized complex orthogonal designs are provided.

2.2 Review of OSTBC and Circulant STBC

2.2.1 Orthogonal Space-Time Block Codes

Definition 2.3 (Orthogonal designs [40, 44])**.** *A complex orthogonal design $\mathcal{O}$ is defined as a $R \times Q$ rectangular matrix whose nonzero entries are $\pm s_1, \pm s_2, \cdots, \pm s_K$ or their conjugates $\pm s_1^*, \pm s_2^*, \cdots, \pm s_K^*$, where $s_1, s_2, \cdots, s_K$ are indeterminates over the complex field $\mathbb{C}$, such that*

$$\mathcal{O}^\dagger \mathcal{O} = (|s_1|^2 + |s_1|^2 + \cdots + |s_K|^2)\boldsymbol{I}_Q. \tag{2.12}$$

The matrix $\mathcal{O}$ is also said to be a $[R, Q, K]$ complex orthogonal design. When $R = Q$, $\mathcal{O}$ is called a complex square orthogonal design.

Proposition 2.4 ([44])**.** *$\mathcal{O}$ is a complex orthogonal design if and only if the basis matrices A_k and B_k in* (2.4) *satisfy*

$$A_i^\dagger A_i + B_i^\dagger B_i = \boldsymbol{I}_Q, \qquad i = 1, 2, \cdots, K \tag{2.13a}$$

$$A_i^\dagger A_j + B_j^\dagger B_i = \mathbf{0}_Q, \qquad 1 \le i < j \le K \tag{2.13b}$$

$$A_i^\dagger B_j + A_j^\dagger B_i = \mathbf{0}_Q, \qquad i, j = 1, 2, \cdots, K. \tag{2.13c}$$

To construct STBC for Q transmit antennas from orthogonal designs (OSTBC), the orthogonal design $[R, Q, K]$ is used, and the indeterminates are replaced by transmitted symbols. For example, the OSTBC for 2 and 4 transmit antennas are given below:

$$\mathcal{O}_2 = \begin{bmatrix} s_1 & s_2 \\ -s_2^* & s_1^* \end{bmatrix}, \tag{2.14}$$

$$\mathcal{O}_4 = \begin{bmatrix} s_1 & s_2 & s_3 & 0 \\ -s_2^* & s_1^* & 0 & -s_3 \\ -s_3^* & 0 & s_1^* & s_2 \\ 0 & s_3^* & -s_2^* & s_1 \end{bmatrix}. \tag{2.15}$$

The OSTBC for 2 transmit antennas is the well-known STBC proposed by Alamouti [82]. The Alamouti code has rate-one. However, when the number of transmit antennas increases, the code rate of OSTBC decreases. The maximal code rate of existing OSTBC is given as follows.

Proposition 2.5 ([44])**.** *The maximal code rate of OSTBC for $Q = 2a - 1$ or $Q = 2a$, where a is any positive integer, is*

$$R_{\mathcal{O},Q} = \frac{a+1}{2a}. \tag{2.16}$$

Thus, the rate-one OSTBC exists for 2 transmit antennas only. Furthermore, the rate approaches 1/2 for a large number of antennas. The subscript Q of $\mathcal{O}_Q$ is added to highlight that the OSTBC is designed for Q transmit antennas. Note that there are several design criteria existing for OSTBC, such as delay-optimal codes with $R = Q$ (or square orthogonal designs) [59] or rate-optimal, i.e. the code rate is maximized [44].

To guarantee the transmit power constraint (2.2), a scaling factor is required. Thus, the OSTBC code matrix with normalized power is $\sqrt{\kappa}\mathcal{O}_Q$. We can show that

$$\kappa = \frac{1}{Q\mathsf{R}_{\mathcal{O},Q}} \tag{2.17}$$

as follows.

Proof. The total energy $\mathcal{E}_{\mathcal{O}}$ of OSTBC code matrices is

$$\mathcal{E}_{\mathcal{O}} = \mathbb{E}\left[\mathrm{trace}(\mathcal{O}^{\dagger}\mathcal{O}\right] = \kappa Q\mathbb{E}[\sum_{k=1}^{K}|s_k|^2] = \kappa KQ\,\mathbb{E}[|s_k|^2] = \kappa KQ.$$

From (2.2), one has $\kappa KQ = T$ or $\kappa = \frac{1}{Q\mathsf{R}_{\mathcal{O},Q}}$. □

For example, the Alamouti code has $\kappa_2 = 1/2$.

The coding gain of OSTBC can be easily found to be

$$G_{\mathcal{O},Q} = \frac{1}{Q\mathsf{R}_{\mathcal{O},Q}}\, d^2_{\min} \tag{2.18}$$

where $d_{\min}$ is the minimum distance of the input constellation from which s_k are chosen.

2.2.2 Linear Threaded Algebraic Space-Time Codes

The idea of employing circulant matrices [64] to build rate-one STBC has appeared in [20, 101]. We may call such codes circulant STBC. Let $\boldsymbol{u} = \begin{bmatrix} u_1 & u_2 & \cdots & u_M \end{bmatrix}$ be the input modulation vector of M symbols. The code matrix of circulant STBC for M transmit antennas is

$$C_r(\boldsymbol{u}) = \begin{bmatrix} u_1 & u_2 & \cdots & u_M \\ u_M & u_1 & \cdots & u_{M-1} \\ \vdots & \vdots & & \vdots \\ u_2 & u_3 & \cdots & u_1 \end{bmatrix}. \tag{2.19}$$

Since circulant matrices are not always full-rank, they cannot be directly applied with typical signal constellations to design STBC with full diversity [101]. To achieve full

diversity, modulation symbols are drawn from the same signal constellation and rotated differently, i.e. the transmitted symbols u_i are virtually drawn from different alphabets [20]. The selection of rotation angles heavily impacts the coding gain. We next briefly review how the rotation angles are selected in [20].

Let S be the input symbol constellation with the minimum Euclidean distance $d_{\min}$. A block of M constellation symbols is arranged in a vector $\boldsymbol{s} = [s_1, s_2, \cdots, s_M]^{\mathsf{T}}$. Each symbol s_i is rotated by an angle $\phi^{(i-1)/M}$, where ϕ is a Diophantine number [20, 103]. Let $\Theta = \mathrm{diag}[\,1,\ \phi^{1/M},\ \cdots,\ \phi^{(M-1)/M}\,]$, the transmitted vector $\boldsymbol{u}$ is as

$$\boldsymbol{u} = \Theta \boldsymbol{s} \tag{2.20}$$

The LTAST code matrices are circulants given by

$$\mathcal{T} = \frac{1}{\sqrt{M}} C_r(\boldsymbol{u})\,. \tag{2.21}$$

The rate of the resulting LTAST code due to this construction is one. The upper bound of the coding gain is as follows.

Proposition 2.6 (eq. (7), [20])**.** *The coding gain of the rate-one LTAST codes is upper-bounded as* $G_{\mathcal{C},M} \leq \frac{1}{M} d^2_{\min}$.

To achieve full diversity, the Diophantine number is chosen as $\phi = e^{\mathsf{j}\,\alpha}$ ($\mathsf{j}^2 = -1$). Thus, the ith symbol s_i is rotated by an angle $\frac{i-1}{M}\alpha$. The optimal values of ϕ that maximize the coding gain are given below.

Proposition 2.7 (Theorem 2, [20])**.** *For* $M = 2^r, r \geq 1$*, the optimal coding gain of rate-one LTAST codes, i.e.* $G_{\mathcal{C},M} = \frac{1}{M} d^2_{\min}$*, can be obtained by choosing the Diophantine number* $\phi = \mathsf{j}$ *and constellations* $\mathcal{S}$ *carved from the ring of Gaussian integers (including QAM), and for* $M = 2^{r_0}3^{r_1}, r_0, r_1 \geq 0$ *by choosing* $\phi = e^{2\mathsf{j}\,\pi/6}$ *and constellations* $\mathcal{S}$ *carved from the ring of Einstein integers (including hexagonal (HEX) constellations [104]).*

[20, Theorem 1] also suggests how to select ϕ for PSK constellations; however, computer search is required to find the ϕ that maximizes the coding gain. Additionally, for $M \neq 2^r$ or $M = 2^{r_0}3^{r_1}$, only local maxima of the coding gain are guaranteed by computer search. However, for a special case with $M = 2$, we will show that the results of reference [105] can be readily applied to find the optimal rotations for any two-dimensional signal PSK.

Proposition 2.8 ([105]). *Consider the rate-one LTAST codes for $M = 2$. One of the two transmitted symbols is drawn from an $\mathcal{M}$-ary PSK constellation S and the other one is drawn from $e^{\mathrm{j}\alpha}\mathsf{S}$. The coding gain of LTAST is maximized if and only if the rotation angle α is $\frac{(2k+1)\pi}{\mathcal{M}}$ for $k = 0, 1, ..., \mathcal{M}-1$ if $\mathcal{M}$ is even and $\frac{(2k+1)\pi}{\mathcal{M}}$, $k = 0, 1, ..., 2\mathcal{M}-1$ if $\mathcal{M}$ is odd.*

We will show that OEST codes include LTAST codes as a special case. Thus, Proposition 2.8 can be verified when we present the properties of OEST codes in the next section.

2.3 Constructions and Properties of Orthogonality-Embedded Space-Time Codes

In this section, we develop OEST codes by deriving their main properties, such as the code rate, diversity order and coding gain. Several existing codes are shown to be special cases of OEST codes. The group decoding property is fully investigated. The orthogonality among the group symbols implies the existence of the orthogonal (spatial) signatures of the data vectors [32, 48]; our main task will be to show these spatial signatures. We also derive an explicit form of the equivalent channel of OEST codes, which is used later to analyze the maximum mutual information of OEST codes.

2.3.1 Constructions of OEST Codes

To construct OEST codes form OSTBC, we replace the symbols s_k in (2.4) by circulant matrices and the scalar product by the Kronecker product. The resulting OEST codes have higher rates than that of OSBTC and, importantly, OEST codes offer several code designs for the same number of transmit antennas with desirable tradeoffs among rate, performance, decoding complexity and delay. Furthermore, the new results of OEST codes shed light on existing codes, such as QSTBC and LTAST [20, 47]. For example, the maximum mutual information, equivalent channel and general decoder for QSTBC and LTAST are obtained as a byproduct of the OEST results.

Let the number of transmit antennas be $M = PQ$, where P and Q are positive integers, and let A_k and B_k $(k = 1, 2, \cdots, K)$ be the basis matrices of $R \times Q$ orthogonal designs. A block of $K \times P$ input symbols are divided into K vectors $\boldsymbol{s}_k$, each of size $P \times 1$.

We propose two constructions of OEST codes as follows:

Construction I:

$$\mathcal{D} = \sqrt{\frac{\kappa}{P}} \sum_{k=1}^{K} \Big(A_k \otimes \mathcal{C}_k + B_k \otimes \mathcal{C}_k^{\dagger} \Big), \tag{2.22}$$

Construction II:

$$\mathcal{D} = \sqrt{\frac{\kappa}{P}} \sum_{k=1}^{K} \Big(\mathcal{C}_k \otimes A_k + \mathcal{C}_k^{\dagger} \otimes B_k \Big). \tag{2.23}$$

Since A_k and B_k have the same size, $\mathcal{C}_k$ is a square matrix, and the two matrices $(A_k \otimes \mathcal{C}_k)$ and $(\mathcal{C}_k \otimes A_k)$ are permutation equivalent (the same relation holds for $(B_k \otimes \mathcal{C}_k^{\dagger})$ and $(\mathcal{C}_k^{\dagger} \otimes B_k)$) [95, corollary 4.3.10]. Hence, Constructions I and II are permutation equivalent. We will, therefore, derive the properties of the OEST codes for Construction I only.

It is of interest to find the linear dispersion form (2.4) of OEST codes. Let $\boldsymbol{u}_k = [u_{k1} \; u_{k2} \; \cdots \; u_{kP}]^{\mathsf{T}}$ $(k = 1, 2, \ldots, K)$ denote the kth input vector to the circulant space-time encoder (2.21). We know that a circulant matrix has the following decomposition

$$C_r(\boldsymbol{u}_k) = \sum_{i=1}^{P} u_{ki} \pi^{i-1} \tag{2.24}$$

where *forward shift permutation* matrix π is given by [64, p. 68]

$$\pi = \begin{bmatrix} 0 & 1 & 0 & 0 & \cdots & 0 \\ 0 & 0 & 1 & 0 & \cdots & 0 \\ \vdots & \vdots & \vdots & \vdots & \vdots & \vdots \\ 1 & 0 & 0 & 0 & \cdots & 0 \end{bmatrix}. \tag{2.25}$$

From (2.22) and (2.25), the linear dispersion form of OEST code matrix is as follows:

$$\begin{aligned} D &= \sqrt{\frac{\kappa}{P}} \sum_{k=1}^{K} \left[A_k \otimes \left(\sum_{i=1}^{P} u_{kp} \pi^{p-1} \right) + B_k \otimes \left(\sum_{p=1}^{P} u_{kp}^{*} \pi^{1-p} \right) \right] \\ &= \sqrt{\frac{\rho\kappa}{P}} \sum_{k=1}^{K} \sum_{p=1}^{P} \left[u_{kp} \left(A_k \otimes \pi^{p-1} \right) + u_{kp}^{*} \left(B_k \otimes \pi^{1-p} \right) \right]. \end{aligned} \tag{2.26}$$

This represention will later be used to derive the group decoder.

Since several different constructions exist for OSTBC [44,59,106], in combination with the circulant codes, we can generate several OEST codes for a given number of transmit antennas. Moreover, OEST codes subsume several existing STBC as we will show below.

1. OSTBC: If $P = 1$, the circulant matrix $\mathcal{C}_k$ reduces to a single symbol, and we revert to the original construction of OSTBC codes.

2. QSTBC: If $Q = 2$, the Construction II is identical with the QSTBC codes given by Tirkkonen *et al.* [47].

   The QSTBC in [47] is known as ABBA codes [2]. This construction for $M = 2Q$ transmit antennas is as follows

$$\mathcal{Q} = \begin{bmatrix} \mathcal{A} & \mathcal{B} \\ \mathcal{B} & \mathcal{A} \end{bmatrix} \tag{2.27}$$

   where $\mathcal{A}$ and $\mathcal{B}$ are two matrices of OSTBC codes designed for Q transmit antennas. Hence, $\mathcal{A}$ and $\mathcal{B}$ can be represented as $\mathcal{A} = \sum_{k=1}^{K} (s_k A_k + s_k^* B_k), \mathcal{B} = \sum_{k=1}^{K} \left(s_{k+K} A_k + s_{k+K}^* B_k\right)$, where A_k and B_k, $(k = 1, 2, \cdots, K)$ are the basis matrices of OSTBC for Q transmit antennas. Substitute $\mathcal{A}$ and $\mathcal{B}$ into (2.27), and we have

$$\begin{aligned} \mathcal{Q} &= \begin{bmatrix} \sum_{k=1}^{K} (s_k A_k + s_k^* B_k) & \sum_{k=1}^{K} \left(s_{k+K} A_k + s_{k+K}^* B_k\right) \\ \sum_{k=1}^{K} \left(s_{k+K} A_k + s_{k+K}^* B_k\right) & \sum_{k=1}^{K} (s_k A_k + s_k^* B_k) \end{bmatrix} \\ &= \sum_{k=1}^{K} \underbrace{\begin{bmatrix} s_k & s_{k+K} \\ s_{k+K} & s_k \end{bmatrix}}_{\mathcal{C}_k} \otimes A_k + \sum_{k=1}^{K} \underbrace{\begin{bmatrix} s_k^* & s_{k+K}^* \\ s_{k+K}^* & s_k^* \end{bmatrix}}_{\mathcal{C}_k^\dagger} \otimes B_k \\ &= \sum_{k=1}^{K} (\mathcal{C}_k \otimes A_k + \mathcal{C}_k^\dagger \otimes B_k). \end{aligned} \tag{2.28}$$

   The above expression is exactly the Construction II of OEST codes in (2.23).

   Note that to achieve full diversity and optimal coding gain for QSTBC, signal rotations are also required. Thus, the optimal rotations of rate-one LTAST codes with $P = 2$ (see Proposition 2.7) can be applied for QSTBC with QAM and Hex constellations. Vice *versa*, the optimal rotations of QSTBC (see [61, 105] and references therein) can be applied for rate-one LTAST codes; this result is provided in Proposition 2.8.

3. Rate-one LTAST codes [20]: In this case, $Q = 1$, $A_1 = \boldsymbol{I}_1$, $B_1 = \mathbf{0}_1$.

We will next examine the properties of OEST codes with the multi-group decoding property being presented first.

[2] There are other QSTBC designed for 4 and 8 transmit antennas proposed by Jafarkhani [46]. However, the QSTBC for 8 transmit antennas given in [46] cannot be constructed from the code designed for 4 transmit antennas; The code for 8 antennas was designed by proper selection and arrangement of the specific OSTBCs' designed for 4 transmit antennas. Thus, the exemplary structures of QSTBC given in [46] are not general for an arbitrary number of transmit antennas.

2.3.2 Properties of OEST Codes

1. Multi-Group Decoding

From the construction of OEST codes, there are K vectors embedded in K circulant matrices. The first important property of OEST codes is their multi-group decodability stated below.

Theorem 2.9. *By Constructions I and II, the OEST codes are K-group decodable.*

One can use the linear dispersion form (2.26) and Theorem 2.2 to prove. However, we will follow a slightly different approach so that the same proof can be used later to derive other properties of OEST codes, such as diversity order and optimal signal transformations.

Proof. From the proof of Theorem 2.2, we need to show that if $\mathcal{D}$ is a code matrix of OEST codes, then from (2.10), the product $\mathcal{D}^\dagger\mathcal{D}$ must be decomposed into a linear sum of K submetrics, each submetric involves only the symbols of one data vector. We have

$$\begin{aligned}\frac{\mathcal{D}^\dagger\mathcal{D}}{\kappa/P} &= \sum_{i=1}^{K}(A_i\otimes\mathcal{C}_i + B_i\otimes\mathcal{C}_i^\dagger)^\dagger\cdot\sum_{j=1}^{K}(A_i\otimes\mathcal{C}_i + B_i\otimes\mathcal{C}_i^\dagger)\\ &= \underbrace{\sum_{i=1}^{K}\sum_{j=1}^{K}(A_i^\dagger A_j)\otimes(\mathcal{C}_i^\dagger\mathcal{C}_j) + \sum_{i=1}^{K}\sum_{j=1}^{K}(B_i^\dagger B_j)\otimes(\mathcal{C}_i\mathcal{C}_j^\dagger)}_{X_1}\\ &\quad + \underbrace{\sum_{i=1}^{K}\sum_{j=1}^{K}(A_i^\dagger B_j)\otimes(\mathcal{C}_i^\dagger\mathcal{C}_j^\dagger)}_{X_2} + \underbrace{\sum_{i=1}^{K}\sum_{j=1}^{K}(B_i^\dagger A_j)\otimes(\mathcal{C}_i\mathcal{C}_j)}_{X_3}.\end{aligned} \tag{2.29}$$

Note that $\mathcal{C}_i$ is circulant, then $\mathcal{C}_i^\dagger$ is also circulant; we can apply the commutativity of circulant matrices to derive the three terms X_i ($i=1,2,3$) in (2.29).

$$\begin{aligned}X_2 &= \sum_{i=1}^{K}\sum_{j=1}^{K}(A_i^\dagger B_j)\otimes(\mathcal{C}_i^\dagger\mathcal{C}_j^\dagger)\\ &= \frac{1}{2}\left(\sum_{i=1}^{K}\sum_{j=1}^{K}(A_i^\dagger B_j)\otimes(\mathcal{C}_i^\dagger\mathcal{C}_j^\dagger) + \sum_{j=1}^{K}\sum_{i=1}^{K}(A_j^\dagger B_i)\otimes(\mathcal{C}_j^\dagger\mathcal{C}_i^\dagger)\right)\\ &= \frac{1}{2}\sum_{i=1}^{K}\sum_{j=1}^{K}(A_i^\dagger B_j + A_j^\dagger B_i)\otimes(\mathcal{C}_i^\dagger\mathcal{C}_j^\dagger).\end{aligned} \tag{2.30}$$

Using the constraint (2.13c) of OSTBC, we have $A_i^\dagger B_j + A_j^\dagger B_i = \mathbf{0}_Q$. Therefore, $X_2 = \mathbf{0}_M$. Similarly, we can show that $X_3 = \mathbf{0}_M$.

To calculate X_1, we first swap the indices i, j of the second term of X_1 and exploit the commutativity of circulant matrices to get

$$\begin{aligned} X_1 &= \sum_{i=1}^{K}\sum_{j=1}^{K}(A_i^\dagger A_j)\otimes(\mathcal{C}_i^\dagger\mathcal{C}_j) + \sum_{i=1}^{K}\sum_{j=1}^{K}(B_i^\dagger B_j)\otimes(\mathcal{C}_i\mathcal{C}_j^\dagger) \\ &= \sum_{i=1}^{K}\sum_{j=1}^{K}(A_i^\dagger A_j + B_j^\dagger B_i)\otimes(\mathcal{C}_i^\dagger\mathcal{C}_j) \\ &= \sum_{i=1}^{K}\sum_{j=1,j\neq i}^{K}(A_i^\dagger A_j + B_j^\dagger B_i)\otimes(\mathcal{C}_i^\dagger\mathcal{C}_j) + \sum_{i=1}^{K}(A_i^\dagger A_i + B_i^\dagger B_i)\otimes(\mathcal{C}_i^\dagger\mathcal{C}_i). \end{aligned} \tag{2.31}$$

From the orthogonality constraint (2.13b), the first term of (2.31) vanishes and from (2.13a), $A_i^\dagger A_i + B_i^\dagger B_i = \boldsymbol{I}_Q$. Thus, $X_1 = \sum_{i=1}^{K}\boldsymbol{I}_Q\otimes(\mathcal{C}_i^\dagger\mathcal{C}_i) = \boldsymbol{I}_Q\otimes\left(\sum_{k=1}^{K}\mathcal{C}_k^\dagger\mathcal{C}_k\right)$. Substituting the results in (2.30) and (2.31) into (2.29), we have

$$\mathcal{D}^\dagger\mathcal{D} = \frac{\kappa}{P}\boldsymbol{I}_Q\otimes\sum_{i=1}^{K}\mathcal{C}_i^\dagger\mathcal{C}_i. \tag{2.32}$$

This completes the proof. □

We next examine the performance of OEST codes. The diversity order and coding gain are the two main performance metrics for designing OEST codes (Section 1.3). Of the primary importance, the diversity order is investigated first.

2. Diversity order

We derive the conditions so that OEST codes achieve full diversity.

Theorem 2.10. *An OEST code achieves full diversity if and only if the underlying circulant STBC has full diversity.*

Proof. We first show the necessary part of Theorem 2.10. We now apply the diversity criterion (Section 1.3) to examine the diversity order of OEST codes. For two distinct OEST code matrices D and $\hat{D}$, the matrix P_D defined as

$$\begin{aligned} P_D &\triangleq (D-\hat{D})^\dagger(D-\hat{D}) \\ &= \frac{\kappa}{P}\boldsymbol{I}_Q\otimes\left(\sum_{k=1}^{K}\Delta_{\mathcal{C}_k}^\dagger\Delta_{\mathcal{C}_k}\right) \end{aligned} \tag{2.33}$$

where $\Delta_{\mathcal{C}_k} = \mathcal{C}_k - \hat{\mathcal{C}}_k$. If P_D is full rank for all distinct code matrices D and $\hat{D}$, then the OEST code achieves full diversity.

Since $D \neq \hat{D}$, there exists at least one pair of $\mathcal{C}_i$ and $\hat{\mathcal{C}}_i$ such that $\mathcal{C}_i \neq \hat{\mathcal{C}}_i$ or $\Delta^{\dagger}_{\mathcal{C}_i}\Delta_{\mathcal{C}_i}$ is positive definite. Then the matrix $\left(\sum_{k=1}^{K} \Delta^{\dagger}_{\mathcal{C}_k}\Delta_{\mathcal{C}_k}\right)$ is always positive definite for any pairs of distinct code matrices. Therefore, the matrix P_D is always of full rank and OEST codes achieve full diversity. This completes the necessary part of Theorem 2.9.

To prove the sufficient part of Theorem 2.10, if the OEST code achieves full diversity, we must show that the underlying circulant STBC must be full diversity. From (2.33), if the worst case happens, there is only one non-zero difference matrix $(\mathcal{C}_i - \hat{\mathcal{C}}_i)$ for $1 \leq i \leq K$. If P_D is full-rank, the matrix $\Delta^{\dagger}_{\mathcal{C}_i}\Delta_{\mathcal{C}_i}$ must be full rank as well; this holds for all possible worst-case pairs of OEST code matrices. Therefore, for all possible matrices $(\mathcal{C}_i - \hat{\mathcal{C}}_i)$ are of full rank and the circulant STBC is full diversity. The proof of the sufficient part is completed. □

3. Coding gain

When OEST achieve full diversity, the coding gain (1.6) immediately follows:

$$\begin{aligned} G_{\mathcal{D},M} &= \frac{\kappa}{P} \min_{D \neq \hat{D}} \det P_D \\ &= \frac{\kappa}{P} \min_{D \neq \hat{D}} \left[\det \left(\sum_{k=1}^{K} \Delta^{\dagger}_{\mathcal{C}_k}\Delta_{\mathcal{C}_k} \right) \right]^{Q/M}. \end{aligned} \tag{2.34}$$

In the worst case, where there only exists one pair of $\mathcal{C}_i$ and $\hat{\mathcal{C}}_i$ such that $\mathcal{C}_i \neq \hat{\mathcal{C}}_i$, the coding gain is

$$\begin{aligned} G_{\mathcal{D},M} &= \frac{\kappa}{P} \min_{C_i \neq \hat{C}_i} \left[\det \left(\Delta^{\dagger}_{\mathcal{C}_i}\Delta_{\mathcal{C}_i} \right) \right]^{1/P} \\ &= \kappa\, G_{\mathcal{C},P}. \end{aligned} \tag{2.35}$$

Thus, using Proposition 2.6 and (2.16), we have the following result.

Corollary 2.11. *The coding gain $G_{\mathcal{D},M}$ of OEST codes is upper bounded as*

$$G_{\mathcal{D},M} \leq \frac{1}{Q\mathsf{R}_{\mathcal{O},Q}} \frac{d^2_{\min}}{P} = \frac{d^2_{\min}}{M\mathsf{R}_{\mathcal{O},Q}}. \tag{2.36}$$

Thus, one can select the optimal rotation of LTAST codes to maximize the coding gain of OEST codes as specified in Proposition 2.7 or Proposition 2.8 for $P = 2$ and PSK.

4. Code Rate

From the construction of OEST codes, compared with the basis OSTBC, the number of symbols parsed in an OEST code matrix increases P times. However, the length of the code matrix also increases P times; the code rate of an OEST code for $M = QP$ transmit antennas is, therefore, equal to the rate of OSTBC for Q transmit antennas used to construct this OEST code. We thus have the following results.

Corollary 2.12. *The rate of an OEST code for $M = PQ$ transmit antennas is equal to the rate of an OSTBC for Q transmit antennas, $\mathsf{R}_{\mathcal{D},M} = \mathsf{R}_{\mathcal{O},Q}$, which is used to construct this OEST code. The upper bound of the code rate for $Q = 2a - 1$ or $Q = 2a$ is $\frac{a+1}{2a}$.*

5. Column orthogonality

From (2.32), the orthogonality property of OEST code matrices can be stated as follows.

Corollary 2.13. *The $M = PQ$ columns of OEST code matrices (for $M = PQ$ transmit antennas) can be divided into Q separate groups, each of P consecutive columns, counting from left to right. Then the columns of the same group are not orthogonal to each other, but they are all orthogonal to the columns of the other groups.*

2.3.3 A Note on the Maximal Rate of OEST Codes

The rate of OEST codes is less than or equal to 1 symbol pcu. One may ask whether there is any STBC with group decoding property and with rate larger than one symbol pcu? We provide a partial answer to this question in the following.

OEST codes are designed with a special property of circulant matrices: If C_1 is a circulant matrix, then $C_1^\dagger$ is also a circulant matrix; C_1 and $C_1^\dagger$ inherit the commutative property of circulant matrices. Now, we consider a more general setting, a family $\mathcal{L}$ of matrices with the following properties: (1) All the matrices of $\mathcal{L}$ are commutative, i.e. if $C_1, C_2 \in \mathcal{L}$, then $C_1C_2 = C_2C_1$; (2) If $C_1 \in \mathcal{L}$, then $C_1^\dagger \in \mathcal{L}$. Thus, the circulant structure is not imposed to the matrices of $\mathcal{L}$. Our question is: what is the maximum rate of the STBC constructed by parsing the data symbols into the matrices of the set $\mathcal{L}$?

Let $C_1 \in \mathcal{L}$, then $C_1^\dagger \in \mathcal{L}$ and, therefore, $C_1C_1^\dagger = C_1^\dagger C_1$. Thus, $\mathcal{L}$ is a commutating family of normal matrices. All the matrices of $\mathcal{L}$ are simultaneously diagonalizable by the same unitary matrix [63, Theorem 2.5.5]. The input information symbols can only

be encoded to produce the diagonal entries of the diagonal matrix because the common unitary matrix cannot deliver any information. Since the number of independent entries of diagonal matrix is equal to the number of the column, the code rate is, therefore, not more than one symbol pcu. This is similar to the design of DST codes [49]. And in fact, rate-one circulant LTAST codes are equivalent to rate-one DST codes [20]. Thus, using the commutating normal matrices to construct OEST codes, codes with rate larger than one symbol pcu cannot be obtained.

Having presented the basic properties of OEST codes, we next show how to design an efficient decoder so that multi-group decoding ís possible without the exponential complexity of typical maximum likelihood search.

2.3.4 Decoder

In general, OEST codes can be decoded using the matrix-vector method proposed in [33], followed by a sphere decoder [107,108]. Therefore, we next show how to efficiently decouple the transmitted symbols into groups to greatly simplify symbol detection at the receiver.

Since the OEST code rate is not more than 1 symbol pcu, it is possible to use only one receive antenna with an efficient maximum likelihood decoder such as a sphere decoder [108]. For the sake of clarity and simplicity, we first consider the case with $N = 1$ receive antennas, and then generalize the results for $N \geq 1$.

Let $\boldsymbol{h} = [h_1\ h_2\ \cdots\ h_M]$ denote the channel gain between the mth $(m = 1, 2, \ldots, M)$ transmit antenna and the receive antenna. Let $D \in \mathcal{D}$ be a transmitted code matrix, the receive signal vector $\boldsymbol{y}$ is adopted from the system model (2.3) as

$$\boldsymbol{y} = \sqrt{\frac{\rho\kappa}{P}}\, D\boldsymbol{h} + \boldsymbol{w}\,. \tag{2.37}$$

We can use maximum likelihood decoding. The detected code matrix $\widetilde{D}$ is given by

$$\widetilde{D} = \arg\min_{\hat{D}\in\mathcal{D}} \|\boldsymbol{y} - \sqrt{\frac{\rho\kappa}{P}}\, \hat{D}\boldsymbol{h}\|_F^2\,. \tag{2.38}$$

This approach will lead to the separation of groups of symbols for detection. However, we will present another equivalent derivation to emphasize the orthogonal property of OEST codes. Moreover, this approach leads to an interesting representation of the equivalent channel of OEST codes.

Substituting the code matrix D in (2.26) to (2.37), we have

$$\boldsymbol{y} = \sqrt{\frac{\rho\kappa}{P}} \sum_{k=1}^{K} \sum_{p=1}^{P} \left[u_{kp} \left(A_k \otimes \pi^{p-1} \right) \boldsymbol{h} + u_{kp}^{*} \left(B_k \otimes \pi^{1-p} \right) \boldsymbol{h} \right] + \boldsymbol{w} \,. \tag{2.39}$$

Let

$$\boldsymbol{e}_{kp} = \left(A_k \otimes \pi^{p-1} \right) \boldsymbol{h} \,, \tag{2.40a}$$

$$E_k = \begin{bmatrix} \boldsymbol{e}_{k1} & \boldsymbol{e}_{k2} & \cdots & \boldsymbol{e}_{kP} \end{bmatrix} \,, \tag{2.40b}$$

$$\boldsymbol{f}_{kp} = \left(B_k \otimes \pi^{1-p} \right) \boldsymbol{h} \,, \tag{2.40c}$$

$$F_k = \begin{bmatrix} \boldsymbol{f}_{k1} & \boldsymbol{f}_{k2} & \cdots & \boldsymbol{f}_{kP} \end{bmatrix} \,. \tag{2.40d}$$

We can rewrite (2.39) as

$$\begin{aligned} \boldsymbol{y} &= \sqrt{\frac{\rho\kappa}{P}} \sum_{k=1}^{K} \sum_{p=1}^{P} \left(\boldsymbol{e}_{kp} u_{kp} + \boldsymbol{f}_{kp} u_{kp}^{*} \right) + \boldsymbol{w} \\ &= \sqrt{\frac{\rho\kappa}{P}} \begin{bmatrix} E_1 & F_1 & E_2 & F_2 & \cdots & E_K & F_K \end{bmatrix} \\ &\quad \times \begin{bmatrix} \boldsymbol{u}_1^{\mathsf{T}} & \boldsymbol{u}_1^{\dagger} & \boldsymbol{u}_2^{\mathsf{T}} & \boldsymbol{u}_2^{\dagger} & \cdots & \boldsymbol{u}_K^{\mathsf{T}} & \boldsymbol{u}_K^{\dagger} \end{bmatrix}^{\mathsf{T}} + \boldsymbol{w} \,. \end{aligned} \tag{2.41}$$

Furthermore, the following equation is equivalent to (2.41)

$$\begin{bmatrix} \boldsymbol{y} \\ \boldsymbol{y}^{*} \end{bmatrix} = \sqrt{\frac{\rho\kappa}{P}} \underbrace{\begin{bmatrix} E_1 & F_1 & \cdots & E_K & F_K \\ F_1^{*} & E_1^{*} & \cdots & F_K^{*} & E_K^{*} \end{bmatrix}}_{W} \begin{bmatrix} \boldsymbol{u}_1^{\mathsf{T}} & \boldsymbol{u}_1^{\dagger} & \cdots & \boldsymbol{u}_K^{\mathsf{T}} & \boldsymbol{u}_K^{\dagger} \end{bmatrix}^{\mathsf{T}} + \begin{bmatrix} \boldsymbol{w} \\ \boldsymbol{w}^{*} \end{bmatrix} . \tag{2.42}$$

An important property of W is that the its columns are orthogonal and can be shown in the following.

We have to show that the following equations hold:

$$\begin{bmatrix} E_k \\ F_k^{*} \end{bmatrix}^{\dagger} \begin{bmatrix} E_l \\ F_l^{*} \end{bmatrix} = E_k^{\dagger} E_l + F_k^{\mathsf{T}} F_l^{*} = \mathbf{0}_P \qquad \text{for } k \neq l, \tag{2.43a}$$

$$\begin{bmatrix} E_k \\ F_k^{*} \end{bmatrix}^{\dagger} \begin{bmatrix} F_l \\ E_l^{*} \end{bmatrix} = E_k^{\dagger} F_l + F_k^{\mathsf{T}} E_l^{*} = \mathbf{0}_P, \tag{2.43b}$$

We just provide the proof for (2.43a); (2.43b) can be shown similarly.

The following properties of the forward permutation matrix π will be useful for our next derivation [64, page 27].

$$\pi^{\mathsf{T}} = \pi^{\dagger} = \pi^{-1} = \pi^{P-1}. \tag{2.44}$$

Consequently, one has $\pi^0 = \pi^P = \boldsymbol{I}_P$.

From (2.40), the size of matrix $Z_{kl} = (E_k^\dagger E_l + F_k^\mathsf{T} F_l^*)$ is $P \times P$. The element $[Z_{kl}]_{ij}$ of Z_{kl} can be calculated from (2.40) as

$$\begin{aligned}
[Z_{kl}]_{ij} &= \boldsymbol{e}_{ki}^\dagger \boldsymbol{e}_{lj} + \boldsymbol{f}_{ki}^\mathsf{T} \boldsymbol{f}_{lj}^* \\
&= \boldsymbol{h}^\dagger (A_k^\dagger \otimes \pi^{-i+1})(A_l \otimes \pi^{j-1})\boldsymbol{h} + \boldsymbol{h}^\mathsf{T}(B_k^\mathsf{T} \otimes \pi^{i-1})(B_l^* \otimes \pi^{-j+1})\boldsymbol{h}^* \\
&= \boldsymbol{h}^\dagger [(A_k^\dagger A_l) \otimes (\pi^{j-i})]\boldsymbol{h} + \boldsymbol{h}^\mathsf{T}[(B_k^\mathsf{T} B_l^*) \otimes (\pi^{i-j})]\boldsymbol{h}^* \\
&= \boldsymbol{h}^\dagger [(A_k^\dagger A_l) \otimes (\pi^{j-i})]\boldsymbol{h} + \boldsymbol{h}^\dagger [(B_k^\dagger B_l) \otimes (\pi^{j-i})]\boldsymbol{h} = \boldsymbol{h}^\dagger [(A_k^\dagger A_l + B_k^\dagger B_l) \otimes (\pi^{j-i})]\boldsymbol{h} \\
&= \begin{cases} 0, & k \neq l; \\ \boldsymbol{h}^\dagger (\boldsymbol{I}_Q \otimes \pi^{j-i})\boldsymbol{h}, & k = l. \end{cases}
\end{aligned} \tag{2.45}$$

Thus, $Z_{kl} = \boldsymbol{0}_P$ if $k \neq l$ or the columns of W are orthogonal.

Since for $k = l$, the matrices Z_{kk} do not depend on the value of k; we drop the subscript k for brevity. Hence, the entries of Z are

$$z_{ij} = \boldsymbol{h}^\dagger (\boldsymbol{I}_Q \otimes \pi^{j-i})\boldsymbol{h}. \tag{2.46}$$

Let $\hat{\boldsymbol{h}}_q = \begin{bmatrix} h_{(q-1)P+1} & h_{(q-1)P+2} & \cdots & h_{(q-1)P+P} \end{bmatrix}^\mathsf{T}$ for $q = 1, 2, \ldots, Q$. Then $\boldsymbol{h} = \begin{bmatrix} \hat{\boldsymbol{h}}_1^\mathsf{T} & \hat{\boldsymbol{h}}_2^\mathsf{T} & \cdots & \hat{\boldsymbol{h}}_Q^\mathsf{T} \end{bmatrix}^\mathsf{T}$, and z_{ij} in (2.46) can be rewritten as

$$z_{ij} = \sum_{q=1}^{Q} \hat{\boldsymbol{h}}_q^\dagger \pi^{j-i} \hat{\boldsymbol{h}}_q. \tag{2.47}$$

The element z_{ij} (2.47) exhibits a strong structure of Z. To examine further the matrix Z, we recall another representation of circulant matrix built from an arbitrary vector $\boldsymbol{x}$ below [64]:

$$C_r^\mathsf{T}(\boldsymbol{x}) = \begin{bmatrix} \pi^0 \boldsymbol{x} & \pi^{-1}\boldsymbol{x} & \cdots & \pi^{1-P}\boldsymbol{x} \end{bmatrix}. \tag{2.48}$$

We now check for the entry (i, j) of the product matrix $C_r^\dagger(\boldsymbol{x})C_r(\boldsymbol{x})$ using (2.48):

$$[C_r^\dagger(\boldsymbol{x})C_r(\boldsymbol{x})]_{ij} = [C_r(\boldsymbol{x})C_r^\dagger(\boldsymbol{x})]_{ij} = \boldsymbol{x}^\mathsf{T}\pi^i\pi^{-j}\boldsymbol{x}^* = \boldsymbol{x}^\dagger\pi^{j-i}\boldsymbol{x}. \tag{2.49}$$

Comparing (2.47) and (2.49), interestingly, we find an elegant representation of Z below:

$$Z = \sum_{q=1}^{Q} C_r^\dagger(\hat{\boldsymbol{h}}_q) C_r(\hat{\boldsymbol{h}}_q). \tag{2.50}$$

Since $C_r(\hat{\boldsymbol{h}}_q)$ is circulant, $C_r^{\dagger}(\hat{\boldsymbol{h}}_q)$ is also circulant; the product of two circulant matrices is also circulant and the sum of circulant matrices is also circulant [64], thus Z *is also a circulant* matrix.

To separate the transmitted vector $\boldsymbol{u}_k$ at the receiver, we multiply the two sides of (2.42) with $\begin{bmatrix} E_k^{\dagger} & F_k^{\mathsf{T}} \end{bmatrix}$ to get

$$E_k^{\dagger}\boldsymbol{y} + F_k^{\mathsf{T}}\boldsymbol{y}^* = Z\boldsymbol{u}_k + \underbrace{(E_k^{\dagger}\boldsymbol{w} + F_k^{\mathsf{T}}\boldsymbol{w}^*)}_{\hat{\boldsymbol{w}}_k}. \tag{2.51}$$

The covariance matrix of noise $V\,\mathbb{E}[\hat{\boldsymbol{w}}_k\hat{\boldsymbol{w}}_k^{\dagger}]$ follows

$$\begin{aligned} V &= \mathbb{E}\left[(E_k^{\dagger}\boldsymbol{w} + F_k^{\mathsf{T}}\boldsymbol{w}^*)(E_k^{\dagger}\boldsymbol{w} + F_k^{\mathsf{T}}\boldsymbol{w}^*)^{\dagger}\right] \\ &= E_k^{\dagger}\,\mathbb{E}[\boldsymbol{w}\boldsymbol{w}^{\dagger}]E_k + F_k^{\mathsf{T}}\,\mathbb{E}[\boldsymbol{w}^*\boldsymbol{w}^{\mathsf{T}}]F_k^* + E_k^{\dagger}\,\mathbb{E}[\boldsymbol{w}\boldsymbol{w}^{\mathsf{T}}]F_k^* + F_k^{\mathsf{T}}\,\mathbb{E}[\boldsymbol{w}^*\boldsymbol{w}^{\dagger}]E_k \\ &= E_k^{\dagger}E_k + F_k^{\dagger}F_k = Z. \end{aligned} \tag{2.52}$$

During the derivation of (2.52), we have used the fact that for the vector $\boldsymbol{w}$ of circularly complex Gaussian random variables, $\mathbb{E}[\boldsymbol{w}\boldsymbol{w}^{\mathsf{T}}] = \boldsymbol{0}_M$.

The noise covariance matrix is not an identity matrix, but the noise vector can be whitened by multiplying the two sides of (2.51) with a whitening matrix $Z^{-\frac{1}{2}}$. The received signal with whitened noise is

$$Z^{-\frac{1}{2}}(E_k^{\dagger}\boldsymbol{y} + F_k^{\mathsf{T}}\boldsymbol{y}^*)Z^{\frac{1}{2}}\boldsymbol{u}_k + \underbrace{Z^{-\frac{1}{2}}\hat{\boldsymbol{w}}_k}_{\bar{\boldsymbol{w}}} \tag{2.53}$$

where the elements of $\bar{\boldsymbol{w}}$ are $\mathcal{CN}(0,1)$.

From (2.53), we conclude that all of the transmitted vectors $\boldsymbol{u}_k$ experience the same equivalent channel, i.e. the same equivalent channel gain and additive noise statistics. Thus, all of the transmitted vectors have the same PEP.

We now generalize the result of (2.53) for the case of multiple receive antennas, $N \geq 1$. The subscript n $(n = 1, 2, \ldots, N)$ is added to the channel gain vector $\boldsymbol{h}$. The channel matrix H is therefore written as $H = \begin{bmatrix} \boldsymbol{h}_1 & \boldsymbol{h}_2 & \cdots & \boldsymbol{h}_N \end{bmatrix}$, where $\boldsymbol{h}_n \begin{bmatrix} h_{1n} & h_{2n} & \cdots & h_{Mn} \end{bmatrix}^{\mathsf{T}}$.

When multiplying the two sides of (2.42) with $\begin{bmatrix} E_k^{\dagger} & F_k^{\mathsf{T}} \end{bmatrix}$, we actually perform *spatial maximal ratio combining* [109, 110] or *spatial matched filtering* [48]. The equivalent channel in (2.50) becomes

$$\boldsymbol{Z} = \sum_{n=1}^{N} Z_n = \sum_{n=1}^{N}\sum_{q=1}^{Q} C_r^{\dagger}(\hat{\boldsymbol{h}}_{q,n})C_r(\hat{\boldsymbol{h}}_{q,n}) \tag{2.54}$$

where $\hat{\boldsymbol{h}}_{q,n} = \begin{bmatrix} h_{(q-1)P+1,n} & h_{(q-1)P+2,n} & \cdots & h_{(q-1)P+P,n} \end{bmatrix}^{\mathsf{T}}$ for $q = 1, 2, \ldots, Q$, $n = 1, 2, \ldots, N$.

Therefore, with multiple antennas and constellation rotation in (2.20), the detection equation (2.53) is generalized for data detection with multiple receive antennas as

$$\underbrace{\boldsymbol{Z}^{-\frac{1}{2}} \sum_{n=1}^{N} (E_{kn}^{\dagger} \boldsymbol{y}_n + F_{kn}^{\mathsf{T}} \boldsymbol{y}_n^*)}_{\hat{\boldsymbol{y}}_k} \boldsymbol{Z}^{\frac{1}{2}} \boldsymbol{u}_k + \boldsymbol{W} = \boldsymbol{Z}^{\frac{1}{2}} \Theta \boldsymbol{s}_k + \boldsymbol{W} \tag{2.55}$$

where $\boldsymbol{y}_n$ is the received signal vector of the nth antenna,

$$E_{kn} = \begin{bmatrix} \boldsymbol{e}_{k1,n} & \boldsymbol{e}_{k2,n} & \cdots & \boldsymbol{e}_{kP,n} \end{bmatrix}, \tag{2.56a}$$

$$\boldsymbol{e}_{kp,n} = \left(A_k \otimes \pi^{p-1} \right) \boldsymbol{h}_n \tag{2.56b}$$

$$\text{for } k = 1, 2, \ldots, K; p = 1, 2, \ldots, P,$$

$$F_{kn} = \begin{bmatrix} \boldsymbol{f}_{k1,n} & \boldsymbol{f}_{k2,n} & \cdots & \boldsymbol{f}_{kP,n} \end{bmatrix}, \tag{2.56c}$$

$$\boldsymbol{f}_{kp,n} = \left(B_k \otimes \pi^{1-p} \right) \boldsymbol{h}_n \,, \tag{2.56d}$$

$$[Z_n]_{ij} = \sum_{q=1}^{Q} C_r^{\dagger}(\hat{\boldsymbol{h}}_{q,n}) C_r(\hat{\boldsymbol{h}}_{q,n}) \quad \text{for } i, j = 1, 2, \ldots, P \,, \tag{2.56e}$$

and $\boldsymbol{W} \sim \mathcal{CN}(0, N)$; however, we do not need to divide both sides of (2.55) by N.

Notice: By similar derivation with suitable modifications, the transmitted symbols of OEST code matrices of Construction II are also separated into groups as (2.55). However, the main difference is that the elements of matrix Z are

$$z_{ij} = \boldsymbol{h}^{\dagger} (\pi^{j-i} \otimes \boldsymbol{I}_Q) \boldsymbol{h} \,, \tag{2.57}$$

which will not lead to a compact representation of Z as in (2.54).

One can use K sphere decoders (see, e.g. [108]) running in parallel, each is to solve (2.55). Therefore, the decoding complexity and decoding time are greatly reduced.

The matrix $\boldsymbol{Z}^{\frac{1}{2}}$ can be considered as the equivalent channel of OEST codes. Since $\boldsymbol{Z}$ is a circulant matrix, using [64, Theorem 3.2.3, p. 73], we can show that $\boldsymbol{Z}^{\frac{1}{2}}$ is also a circulant matrix. It means that *when multiple data vectors are encoded in circulant matrices and mapped to an OEST code matrix, the data vectors can be completely decoupled at the receiver. Each data vector is equivalently experienced the same circulant channel matrix, which is a superposition of multiple circulant matrices.*

In the following, as a sanity check, we verify the general detection equation (2.55) for two special cases: OSTBC and circulant STBC [101].

Detection of OSTBC

For OSTBC, $P = 1, Q = M$ and hence,

$$E_{kn} = \boldsymbol{e}_{k1,n} = A_k \boldsymbol{h}_n \,, \tag{2.58a}$$

$$F_{kn} = \boldsymbol{f}_{k1,n} = B_k \boldsymbol{h}_n \,, \tag{2.58b}$$

$$Z_n = [Z_n]_{11} = \|\boldsymbol{h}_n\|_{\mathsf{F}}^2. \tag{2.58c}$$

$$\boldsymbol{Z} = \sum_{n=1}^{N} Z_n = \sum_{n=1}^{N} \|\boldsymbol{h}_n\|_{\mathsf{F}}^2 = \|H\|_{\mathsf{F}}^2, \tag{2.58d}$$

and $\Theta = \boldsymbol{I}_1$, then (2.55) becomes

$$\underbrace{\|H\|_{\mathsf{F}}^{-1} \sum_{n=1}^{N} (\boldsymbol{h}_n^{\dagger} A_k^{\dagger} \boldsymbol{y}_n + \boldsymbol{h}_n^{\mathsf{T}} B_k^{\mathsf{T}} \boldsymbol{y}_n^{*})}_{\hat{y}_k} \|H\|_{\mathsf{F}} u_k + \hat{w} \,. \tag{2.59}$$

From (2.59), a similar detection equation for single symbol u_k to the metrics given in [59, 62, 111] can be derived.

Detection of circulant STBC [101]

For circulant STBC, $K = Q = 1$, $A_1 = \boldsymbol{I}_1$, $B_1 = \boldsymbol{0}_1$.

From (2.48), (2.56a) and (2.56b), we have $E_{1,n} = C_r(\boldsymbol{h}_n)$; from (2.56a) and (2.56b), $F_{1,n} = \boldsymbol{0}_P \ \forall n$; from (2.54), $\boldsymbol{Z} = \sum_{n=1}^{N} C_r^{\dagger}(\hat{\boldsymbol{h}}_n) C_r(\hat{\boldsymbol{h}}_n)$. Substituting $E_{1,n}$ and $F_{1,n}$ into (2.55), we obtain

$$\boldsymbol{Z}^{-\frac{1}{2}} \sum_{n=1}^{N} [C_r^{\dagger}(\boldsymbol{h}_n) \boldsymbol{y}_n] \boldsymbol{Z}^{\frac{1}{2}} \boldsymbol{u}_k + \boldsymbol{W} \,. \tag{2.60}$$

Although (2.60) holds for maximum likelihood detection, it can be easily modified for the zero-forcing (ZF) or minimum mean square error (MMSE) receivers proposed in [101].

2.3.5 Maximum Mutual Information

Since OEST codes decompose the MIMO channels with $M = PQ$ transmit and N receive antennas into K parallel equivalent MIMO channels of the same size, $P \times P$, we can calculate the maximum mutual information of OEST codes by taking the sum capacity of these K identical MIMO channels. Thus, the maximum mutual information of OEST codes

can be calculated using the equivalent channel in (2.61) as follows [10]:

$$\mathsf{C}_{\mathcal{D}} = \frac{K}{PR}\,\mathbb{E}\left\{\log_2\det\left[\boldsymbol{I}_P + \frac{\rho\kappa}{P}\sum_{n=1}^{N}\sum_{q=1}^{Q} C_r^{\dagger}(\hat{\boldsymbol{h}}_{q,n})C_r(\hat{\boldsymbol{h}}_{q,n})\right]\right\} \tag{2.61}$$

where R is the code length of underlying the OSTBC code. The coefficient $\frac{K}{PR}$ appears because the maximum mutual information of OEST codes is a sum of maximum mutual information of K vectors averaged over $T = PR$ channel uses.

We can use a $P \times P$ unitary discrete Fourier transform (DFT) matrix to diagonalize the circulant matrices $C_r(\hat{\boldsymbol{h}}_{q,n})$ without changing the distribution of $\mathsf{C}_{\mathcal{D}}$. Let $\lambda_{q,n}(p)$ $(p = 1, 2, \ldots P)$ be the eigenvalues of $C_r(\hat{\boldsymbol{h}}_{qn})$. It is well-known that the vectors of eigenvalues are the DFT of the channel vector $\hat{\boldsymbol{h}}_{qn}$. Thus, $\lambda_{qn}(p)$ are independent and $\lambda_{qn}(p) \sim \mathcal{CN}(0, P)$. Let $\lambda_{qn}(p) = \sqrt{P}\hat{h}_{qn}(p)$, then $\hat{h}_{qn}(p) \sim \mathcal{CN}(0, 1)$.

By denoting $\boldsymbol{\Lambda}_{qn} = \mathrm{diag}(\hat{h}_{qn}(1), \hat{h}_{qn}(2), \cdots, \hat{h}_{qn}(P))$, (2.61) becomes

$$\begin{aligned}\mathsf{C}_{\mathcal{D}} &= \frac{\mathsf{R}_{\mathcal{O},Q}}{P}\,\mathbb{E}\left\{\log_2\det\left[\boldsymbol{I}_P + \rho\kappa\sum_{n=1}^{N}\sum_{q=1}^{Q}(\boldsymbol{\Lambda}_{qn}^{\dagger}\boldsymbol{\Lambda}_{qn})\right]\right\} \\ &= \mathsf{R}_{\mathcal{O},Q}\,\mathbb{E}\left\{\log_2\det\left[1 + \frac{\rho}{Q\mathsf{R}_{\mathcal{O},Q}}\sum_{n=1}^{N}\sum_{q=1}^{Q}|\hat{h}_{qn}(p)|^2\right]\right\}. \end{aligned}\tag{2.62}$$

In (2.62), $\mathsf{C}_{\mathcal{D}}$ is independent of the index p; therefore, the index p is omitted without loss of generality. Furthermore, let $\hat{H} = [\hat{h}_{qn}] \in \mathbb{C}^{Q\times N}$, we have $\sum_{n=1}^{N}\sum_{q=1}^{Q}|\hat{h}_{qn}|^2 = \|\hat{H}\|_{\mathsf{F}}^2$. We arrive at the new expression of $\mathsf{C}_{\mathcal{D}}$:

$$\begin{aligned}\mathsf{C}_{\mathcal{D}} &= \mathsf{R}_{\mathcal{O},Q}\,\mathbb{E}\left\{\log_2\det\left[1 + \frac{\rho}{Q\mathsf{R}_{\mathcal{O},Q}}\|\hat{H}\|_{\mathsf{F}}^2\right]\right\} \\ &= \mathsf{C}_{\mathcal{O},Q}\end{aligned}\tag{2.63}$$

where $\mathsf{C}_{\mathcal{O},Q}$ is the maximum mutual information of OSTBC designed for Q transmit antennas [112]. Thus, *the maximum mutual information of OEST codes does not depend on the value of P, the size of data vectors. When increasing the number of transmit antennas M, but keeping the basis orthogonal matrices, one obtains higher diversity but not capacity benefit.* This result also hold for QSTBC.

The results of this section is summarized in the following theorem.

Theorem 2.14. *The maximum mutual information of an OEST code for $M = PQ$ antennas is the same as that of the OSTBC for Q antennas used to construct this OEST code.*

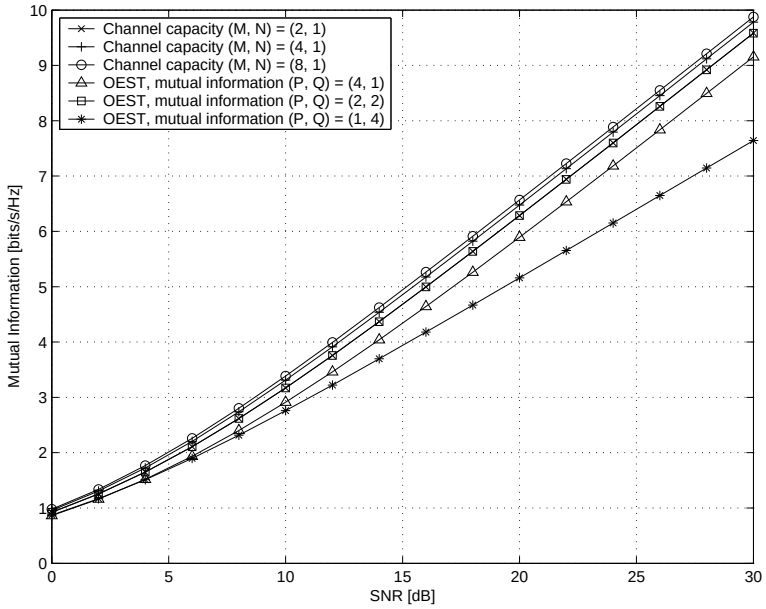

Figure 2.2: Channel capacity and maximum mutual information of OEST, (4, 1) system.

The maximum mutual information of OEST codes for different parameter sets are plotted in Figs. 2.2 and 2.3. For one receive antenna or the MISO channel, in Fig. 2.2, SAST codes corresponding to $Q = 2$ nearly attain the channel capacity. Other configurations suffer from remarkable capacity loss. These losses are more significant for $N > 1$ (see Fig. 2.3). This result is expected because the rates of OEST codes are not more than 1 symbol pcu, while MIMO channels support rates of $\min(M, N)$.

2.3.6 Semi-Orthogonal Algebraic Space-Time Codes

We can identify a special case where $Q = 2$ or the OEST constructed from the Alamouti code. This code has the feature that the columns of the right and the left halves are orthogonal. Thus, we call this code semi-orthogonal algebraic space-time (SAST) code. Additionally, there are several points that make SAST codes important.

1. Since the Alamouti code achieves full capacity of (2, 1) channel, hence, SAST codes achieve significant capacity of the MISO (multiple-input single-output) channel.

2. SAST codes have rate of 1 symbol pcu, the highest rate achievable by OEST codes.

Fig. 2.4 plots the maximum mutual information of SAST and circulant STBC (or LTAST) codes, two subclass of OEST codes having the same code rate of 1 symbol pcu,

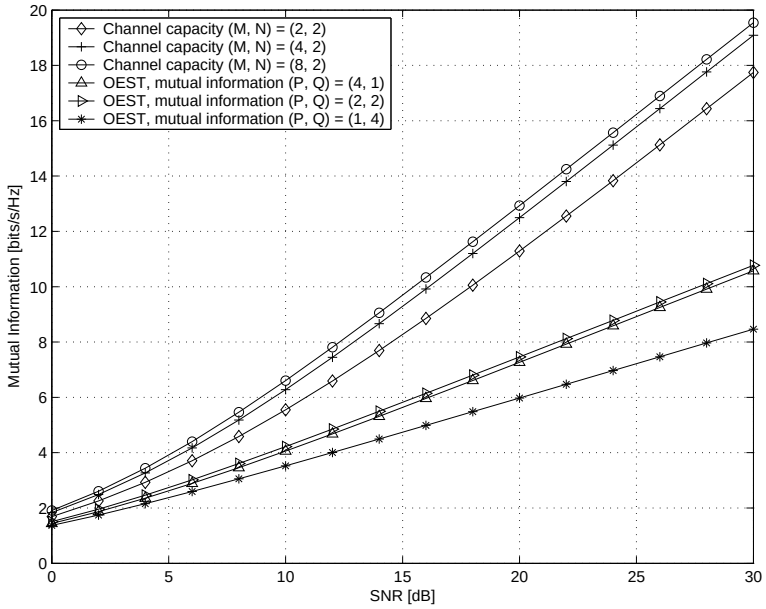

Figure 2.3: Channel capacity and maximum mutual information of OEST, (4, 2) system.

together with the capacity of MISO channels for $M = 2, 4, 8, 16$. Fig. 2.5 illustrates the relative channel capacity attained by the two codes. The numerical results show that for $M = 4$, SAST codes attain more than 95% and up to 98% of channel capacity. For M = 16, SAST codes achieve not less than about 92% channel capacity. This is because for a specific high SNR, the channel capacity does not actually increase when the number of transmit antennas increases, but the number of receive antennas is fixed [14]. Fig. 2.4 also shows that the capacity increment of the MISO channel is negligible when the number of transmit antennas increases from 8 to 16. Therefore, SAST codes nearly attain the capacity of MISO channels.

The next section will present the constructions and performances of OEST codes for 4, 6 and 12 antennas.

2.4 Examples of OEST Codes

Given a value of M, one can find the sets of all pairs $\{(P, Q)|P, Q \in \mathbb{N}, PQ = M\}$. Note that one can delete one or several columns of OEST codes for M transmit antennas to construct OEST codes for the smaller numbers of transmit antennas.

In the following, we will present OEST codes for 4 and 6 transmit antennas using

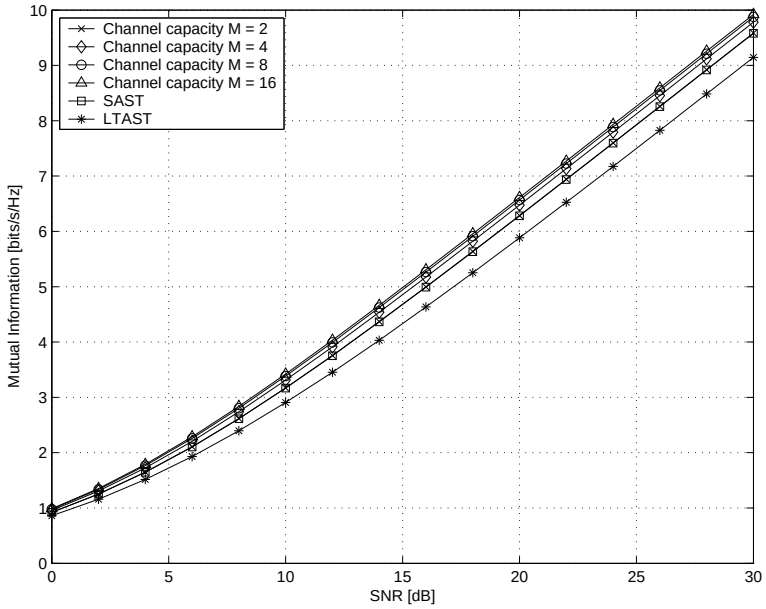

Figure 2.4: Maximum mutual information of SAST and LTAST codes over MISO channels.

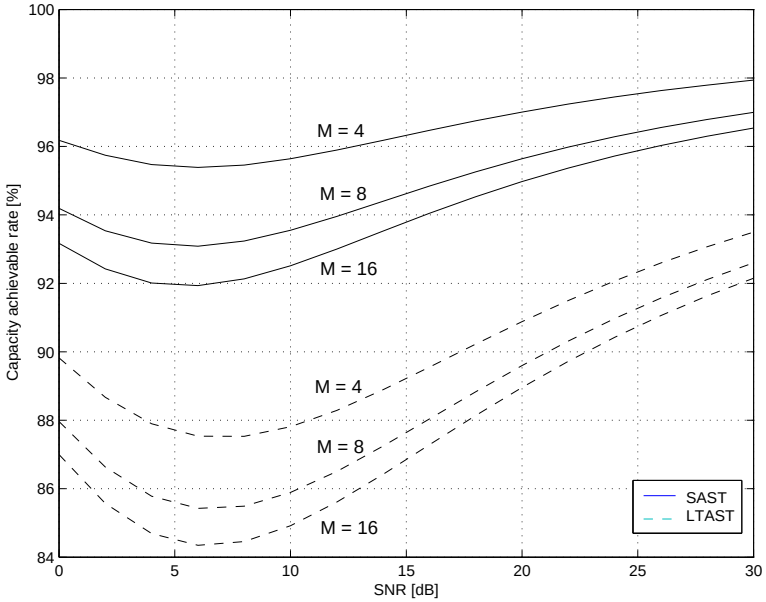

Figure 2.5: Capacity achievable rates of SAST and LTAST codes compared with the capacity of open-loop MISO channels.

Construction I and their performances in quasi-static flat fading channels.

2.4.1 Code Construction Examples

Let us denote OEST codes designed for the set of parameters P, Q as $\mathcal{D}_{P,Q}$. For $M = 4$ transmit antennas, there are at least three variants of OEST codes as follows.

$$\mathcal{D}_{1,4} = \frac{1}{\sqrt{3}}\mathcal{O}_4 = \frac{1}{\sqrt{3}}\begin{bmatrix} u_1 & u_2 & u_3 & 0 \\ -u_2^* & u_1^* & 0 & -u_3 \\ -u_3^* & 0 & u_1^* & u_2 \\ 0 & u_3^* & -u_2^* & u_1 \end{bmatrix}. \tag{2.64a}$$

$$\mathcal{D}_{2,2} = \frac{1}{\sqrt{4}}\begin{bmatrix} u_1 & u_2 & u_3 & u_4 \\ u_2 & u_1 & u_4 & u_3 \\ -u_3^* & -u_4^* & u_1^* & u_2^* \\ -u_4^* & -u_3^* & u_2^* & u_1^* \end{bmatrix}$$

$$= \mathcal{S}_4 \equiv \mathcal{Q}_4. \tag{2.64b}$$

$$\mathcal{D}_{4,1} = \frac{1}{\sqrt{4}}\begin{bmatrix} u_1 & u_2 & u_3 & u_4 \\ u_4 & u_1 & u_2 & u_3 \\ u_3 & u_4 & u_1 & u_2 \\ u_2 & u_3 & u_4 & u_1 \end{bmatrix}$$

$$= \mathcal{C}_4. \tag{2.64c}$$

For $M = 6$, there are at least 4 variants as follows.

$$\mathcal{D}_{1,6} = \frac{1}{\sqrt{4}}\mathcal{O}_6 \qquad \text{(see [44, (101)])}. \tag{2.65a}$$

$$\mathcal{D}_{2,3} = \frac{\sqrt{2}}{3}\begin{bmatrix} u_1 & u_2 & u_3 & u_4 & u_5 & u_6 \\ u_2 & u_1 & u_4 & u_3 & u_6 & u_5 \\ -u_3^* & -u_4^* & u_1^* & u_2^* & 0 & 0 \\ -u_4^* & -u_3^* & u_2^* & u_1^* & 0 & 0 \\ -u_5^* & -u_6^* & 0 & 0 & u_1^* & u_2^* \\ -u_6^* & -u_5^* & 0 & 0 & u_2^* & u_1^* \\ 0 & 0 & u_5^* & u_6^* & -u_3^* & -u_4^* \\ 0 & 0 & u_6^* & u_5^* & -u_4^* & -u_3^* \end{bmatrix}$$

$$\equiv \mathcal{Q}_6. \tag{2.65b}$$

$$\mathcal{D}_{3,2} = \frac{1}{\sqrt{6}}\begin{bmatrix} u_1 & u_2 & u_3 & u_4 & u_5 & u_6 \\ u_3 & u_1 & u_2 & u_6 & u_4 & u_5 \\ u_2 & u_3 & u_1 & u_5 & u_6 & u_4 \\ -u_4^* & -u_6^* & -u_5^* & u_1^* & u_3^* & u_2^* \\ -u_5^* & -u_4^* & -u_6^* & u_2^* & u_1^* & u_3^* \\ -u_6^* & -u_5^* & -u_4^* & u_3^* & u_2^* & u_1^* \end{bmatrix}$$

$$= \mathcal{S}_6. \tag{2.65c}$$

$$\mathcal{D}_{6,1} = \frac{1}{\sqrt{6}} \begin{bmatrix} u_1 & u_2 & u_3 & u_4 & u_5 & u_6 \\ u_6 & u_1 & u_2 & u_3 & u_4 & u_5 \\ u_5 & u_6 & u_1 & u_2 & u_3 & u_4 \\ u_4 & u_5 & u_6 & u_1 & u_2 & u_3 \\ u_3 & u_4 & u_5 & u_6 & u_1 & u_2 \\ u_2 & u_3 & u_4 & u_5 & u_6 & u_1 \end{bmatrix}$$
$$= \mathcal{C}_6. \tag{2.65d}$$

To construct $\mathcal{D}_{2,3}$, we have used Construction I and the orthogonal basis matrices of OSTBC $\mathcal{O}_3$ [59] by deleting the last columns of (2.64a). If Construction II was used, the resulting OEST code would be equivalent to a QSTBC for $M = 6$ as we have shown in Section 2.3.1.

The OEST codes presented above for $M = 4, 6$ are equivalent to the previously known codes since there are only a few choices for the pairs of parameters P and Q. Nevertheless, other new OEST codes for $M = 6$ can be obtained by deleting some columns of the OEST codes designed for $M \geq 8$. For larger values of M, for example $M = 12$, we have more freedom to select the values of the pairs (P, Q): $(1, 12), (2, 6), (3, 4), (4, 3), (6, 2)$, and $(12, 1)$. We can construct several completely new OEST codes for the values of parameters (P, Q): $(3, 4)$ or $(4, 3)$. The details are omitted for brevity.

The main parameters of OEST codes for $M = 4, 6, 12$ are summarized in Table 2.1. The OSTBC with maximal rates in [44] are selected to constructed OEST codes.

2.4.2 Simulation Results

Comparison of OEST codes implementations

We have performed simulations to compare the performance of different implementations of OEST codes for 4, 6 and 12 transmit antennas. The input constellations are selected so that the bit rate is 3 bits pcu. A summary of OEST codes combined with signal constellations is given in Table 2.2. However, except for $\mathcal{D}_{1,6}$ (or $\mathcal{O}_6$) and $\mathcal{D}_{2,6}$ (or $\mathcal{Q}_{12}$) with symbol rate of 2/3 symbol pcu, there is no constellation that matches the bit rate of 3 bits pcu. Thus, 16QAM is selected, resulting in the bit rate $8/3$ bits pcu. Note that the minimum Euclidean distances of 16QAM is 0.6325, and of 8QAM and 8Hex are 0.8165 and 0.9631, respectively. The shapes of 8QAM and 8Hex [104] are sketched in Fig. 2.6.

For $M = 4$, all OEST code variants have the same spectral efficiency of 3 bits pcu.

Table 2.1: Comparisons of Several OEST Codes

M	OEST codes	Known as	G_c	Rate	Decoding complexity	Delay
4	$\mathcal{D}_{1,4}$	$\mathcal{O}_4$	$\frac{1}{3}\,d^2_{\min}$	$\frac{3}{4}$	1 symbol	4
4	$\mathcal{D}_{2,2}$	$\mathcal{S}_4$	$\frac{1}{4}\,d^2_{\min}$	1	2 symbols	4
4	$\mathcal{D}_{4,1}$	$\mathcal{T}_4$	$\frac{1}{4}\,d^2_{\min}$	1	4 symbols	4
6	$\mathcal{D}_{1,6}$	$\mathcal{O}_6$	$\frac{1}{4}\,d^2_{\min}$	$\frac{2}{3}$	1 symbol	30
6	$\mathcal{D}_{2,3}$	new, $\equiv \mathcal{Q}_6$	$\frac{2}{9}\,d^2_{\min}$	$\frac{3}{4}$	2 symbols	8
6	$\mathcal{D}_{3,2}$	$\mathcal{S}_6$	$\frac{1}{6}\,d^2_{\min}$	1	3 symbols	6
6	$\mathcal{D}_{6,1}$	$\mathcal{T}_6$	$\frac{1}{6}\,d^2_{\min}$	1	6 symbols	6
12	$\mathcal{D}_{1,12}$	$\mathcal{O}_{12}$	$\frac{1}{7}\,d^2_{\min}$	$\frac{7}{12}$	1 symbol	792
12	$\mathcal{D}_{2,6}$	new, $\equiv \mathcal{Q}_{12}$	$\frac{1}{8}\,d^2_{\min}$	$\frac{8}{12}$	2 symbols	60
12	$\mathcal{D}_{3,4}$	new	$\frac{1}{9}\,d^2_{\min}$	$\frac{9}{12}$	3 symbols	12
12	$\mathcal{D}_{4,3}$	new	$\frac{1}{9}\,d^2_{\min}$	$\frac{9}{12}$	4 symbols	16
12	$\mathcal{D}_{6,2}$	$\mathcal{S}_{12}$	$\frac{1}{12}\,d^2_{\min}$	1	6 symbols	12
12	$\mathcal{D}_{12,1}$	$\mathcal{T}_{12}$	$\frac{1}{12}\,d^2_{\min}$	1	12 symbols	12

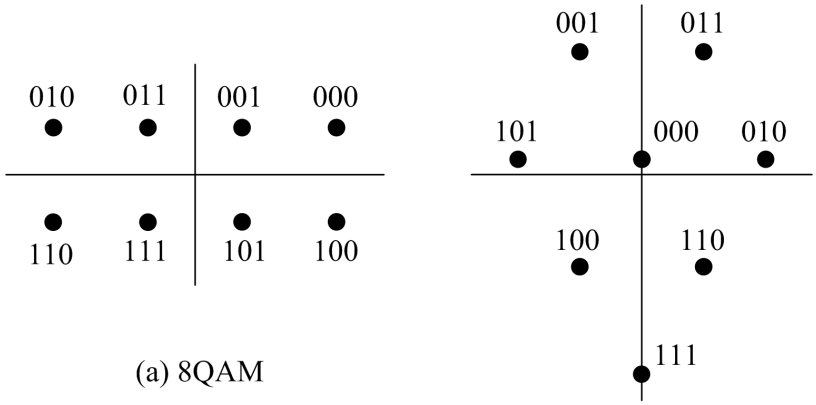

Figure 2.6: Geometrical shapes of 8QAM and 8Hex constellations.

The optimal rotations in Proposition 2.7 can be used for $\mathcal{S}_4$ and $\mathcal{T}_4$. $\mathcal{S}_4$ with 8Hex (large Euclidean distance) outperforms $\mathcal{O}_4$. Note that for $M = 4$, $\mathcal{S}_4$ and $\mathcal{Q}_4$ are equivalent; this observation is also made in [61]. Using the same 8QAM, however, $\mathcal{S}_4$ code gains 1.7 dB over $\mathcal{T}_4$. On the other hand, performance of $\mathcal{S}_4$ with 8QAM is inferior to that of $\mathcal{O}_4$, even

Table 2.2: OEST Codes and Simulation Parameters

M	Codes	Modulation	Coding gain	Bit rate
4	$\mathcal{D}_{1,4}$ / $\mathcal{O}_4$	16QAM	0.1334	3
4	$\mathcal{D}_{2,2}$ / $\mathcal{Q}_4$ / $\mathcal{S}_4$	8QAM / 8Hex	0.1667 / 0.2319	3
4	$\mathcal{D}_{4,1}$ / $\mathcal{T}_4$	8QAM / 8Hex	0.1667 / 0.2319	3
6	$\mathcal{D}_{1,6}$ / $\mathcal{O}_6$	16QAM	0.1	8/3
6	$\mathcal{D}_{2,3}$ / $\equiv \mathcal{Q}_6$	16QAM	0.0889	3
6	$\mathcal{D}_{3,2}$ / $\mathcal{S}_6$	8QAM / 8Hex	< 0.1111 / 0.1546	3
6	$\mathcal{D}_{6,1}$ / $\mathcal{T}_6$	8QAM / 8Hex	0.1111 / 0.1546	3
12	$\mathcal{D}_{2,6}$ / $\equiv \mathcal{Q}_{12}$	16QAM	0.05	8/3
12	$\mathcal{D}_{3,4}$	16QAM	< 0.0445	3
12	$\mathcal{D}_{4,3}$	16QAM	0.0445	3
12	$\mathcal{D}_{6,2}$	8QAM	< 0.0556	3
12	$\mathcal{D}_{12,1}$ / $\mathcal{T}_{12}$	8QAM	< 0.0556	3

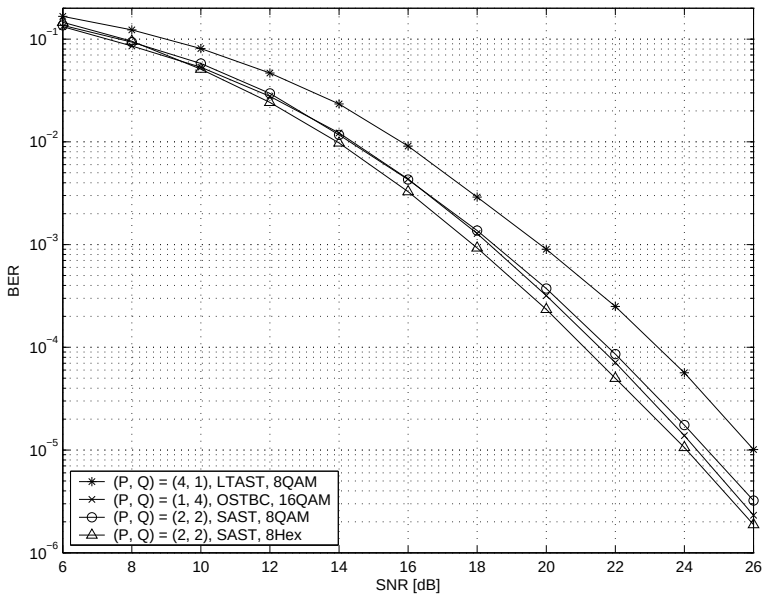

Figure 2.7: Performance of OEST codes with 3 bits pcu, (4, 1) system.

though its coding gain is higher.

For $M = 6$, with 8QAM and 6 transmit antennas, the optimal rotations for circulant STBC are not available analytically. By computer search, the best found rotation angles

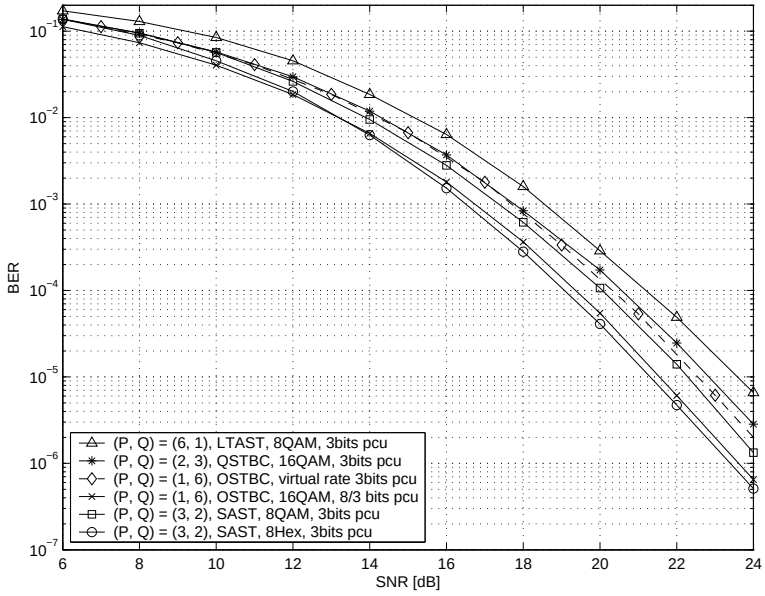

Figure 2.8: Performance of four implementations of OEST codes for 6 transmit antennas with 3 bits pcu, except $\mathcal{D}_{1,6}$ (or $\mathcal{O}_6$) with $8/3$ bits pcu.

are approximately $\phi = e^{\mathrm{j}\pi/4}$ for the $\mathcal{S}_6$ and $\phi = e^{\mathrm{j}\pi/3}$ for $\mathcal{T}_6$. From Fig. 2.8, $\mathcal{S}_6$ also yields better performance among the investigated OEST codes. $\mathcal{S}_6$ with 8QAM gains about 0.5 and 1.2 dB over $\mathcal{T}_6$ and $\mathcal{O}_6$, respectively. Moreover, $\mathcal{S}_6$ with 8Hex even outperforms OSTBC, which has lower spectral efficiency.

Even though the rate of $\mathcal{O}_6$ is 8/3 bits pcu, we can still compare its performance with other codes with a rate of 3 bits pcu. Recall the fact that OSTBC convert the MIMO channel to the scalar (SISO) channel (Section 1.4.2). Also, in the scalar channel, to obtain 1 more bit of spectral efficiency using QAM, an additional SNR of at least 3 dB is required [113] at high SNR. Additionally, in the space-time system, it is shown by Zheng and Tse [114] that among OSTBC, only the Alamouti code achieve the optimal diversity-multiplexing tradeoff for 2 transmit/1 receive MIMO system. It is also confirmed that with the Alamouti code and QAM, to gain an additional rate of 1 bit, the SNR increment is at least 3 dB [115]. In our simulation, the OSTBC $\mathcal{O}_6$ do not achieve the optimal diversity-multiplexing tradeoff. Therefore, more than 3 dB is expected to gain 1 bit of data rate. To reach the rate of 3 bits pcu from the current rate of 8/3 bits pcu, one needs to increase the data rate by 1/3 bit pcu, which requires more than 1 dB of SNR. In Fig 2.8, we plot another the BER curve of $\mathcal{O}_6$ with a virtual rate of 3 bits pcu by shifting the a part of BER curve of $\mathcal{O}_6$ (starting from

SNR = 10 dB) to the right by 1 dB. With this virtual rate, $\mathcal{O}_6$ perform slightly better than QSTBC $\mathcal{Q}_6$. This result is different from the case of 4 transmit antennas, where OSTBC is inferior to QSTBC. The virtual rate concept may not provide a precise comparison for the codes with similar performance. However, it helps to close the gap of rate mismatch for asymptotic comparisons.

The performances of five variants of OEST codes for 12 transmit antennas are illustrated in Fig. 2.9. The OSTBC $\mathcal{O}_{12}$ is not presented due to this code entails a long delay of 792 channel uses [106]. For QSTBC $\mathcal{Q}_{12}$ with rate of 8/3 bits pcu, the virtual rate concept is again applied enabling the reasonable performance comparison. With 12 transmit antennas, except $\mathcal{D}_{4,3}$ and $\mathcal{D}_{12,1}$ (or LTAST code $\mathcal{T}_{12}$), the other three variants of OEST codes $\mathcal{D}_{6,2}$ (or SAST code $\mathcal{S}_{12}$), $\mathcal{D}_{3,4}$, and $\mathcal{D}_{2,6}$ (or QSTBC $\mathcal{Q}_{12}$ with virtual rate of 3 bits pcu) clearly show a performance-complexity tradeoff: the higher decoding complexity, the better performance. The decoding complexity of $\mathcal{D}_{4,3}$ is slightly higher than that of $\mathcal{D}_{3,4}$ (see Table I), but the latter yields a small SNR gain of 0.1 dB over the former. The LTAST code $\mathcal{T}_{12}$ has highest decoding complexity, but BER is inferior to the other codes at low and medium SNR. Only when SNR > 18 dB, the LTAST code performs slightly better than $\mathcal{D}_{3,4}$, $\mathcal{D}_{4,3}$, and $\mathcal{D}_{2,6}$; but its performance is still about 0.6 dB worse than that of the SAST code.

Comparison of SAST codes and other codes

In this section, we compare the performance of SAST codes and other STBC of rate-one symbol pcu or less. Unless otherwise stated, the BER curves are obtained by maximum likelihood detection.

Fig. 2.10 plots the BER of SAST and LTAST codes for a MISO channel with 4 transmit antennas system using 4-, 16- and 64-QAM (with spectral efficiencies 2, 4 and 6 bits pcu accordingly). The SNR gain of SAST codes over LTAST codes is substantial. For example, the SNR gain is about 1.3, 2, 2.5 dB for 2, 4, 6 bits pcu, respectively. The gains increase with the spectral efficiency.

Similar gains can be observed for a higher number of transmit antennas. Fig. 2.11 compares the BER of SAST and LTAST codes for MISO channel with 8 transmit antennas. Again, SAST codes outperform LTAST codes. The SNR gain is 0.7 and 1.3 dB with 2 and 6 bits pcu, respectively.

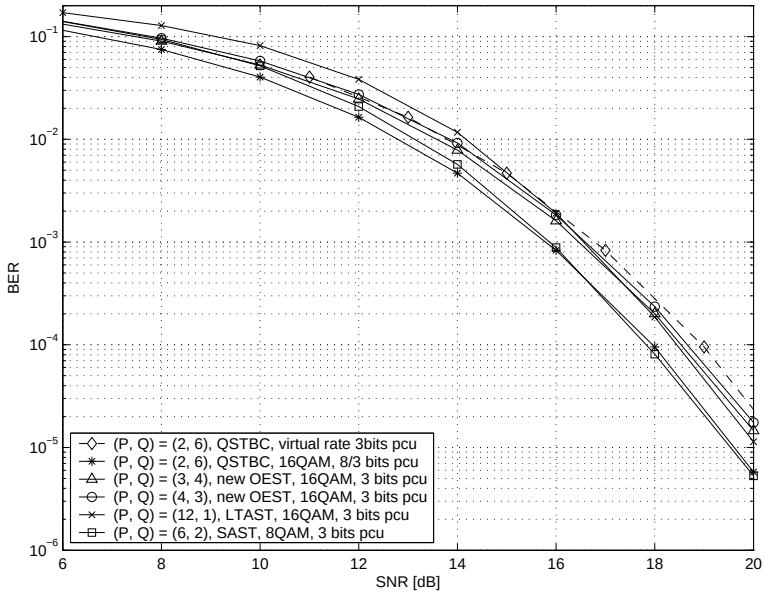

Figure 2.9: Performance of OEST codes with 3 bits pcu, except $\mathcal{D}_{2,6}$ (or $\mathcal{Q}_{12}$) with $8/3$ bits pcu, (12, 1) system.

While our theoretical analysis is carried out for even numbers of transmit antennas, SAST codes for an odd number of transmit antennas can be obtained by deleting one column of SAST codewords (or switching off one transmit antenna) and by setting the channel gain associated with the switched-off antenna to zero at the decoder.

Fig. 2.12 illustrates the performance of SAST codes and space-time linear constellation precoding (ST-LCP) codes [51] with the same 2 bits pcu (4-QAM). ST-LCP codes, in fact, are equivalent to DAST codes proposed in [49]; by using discrete Fourier transform (DFT), one can convert LTAST codes to DAST codes (see [20]). The slopes of the BER curves of SAST and ST-LCP codes are almost parallel, indicating that the former achieve full diversity. Furthermore, notable gains of 1 and 1.5 dB over ST-LCP codes are obtained for $M = 3$ and $M = 5$, respectively. Thus, SAST codes perform better compared with LTAST codes for any number of transmit antennas.

Fig. 2.13 compares performance of SAST, ST-LCP and linear dispersion codes [33] for spectral efficiency 2 and 6 bits pcu (4- and 64-QAM, respectively) and with $M = 3, N = 1$. Fig. 2.13 shows that SAST codes perform better than ST-LCP codes for all bit rates. SAST codes also perform better than the linear dispersion code with the same delay $T = 4$ at high SNR. With 2 and 6 bits pcu, SAST codes gain about 0.4 and 0.7 dB over the linear

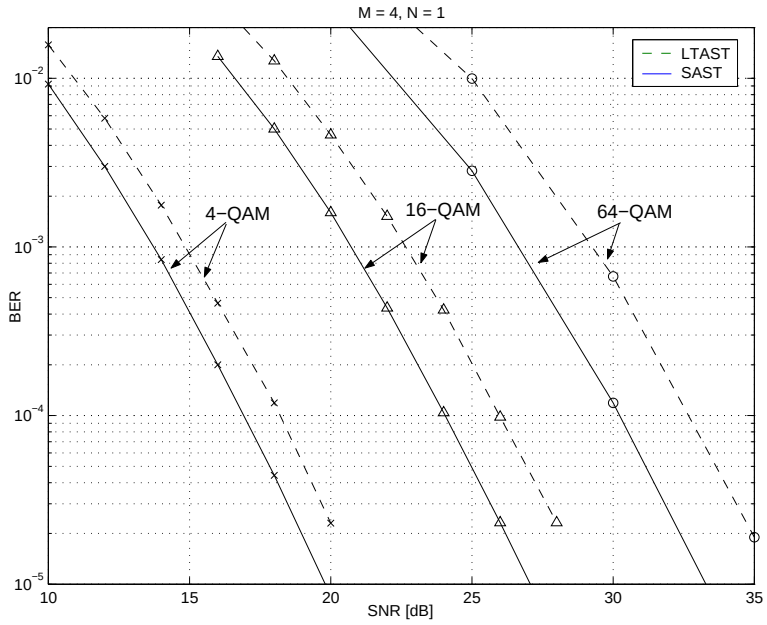

Figure 2.10: Performances of SAST and LTAST codes, (4, 1) system.

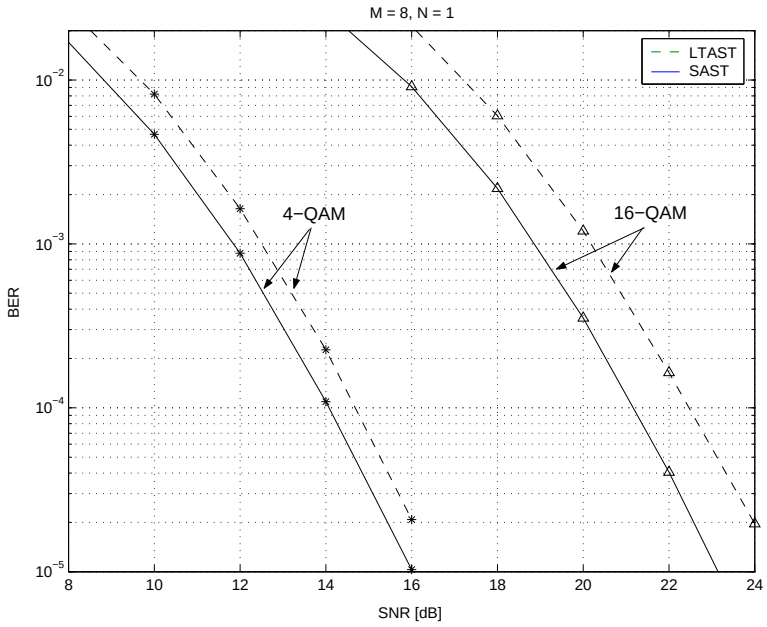

Figure 2.11: Performances of SAST and LTAST codes, (8, 1) system.

dispersion codes at a BER of 10^{-4}. With higher delay design $T = 6$ and for 2 bits pcu, SAST codes perform the same as the linear dispersion codes at low SNR, but outperform them at high SNR. SAST codes improve over the linear dispersion codes because the design criterion of the linear dispersion codes aims at maximizing the mutual information, which

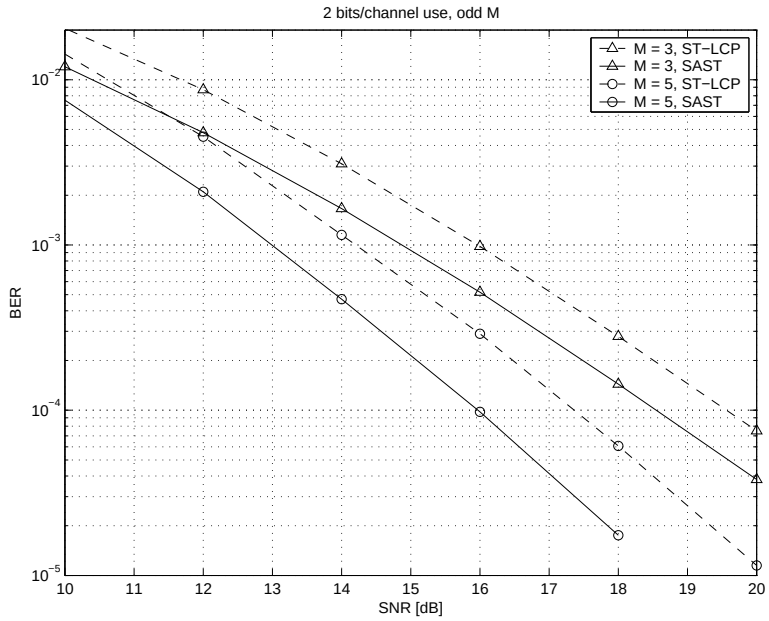

Figure 2.12: Performances of SAST and ST-LCP codes with 4-QAM, $M = 3, 5$, $N = 1$.

may not extract full diversity. Therefore, the performance of the linear dispersion codes is worse than that of SAST codes at high SNR. Note that the decoding complexity of linear dispersion codes is always higher than that of SAST codes.

We have investigated the error-rate performance of SAST codes. The results show that SAST codes outperform LTAST, ST-LCP/DAST, QSTBC, and linear dispersion codes. Since the performance of OSTBC is inferior to these codes [33, 49, 51, 61], SAST codes also outperform OSTBC codes.

Since suboptimal detectors may sometimes be employed to reduce the detection complexity, we examine the performance of LTAST and SAST codes with 16-QAM, using the V-BLAST optimal nulling and cancellation receiver or the optimal zero-forcing decision feedback equalization (ZF-DFE) receiver [94]. Fig. 2.14 depicts the performance of the two codes with the ZF-DFE receiver. The BER of SAST codes with $M = 2$ (Alamouti code) and $M = 4, 8$ using sphere decoder, and uncoded BER over single Rayleigh fading channel are also presented for comparison. By comparing the slopes of BER curves, we conclude that with the V-BLAST ZF-DFE receiver, SAST codes achieve a diversity order of 2, while the diversity order of LTAST codes is only 1; moreover, SAST codes have smaller BER than that of LTAST codes. With the ZF-DFE receiver, LTAST codes produce

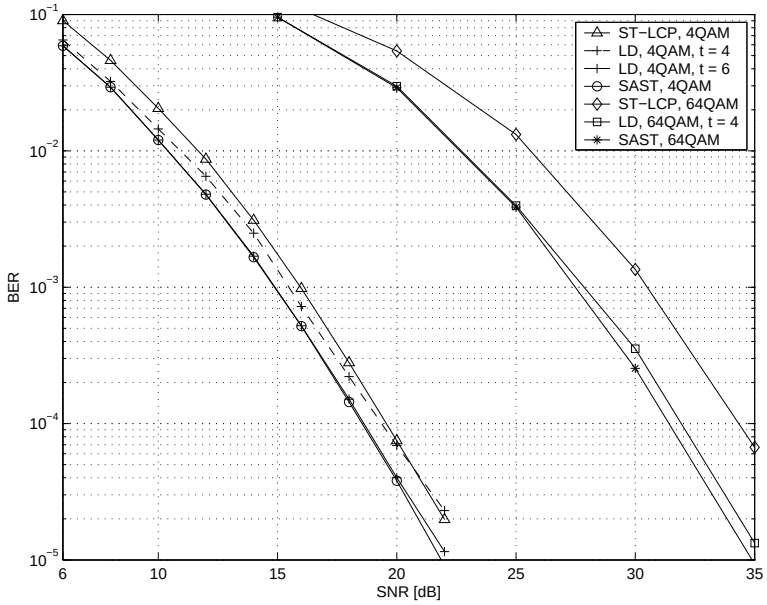

Figure 2.13: Performances of SAST, ST-LCP and linear dispersion codes with 4- and 64-QAM, (3, 1) system.

a marginal gain compared with uncoded data transmitted over single Rayleigh fading channel ($M = N = 1$) case. On the other hand, SAST codes with $M = 4$ and 8 gain about 1-dB and 2.9-dB, respectively, over the Alamouti code. With the ZF-DFE receiver, SAST codes do not achieve full diversity, but still deliver a notable coding gain.

The diversity orders of SAST codes and LTAST codes using ZF-DFE can be intuitively explained by checking back (2.54). With one receive antenna, the elements on the main diagonal of the equivalent channel of SAST codes are the sum of two squares of two channel amplitudes, while the elements on the main diagonal of the equivalent channel of LTAST codes are a square of a channel gain. Thus using the ZF decoder, the diversity orders of SAST codes and LTAST codes are two and one, respectively. The DFE helps to improve the error rate (coding gain) but not diversity order.

From the simulation results, we conclude that SAST codes always perform better than LTAST codes (see also [100]), even thought this two special cases of OEST codes have the same coding gains. The reason is that the distance spectrum of SAST codes is improved compared with LTAST codes. This fact can be verified by counting the number of codewords with minimal coding gain.

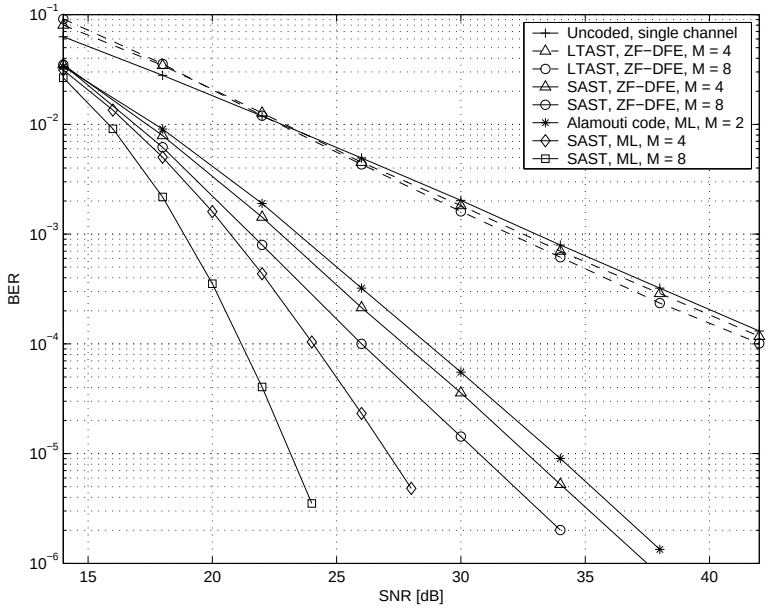

Figure 2.14: Performances of SAST and LTAST codes using V-BLAST optimal nulling and cancellation (or ZF-DFE for short) receiver for 16-QAM, $M = 4, 8$, $N = 1$.

2.4.3 Decoding Complexity

Since SAST codes offer better performance than several STBC, it is of interest to investigate their arithmetic complexity. We thus compare the complexity of SAST codes and LTAST codes, which have the same rate-one, for 8 transmit antennas. The two codes are decoded by a sphere decoder with Fincke-Pohst enumerating method [116] [108], written in Matlab Release 13. Note that the decoding of SAST codes is to decode two data vectors, each with 4 complex symbols; while with LTAST code, we need to decode only one data vector of 8 complex symbols. Therefore, we have to verify whether the total number of arithmetic operations to decode two length-4 data vectors of SAST codes is less than that of the decoding of one length-8 data vector of LTAST codes.

We differentiate "hard" operations, including multiplication, division and square, and simple addition. The results for a (8, 1) system with 16-QAM are plotted in Fig. 2.15. Clearly, the decoding complexity of LTAST codes higher than SAST codes 27 times at 14 dB (low SNR), 16.3 times at 20 dB (medium SNR) and 3.1 times at 30 dB (high SNR). Thus much arithmetic computation savings can be obtained by using 2-group SAST codes compared with 1-group LTAST codes. This is a good evidence to highlight the efficiency of multi-group STBC in complexity reduction.

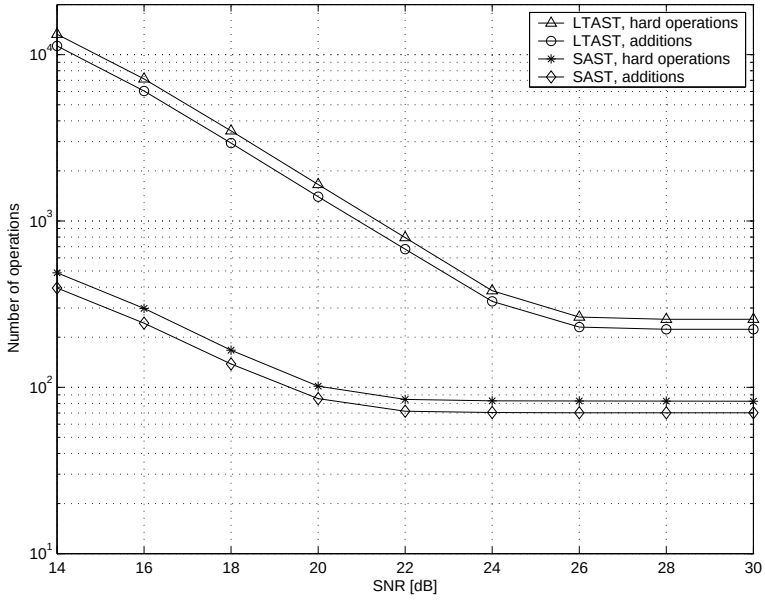

Figure 2.15: Comparison the arithmetic complexity of SAST codes and LTAST codes for (8, 1) system using 16-QAM.

2.5 Summary

We have derived the necessary and sufficient conditions for multi-group decodable STBC. Based on these conditions, we have presented a new general class of space-time codes called OEST codes. Their full-diversity and optimal coding gain are achieved by rotating the input constellations. The blocks of transmitted symbols in the OEST codewords can be maximum-likelihood decoded separately at the receiver without any interference from other blocks. This is a highly desirable decoding-complexity-reduction property for practical systems. The OEST framework sheds new light on the previously known STBC, including OSTBC, QSTBC, and rate-one LTAST codes. Furthermore, a new class of rate-one STBC, namely semi-orthogonal space-time codes, is identified. For a given number of transmit antennas, OEST code variants can be derived with flexible tradoffs among rate, performance, and decoding complexity.

In the next two chapters, we will develop two STBC from OEST, which are the extensions of QSTBC and SAST codes, with even lower decoding complexity. More sophisticated encoding will be designed to utilize the lower decoding complexity compared with the original codes.

Chapter 3

Minimum Decoding Complexity Space-Time Block Codes

In Section 2.3.1 of the previous chapter, we have shown that ABBA codes, proposed by Tirkkonen, Boariu, and Hottinen [47], are a special case of Construction II of OEST codes (see (2.23)). Even though the two constructions of OEST codes are permutation equivalent, the equivalent channels of the two constructions are different (see (2.54) and (2.57)). We have derived the equivalent channel of Construction I of OEST codes, but omitted the details of Construction II. In this chapter, we derive the equivalent channel of ABBA codes, which is a special case of OEST Construction II. Many further important results can be developed based on the equivalent channels of ABBA codes. For example, the original ABBA codes allow pair-wise complex-symbol decoding complexity. However, ABBA codes also allow single-complex symbol decoding, the feature which was known to associate with only OSTBC.

3.1 Existing Results and Open Issues of ABBA Codes

ABBA codes [47], a class of QSTBC, have been proposed to increase the code rate of OSTBC [40, 44]. Since ABBA QSTBC have low complexity pair-wise complex-symbol decoding and perform better than OSTBC [61], they have been widely studied for various applications such as coherent and non-coherent MIMO communications, beamforming, precoding, and others (see, e.g., [19, 117–119]).

Recently, Yuen *et al.* [120] have shown that the ABBA codes also enable pair-wise real-symbol decoding, which is the *minimum decoding complexity* (MDC) achievable by

non-orthogonal STBC; they call such codes MDC codes. Thus, while their code rate is higher than that of OSTBC, their decoding complexity is equal to single complex symbol decoding. In the following, we reserve the term "ABBA" for the QSTBC proposed by Tirkkonen *et al.* [47] with pair-wise complex-symbol decoding [61] and the term "MDC-ABBA" for the ABBA codes with pair-wise real-symbol decoding [120].

Single complex symbol decoding for ABBA codes is possible using phase feedback schemes. Specifically, these schemes are tailored for ABBA codes with 4 [121, 122], 6 [123], and 8 antennas [124]. However, these methods may be unnecessary since the ABBA codes are already single-symbol decodable.

To design MDC-ABBA codes with full-diversity, conventional quadrature amplitude modulation (QAM) or phase-shift keying (PSK) signals need to be transformed [120, 125]. Yuen *et al.* [120] and Wang *et al.* [125] employ the coding gain metric [16] to derive the optimal signal transformations[1] for QAM and 8PSK. Their analytical results are reported for QAM only. However, maximizing the coding gain is, in fact, to minimize the worst-case codeword PEP; this provides no guarantee for minimizing the symbol error rate (SER). In general, finding the optimal signal transformations for QAM, PSK, and other constellation with good minimum Euclidean distance, such as lattice of equilateral triangular (TRI) (also called hexagonal (HEX)) or amplitude PSK (APSK) [104, 126] in terms of minimal SER, is still an open problem.

Furthermore, despite extensive research, a general decoding method for ABBA codes for arbitrary numbers of transmit and receive antennas is not available. One reason for this gap is that the equivalent channel for ABBA codes is not known in the most general case. Several decoders for ABBA codes have been proposed, but only for some specific cases, for example with 4 or 6 antennas in [127–129].

In this chapter, we will systematically solve the fundemental open problems of ABBA QSTBC. They include the general decoder and optimal signal transformations in the minimal SER sense. We first derive general decoders of ABBA codes and apply these decoders for the signal transformations proposed by Yuen *et al.* [120] and Wang *et al.* [125]. The exact symbol pair-wise error probability (PEP) and union bound on the SER are derived.

[1] By using the term "transformation", we imply that the transformation matrix is not necessarily orthogonal. On the other hand, the term "rotation" is used only whenever the transformation matrix is orthogonal.

The union bound can be used to precisely predict the performance of MDC-ABBA codes and, moreover, to optimize the signal transformations for any constellation. Furthermore, for the constellations with inphase-quadrature power-imbalance, such as rectangular QAM (QAM-R), we propose a new method combining signal rotation and power allocation. Our new signal transformations for QAM-R perform better and have lower encoding/decoding complexities than that proposed in [125]. Since antenna selection is an effective method to improve the performance of space-time codes, as well as to simplify the structure of transmitter/receiver, we investigate the performance of MDC-ABBA codes with transmit and receive antenna selection. We show that MDC-ABBA codes achieve full diversity in the systems with antenna selection and with limited feedback [130].

3.2 Decoding of ABBA QSTBC Codes

We briefly review the construction of ABBA codes. Let A_k and B_k $(k = 1, 2, \cdots, K)$ be the $t \times m$ basis matrices of an OSTBC $\mathcal{O}_m$. Two blocks of data, each of K symbols, are mapped into two code matrices $\mathcal{A}$ and $\mathcal{B}$ of $\mathcal{O}_m$ as $\mathcal{A} = \sum_{k=1}^{K} (s_k A_k + s_k^* B_k), \mathcal{B} = \sum_{k=1}^{K} \left(s_{k+K} A_k + s_{k+K}^* B_k\right)$.

The ABBA code matrices for $M = 2m$ transmit antennas are constructed from $\mathcal{O}_m$ as $\mathcal{Q}_M = \begin{bmatrix} \mathcal{A} & \mathcal{B} \\ \mathcal{B} & \mathcal{A} \end{bmatrix}$, or

$$\begin{aligned} \mathcal{Q}_M &= \sum_{k=1}^{K} \underbrace{\begin{bmatrix} s_k & s_{k+K} \\ s_{k+K} & s_k \end{bmatrix}}_{\mathcal{C}_k} \otimes A_k + \sum_{k=1}^{K} \underbrace{\begin{bmatrix} s_k^* & s_{k+K}^* \\ s_{k+K}^* & s_k^* \end{bmatrix}}_{\mathcal{C}_k^\dagger} \otimes B_k \\ &= \sum_{k=1}^{K} (\mathcal{C}_k \otimes A_k + \mathcal{C}_k^\dagger \otimes B_k). \end{aligned} \tag{3.1}$$

The above expression have been shown in (2.28). Let $\pi = \begin{bmatrix} 0 & 1 \\ 1 & 0 \end{bmatrix}$, then $\pi = \pi^{-1}, \pi^2 = \boldsymbol{I}_2$, and

$$\mathcal{C}_k = (s_k \pi^0 + s_{k+K} \pi). \tag{3.2}$$

For example, the code matrix of the MDC-ABBA code for 4 transmit antennas built

from the Alamouti code [26] is given below:

$$\mathcal{Q}_4 = \begin{bmatrix} s_1 & s_2 & s_3 & s_4 \\ -s_2^* & s_1^* & -s_4^* & s_3^* \\ s_3 & s_4 & s_1 & s_2 \\ -s_4^* & s_3^* & -s_2^* & s_1^* \end{bmatrix}.$$

We next derive the equivalent channel of ABBA and MDC-ABBA codes, which is similar to the steps of deriving the equivalent channel of Construction I of OEST codes. The number of receive antenna $N = 1$ is considered first and then the results are generalized for multiple receive antennas.

Let $\boldsymbol{h} = [h_1\ h_2\ \cdots\ h_M]^\mathsf{T}$ denote the channel vector with $h_i \sim \mathcal{CN}(0,1)$. Let $Q \in \mathcal{Q}_M$ be a transmitted code matrix, the receive signal vector is $\boldsymbol{y} = \sqrt{\frac{\rho\kappa}{2}}Q\boldsymbol{h} + \boldsymbol{w}$, where $\boldsymbol{w}$ is noise vector with independently, identically distributed (i.i.d.) entries $\sim \mathcal{CN}(0,1)$; ρ is the average receive signal-to-noise ratio (SNR).

From (3.1) and (3.2), the received signal vector can be expressed as

$$\boldsymbol{y} = \sqrt{\frac{\rho\kappa}{2}} \sum_{k=1}^{K} \sum_{i=1}^{2} \left[\left(\pi^{i-1} \otimes A_k\right) \boldsymbol{h} s_{k+(i-1)K} + \left(\pi^{1-i} \otimes B_k\right) \boldsymbol{h} s_{k+(i-1)K}^* \right] + \boldsymbol{w}\,. \quad (3.3)$$

Let $\boldsymbol{e}_{ki} = \left(\pi^{i-1} \otimes A_k\right)\boldsymbol{h}, E_k = \begin{bmatrix}\boldsymbol{e}_{k1} & \boldsymbol{e}_{k2}\end{bmatrix}, \boldsymbol{f}_{ki} = \left(\pi^{1-i} \otimes B_k\right)\boldsymbol{h}, F_k = \begin{bmatrix}\boldsymbol{f}_{k1} & \boldsymbol{f}_{k2}\end{bmatrix}$, and $\boldsymbol{s}_k = \begin{bmatrix}s_k & s_{k+K}\end{bmatrix}^\mathsf{T}$, (3.3) can be rewritten as

$$\boldsymbol{y} = \sqrt{\frac{\rho\kappa}{2}} \begin{bmatrix} E_1 & F_1 & E_2 & F_2 & \cdots & E_K & F_K \end{bmatrix} \times \begin{bmatrix} \boldsymbol{s}_1^\mathsf{T} & \boldsymbol{s}_1^\dagger & \boldsymbol{s}_2^\mathsf{T} & \boldsymbol{s}_2^\dagger & \cdots & \boldsymbol{s}_K^\mathsf{T} & \boldsymbol{s}_K^\dagger \end{bmatrix}^\mathsf{T} + \boldsymbol{w}\,. \quad (3.4)$$

We now use a trick in [111] to decode OSTBC for our next derivation. The following equation is equivalent to (3.4):

$$\begin{bmatrix} \boldsymbol{y} \\ \boldsymbol{y}^* \end{bmatrix} = \sqrt{\frac{\rho\kappa}{2}} \underbrace{\begin{bmatrix} E_1 & F_1 & \cdots & E_K & F_K \\ F_1^* & E_1^* & \cdots & F_K^* & E_K^* \end{bmatrix}}_{W} \times \begin{bmatrix} \boldsymbol{s}_1^\mathsf{T} & \boldsymbol{s}_1^\dagger & \cdots & \boldsymbol{s}_K^\mathsf{T} & \boldsymbol{s}_K^\dagger \end{bmatrix}^\mathsf{T} + \begin{bmatrix} \boldsymbol{w} \\ \boldsymbol{w}^* \end{bmatrix}. \quad (3.5)$$

We can show that the columns of matrix W are orthogonal. To do this, we need to show that the following equations hold:

$$\begin{bmatrix} E_k \\ F_k^* \end{bmatrix}^\dagger \begin{bmatrix} E_l \\ F_l^* \end{bmatrix} = E_k^\dagger E_l + F_k^\mathsf{T} F_l^* = \mathbf{0}_2 \qquad \text{for } k \neq l, \quad (3.6a)$$

$$\begin{bmatrix} E_k \\ F_k^* \end{bmatrix}^\dagger \begin{bmatrix} F_l \\ E_l^* \end{bmatrix} = E_k^\dagger F_l + F_k^\mathsf{T} E_l^* = \mathbf{0}_2 \qquad \forall k, l. \quad (3.6b)$$

We just provide the proof for (3.6a); (3.6b) can be shown similarly. Let $Z_{kl} = (E_k^\dagger E_l + F_k^\mathsf{T} F_l^*)$, its element can be calculated as

$$\begin{aligned}
[Z_{kl}]_{ij} &= \boldsymbol{e}_{ki}^\dagger \boldsymbol{e}_{lj} + \boldsymbol{f}_{ki}^\mathsf{T} \boldsymbol{f}_{lj}^* \\
&= \boldsymbol{h}^\dagger [(\pi^{j-i}) \otimes (A_k^\dagger A_l)] \boldsymbol{h} + \boldsymbol{h}^\mathsf{T} [(\pi^{i-j}) \otimes (B_k^\mathsf{T} B_l^*)] \boldsymbol{h}^* \\
&= \boldsymbol{h}^\dagger [(\pi^{j-i}) \otimes (A_k^\dagger A_l + B_k^\dagger B_l)] \boldsymbol{h} \\
&= \begin{cases} 0, & k \neq l; \\ \boldsymbol{h}^\dagger (\pi^{j-i} \otimes \boldsymbol{I}_m) \boldsymbol{h}, & k = l. \end{cases}
\end{aligned} \tag{3.7}$$

Thus, $Z_{kl} = \mathbf{0}_2$ if $k \neq l$. Since for $k = l$, the matrices $Z_{kk} = Z \, \forall k$, where the entries of Z are $z_{ij} = \boldsymbol{h}^\dagger (\pi^{j-i} \otimes \boldsymbol{I}_m) \boldsymbol{h}$. In particular, $z_{1,1} = z_{2,2} = \|\boldsymbol{h}\|_\mathsf{F}^2$, $z_{1,2} = z_{2,1} = \sum_{i=1}^m (h_i h_{i+m}^* + h_i^* h_{i+m})$. Therefore, Z is also a circulant real matrix and can be represented as

$$Z = \sum_{i=1}^{m} H_i^\dagger H_i \tag{3.8}$$

where $H_i = \begin{bmatrix} h_i & h_{i+m} \\ h_{i+m} & h_i \end{bmatrix}$. To separate the transmitted vector $\boldsymbol{s}_k (k = 1, 2, \ldots K)$ at the receiver, we can multiply the two sides of (3.5) with $\begin{bmatrix} E_k^\dagger & F_k^\mathsf{T} \end{bmatrix}$ to get

$$E_k^\dagger \boldsymbol{y} + F_k^\mathsf{T} \boldsymbol{y}^* = \sqrt{\frac{\rho\kappa}{2}} Z \boldsymbol{s}_k + (E_k^\dagger \boldsymbol{w} + F_k^\mathsf{T} \boldsymbol{w}^*) \, . \tag{3.9}$$

Thus, $\begin{bmatrix} E_k^\dagger & F_k^\mathsf{T} \end{bmatrix}$ plays the role of the spatial signature of the data vector $\boldsymbol{s}_k$.

We now generalize the result of (3.9) for the case of multiple receive antennas, $N \geq 1$. The subscript n $(n = 1, 2, \ldots, N)$ is added to the channel gain vector $\boldsymbol{h}$. The channel matrix $\mathcal{H}$ is therefore written as $\mathcal{H} = \begin{bmatrix} \boldsymbol{h}_1 & \boldsymbol{h}_2 & \cdots & \boldsymbol{h}_N \end{bmatrix}$, where $\boldsymbol{h}_n = \begin{bmatrix} h_{1n} & h_{2n} & \cdots & h_{Mn} \end{bmatrix}^\mathsf{T}$.

We can show that the matrix Z in (3.8) becomes

$$Z = \sum_{j=1}^{N} \sum_{i=1}^{m} H_{i,j}^\dagger H_{i,j} \tag{3.10}$$

where $H_{i,j} = \begin{bmatrix} h_{i,j} & h_{i+m,j} \\ h_{i+m,j} & h_{i,j} \end{bmatrix}$. Therefore, (3.9) is generalized for multiple receive antennas as follows:

$$\underbrace{\sum_{n=1}^{N} (E_{kn}^\dagger \boldsymbol{y}_n + F_{kn}^\mathsf{T} \boldsymbol{y}_n^*)}_{\hat{\boldsymbol{y}}_k} = \sqrt{\frac{\rho\kappa}{2}} Z \boldsymbol{s}_k + \underbrace{\sum_{n=1}^{N} (E_{kn}^\dagger \boldsymbol{w}_n + F_{kn}^\mathsf{T} \boldsymbol{w}_n^*)}_{\hat{\boldsymbol{w}}_k} \tag{3.11}$$

where $\boldsymbol{y}_n$ is the received signal vector of the nth antenna,

$$E_{kn} = \begin{bmatrix} \boldsymbol{e}_{k1,n} & \boldsymbol{e}_{k2,n} \end{bmatrix}, \qquad \text{for } k = 1, 2, \ldots, K, \tag{3.12a}$$

$$\boldsymbol{e}_{ki,n} = \left(A_k \otimes \pi^{i-1} \right) \boldsymbol{h}_n, \qquad \text{for } i = 1, 2, \tag{3.12b}$$

$$F_{kn} = \begin{bmatrix} \boldsymbol{f}_{k1,n} & \boldsymbol{f}_{k2,n} \end{bmatrix}, \tag{3.12c}$$

$$\boldsymbol{f}_{ki,n} = \left(B_k \otimes \pi^{1-i} \right) \boldsymbol{h}_n. \tag{3.12d}$$

The noise vector $\hat{\boldsymbol{w}}_k$ is colored with covariance matrix $V = \mathbb{E}[\hat{\boldsymbol{w}}_k \hat{\boldsymbol{w}}_k^\dagger] = Z \neq \boldsymbol{I}_M$. Let $\hat{H} = Z^{\frac{1}{2}}$. This color noise can be whitened by a whitening matrix $\hat{H}^{-1} = Z^{-\frac{1}{2}}$.

Since Z is real, we can rewrite (3.11) by decoupling the real and imaginary parts of the two sides of (3.11) as

$$\underbrace{\begin{bmatrix} \Re(\hat{\boldsymbol{y}}_k) \\ \Im(\hat{\boldsymbol{y}}_k) \end{bmatrix}}_{\tilde{\boldsymbol{y}}_k} = \sqrt{\frac{\rho\kappa}{2}} \underbrace{\begin{bmatrix} Z & \boldsymbol{0}_2 \\ \boldsymbol{0}_2 & Z \end{bmatrix}}_{\tilde{H}} \begin{bmatrix} \Re(\boldsymbol{s}_k) \\ \Im(\boldsymbol{s}_k) \end{bmatrix} + \underbrace{\begin{bmatrix} \Re(\hat{\boldsymbol{w}}_k) \\ \Im(\hat{\boldsymbol{w}}_k) \end{bmatrix}}_{\tilde{\boldsymbol{w}}_k}. \tag{3.13}$$

Thus, the real and imaginary parts of the transmitted vector $\boldsymbol{s}_k$ can be separately detected. Including the noise whitening matrix $\hat{H}^{-1}$, the general equivalent transmit/receive signal relation of MDC-ABBA codes are:

$$\hat{H}^{-1}\Re(\hat{\boldsymbol{y}}_k) = \sqrt{\frac{\rho\kappa}{2}} \hat{H}\Re(\boldsymbol{s}_k) + \hat{H}^{-1}\Re(\hat{\boldsymbol{w}}_k), \tag{3.14a}$$

$$\hat{H}^{-1}\Im(\hat{\boldsymbol{y}}_k) = \sqrt{\frac{\rho\kappa}{2}} \hat{H}\Im(\boldsymbol{s}_k) + \hat{H}^{-1}\Im(\hat{\boldsymbol{w}}_k). \tag{3.14b}$$

In (3.14), $\hat{H}$ is the *equivalent channel* of MDC-ABBA codes. We have some important properties of $\hat{H}$ as follows.

Lemma 3.1. *The equivalent channel matrix of ABBA codes and its inversion are real and circulant.*

Proof. Since Z is a 2×2 normal circulant matrix, its two eigenvalues λ_1 and λ_2 are non-negative; Z can be diagonalized by a 2×2 (real) Fourier transform matrix $F_2 = \frac{1}{\sqrt{2}} \begin{bmatrix} 1 & 1 \\ 1 & -1 \end{bmatrix}$ as $Z = F_2^\dagger \operatorname{diag}(\lambda_1,\ \lambda_2) F_2$. If $\hat{H}^2 = Z$, then $\hat{H} = F_2^\dagger \operatorname{diag}(\sqrt{\lambda_1},\ \sqrt{\lambda_2}) F_2$. Thus, $\hat{H}$ is real. One can also verify that $\hat{H}$ is a circulant matrix. The matrix $\hat{H}^{-1}$ can be similarly shown to be a real and circulant matrix. The proof is completed. □

Note that, in general, the equivalent channel of Construction II of OEST codes is not circulant. However, with the special case of ABBA QSTBC, the equivalent channel is also circulant.

The detection of vectors $\Re(\boldsymbol{s}_k)$ and $\Im(\boldsymbol{s}_k)$ in (3.14) involves only 2 real symbols. Therefore, maximum likelihood detection of MDC-ABBA codes becomes single complex-symbol decoding, a feature previously known to be possessed by OSTBC only.

In order to achieve full-diversity, optimal signal transformations are required before transmission and these are derived for MDC-ABBA codes. We first analyze the encoding and decoding of existing signal transformations proposed by (1) Yuen, Guan, and Tjhung (YGT) [120] and (2) Wang, Wang, and Xia (WWX) [125]. Note that the coding gain metric [16] is used to optimize signal transformation in [120, 125], which may not be optimal in terms of minimal SER.

3.3 Analyzing the Existing Signal Transformations

Let the input symbols be $d_k = a_k + \mathsf{j}\, b_k, d_{k+K} = a_{k+K} + \mathsf{j}\, b_{k+K}, (k = 1, 2, \ldots, K)$; they are drawn from a unit average energy constellation $\mathcal{S}$, for example QAM, PSK. Let $s_k = p_k + \mathsf{j}\, q_k, s_{k+K} = p_{k+K} + \mathsf{j}\, q_{k+K}$ be the transmitted symbols. We can jointly transform the real input symbols a_k, b_k, a_{k+K} and b_{k+K} by a real transformation $\mathcal{R}$ to generate transmitted symbols p_k, q_k, p_{k+K}, and q_{k+K} as

$$\begin{aligned}\begin{bmatrix}\Re(\boldsymbol{s}_k)^{\mathsf{T}} & \Im(\boldsymbol{s}_k)^{\mathsf{T}}\end{bmatrix}^{\mathsf{T}} &= \begin{bmatrix}p_k & p_{k+K} & q_k & q_{k+K}\end{bmatrix}^{\mathsf{T}} \\ &= \mathcal{R}\underbrace{\begin{bmatrix}a_k & b_k & a_{k+K} & b_{k+K}\end{bmatrix}^{\mathsf{T}}}_{\hat{\boldsymbol{c}}_k}. \end{aligned} \tag{3.15}$$

1. *Signal rotation proposed by Yuen et al.* [120]:

In [120], the transmitted symbols are generated as follows:

$$\Re(\boldsymbol{s}_k) = \begin{bmatrix}p_k & p_{k+K}\end{bmatrix}^{\mathsf{T}} = R\begin{bmatrix}a_k & b_k\end{bmatrix}^{\mathsf{T}}, \tag{3.16a}$$

$$\Im(\boldsymbol{s}_k) = \begin{bmatrix}q_k & q_{k+K}\end{bmatrix}^{\mathsf{T}} = R\begin{bmatrix}a_{k+K} & b_{k+K}\end{bmatrix}^{\mathsf{T}} \tag{3.16b}$$

where R is a unitary matrix,

$$R = \begin{bmatrix}\cos(\alpha) & \sin(\alpha) \\ \sin(\alpha) & -\cos(\alpha)\end{bmatrix}. \tag{3.17}$$

and optimal angle, in terms of coding gain [16], for QAM is $\alpha = \frac{1}{2}\arctan(\frac{1}{2}) = 13.2825^{\circ}$. Thus, the signal rotation $\mathcal{R}$ is of the form

$$\mathcal{R} = \begin{bmatrix} R & \mathbf{0}_2 \\ \mathbf{0}_2 & R \end{bmatrix}. \tag{3.18}$$

2. *Signal transformation proposed by Wang et al.* [125]:

Wang *et al.* [125] present a general format of signal transformations and show that there are three cases that can be used to achieve pair-wise real-symbol decoding. However, these three cases are permutation-equivalent. We thus consider only the first case with the following signal transformation:

$$\begin{bmatrix} p_k & q_k & p_{k+K} & q_{k+K} \end{bmatrix}^{\mathsf{T}} = \mathcal{R}_W \hat{\boldsymbol{c}}_k \tag{3.19}$$

where

$$\mathcal{R}_W = \begin{bmatrix} U_1 & U_2 \\ U_1 R_1 & U_2 R_2 \end{bmatrix}, \tag{3.20}$$

and U_1, U_2, R_1, R_2 are 2×2 real matrices, $R_1^2 = \boldsymbol{I}_2, R_2^2 = \boldsymbol{I}_2$.

However, the symbol mapping in [125] is slightly different from (3.15): the p_{k+K} and q_k are permuted compared with the arrangement in (3.15) such that

$$\begin{aligned} \begin{bmatrix} \Re(\boldsymbol{s}_k)^{\mathsf{T}} & \Im(\boldsymbol{s}_k)^{\mathsf{T}} \end{bmatrix}^{\mathsf{T}} &= \begin{bmatrix} p_k & p_{k+K} & q_k & q_{k+K} \end{bmatrix}^{\mathsf{T}} \\ &= \pi \begin{bmatrix} p_k & q_k & p_{k+K} & q_{k+K} \end{bmatrix}^{\mathsf{T}} = \underbrace{\pi \mathcal{R}_W}_{\widehat{\mathcal{R}}_W} \hat{\boldsymbol{c}}_k \end{aligned} \tag{3.21}$$

where

$$\pi = \begin{bmatrix} 1 & 0 & 0 & 0 \\ 0 & 0 & 1 & 0 \\ 0 & 1 & 0 & 0 \\ 0 & 0 & 0 & 1 \end{bmatrix}. \tag{3.22}$$

Substituting $\widehat{\mathcal{R}}_W$ into (3.13), we have

$$\bar{\boldsymbol{y}}_k = \sqrt{\frac{\rho\kappa}{2}} \widetilde{H} \widehat{\mathcal{R}}_W \hat{\boldsymbol{c}}_k + \bar{\boldsymbol{w}}_k. \tag{3.23}$$

The matrix $\widetilde{H}\widehat{\mathcal{R}}_W$ in (3.23) is not block-diagonal; thus, pair-wise real-symbol decoding seems to be impossible. However, by multiplying to sides of (3.23) with $\widehat{\mathcal{R}}_W^{\mathsf{T}}$, we again obtain another block diagonal matrix $\widehat{\mathcal{R}}_W^{\mathsf{T}} \widetilde{H} \widehat{\mathcal{R}}_W$.

We first can show that the product $\pi^{\mathsf{T}}\widetilde{H}\pi = \begin{bmatrix} z_1\boldsymbol{I}_2 & z_2\boldsymbol{I}_2 \\ z_2\boldsymbol{I}_2 & z_1\boldsymbol{I}_2 \end{bmatrix}$. Then,

$$\bar{H} = \widehat{\mathcal{R}}_W^{\mathsf{T}}\widetilde{H}\widehat{\mathcal{R}}_W = \mathcal{R}_W^{\mathsf{T}}\pi^{\mathsf{T}}\widetilde{H}\pi\mathcal{R}_W = \begin{bmatrix} X_1 & \mathbf{0}_2 \\ \mathbf{0}_2 & X_2 \end{bmatrix} \tag{3.24}$$

where

$$X_1 = z_1U_1^{\mathsf{T}}U_1 + z_2R_1^{\mathsf{T}}U_1^{\mathsf{T}}U_1 + z_2U_1^{\mathsf{T}}U_1R_1 + z_1R_1^{\mathsf{T}}U_1^{\mathsf{T}}U_1R_1,$$
$$X_2 = z_1U_2^{\mathsf{T}}U_2 + z_2R_2^{\mathsf{T}}U_2^{\mathsf{T}}U_2 + z_2U_2^{\mathsf{T}}U_2R_2 + z_1R_2^{\mathsf{T}}U_2^{\mathsf{T}}U_2R_2.$$

where, z_1 and z_2 are the elements of Z such that $Z = \begin{bmatrix} z_1 & z_2 \\ z_2 & z_1 \end{bmatrix}$.

Now, multiplying both sides of (3.23), one gets:

$$\widehat{\mathcal{R}}_W\bar{\boldsymbol{y}}_k = \sqrt{\frac{\rho\kappa}{2}}\begin{bmatrix} X_1 & \mathbf{0}_2 \\ \mathbf{0}_2 & X_2 \end{bmatrix}\boldsymbol{c}_k + \widehat{\mathcal{R}}_W\bar{\boldsymbol{w}}_k. \tag{3.25}$$

The noise vector $\widehat{\mathcal{R}}_W\bar{\boldsymbol{w}}_k$ can be shown to have covariance matrix $\bar{H}$. Thus, we can use the noise whitening matrix $\bar{H}^{-\frac{1}{2}}$. Eq. (3.25) becomes

$$\begin{bmatrix} X_1^{-\frac{1}{2}} & \mathbf{0}_2 \\ \mathbf{0}_2 & X_2^{-\frac{1}{2}} \end{bmatrix}\widehat{\mathcal{R}}_W\bar{\boldsymbol{y}}_k = \sqrt{\frac{\rho\kappa}{2}}\begin{bmatrix} X_1^{\frac{1}{2}} & \mathbf{0}_2 \\ \mathbf{0}_2 & X_2^{\frac{1}{2}} \end{bmatrix}\boldsymbol{c}_k + \bar{H}^{-\frac{1}{2}}\bar{\boldsymbol{w}}_k. \tag{3.26}$$

Let $\widehat{\mathcal{R}}_W\bar{\boldsymbol{y}}_k = [\check{\boldsymbol{y}}_{k,1}^{\mathsf{T}} \;\; \check{\boldsymbol{y}}_{k,2}^{\mathsf{T}}]^{\mathsf{T}}$, where $\check{\boldsymbol{y}}_{k,1}^{\mathsf{T}}$ and $\check{\boldsymbol{y}}_{k,2}^{\mathsf{T}}$ are 2×1 real vectors, $\bar{H}^{-\frac{1}{2}}\bar{\boldsymbol{w}}_k = [\check{\boldsymbol{w}}_{k,1}^{\mathsf{T}} \;\; \check{\boldsymbol{w}}_{k,2}^{\mathsf{T}}]^{\mathsf{T}}$, where $\check{\boldsymbol{w}}_{k,1}^{\mathsf{T}}$ and $\check{\boldsymbol{w}}_{k,2}^{\mathsf{T}}$ are 2×1 vectors with i.i.d. real Gaussian elements, (3.26) is equivalent to

$$X_1^{-\frac{1}{2}}\check{\boldsymbol{y}}_{k,1} = \sqrt{\frac{\rho\kappa}{2}}X_1^{\frac{1}{2}}\boldsymbol{c}_k + \check{\boldsymbol{w}}_{k,1}\,, \tag{3.27a}$$

$$X_2^{-\frac{1}{2}}\check{\boldsymbol{y}}_{k,2} = \sqrt{\frac{\rho\kappa}{2}}X_2^{\frac{1}{2}}\boldsymbol{c}_{k+K} + \check{\boldsymbol{w}}_{k,2}. \tag{3.27b}$$

The maximum likelihood detection equations for MDC-ABBA codes with signal transformation from [125] are

$$\hat{\boldsymbol{c}}_k = \arg\min_{\boldsymbol{c}_k}\left(\rho\kappa\boldsymbol{c}_k^{\mathsf{T}}X_1\boldsymbol{c}_k - 2\sqrt{\frac{\rho\kappa}{2}}\boldsymbol{c}_k^{\mathsf{T}}\check{\boldsymbol{y}}_{k,1})\right), \tag{3.28a}$$

$$\hat{\boldsymbol{c}}_{k+K} = \arg\min_{\boldsymbol{c}_{k+K}}\left(\rho\kappa\boldsymbol{c}_{k+K}^{\mathsf{T}}X_2\boldsymbol{c}_{k+K} - 2\sqrt{\frac{\rho\kappa}{2}}\boldsymbol{c}_{k+K}^{\mathsf{T}}\check{\boldsymbol{y}}_{k,2}\right). \tag{3.28b}$$

Thus, the decoding of MDC-ABBA codes with WWX-transformation reduces to pair-wise real-symbol decoding.

We have some comparisons on the signal transformations by Yuen *et al.* [120] and Wang *et al.* [125] as follows.

- Encoding complexity: The 4×4 transformation $\mathcal{R}_W$ of Wang *et al.* [125] has higher encoding complexity compared with the 2×2 rotation R of Yuen *et al.* [120].

- Decoding complexity: However, the multiplication of $\widehat{\mathcal{R}}_W$ and $\bar{\boldsymbol{y}}_k$ in (3.25) slightly increase the complexity, compare with the decoding of MDC-ABBA codes with YGT-rotation.

- Performance: For square QAM (QAM-S), the transformation in [125, Theorem 2] provides no SNR gain compared with the rotation proposed by Yuen *et al.* [120]. The transformation in [125, Theorem 3] performs better with rectangular QAM (QAM-R) at the cost of higher encoding/decoding complexities.

3.4 Optimal Signal Transformations

We will only consider the signal rotation of Yuen *et al.* [120] for deriving the exact symbol PEP because their rotation is mathematically convenient. More important, we will show that by combining power allocation and signal rotation for inphase-quadrature power-unbalanced constellations like QAM-R, we can achieve not only better performance but also less complexity than by using the transformation in [125, Theorem 3].

3.4.1 Exact Symbol Pair-Wise Error Probability

From (3.15) and (3.16), we can rewrite (3.14) as

$$\hat{H}^{-1}\Re(\hat{\boldsymbol{y}}_k) = \sqrt{\frac{\rho\kappa}{2}}\hat{H}R\begin{bmatrix} a_k & b_k \end{bmatrix}^{\mathsf{T}} + \Re(\hat{\boldsymbol{w}}_k), \tag{3.29a}$$

$$\hat{H}^{-1}\Im(\hat{\boldsymbol{y}}_k) = \sqrt{\frac{\rho\kappa}{2}}\hat{H}R\begin{bmatrix} a_{k+K} & b_{k+K} \end{bmatrix}^{\mathsf{T}} + \Im(\hat{\boldsymbol{w}}_k). \tag{3.29b}$$

Since $\hat{H}^{-1}\Re(\hat{\boldsymbol{w}}_k)$ and $\hat{H}^{-1}\Im(\hat{\boldsymbol{w}}_k)$ are real random Gaussian vectors with i.i.d. entries (zero-mean and variance $N_0 = 1/2$), the information vectors $\begin{bmatrix} a_k & b_k \end{bmatrix}^{\mathsf{T}}$ and $\begin{bmatrix} a_{k+K} & b_{k+K} \end{bmatrix}^{\mathsf{T}}$ $(k = 1, 2, \ldots, K)$ experience the same channels; they are subject to the same error probability. We thus can consider the error probability of one of the two vectors only; the subscript of symbols can be omitted for brevity. Furthermore, the pair-wise error probability of each vector is also the symbol PEP.

Consider two distinct symbols $d = a + \mathrm{j}\, b$ and $\hat{d} = \hat{a} + \mathrm{j}\, \hat{b}$. Let $\delta_1 = a - \hat{a}, \delta_2 = b - \hat{b}, \Delta = [\delta_1 \ \ \delta_2]^{\mathsf{T}}$, the conditional symbol PEP of d and $\hat{d}$ can be expressed by the Gaussian Q-function as [32]

$$P(d \to \hat{d}|\hat{H}) = Q\left(\sqrt{\frac{\rho\kappa|\hat{H}R\Delta|^2}{4N_0}}\right). \tag{3.30}$$

We have shown that $\hat{H}$ is a 2×2 real circulant matrix in Lemma 3.1. Hence, $\hat{H}^\dagger\hat{H} = \hat{H}\hat{H} = \hat{H}^2 = Z$, where Z is given in (3.10). We can use eigenvalue decomposition for $H_{i,j}$ so that $H_{i,j} = F_2^\dagger \Lambda_{i,j} F_2$, where $\Lambda_{i,j} = \mathrm{diag}(\lambda_{i,j,1}, \lambda_{i,j,2})$ and $[\lambda_{i,j,1} \ \ \lambda_{i,j,2}]^{\mathsf{T}} = F_2[h_{i,j} \ h_{i+M/2,j}]^{\mathsf{T}}$. Since $h_{i,j}$ and $h_{i+M/2,j}$ are i.i.d. $\sim \mathcal{CN}(0,1)$, so are the $\lambda_{i,j,1}$ and $\lambda_{i,j,2}$. Thus,

$$Z = \sum_{j=1}^{N}\sum_{i=1}^{M/2} F_2\, \mathrm{diag}(|\lambda_{i,j,1}|^2, |\lambda_{i,j,2}|^2)F_2. \tag{3.31}$$

Let $x \triangleq |\hat{H}R\Delta|^2 = (R\Delta)^\dagger\hat{H}^\dagger\hat{H}(R\Delta)$, one has

$$\begin{aligned} x &= \sum_{j=1}^{N}\sum_{i=1}^{M/2} \left[(F_2R\Delta)^\dagger\, \mathrm{diag}(|\lambda_{i,j,1}|^2, |\lambda_{i,j,2}|^2)(F_2R\Delta)\right] \\ &= \sum_{j=1}^{N}\sum_{i=1}^{M/2} \left[\beta_1^2|\lambda_{i,j,1}|^2 + \beta_2^2|\lambda_{i,j,2}|^2\right] \end{aligned} \tag{3.32}$$

where $[\beta_1 \ \beta_2]^{\mathsf{T}} = F_2R\Delta$, and β_1 and β_2 are real.

We can apply the Craig's formula [131] to derive the conditional symbol PEP in (3.30).

$$\begin{aligned} P(d \to \hat{d}|\hat{H}) &= Q\left(\sqrt{\frac{\rho\kappa x}{2}}\right) = \frac{1}{\pi}\int_0^{\pi/2} \exp\left(\frac{-\rho\kappa x}{4\sin^2\theta}\right) d\theta \\ &= \frac{1}{\pi}\int_0^{\pi/2} \prod_{j=1}^{N}\prod_{i=1}^{M/2} \exp\left(-\frac{\rho\kappa\left(\beta_1^2|\lambda_{i,j,1}|^2 + \beta_2^2|\lambda_{i,j,2}|^2\right)}{4\sin^2\theta}\right) d\theta. \end{aligned} \tag{3.33}$$

Since $\lambda_{i,j,1}$ and $\lambda_{i,j,2}$ are i.i.d $\sim \mathcal{CN}(0,1)$, we can apply a method based on the moment generation function (MGF) [132, 133] to obtain the unconditional symbol PEP in the following:

$$P(d \to \hat{d}) = \frac{1}{\pi}\int_0^{\pi/2} \underbrace{\left[\left(1 + \frac{\rho\kappa\beta_1^2}{4\sin^2\theta}\right)\left(1 + \frac{\rho\kappa\beta_2^2}{4\sin^2\theta}\right)\right]^{-MN/2}}_{G(x)} d\theta. \tag{3.34}$$

We can further derive another closed form of symbol PEP to avoid integral operation. Let $x = \sin^2\theta$, $\epsilon_1 = \frac{4}{\rho\kappa\beta_1^2}, \epsilon_2 = \frac{4}{\rho\kappa\beta_2^2}$, and $\widehat{L} = MN/2$. Using the partial fraction for the equation inside the integral (3.34), one has

$$G(x) = \frac{1}{(1+x/\epsilon_1)^{\widehat{L}}(1+x/\epsilon_2)^{\widehat{L}}} = (\epsilon_1\epsilon_2)^{\widehat{L}} \left(\sum_{i=0}^{\widehat{L}-1} \frac{u_i}{(x+\epsilon_1)^{m-i}} + \sum_{k=0}^{\widehat{L}-1} \frac{v_k}{(x+\epsilon_2)^{m-k}} \right) \tag{3.35}$$

where

$$u_i = \frac{(-1)^i \widehat{L}(\widehat{L}+1)\dots(\widehat{L}+i-1)}{i!(\epsilon_2-\epsilon_1)^{\widehat{L}+i}}, \tag{3.36a}$$

$$v_k = \frac{(-1)^k \widehat{L}(\widehat{L}+1)\dots(\widehat{L}+k-1)}{k!(\epsilon_1-\epsilon_2)^{\widehat{L}+k}}. \tag{3.36b}$$

Substituting $G(x), u_i, v_k$ into (3.34) and after algebraic manipulations, we get

$$\begin{aligned} &P(d \to \hat{d}) \\ &= (\epsilon_1\epsilon_2)^{\widehat{L}} \left(\sum_{i=0}^{\widehat{L}-1} \frac{u_i}{\epsilon_1^{\widehat{L}-i}} \frac{1}{\pi} \int_0^{\pi/2} \frac{d\theta}{(1+\frac{1}{\epsilon_1}\sin^2\theta)^{\widehat{L}-i}} + \sum_{i=0}^{\widehat{L}-1} \frac{v_i}{\epsilon_2^{\widehat{L}-i}} \frac{1}{\pi} \int_0^{\pi/2} \frac{d\theta}{(1+\frac{1}{\epsilon_2}\sin^2\theta)^{\widehat{L}-i}} \right). \end{aligned} \tag{3.37}$$

Since $\frac{1}{\pi}\int_0^{\pi/2} \frac{d\theta}{(1+\frac{1}{\epsilon_1}\sin^2\theta)^{\widehat{L}-i}}$ (and also $\frac{1}{\pi}\int_0^{\pi/2} \frac{d\theta}{(1+\frac{1}{\epsilon_2}\sin^2\theta)^{\widehat{L}-i}}$) is the symbol PEP of a maximal ratio combining (MRC) system with $(\widehat{L}-i)$ receive antennas [32], we obtain

$$\mathcal{M}_{1,i} =: \frac{1}{\pi}\int_0^{\pi/2} \frac{d\theta}{(1+\frac{1}{\epsilon_1}\sin^2\theta)^{\widehat{L}-i}} = \left(\frac{1-\eta_1}{2}\right)^{\widehat{L}-i} \sum_{l=0}^{\widehat{L}-i-1} \binom{\widehat{L}-i-1+l}{l} \left(\frac{1+\eta_1}{2}\right)^l, \tag{3.38a}$$

$$\mathcal{M}_{2,i} =: \frac{1}{\pi}\int_0^{\pi/2} \frac{d\theta}{(1+\frac{1}{\epsilon_2}\sin^2\theta)^{\widehat{L}-i}} = \left(\frac{1-\eta_2}{2}\right)^{\widehat{L}-i} \sum_{l=0}^{\widehat{L}-i-1} \binom{\widehat{L}-i-1+l}{l} \left(\frac{1+\eta_2}{2}\right)^l. \tag{3.38b}$$

where $\eta_1 = \sqrt{1/(1+\epsilon_1)}, \eta_2 = \sqrt{1/(1+\epsilon_2)}$.

The symbol PEP of MDC-ABBA codes can be found below.

$$P(d \to \hat{d}) = \sum_{i=0}^{\widehat{L}-1} \left(u_i \epsilon_1^i \epsilon_2^{\widehat{L}} \mathcal{M}_{1,i} + v_i \epsilon_1^{\widehat{L}} \epsilon_2^i \mathcal{M}_{2,i} \right). \tag{3.39}$$

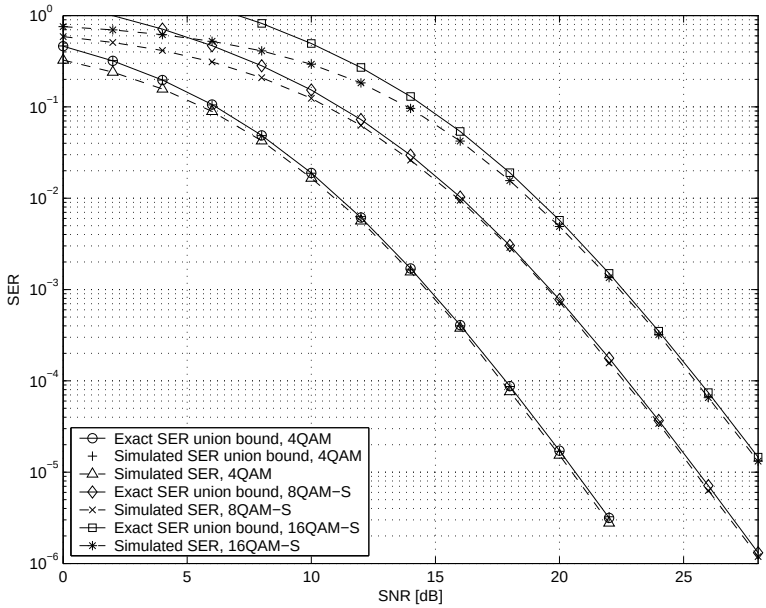

Figure 3.1: Union bound on SER compared with simulated SER of QAM signals, (4, 1) system.

3.4.2 Optimal Signal Rotations Based on Tight SER Union Bound

Assume that d_i and d_j, $i, j = 1, \ldots, \Omega$, are signals drawn from a constellation $\mathcal{S}$ of size Ω. Using the symbol PEP expression (3.34), we compute the union bound on SER of MDC-ABBA codes with constellation $\mathcal{S}$ as

$$P_u(\mathcal{S}) = \frac{2}{\Omega} \sum_{i=1}^{\Omega-1} \sum_{j=i+1}^{\Omega} P(d_i \to d_j). \tag{3.40}$$

The SER union bound of square QAM (QAM-S) with signal rotation in (3.17) and $\alpha = 13.2825^\circ$ are plotted in Fig. 3.1. The geometrical shape of 8QAM-S (and also other 8-ary constellations) can be found in Fig. 3.2. The bit mapping is designed such that the average number of different bits of neighbor symbols is minimized.

The union bound is only about 0.1 dB apart from the simulated SER when SER $< 10^{-2}$. Therefore, the SER union bound can be used to predict the SER performance of MDC-ABBA codes accurately. Furthermore, this bound can be used to optimize the signal rotation R.

We run a computer search to find the optimal rotation in terms of minimizing the SER union bound for popular constellations. During the search, the incremental step size of rotation angle is 0.001°. The optimal angle is searched in the range $[0^\circ, 45^\circ]$, because if α

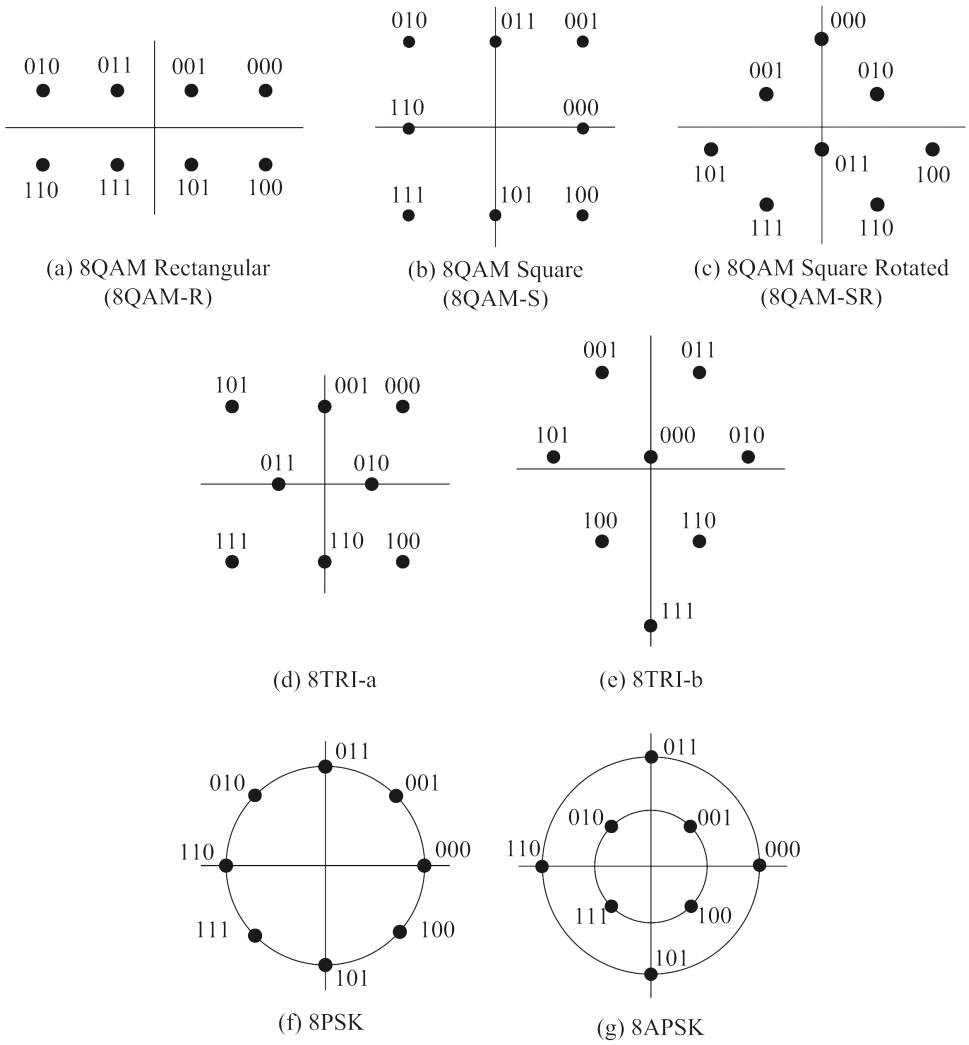

Figure 3.2: Geometrical shapes of 8-ary constellations.

is an optimal angle, the following angles are also optimal $-\alpha, 90^\circ \pm \alpha, 180^\circ \pm \alpha, 270^\circ \pm \alpha$. The SNR is chosen such that the SER of corresponding optimal rotation angle is about 10^{-8}. At such low SER, the optimal rotation angles also yield full-diversity MDC-ABBA codes. The results are summarized for the optimal angle in the range $[0^\circ, 45^\circ]$ in Table 3.1.

The SER union bounds of several 4-, 8- and 16-ary constellations are illustrated in Fig. 3.3. Compared with QAM, TRI performs quite well when they are used for fading channels [104, 126], and for OSTBC and ABBA codes [61, 105]. The constellations with larger minimum Euclidean distance tend to perform better. However, this conclusion may not be valid for MDC-ABBA codes. For example, 8TRI-b has the best minimum Euclidean distance among 8-ary constellations, but its performance is worse than 8QAM.

Table 3.1: Optimal Rotation Angles of Popular Constellations

Signal	Optimal α	Signal	Optimal α
4QAM	$14.382°$	8QAM-S	$12.268°$
4TRI	$31.155°$	8QAM-R	$13.166°$
8PSK	$5.915°$, $39.085°$	8QAM-SR	$31.964°$
8APSK	$33.472°$	16PSK	$24.883°$, $42.617°$
8TRI-a	$30.284°$	16TRI	$0°$
8TRI-b	$0°$	16QAM-S	$13.195°$

We also compare the frame error rate[2] (FER) of MDC-ABBA codes with the new optimal signal rotation and existing transformations for square-rotated 8QAM (8QAM-SR) in Fig. 3.4. Our new optimal signal rotation gains remarkable SNR at high SNR compared with the signal rotation in [120] and performs slightly better than the signal transformation in [125], however, with lower encoding/decoding complexities.

Note that in Fig. 3.4, while ABBA codes (with pair-wise complex-symbol decoding) have a better FER compared with MDC-ABBA codes, the BER of the former is inferior to that of the latter. Gray-bit mapping may not be optimal for ABBA codes with 8QAM-SR.

The new optimal rotation angles for QAM (square or rectangular) constellations are very close to the proposed angle $\alpha = 13.2825°$ by minimizing codeword PEP [120]. Therefore, the SNR gains in these cases are negligible compared to the results of [120] and [125, Theorem 2]. We will next present a new approach, which is applicable to find the optimal rotation angle for QAM-R so that the MDC-ABBA codes perform better but have lower encoding/decoding complexity than that proposed in [125, Theorem 3].

3.5 Optimal Signal Rotations with Power Allocations

For QAM-R, for example 8QAM-R in Fig. 3.3, the average powers of the real and imaginary parts of the signal points are different. We may change the power allocation of the real and imaginary parts of QAM-R signals to a get better overall SER.

[2]Since a frame or vector of symbol data is mapped into a codeword, the term "frame error rate" bears the meaning of "codeword error rate".

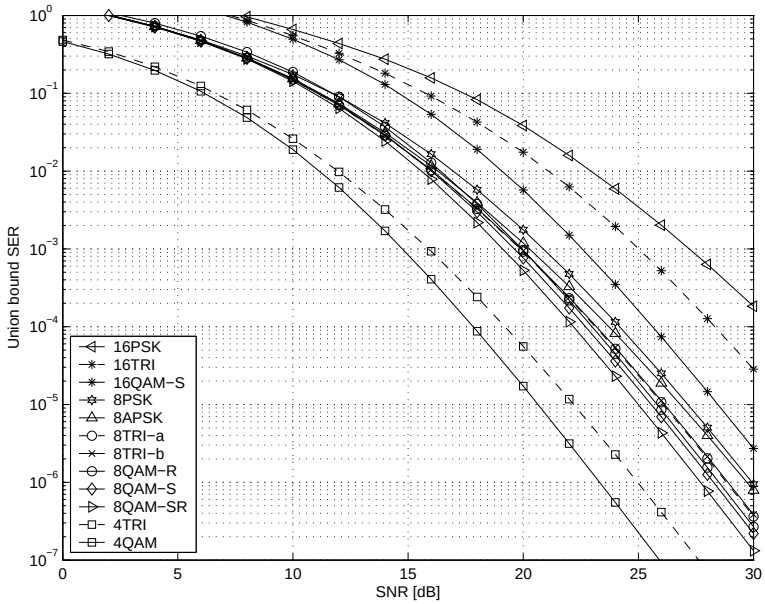

Figure 3.3: SER union bound of 4-, 8-, 16-ary constellations, (4, 1) system.

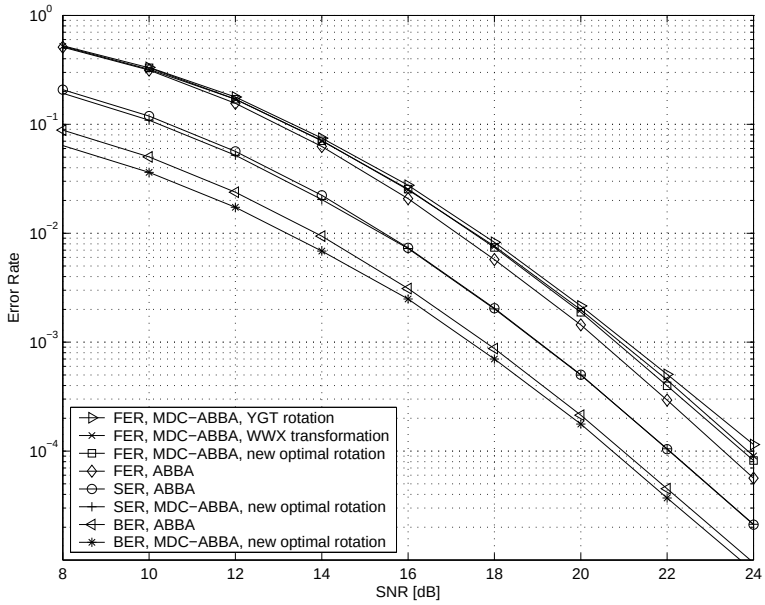

Figure 3.4: Performances of ABBA codes and MDC-ABBA codes using 8QAM-SR, (4, 1) system.

In particular, the real and imaginary parts of QAM-R signals are scaled by constants μ_1 and μ_2, respectively, before they are rotated. For example, let $\mathcal{S}$ be a constellation with signal set $\mathcal{S} = \{d \mid d = a + \mathrm{j}\, b, a, b \in \mathbb{R}\}$, the new constellation with new power allocation is $\bar{\mathcal{S}} = \{\bar{d} \mid \bar{d} = \mu_1 a + \mathrm{j}\, \mu_2 b; a, b \in \mathbb{R}\}$. The average energy of the constellation is kept

Table 3.2: Optimal Power Allocation and Signal Rotation for QAM-R

Constellation	μ_1	μ_2	Optimal α
8QAM-R	0.9055	1.3784	$0°$
32QAM-R	0.8972	1.3487	$1.954°$

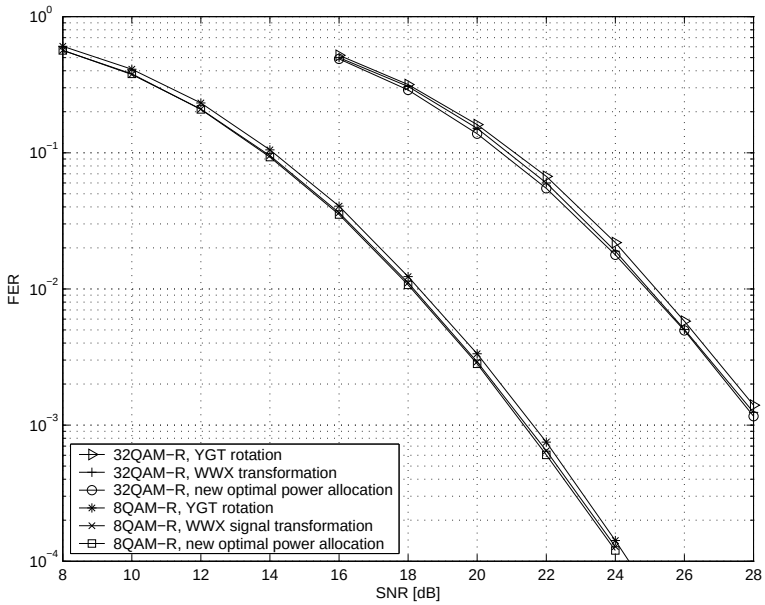

Figure 3.5: Performance of MDC-ABBA codes with new optimal power allocation and existing signal transformations for QAM-R, (4, 1) system.

unchanged. Scalars μ_1 and μ_2 are called power loading coefficients. For example, the 8QAM-R with signal points $\{(\pm 3 \pm \mathrm{j}, \pm 1 \pm \mathrm{j})/\sqrt{48}\}$ has a constraint equation for power loading coefficients μ_1 and μ_2 as $5\mu_1^2 + \mu_2^2 = 6$. We ran an exhaustive computer search to find the best power loading coefficients and rotation angle for 8- and 32QAM-R. The results are given in Table 3.2.

The FER of MDC-ABBA codes with our new power loading scheme for QAM-R is compared with the existing signal transformations in Fig. 3.5. Our proposed scheme performs better compared with the signal rotation method of Yuen-Guan-Tjhung and also performs slightly better than the signal transformation method of Wang-Wang-Xia with lower encoding/decoding complexities.

We can apply the power allocation method for other constellations, such as 8TRI-b and 16TRI. With such power scaling, the square or equilateral triangle of lattices are actually

distorted, which reduces the minimum Euclidean distance of the constellations. Therefore, we again confirm that, in contrast with OSTBC, maximization of the minimum Euclidean distance is not essential for MDC-ABBA codes.

3.6 MDC-ABBA Codes with Antenna Selection

When a low-rate feedback channel exist between receiver and transmitter, several feedback schemes have been proposed for OSTBC. Among these schemes, transmit/receive antenna selection is simple, yet provides significant SNR gain compared with the open-loop OSTBC [130, 134–136]. We will therefore investigate the performance of MDC-ABBA codes with transmit/receive antenna selection and compare MDC-ABBA codes with OSTBC with antenna selection. The transmit (or receive) antennas are selected so that the Frobenius norm of the channel is maximized.

From (3.32), let $\bar{\beta}_1 = \min(|\beta_1|, |\beta_2|), \bar{\beta}_2 = \max(|\beta_1|, |\beta_2|)$, we have

$$x \geq \sum_{j=1}^{N} \sum_{i=1}^{M/2} \left[\bar{\beta}_1^2 \left(|\lambda_{i,j,1}|^2 + |\lambda_{i,j,2}|^2 \right) \right],$$

$$x \leq \sum_{j=1}^{N} \sum_{i=1}^{M/2} \left[\bar{\beta}_2^2 \left(|\lambda_{i,j,1}|^2 + |\lambda_{i,j,2}|^2 \right) \right].$$

Since $[\lambda_{i,j,1} \ \lambda_{i,j,2}]^{\mathsf{T}} = F_2 [h_{i,j} \ h_{i+M/2,j}]^{\mathsf{T}}$, we get

$$|\lambda_{i,j,1}|^2 + |\lambda_{i,j,2}|^2 = |h_{i,j}|^2 + |h_{i+M/2,j}|^2. \tag{3.41}$$

Therefore,

$$\bar{\beta}_1^2 \| \mathcal{H} \|^2 \leq x \leq \bar{\beta}_2^2 \| \mathcal{H} \|^2. \tag{3.42}$$

Actually, $\hat{H}$ is dependent on $\mathcal{H}$. We thus rewrite the upper and lower bounds of conditional symbol PEP as

$$Q\left(\sqrt{\frac{\rho \kappa \bar{\beta}_2^2 \| \mathcal{H} \|_{\mathsf{F}}^2}{2}} \right) \leq P(d \to \hat{d} | \mathcal{H}) \leq Q\left(\sqrt{\frac{\rho \kappa \bar{\beta}_1^2 \| \mathcal{H} \|_{\mathsf{F}}^2}{2}} \right). \tag{3.43}$$

If both $\bar{\beta}_1$ and $\bar{\beta}_2$ are nonzero for all distinct pairs of symbols, the lower and upper bounds of symbol PEP of MDC-QSTBC in (3.43) are simply a symbol PEP of some OSTBC transmitted over the same channel $\mathcal{H}$ with different SNR scales. Therefore, as long

as $\bar{\beta}_1$ and $\bar{\beta}_2$ are nonzero, the symbol PEP of MDC-ABBA codes is bounded by two full-diversity symbol PEP curves. Hence, MDC-ABBA codes must achieve full diversity. From (3.34), if $\bar{\beta}_1$ and $\bar{\beta}_2$ are nonzero for all distinct pairs of symbols, the MDC-ABBA codes are full diversity; this condition also holds for the signal transformations using the rank-determinant criteria with codeword PEP [16, 120].

In the case of transmit antenna selection, only M out of M_t available transmit antennas are used. The effective channel of MDC-ABBA codes with transmit antenna selection is $\bar{\mathcal{H}}$, which consists of M columns with the largest Frobenius norm of the matrix $\mathcal{H}$. In this case, the matrix $\mathcal{H}$ in (3.43) is replaced by $\bar{\mathcal{H}}$. It is similar to the case of OSTBC with transmit antenna selection [130]. Since OSTBC achieve full diversity with transmit antenna selection, MDC-ABBA codes also achieve full diversity with transmit antenna selection.

More importantly, full diversity can be obtained with limited feedback [130]. The concept of antenna selection with limited feedback can be explained as follows. With full information feedback, choosing M out of M_t transmit antennas requires $b = \lceil \log_2 \binom{M_t}{M} \rceil$ bits and the number of feedback bits b may be large. In some scenarios, it is required to keep b small. Therefore, instead of picking one group of M antennas from the set of $\binom{M_t}{M}$ possible choices, the M antennas are selected from the set with smaller cardinality; thus, the number of feedback bits is reduced. This method is called limited feedback. Obviously, the selected M antennas may not be optimal with limited feedback, but the bandwidth of feedback channel can be set small and also the time to send the feedback would be shorter. It is shown that OSTBC can achieve full diversity with limited feedback [130]. Therefore, MDC-ABBA codes also achieve full diversity with limited feedback.

The similar explanation can be given with receive antenna selection [134]. Therefore, with transmit antenna selection and receive antenna selection, MDC-ABBA codes always achieve full diversity with full or limited feedback.

3.7 Simulation Results

Simulation results are next presented using the new decoders for ABBA and MDC-ABBA codes to compare their performances. The diversity order of MDC-ABBA codes with antenna selection is also verified. All signal constellations use Gray-bit mapping.

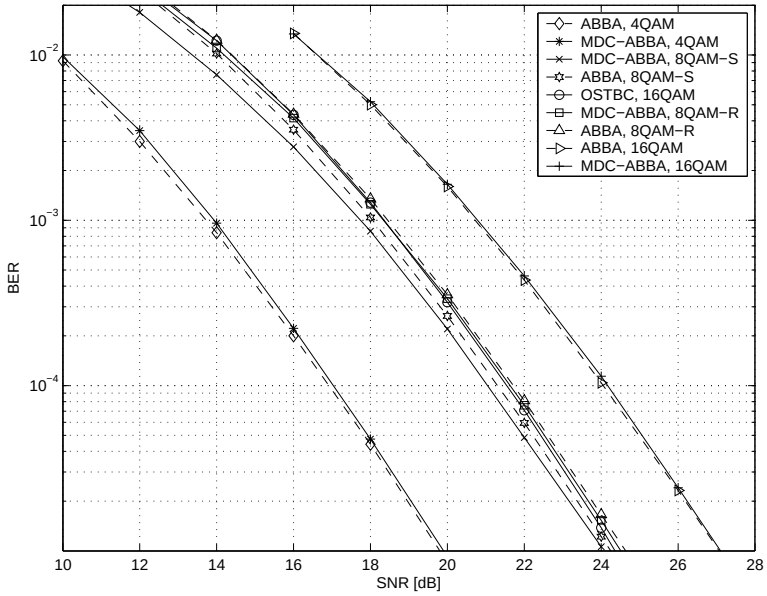

Figure 3.6: Performances of MDC-ABBA codes compared with ABBA codes and OSTBC, (4, 1) system.

3.7.1 Performance of MDC-ABBA, OSTBC, and ABBB Codes

The performances of ABBA and MDC-ABBA codes for an open loop 4 Tx/1 Rx antenna system are compared in Fig. 3.6. Performance of OSTBC rate 3/4 symbol pcu [44] with 16QAM (3 bits pcu) is also plotted in Fig. 3.6. While the performance of MDC-ABBA codes with 4- and 16QAM closely approach to that of ABBA codes, the former outperforms the latter with 8QAM-S with signal points. Therefore, the Gray-bit mapping may be not the optimal bit mapping for ABBA codes. With another 8QAM-R, MDC-ABBA code also performs better than the ABBA code but slightly worse than OSTBC. The MDC-ABBA code with 8QAM-S gains 0.5 dB over OSTBC with the same spectral efficiency of 3 bits pcu.

3.7.2 Performance of MDC-ABBA Codes with Antenna Selection

1. Diversity order of MDC-ABBA codes with transmit antenna selection and limited feedback

We examine the diversity order of MDC-ABBA codes with transmit antenna selection using limited feedback. One can choose $M = 3$ out of $M_t = 4$ available transmit antennas. Full complexity systems require $b = \left\lceil \log_2 \binom{4}{3} \right\rceil = 2$ bits to be sent back from the receiver

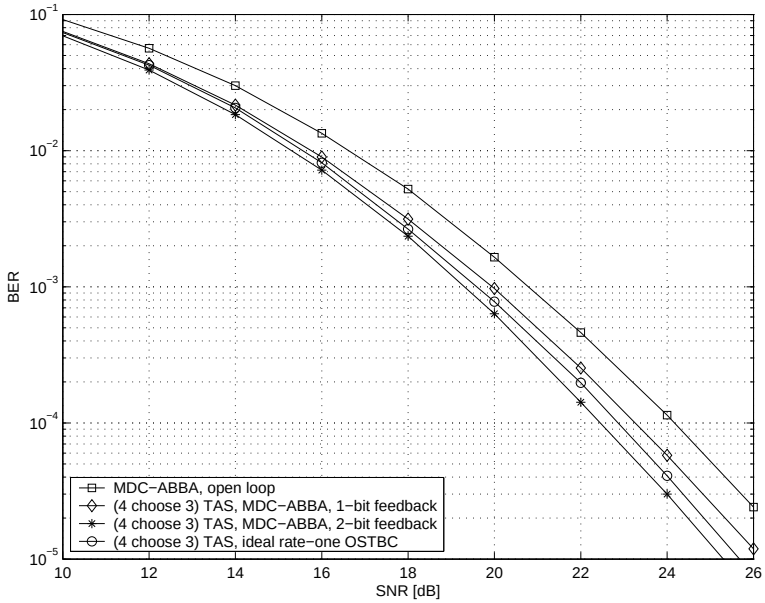

Figure 3.7: Performances of MDC-ABBA codes with limited and full feedback, choose $M = 3$ transmit antennas from $M_t = 4$ antennas, and 1 receive antenna, 16QAM.

to the transmitter. In the limited feedback system, there are only 2 possible choices to choose 3 out of 4 antennas. Thus only 1-bit feedback is needed. In Fig 3.7, performances of MDC-ABBA codes with full and limited feedback schemes are compared for $N = 1$ and using 16QAM. There is a loss of 0.5 dB when using 1-bit feedback compared with optimal transmit antenna selection (2-bit feedback). However, the 1-bit limited feedback scheme still improves 0.9 dB over the performance of the open-loop MDC-ABBA code. Performances of the two feedback schemes are compared with that of the ideal rate-one OSTBC with transmit antenna selection, which serves as the lower bound on the performance of the MDC-ABBA code with transmit antenna selection. The performance gap between the limited feedback MDC-ABBA code and the lower bound is about 0.8 dB.

2. Comparing MDC-ABBA and OSTBC with antenna selection

Performances of an MDC-ABBA code designed for 3 transmit antennas with transmit antenna selection is presented in Fig. 3.8. The number of available antennas $M_t = 4$ and 1 receive antenna. Compared with the open loop case, the MDC-ABBA code with transmit antenna selection and 16QAM gains about 1.2 dB. Especially, the performance of $\binom{4}{3}$ transmit antenna selection is slightly better than that of an ideal imaginative rate-one OSTBC using the same 16QAM. Note that the performance of an ideal hypothetical

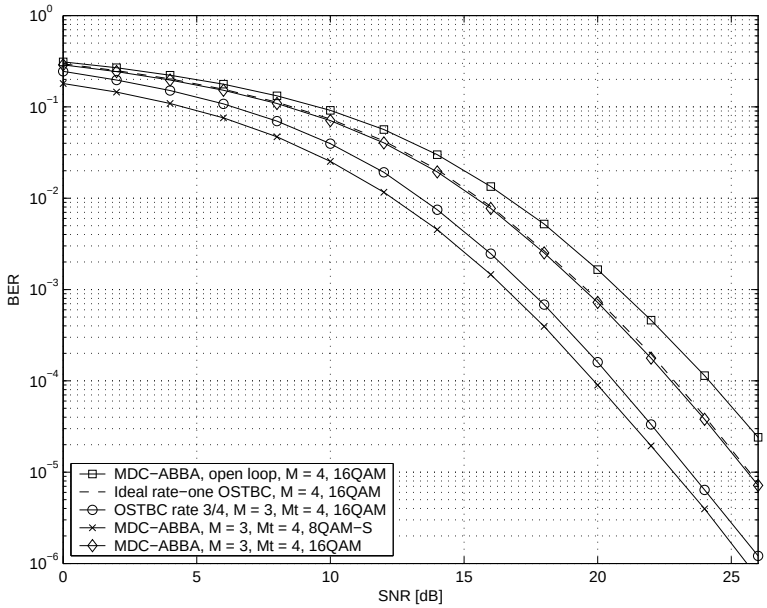

Figure 3.8: Performances of MDC-ABBA codes and OSTBC designed for $M = 3$ with transmit antennas selection, number of available antennas $M_t = 4$, and 1 receive antenna.

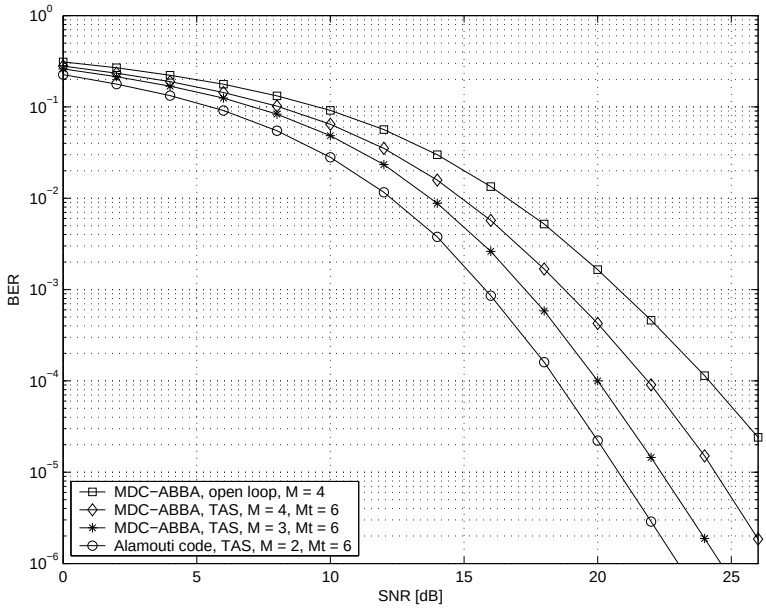

Figure 3.9: Performances of MDC codes with transmit antennas selection, 16QAM (4 bits pcu), number of available antennas $M_t = 6$, number of active antennas $M = 2, 3, 4$, and 1 receive antenna.

rate-one OSTBC is also the performance limit of ABBA-QSTBC with phase feedback schemes [122–124]. Compared with OSTBC for the same spectral efficiency of 3 bits pcu and transmit antenna selection, MDC-ABBA code gains 0.8 dB.

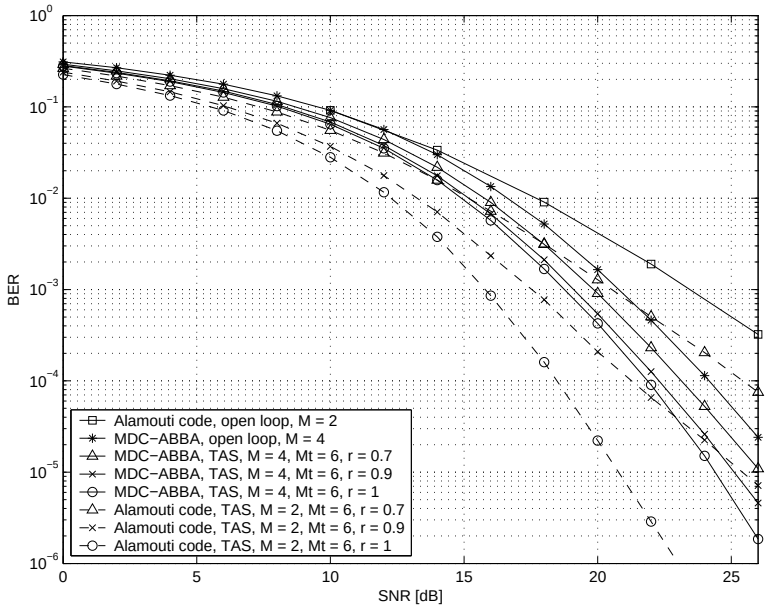

Figure 3.10: Performances of MDC codes compared with the Alamouti code when feedback is delayed, 16QAM (4 bits pcu), number of available antennas $M_t = 6$, number of active antennas $M = 2, 4$, and 1 receive antenna.

In Fig. 3.9, we compare the performances of MDC-ABBA codes for 3 and 4 transmit antennas with that of the Alamouti code. All these STBC are considered with transmit antenna selection, where the available transmit antennas $M_t = 6$ and 1 receive antenna, and all codes have rates of 1 symbol pcu and use 16QAM. The Alamouti code performs significantly better than MDC-ABBA codes. However, this excellent improvement is obtained with a perfect assumption: there is no feedback delay. In case of delayed feedback, the transmitter has the outdated channel state information. We provide the simulation results with correlation covariance coefficient of the actual and outdated channel gains $r = 0.9$ and 0.7 in Fig. 3.10. The advantage of the Alamouti code over MDC-ABBA codes with transmit antenna selection vanishes quickly when $r = 0.7$; the Alamouti code performs worse than MDC-ABBA codes when SNR > 17.5 dB.

3.8 Summary

In this chapter, we have applied the framework of OEST codes to thoroughly analyze ABBA QSTBC. We have derived the general decoder of ABBA codes, to allow either pairwise or single complex symbol decoding. Existing signal transformations were adapted for

the newly proposed decoder of MDC-ABBA codes. A tight union bound on the SER was presented and used to optimize the signal rotations for MDC-ABBA codes with various signal constellations. We have also proposed a new method combining the optimal power allocation and signal rotation to find the best signal transformation for inphase-quadrature power-imbalanced constellations such as rectangular QAM. Our new signal transformations perform better than the existing ones and also have lower encoding/decoding complexities. The MDC-ABBA codes have been shown to achieve full diversity with antenna selection and with full or limited feedback. Although our analysis is restricted to the ABBA codes, it can be also extended for other QSTBC in [46, 48] and coordinate interleaved orthogonal designs (CIOD) [92].

Chapter 4

Four-Group Decodable SAST Codes

In Chapter 2, ABBA QSTBC, as a special case of OEST codes, is K-group decodable. In Chapter 3, we show that by a new encoding method, ABBA codes are actually $2K$-group decodable. The single-symbol decoding capability of ABBA codes is obtained because their equivalent channel is a real matrix. In general, the equivalent channels of OEST codes are complex matrices, which make the decoding complexity reduction difficult or impossible. In this chapter, we will solve this problem by proposing a more sophisticated encoding method for OEST codes by exploiting the circulant property of the equivalent channel to obtain lower decoding complexity OEST codes. Hence, OEST codes are $2K$-group decodable in general.

Among subclasses of OEST codes, SAST codes have several distinguishing properties such as near-capacity performance, rate-one for any number of transmit antennas, and better performance than several existing codes. Therefore, we will present the new encoding method to obtain lower decoding complexity for SAST codes. Recall that SAST codes are constructed from the Alamouti code with $K = 2$. Thus, the new encoding method will make SAST codes 4-group decodable.

4.1 General Encoder of $2K$-Group OEST Codes

Recall that in Section 2.3, before mapping a data vector (of P symbols) into a circulant matrix, each element (data symbol) of the data vector is rotated separately by a specific angle to make the OEST codes full diversity. We now consider a joint rotation of all the data symbols, i.e. to rotate the data vectors by a special matrix, namely *inverse discrete*

Fourier transform (IDFT) $\mathcal{F}^\dagger$ [64]. Let $\boldsymbol{x}$ be the data vector, the rotated vector is

$$\boldsymbol{s} = \mathcal{F}^\dagger \boldsymbol{x}. \tag{4.1}$$

We consider the simple case of circulant STBC. The data vector is first rotated as in (4.1), and then mapped to a circulant STBC. Our question is how many groups of symbols can be separated at the receiver for maximum likelihood detection? To answer this question, we need to examine the dispersion matrices of the circulant STBC with respect to Theorem 2.2. Let $x_i = a_i + \mathsf{j}\, b_i$ ($i = 1, \ldots, P$), and $\mathcal{F}^\dagger = \begin{bmatrix} f_{ik} \end{bmatrix} = \begin{bmatrix} \boldsymbol{f}_1 & \boldsymbol{f}_2 & \ldots & \boldsymbol{f}_P \end{bmatrix}$ ($f_{ik} = \frac{1}{\sqrt{P}} e^{\mathsf{j}\, 2\pi(i-1)(k-1)}$), we have

$$\begin{aligned} \mathcal{C}(\boldsymbol{s}) &= \begin{bmatrix} s_1 & s_2 & \ldots & s_P \\ s_P & s_1 & \ldots & s_{P-1} \\ \vdots & \vdots & \ddots & \vdots \\ s_2 & s_3 & \ldots & s_1 \end{bmatrix} \\ &= \sum_{k=1}^{P} a_k A_k + \sum_{k=1}^{P} b_k B_k \end{aligned} \tag{4.2}$$

where

$$A_k = \sum_{i=1}^{P} f_{ik} \pi^{i-1} = \mathcal{C}(\boldsymbol{f}_k), \tag{4.3}$$

$$B_k = \mathsf{j} \sum_{i=1}^{P} f_{ik} \pi^{i-1} = \mathsf{j}\, \mathcal{C}(\boldsymbol{f}_k). \tag{4.4}$$

Let Λ_k be the vector containing the eigenvalues of A_k. Since A_k is circulant, the eigenvalues of A_k can be found by taking the unnormalized DFT of $\boldsymbol{f}_k$ [64]. Therefore, $\Lambda_k = \sqrt{P}\mathcal{F}\boldsymbol{f}_k = \begin{bmatrix} 0 & \ldots & 0 & \sqrt{P} & 0 & \ldots & 0 \end{bmatrix}^\mathsf{T}$ and the only nonzero eigenvalue appears at the k position.

Now we consider two different dispersion matrices A_i and A_j of two real symbols a_i and a_j, respectively, and one has

$$A_i^\dagger A_j + A_j^\dagger A_i = \mathcal{F}^\dagger \operatorname{diag}(\Lambda_i^\dagger) \operatorname{diag}(\Lambda_j) \mathcal{F} + \mathcal{F}^\dagger \operatorname{diag}(\Lambda_j^\dagger) \operatorname{diag}(\Lambda_i) \mathcal{F} = \mathbf{0}\,. \tag{4.5}$$

Thus, according to Theorem 2.2, the real symbols a_i and a_j can be separated at the receiver. Similarly, we can show that real symbols a_i and b_j can be separated as well. It means that all

the real symbols can be decoupled for maximum likelihood detection or we obtain single-real symbol decoding complexity. This result is beyond our expectation since we just try to get two-group decoding for circulant STBC.

However, since the dispersion matrices A_k and B_k have only one nonzero eigenvalue, these dispersion matrices are of rank one; one cannot obtain full diversity circulant STBC. On the other hand, each circulant matrix A_k has only one nonzero eigenvalue at kth position. Therefore, if $\bar{A}$ is a linear combination of P circulant matrices $A_k, k = 1, \ldots, P$, $\bar{A}$ will have P nonzero eigenvalues or $\bar{A}$ is full rank. This means one more time the real symbols a_i (or b_i) must be spread out over the new dispersion matrices, which are the linear combination of P dispersion matrices $A_k, k = 1, \ldots, P$ (or $B_k, k = 1, \ldots, P$).

We summarize the above results as follows.

- With signal rotation (4.1), circulant STBC are single real-symbol decodable. However, the diversity order is only 1.

- To achieve full diversity, the data vector must be rotated by another rotation matrix R before applying the rotation (4.1). Thus, the compound rotation matrix is in the form $\mathcal{F}^\dagger R$. With this two rotating stages, the circulant STBC is two-group decodable. Consequently, the product $\mathcal{C}(\boldsymbol{s})^\dagger \mathcal{C}(\boldsymbol{s})$ can be written as the sum of two terms, each contains the symbols from one group only.

We now consider the general construction of OEST codes, where the circulant matrices are embedded. If the matrices of two-group circulant STBC are substituted to (2.29), we get $2K$ terms. Hence, OEST codes are actually $2K$-group decodable and full-diversity is achievable. We state the main result of this section in the following theorem.

Theorem 4.1. *Using the signal rotation of the form $\mathcal{F}^\dagger R$, OEST codes are $2K$-group decodable and full diversity can be achieved.*

To appreciate the advantages of 4-group SAST codes, we will compare the main parameters of SAST codes and other low-complexity STBC, including OSTBC, QSTBC, MDC-QSTBC, and codes from coordinate-interleaved orthogonal designs (CIOD) [92], for 6 and 8 transmit antennas in Table 4.1. Clearly, the new 4-group SAST codes offer several distinct advantages, such as higher code rate, lower decoding complexity, and lower

Table 4.1: Comparison of Several Low-Complexity STBC for 6 and 8 Antennas

Codes	Γ	Maximal rate	Delay	Real symbol decoding
OSTBC [44, 137]	$2K$ or K	2/3 (5/8)[a]	30 (56)	1 or 2 (1 or 2)
CIOD [92]	K	6/7 (4/5)	14 (50)	2 (2)
MDC-ABBA [120]	K	3/4 (3/4)	8 (8)	2 (2)
QSTBC [47]	$K/2$	3/4 (3/4)	8 (8)	4 (4)
2-group QSTBC [96]	2	1 (1)	8 (8)	8 (8)
SAST	2	1 (1)	6 (8)	6 (8)
4-group QSTBC [93]	4	1 (1)	8 (8)	4 (4)
4-group SAST (new)	4	**1** (**1**)	**6** (**8**)	**3** (**4**)

[a]The numbers in the parentheses indicate the codes' parameters for 8 antennas.

encoding/decoding delay. The 4-group SAST codes also have lower PAPR than that of OSTBC, QSTBC, MDC-QSTBC, and CIOD codes because there are no zeros in the code matrices. Moreover, from extensive simulation results, our 4-group SAST codes also yield significant SNR gains compared with the existing codes.

In the next section, we will present the decoding of OEST codes with two steps. The first step is to separate K transmitted vectors of data symbols, as solved in Chapter 2. The second step will decompose the real and imaginary parts of each data vector for maximum likelihood detection. As mentioned earlier, we will illustrate these two decoding steps for the representative SAST codes.

4.2 Decoder for 4-Group SAST Codes

To obtain 4-group decodable SAST codes, we need two steps. The first step is to decouple the transmitted symbols into two group. The second step will separate each group into two smaller groups. The first step has been solved in Section 2.3.4 of Chapter 2. Nevertheless, for the case of SAST codes, we can develop an alternative approach to design the decoder, which is more computationally efficient by reducing intermediate deriving steps.

We first review the construction of SAST codes introduced in Section 2.3.6. The SAST code matrix is constructed for $M = 2P$ transmit antennas using circulant blocks. Two data

vectors $\boldsymbol{s}_1 = \begin{bmatrix} s_1 & s_2 & \dots & s_P \end{bmatrix}^\mathsf{T}$ and $\boldsymbol{s}_2 = \begin{bmatrix} s_{P+1} & s_{P+2} & \dots & s_{2P} \end{bmatrix}^\mathsf{T}$ are used to generate two circulant matrices:

$$\mathcal{C}(\boldsymbol{s}_1) = \begin{bmatrix} s_1 & s_2 & \dots & s_P \\ s_P & s_1 & \dots & s_{P-1} \\ \vdots & \vdots & \ddots & \vdots \\ s_2 & s_3 & \dots & s_1 \end{bmatrix}, \qquad \mathcal{C}(\boldsymbol{s}_2) = \begin{bmatrix} s_{P+1} & s_{P+2} & \dots & s_{2P} \\ s_{2P} & s_{P+1} & \dots & s_{2P-1} \\ \vdots & \vdots & \ddots & \vdots \\ s_{P+2} & s_{P+3} & \dots & s_{P+1} \end{bmatrix}. \tag{4.6}$$

The SAST code matrix is constructed from $\mathcal{C}(\boldsymbol{s}_1)$ and $\mathcal{C}(\boldsymbol{s}_2)$as

$$\mathcal{S} = \begin{bmatrix} \mathcal{C}(\boldsymbol{s}_1) & \mathcal{C}(\boldsymbol{s}_2) \\ -\mathcal{C}^\dagger(\boldsymbol{s}_2) & \mathcal{C}^\dagger(\boldsymbol{s}_1) \end{bmatrix}. \tag{4.7}$$

For example, the SAST code for 6 transmit antennas is

$$\mathcal{S}_6 = \begin{bmatrix} u_1 & u_2 & u_3 & u_4 & u_5 & u_6 \\ u_3 & u_1 & u_2 & u_6 & u_4 & u_5 \\ u_2 & u_3 & u_1 & u_5 & u_6 & u_4 \\ -u_4^* & -u_6^* & -u_5^* & u_1^* & u_3^* & u_2^* \\ -u_5^* & -u_4^* & -u_6^* & u_2^* & u_1^* & u_3^* \\ -u_6^* & -u_5^* & -u_4^* & u_3^* & u_2^* & u_1^* \end{bmatrix}. \tag{4.8}$$

We introduce another type of circulant matrix called left ciculant, denoted by $\mathcal{C}_L(\boldsymbol{x})$, where the ith row is obtained by circular shifts $(i-1)$ times to the left the row vector $\boldsymbol{x}$.

$$\mathcal{C}_L(\boldsymbol{x}) = \begin{bmatrix} x_1 & x_2 & \dots & x_P \\ x_2 & x_3 & \dots & x_1 \\ \vdots & \vdots & \ddots & \vdots \\ x_P & x_1 & \dots & x_{P-1} \end{bmatrix}. \tag{4.9}$$

Let us define a permutation $\mathit{\Pi}$ on an arbitrary matrix X such that, the $(P-i+2)$th row is permuted with the ith row for $i = 2, 3, ..., \lceil \frac{P}{2} \rceil$, where $\lceil(\cdot)\rceil$ is the ceiling function. One can verify that

$$\mathit{\Pi}(\mathcal{C}_L(\boldsymbol{x})) = \mathcal{C}(\boldsymbol{x}). \tag{4.10}$$

This useful operator will be used for our next derivation.

Let $\boldsymbol{y} = \begin{bmatrix} \boldsymbol{y}_1^\mathsf{T} & \boldsymbol{y}_2^\mathsf{T} \end{bmatrix}^\mathsf{T}$, $\boldsymbol{y}_1 = \begin{bmatrix} y_1 & y_2 & \dots & y_P \end{bmatrix}^\mathsf{T}$, $\boldsymbol{y}_2 = \begin{bmatrix} y_{P+1} & y_{P+2} & \dots & y_M \end{bmatrix}^\mathsf{T}$, $\boldsymbol{h} = \begin{bmatrix} \boldsymbol{h}_1^\mathsf{T} & \boldsymbol{h}_2^\mathsf{T} \end{bmatrix}^\mathsf{T}$, $\boldsymbol{h}_1 = \begin{bmatrix} h_1 & h_2 & \dots & h_P \end{bmatrix}^\mathsf{T}$, $\boldsymbol{h}_2 = \begin{bmatrix} h_{P+1} & h_{P+2} & \dots & h_{2P} \end{bmatrix}^\mathsf{T}$, $\boldsymbol{w} = \begin{bmatrix} \boldsymbol{w}_1^\mathsf{T} & \boldsymbol{w}_2^\mathsf{T} \end{bmatrix}^\mathsf{T}$, $\boldsymbol{w}_1 = \begin{bmatrix} w_1 & w_2 & \dots & w_P \end{bmatrix}^\mathsf{T}$, $\boldsymbol{w}_2 = \begin{bmatrix} w_{P+1} & w_{P+2} & \dots & w_{2P} \end{bmatrix}^\mathsf{T}$.

We can write the transmit-receive signal relation as

$$\begin{bmatrix} \boldsymbol{y}_1 \\ \boldsymbol{y}_2 \end{bmatrix} = \sqrt{\frac{\rho}{M}} \begin{bmatrix} \mathcal{C}(\boldsymbol{s}_1) & \mathcal{C}(\boldsymbol{s}_2) \\ -\mathcal{C}^\dagger(\boldsymbol{s}_2) & \mathcal{C}^\dagger(\boldsymbol{s}_1) \end{bmatrix} \begin{bmatrix} \boldsymbol{h}_1 \\ \boldsymbol{h}_2 \end{bmatrix} + \begin{bmatrix} \boldsymbol{w}_1 \\ \boldsymbol{w}_2 \end{bmatrix}. \tag{4.11}$$

Applying permutation $\mathit{\Pi}$ in (4.10) for the column matrix $\boldsymbol{y}_1$, we obtain [100]:

$$\begin{bmatrix} \bar{\boldsymbol{y}}_1 \\ \bar{\boldsymbol{y}}_2 \end{bmatrix} \triangleq \begin{bmatrix} \mathit{\Pi}(\boldsymbol{y}_1) \\ \boldsymbol{y}_2^* \end{bmatrix} = \sqrt{\frac{\rho}{M}} \underbrace{\begin{bmatrix} H_1 & H_2 \\ H_2^\dagger & -H_1^\dagger \end{bmatrix}}_{\mathcal{H}} \begin{bmatrix} \boldsymbol{s}_1 \\ \boldsymbol{s}_2 \end{bmatrix} + \begin{bmatrix} \bar{\boldsymbol{w}}_1 \\ \bar{\boldsymbol{w}}_2 \end{bmatrix} \tag{4.12}$$

where $H_1 = \mathcal{C}(\boldsymbol{h}_1)$, $H_2 = \mathcal{C}(\boldsymbol{h}_2)$, $\bar{\boldsymbol{w}}_1 = \mathit{\Pi}(\boldsymbol{w}_1)$, $\bar{\boldsymbol{w}}_2 = \boldsymbol{w}_2^*$. The elements of $\bar{\boldsymbol{w}}_1$ and $\bar{\boldsymbol{w}}_2$ have the same statistics, $\mathcal{CN}(0,1)$, as elements of $\boldsymbol{w}_1$ and $\boldsymbol{w}_2$.

We now multiply $\mathcal{H}^\dagger$ with the both sides of (4.12). Let $\hat{\mathcal{H}} = H_1^\dagger H_1 + H_2^\dagger H_2$, we get

$$\begin{aligned} \begin{bmatrix} \hat{\boldsymbol{y}}_1 \\ \hat{\boldsymbol{y}}_2 \end{bmatrix} &= \mathcal{H}^\dagger \begin{bmatrix} \bar{\boldsymbol{y}}_1 \\ \bar{\boldsymbol{y}}_2 \end{bmatrix} = \sqrt{\frac{\rho}{M}} \begin{bmatrix} \hat{\mathcal{H}} & \boldsymbol{0}_P \\ \boldsymbol{0}_P & \hat{\mathcal{H}} \end{bmatrix} \begin{bmatrix} \boldsymbol{s}_1 \\ \boldsymbol{s}_2 \end{bmatrix} + \mathcal{H}^\dagger \begin{bmatrix} \bar{\boldsymbol{w}}_1 \\ \bar{\boldsymbol{w}}_2 \end{bmatrix} \\ &= \sqrt{\frac{\rho}{M}} \begin{bmatrix} \hat{\mathcal{H}} & \boldsymbol{0}_P \\ \boldsymbol{0}_P & \hat{\mathcal{H}} \end{bmatrix} \begin{bmatrix} \boldsymbol{s}_1 \\ \boldsymbol{s}_2 \end{bmatrix} + \underbrace{\begin{bmatrix} \hat{\boldsymbol{w}}_1 \\ \hat{\boldsymbol{w}}_2 \end{bmatrix}}_{\hat{\boldsymbol{w}}}. \end{aligned} \tag{4.13}$$

The covariance matrix of the additive noise vector $\hat{\boldsymbol{w}}$ is

$$E[\boldsymbol{w}\boldsymbol{w}^\dagger] = \begin{bmatrix} \hat{\mathcal{H}} & \boldsymbol{0}_P \\ \boldsymbol{0}_P & \hat{\mathcal{H}} \end{bmatrix}. \tag{4.14}$$

Therefore, noise vectors $\hat{\boldsymbol{w}}_1$ and $\hat{\boldsymbol{w}}_s$ are uncorrelated and have the same covariance matrix $\hat{\mathcal{H}}$. Thus, $\boldsymbol{s}_1$ and $\boldsymbol{s}_2$ can be decoded separately using $\hat{\boldsymbol{y}}_i = \hat{\mathcal{H}}\boldsymbol{s}_i + \hat{\boldsymbol{w}}_i$, $i = 1, 2$. The noise vectors $\hat{\boldsymbol{w}}_1$ and $\hat{\boldsymbol{w}}_s$ can be whiten by the same whitening matrix $\hat{\mathcal{H}}^{-1/2}$. The equivalent equations for transmit-receive signals are

$$\hat{\mathcal{H}}^{-1/2}\hat{\boldsymbol{y}}_i = \sqrt{\frac{\rho}{M}}\hat{\mathcal{H}}^{1/2}\boldsymbol{s}_i + \hat{\mathcal{H}}^{-1/2}\hat{\boldsymbol{w}}_i, \qquad i = 1, 2. \tag{4.15}$$

At this point, the decoding of SAST codes becomes the detection of 2 group of complex symbols $\boldsymbol{s}_i$ $(i = 1, 2)$. Our next step is to separate the real and imaginary parts of vectors $\boldsymbol{s}_i$ by exploiting the properties of $\hat{\mathcal{H}}$.

Recall that $\hat{\mathcal{H}} = H_1^\dagger H_1 + H_2^\dagger H_2$, and both H_1 and H_2 are circulant. Hence, $\hat{\mathcal{H}}$ is also circulant [64]. Let $\mathit{\Lambda}_i = \begin{bmatrix} \lambda_{i,1} & \lambda_{i,2} & \dots & \lambda_{i,P} \end{bmatrix}$ be the P eigenvalues of H_i $(i = 1, 2)$. We can diagonalized H_i by Fourier transform matrix as $H_i = \mathcal{F}^\dagger \mathit{\Lambda}_i \mathcal{F}$. Thus,

$$\hat{\mathcal{H}} = \mathcal{F}^\dagger(\mathit{\Lambda}_1^\dagger\mathit{\Lambda}_1 + \mathit{\Lambda}_2^\dagger\mathit{\Lambda}_2)\,\mathcal{F}\,. \tag{4.16}$$

Let $\mathit{\Lambda}_1^\dagger\mathit{\Lambda}_1 + \mathit{\Lambda}_2^\dagger\mathit{\Lambda}_2 = \mathit{\Lambda}$, then $\mathit{\Lambda}$ has non-negative entries in the main diagonal and

$$\hat{\mathcal{H}}^{1/2} = \mathcal{F}^\dagger \mathit{\Lambda}^{1/2}\,\mathcal{F}, \tag{4.17a}$$

$$\hat{\mathcal{H}}^{-1/2} = \mathcal{F}^\dagger \mathit{\Lambda}^{-1/2}\,\mathcal{F}\,. \tag{4.17b}$$

We have $\boldsymbol{s}_i$ is pre-multiplied (or rotated) by a matrix $\mathcal{F}^\dagger$. Substituting $\boldsymbol{s}_i$ by $\mathcal{F}^\dagger \boldsymbol{s}_i$ and multiplying both sides of (4.15) with $\mathcal{F}$, one obtains

$$\begin{aligned}\Lambda^{-1/2}\mathcal{F}\hat{\boldsymbol{y}}_i &= \sqrt{\frac{\rho}{M}}\mathcal{F}\hat{\mathcal{H}}^{1/2}\mathcal{F}^\dagger \boldsymbol{s}_i + \Lambda^{-1/2}\mathcal{F}\hat{\boldsymbol{w}}_i \\ &= \sqrt{\frac{\rho}{M}}\Lambda^{1/2}\boldsymbol{s}_i + \underbrace{\Lambda^{-1/2}\mathcal{F}\hat{\boldsymbol{w}}_i}_{\check{\boldsymbol{w}}_i}. \end{aligned} \tag{4.18}$$

Since $\Lambda^{1/2}$ has real elements (in the main diagonal), the real and imaginary parts of $\boldsymbol{s}_i$ now can be separated for detection.

$$\Lambda^{-1/2}\Re(\mathcal{F}\hat{\boldsymbol{y}}_i) = \sqrt{\frac{\rho}{M}}\Lambda^{1/2}\Re(\boldsymbol{s}_i) + \Re(\check{\boldsymbol{w}}_i), \tag{4.19a}$$

$$\Lambda^{-1/2}\Im(\mathcal{F}\hat{\boldsymbol{y}}_i) = \sqrt{\frac{\rho}{M}}\Lambda^{1/2}\Im(\boldsymbol{s}_i) + \Im(\check{\boldsymbol{w}}_i). \tag{4.19b}$$

Using (4.19), one can use a sphere decoder to detect the transmitted symbols. The *equivalent channel* of 4-group SAST codes is $\Lambda^{1/2}$.

We thus have derived the general decoder for 4-group SAST codes. The role of the IDFT rotation matrix $\mathcal{F}^\dagger$ is to diagonalize the channel, facilitating the lower decoding complexity for SAST codes. We next analyze the performance of the 4-group SAST codes.

4.3 Performance Analysis

Note that the eigenvalues of $P \times P$ matrices H_1 and H_2 can be found easily using unnormalized Fourier transformation of the channel vectors $\boldsymbol{h}_1$ and $\boldsymbol{h}_2$ [64]. Therefore, the eigenvalues of H_1 and H_2 have distribution $\sim \mathcal{CN}(0, P)$.

We introduce a real orthogonal transformation R to the data vectors $\Re(\boldsymbol{s}_i)$ and $\Im(\boldsymbol{s}_i)$ $(i = 1, 2)$ to make 4-group SAST codes full diversity. Thus, the actual signal rotation of 4-group SAST codes is $\mathcal{F}^\dagger R$.

Since the PEP of vectors $\Re(\boldsymbol{s}_i)$ and $\Im(\boldsymbol{s}_i)$ $(i = 1, 2)$ are the same, we just calculate the PEP of the vector $\Re(\boldsymbol{s}_1)$. Let $\boldsymbol{d} = \Re(\boldsymbol{s}_1) = \begin{bmatrix} a_1 & a_2 & \dots & a_P \end{bmatrix}^\mathsf{T}$.

The PEP of the pair $\boldsymbol{d}$ and $\bar{\boldsymbol{d}}$ can be expressed by the Gaussian tail function as [32]

$$P(\boldsymbol{d} \to \bar{\boldsymbol{d}}|\hat{\mathcal{H}}) = Q\left(\sqrt{\frac{\rho}{8}\frac{|\Lambda^{1/2}R\boldsymbol{\delta}|^2}{4N_0}}\right) \tag{4.20}$$

where $N_0 = 1/2$ is the variance of the elements of the white noise vector $\Re(\check{\boldsymbol{w}}_1)$ in (4.19a), $\boldsymbol{\delta} = \boldsymbol{d} - \bar{\boldsymbol{d}}$. Substituting $\Lambda = \Lambda_1^\dagger \Lambda_1 + \Lambda_2^\dagger \Lambda_2$, one has

$$\begin{aligned} P(\boldsymbol{d} \to \bar{\boldsymbol{d}}|\hat{\mathcal{H}}) &= Q\left(\sqrt{\frac{\rho\left[\boldsymbol{\delta}^\mathsf{T} R^\mathsf{T}(\Lambda_1^\dagger \Lambda_1 + \Lambda_2^\dagger \Lambda_2) R\boldsymbol{\delta}\right]}{16}}\right) \\ &= Q\left(\sqrt{\frac{\rho(\sum_{i=1}^{2}\sum_{j=1}^{P}\beta_j^2|\lambda_{i,j}|^2)}{16}}\right) \end{aligned} \tag{4.21}$$

where $\boldsymbol{\beta} = R\boldsymbol{\delta}$.

We now use the Craig's formula [131] to derive the conditional PEP in (4.20).

$$\begin{aligned} P(\boldsymbol{d} \to \bar{\boldsymbol{d}}|\hat{\mathcal{H}}) &= Q\left(\sqrt{\frac{\rho(\sum_{i=1}^{2}\sum_{j=1}^{P}\beta_j^2|\lambda_{i,j}|^2)}{16}}\right) \\ &= \frac{1}{\pi}\int_0^{\pi/2} \exp\left(\frac{-\rho(\sum_{i=1}^{2}\sum_{j=1}^{P}\beta_j^2|\lambda_{i,j}|^2)}{32\sin^2\alpha}\right) d\alpha. \end{aligned} \tag{4.22}$$

We can apply a method based on the moment generating function (MGF) [132, 133] to obtain the unconditional PEP in the following:

$$P(\boldsymbol{d} \to \bar{\boldsymbol{d}}) = \frac{1}{\pi}\int_0^{\pi/2}\left[\prod_{i=1}^{P}\left(1 + \frac{\rho\beta_i^2}{8\sin^2\alpha}\right)\right]^{-2} d\alpha. \tag{4.23}$$

Since there are four vectors to be decoded in each code matrix, the codeword PEP is therefore equal to 4 times the PEP given in (4.23).

Assume that $\beta_i \neq 0\ \forall i = 1, 2, \ldots, P$. One can find the upper bound on PEP of 4-group SAST codes at high SNR as follows.

$$\begin{aligned} P(\boldsymbol{d} \to \bar{\boldsymbol{d}}) &\approx \left(\frac{2^{6m}\rho^{-2P}}{\pi}\int_0^{\pi/2}(\sin\alpha)^{16}d\alpha\right)\prod_{i=1}^{P}\beta_i^{-4} \\ &= \frac{2^{3M}\rho^{-M}}{2^{17}}\frac{16!}{8!8!}\prod_{i=1}^{M/2}\beta_i^{-4}. \end{aligned} \tag{4.24}$$

The asymptotic bound in (4.24) shows an important property of the 4-group SAST codes at high SNR: The PEP is heavily dependent on the product distance $\prod_{i=1}^{4}\beta_i$ (see, e.g. [138]). The exponent of SNR in (4.24) is $-M$. This indicates that the maximum

diversity order of 4-group QSTBC is 8 and it is achievable if the product distance is non-zero for all possible data vectors. Furthermore, at high SNR, the asymptotic bound becomes very tight to the exact PEP. Therefore, the larger the product distance, the lower FER can be obtained. Thus, we can optimize the rotation by R so that the minimum product distance

$$d_{p,\min} = \min_{\forall \boldsymbol{d}^i, \boldsymbol{d}^j} \prod_{k=1}^{4} |\beta_k| \tag{4.25}$$

is non-zero and maximized.

For QAM signals, the symbols a_i and b_i are in the set $\{\pm 1, \pm 3, \pm 5, \dots\}$, the best-known rotations for QAM that maximizes the minimum product distance are provided in [139, 140]; they are denoted by R_{BOV}.

In [139, 140], the rotated lattice points are generated by $\boldsymbol{x} = \boldsymbol{d} R_{BOV}$, where $\boldsymbol{d} \in \mathbb{Z}^n$ and R_{BOV} is of size $n \times n$. In this representation, $\boldsymbol{x}$ and $\boldsymbol{d}$ are row vectors, while we use column vector notation in our paper. Thus, the rotation matrices R_{BOV} given in [139, 140] will be transposed. For the 3 and 4-dimensional lattices, the rotation matrices are given below.

$$R_{BOV,3} = \begin{bmatrix} -0.3279852776 & -0.7369762291 & -0.5910090485 \\ -0.5910090485 & -0.3279852776 & 0.7369762291 \\ -0.7369762291 & 0.5910090485 & -0.3279852776 \end{bmatrix}, \tag{4.26}$$

$$R_{BOV,4} = \begin{bmatrix} -0.3663925121 & -0.2264430248 & -0.4744647080 & -0.7677000246 \\ -0.7677000238 & -0.4744647078 & 0.2264430248 & 0.3663925106 \\ 0.4230815704 & -0.6845603618 & -0.5049593144 & 0.3120820189 \\ 0.3120820187 & -0.5049593142 & 0.6845603618 & -0.4230815707 \end{bmatrix}. \tag{4.27}$$

Note that in the construction of 4-group SAST codes, the data vectors $\boldsymbol{s}_i$ $(i = 1, 2)$ with proper size are rotated to generate the vectors $\boldsymbol{u}_i$ as $\boldsymbol{u}_i = \mathcal{F}^\dagger R \boldsymbol{s}_i$.

4.4 Simulation Results

4.4.1 Union Bound on FER

It is of interest to investigate the union bound on FER of 4-group SAST codes using the exact PEP in (4.23). The union bound and simulated FER of a 4-group SAST code for 6 antennas is plotted in Fig. 4.1. The bound is only about 0.1 dB from the simulated FER when FER < 10^{-2}. Therefore, instead of optimizing the worst-case PEP, the union bound can be optimized to obtain lower FER.

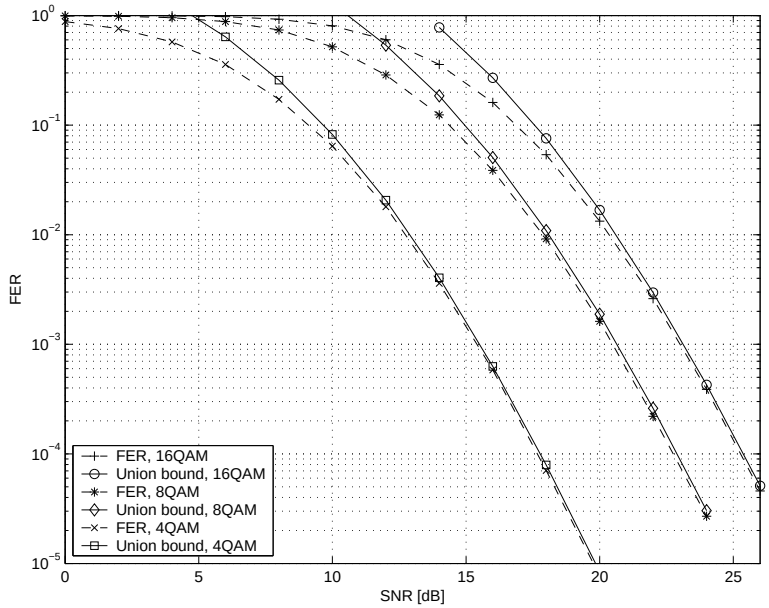

Figure 4.1: Union bound on FER of 4-group SAST codes for (6, 1) system.

4.4.2 Performance of 4-Group SAST Codes

The performance of 4-group SAST codes will be compared with OSTBC, MDC-QSTBC [120], QSTBC [47, 61], DAST [49], 4-group QSTBC [93], and SAST codes. The performance of CIOD codes [92] is not compared because of two reasons: (1) We could not find suitable constellations for maximal-rate CIOD codes [92] so that CIOD codes have the same bit rates with our newly developed codes; (2) Since the minimal-delay CIOD codes have the same code rate and performance as that of MDC-QSTBC [92, 125], it is enough to compare the performance of our codes with that of MDC-QSTBC.

Since 4-group SAST for 4 transmit antennas is equivalent to MDC-ABBA, we thus present the results for 5, 6, and 8 transmit antennas. The number of receive antennas is one in all simulations.

1. Performance 4-group SAST codes for 6 transmit antennas

Since the rate of OSTBC for 6 transmit antennas is $2/3$ symbol pcu [44], we use 8QAM to produce a data rate of 2 bits pcu and compare performances of OSTBC and our new codes in Fig. 4.3. The rate of 4-group QSTBC and 4-group SAST codes is one. We thus use 4QAM to obtain 2 bits pcu. Two columns (4 and 8) of 4-group QSTBC for 8 transmit antennas is deleted to create the code for 6 transmit antennas. With spectral efficiency

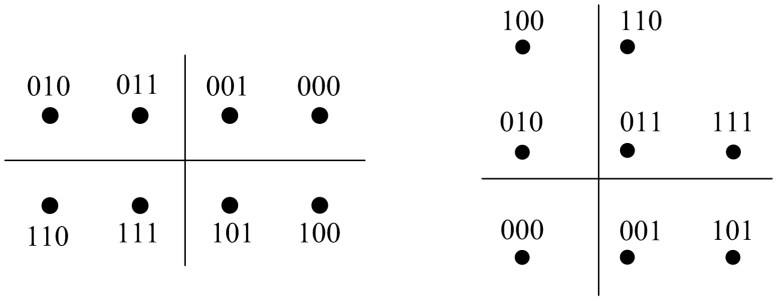

(a) 8QAM-R (b) 8QAM-S

Figure 4.2: Geometrical shapes of 8QAM-R $(d_{e,\min} = 0.8165)$ and 8QAM-S $(d_{e,\min} = 0.9058)$.

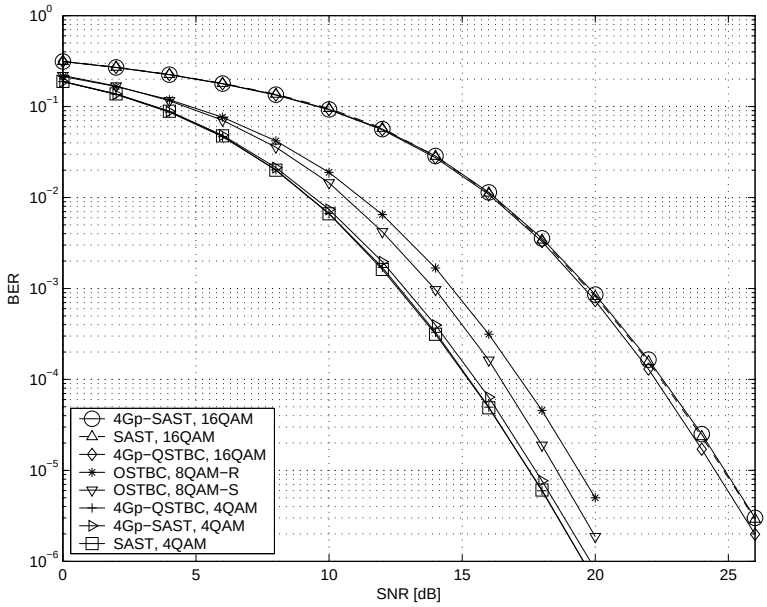

Figure 4.3: Comparing performances of 4-group SAST codes with several STBC for (6, 1) system, 2 and 4 bits pcu.

of 2 bits pcu, 4-group SAST codes gains 0.8 and 1.6 dB over OSTBC with 8QAM-S and 8QAM-R, respectively, while the decoding complexity slightly increases (joint decoding of 3 real symbols). Performance of 4-group SAST codes is slightly inferior to that of 4-group QSTBC (0.2 dB). Note that the decoding complexity of 4-group QSTBC (joint detection of 4 real symbols) is higher than that of 4-group SAST codes (joint detection of 3 real symbols).

In Fig. 4.4, performances of 4-group QSTBC, 4-group SAST codes with 3 bits pcu are presented. With this spectral efficiency, only QSTBC and MDC-QSTBC with rate

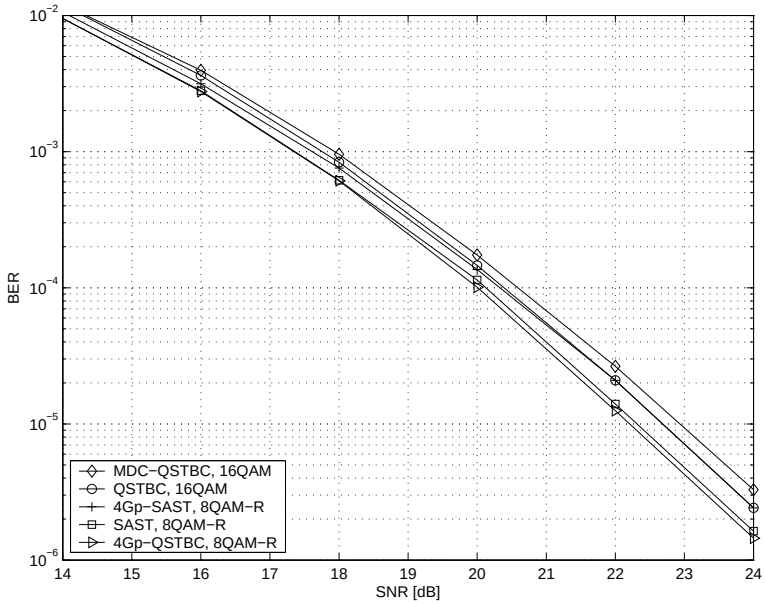

Figure 4.4: Comparing performances of 4-group SAST codes with MDC-QSTBC, QSTBC, and 4-group QSTBC for (6, 1) system, 3 bits pcu.

of 3/4 symbol pcu (using 16QAM) are compared. For 6 transmit antennas, the 4-group SAST codes have 4 groups, each has 3 real symbols. 4-group SAST code yields 0.3 dB improvement over MDC-QSTBC (two real symbol decoding) and performs the same as QSTBC (four real symbol decoding). The 4-group QSTBC using 8QAM-R gains 0.5 dB over 4-group SAST codes at the cost of higher complexity (4-real symbol decoding versus 3-real symbol decoding).

2. Performance 4-group SAST codes for 8 transmit antennas

Performance of 4-group SAST codes are compared with 4-group QSTBC, SAST and DAST codes for 3 and 4 bits spectral efficiency in Fig. 4.5. 4-group SAST codes perform the same as 4-group QSTBC and the two codes have the same decoding complexity (4 real-symbol decoding). However, the two codes gain 0.8 dB over DAST code, which has much higher decoding complexity. The 4-group SAST code is about 0.5 dB worse than SAST codes at high SNR, but keep in mind that the decoding of this SAST code required joint detection of 8 real symbols (see Table 4.1).

For the data rate of 3 bits pcu, 4-group SAST code is also superior to MDC-QSTBC and QSTBC. Our code yields 0.8 and 1 dB gains over MDC-QSTBC and QSTBC, respectively.

3. Performance 4-group SAST codes for 5 transmit antennas

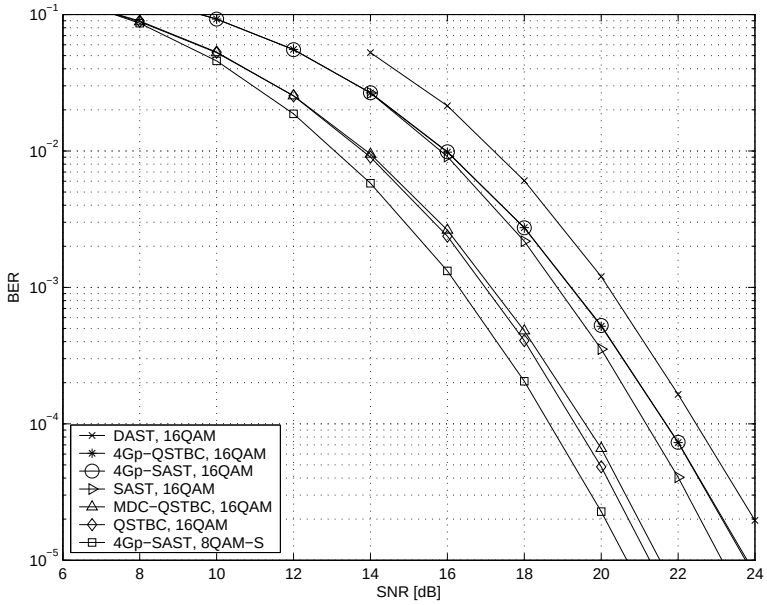

Figure 4.5: Comparing performances of 4-group SAST codes with several STBC for (8, 1) system, 3 and 4 bits pcu.

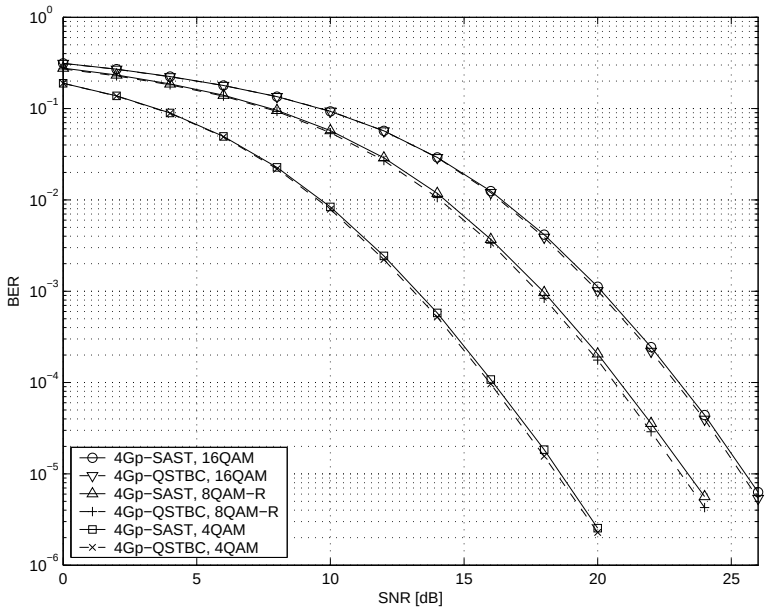

Figure 4.6: Comparing performances of 4-group SAST and 4-group QSTBC for (5, 1) system.

We compare the performances of 4-group QSTBC and 4-group SAST codes in Fig. 4.6. The 4-group QSTBC for 5 transmit antennas is obtained by deleting three columns (4, 7, and 8) of the 4-group QSTBC for 8 transmit antennas. Similarly, the 4-group SAST code for 5 transmit antennas is also created by deleting one column of the SAST code for

6 transmit antennas. Therefore, 4-group SAST code is more delay-efficient and have lower decoding complexity than 4-group QSTBC. With these advantages, 4-group SAST codes incur 0.2 dB loss compared with 4-group QSTBC at high SNR.

4.5 Summary

We have presented a new encoding method so that OEST codes are $2K$-group decodable. The complexity reduction is significant because the number of symbols in each group is reduced by half compared with K-group OEST codes. As a typical example, we obtained 4-group SAST codes from 2-group SAST codes. Extensive simulation results show that 4-group SAST codes perform better than several existing low-complexity STBC, such as OSTBC, MDC-QSTBC, and QSTBC codes. Additionally, 4-group SAST codes have low encoding/decoding delay. Since there are no zeros in SAST code matrices, SAST codes have better PAPR than that of OSTBC. These advantages make 4-group SAST codes suitable for MISO systems, where transmit diversity is one of the available resources to improve the error performance of wireless links.

Chapter 5

Extensions of OEST Framework

In previous chapters, we have derived the multi-group decoding property of OEST codes in general and examined in detail MDC-ABBA and SAST codes, two subclasses of OEST codes. A rigorous approach to decouple the data vectors is to use their orthogonal spatial signatures at the receiver. In this chapter, this approach is extended to investigate other two existing STBC. The first code, called coordinate interleaved orthogonal designs (CIOD), is proposed by Khan and Rajan. Similar to MDC-ABBA codes, CIOD codes are also single-symbol decodable. The second code, 4-group QSTBC, is similar to 4-group SAST codes. However, SAST codes are more delay-efficient than 4-group QSTBC.

5.1 Coordinate Interleaved Orthogonal Designs

5.1.1 Introduction

While OSTBC have minimal decoding complexity, their code rates are low for more than 2 transmit antennas (see Section 1.4.2). To improve the code rate of OSTBC and maintain low decoding complexity, some alternative code designs have been introduced recently. They are (1) minimum decoding complexity (MDC) QSTBC [120, 141] and (2) STBC using coordinate interleaved orthogonal designs (CIOD) [90–92]. These two codes are single (complex) symbol decodable. In Chapter 3, we have studied MDC-ABBA codes, which are similar to MDC-QSTBC. The maximal code rates of OSTBC, MDC-QSTBC (and also MDC-ABBA codes), and CIOD codes are summarized in Table 5.1 for the number of transmit antennas $M = 2, \ldots, 8$. Clearly, CIOD codes offer equal or higher rates than the other codes. This advantage motivates the study of CIOD codes here.

Table 5.1: Code Rates of Single-Symbol Decodable STBC

Codes	$M = 2$	$M = 3, 4$	$M = 5, 6$	$M = 7, 8$
OSTBC	1	3/4	2/3	5/8
MDC-QSTBC		1	3/4	3/4
CIOD		1	6/7	4/5

While OSTBC achieve full diversity for any constellation, CIOD codes may not achieve full-diversity with the conventional constellations, such as QAM or PSK. To achieve full diversity, modulation symbols may need to be rotated by an angle α [90–92]. Proper choice of the rotation angle α will maximize the code diversity gain and also minimize the error performance. The authors in [92] use the coding gain parameter [16] to derive the optimal α for QAM. However, maximizing the coding gain amounts to minimizing the worst-case codeword pair-wise error probability (CPEP), which provides no guarantee for minimization of the symbol error rate (SER). Moreover, references [90–92] did not derive optimal signal rotations for QAM, PSK, and other constellations with good minimum Euclidean distance, such as lattice of equilateral triangular (TRI) (also called hexagonal (HEX)) or amplitude PSK (APSK) [104] in terms of minimal SER.

In this chapter, we will extend the method, which has been used to analyze MDC-ABBA codes to solve several open issues of CIOD codes. First, we derive *equivalent channel* representations. A *new maximum likelihood decoder* is also presented in a simple form. A *closed form symbol pair-wise error probability* (SPEP) is derived. Hence, the *union bound* on the symbol error rate (SER) can be easily evaluated. For all the tested cases, the union bound is within 0.1 dB of the simulated SER. Therefore, this bound can be used to *accurately analyze the performance* of CIOD codes as well as to *optimize the signal rotation* for any constellation with an arbitrary geometrical shape. Similar to MDC-ABBA codes, we present a design of signal transformation for signals with unbalanced powers of real and imaginary parts such as rectangular QAM (QAM-R). The new method combines signal rotation and power (re)allocation yielding better performance than the existing ones in [92, 125] for QAM-R.

5.1.2 Construction of CIOD Codes

The CIOD code for M transmit antennas is constructed from two OSTBC components, $\mathcal{O}_{M_1}$ and $\mathcal{O}_{M_2}$, where $M = M_1 + M_2$ [90–92]. The size of code matrices of $\mathcal{O}_{M_1}$ and $\mathcal{O}_{M_2}$ are $T_1 \times M_1$ and $T_2 \times M_2$, respectively; there are K_1 and K_2 complex symbols embedded in $\mathcal{O}_{M_1}$ and $\mathcal{O}_{M_2}$, respectively. Additionally, the matrices $\mathcal{O}_{M_1}$ and $\mathcal{O}_{M_2}$ are scaled by constants κ_1 and κ_2 to satisfy the power constraint (2.2).

Let $\bar{K}$ be the least common multiple (lcm) of K_1 and K_2, $n_1 = \bar{K}/K_1, n_2 = \bar{K}/K_2$, $\bar{T}_1 = n_1 T_1, \bar{T}_2 = n_2 T_2$. A block of $K = 2\bar{K}$ data (information) symbols $s_i = a_i + \mathrm{j}\, b_i$ ($\mathrm{j}^2 = -1$), $i = 1, 2, \ldots, K$ is mapped to the intermediate symbols x_k ($k = 1, 2, \ldots, K$) as follows:

$$x_k = \begin{cases} a_k + \mathrm{j}\, b_{k+\bar{K}}, & k = 1, 2, \ldots, \bar{K}; \\ a_k + \mathrm{j}\, b_{k-\bar{K}}, & k = \bar{K}+1, \bar{K}+2, \ldots, K. \end{cases} \tag{5.1}$$

By this encoding rule, the coordinates of the symbols $s_1, s_2, \ldots, s_{\bar{K}}$ are interleaved with the coordinates of the symbols $s_{1+\bar{K}}, s_{2+\bar{K}}, \ldots, s_{2\bar{K}}$. Now we construct n_1 OSTBC code matrices $\mathcal{O}_{M_1,i}$ ($i = 1, 2, \ldots, n_1$) and n_2 OSTBC code matrices $\mathcal{O}_{M_2,j}$ ($j = 1, 2, \ldots, n_2$) and arrange them in the intermediate matrices $\mathcal{C}_1$ and $\mathcal{C}_2$ as

$$\mathcal{C}_1 = \begin{bmatrix} \mathcal{O}_{M_1,1}(x_1, x_2, \ldots, x_{K_1}) \\ \mathcal{O}_{M_1,2}(x_{K_1+1}, x_{K_1+2}, \ldots, x_{2K_1}) \\ \vdots \\ \mathcal{O}_{M_1,n_1}(x_{(n_1-1)K_1+1}, x_{(n_1-1)K_1+2}, \ldots, x_{\bar{K}}) \end{bmatrix},$$

$$\mathcal{C}_2 = \begin{bmatrix} \mathcal{O}_{M_2,1}(x_{\bar{K}+1}, x_{\bar{K}+2}, \ldots, x_{\bar{K}+K_2}) \\ \mathcal{O}_{M_2,2}(x_{\bar{K}+K_2+1}, x_{\bar{K}+K_2+2}, \ldots, x_{\bar{K}+2K_2}) \\ \vdots \\ \mathcal{O}_{M_2,n_2}(x_{\bar{K}+(n_2-1)K_2+1}, x_{\bar{K}+(n_2-1)K_2+2}, \ldots, x_{2\bar{K}}) \end{bmatrix}.$$

Hence, the size of $\mathcal{C}_1$ and $\mathcal{C}_2$ are $\bar{T}_1 \times M_1$ and $\bar{T}_2 \times M_2$, respectively.

The CIOD code matrix is formulated by

$$\mathcal{C} = \begin{bmatrix} \sqrt{\kappa_1}\,\mathcal{C}_1 & \mathbf{0}_{\bar{T}_1 \times M_2} \\ \mathbf{0}_{\bar{T}_2 \times M_1} & \sqrt{\kappa_2}\,\mathcal{C}_2 \end{bmatrix}. \tag{5.2}$$

Thus, the size of the CIOD code matrices are $T \times M$, where $T = \bar{T}_1 + \bar{T}_2 = n_1 T_1 + n_2 T_2$, $M = M_1 + M_2$.

For example, here is a CIOD code for 4 transmit antennas, using the 2-by-2 Alamouti code. In this construction, $M_1 = M_2 = 2$, $K_1 = K_2 = 2$, $T_1 = T_2 = 2$. Therefore, the

CIOD code is

$$\mathcal{C}_4 = \begin{bmatrix} a_1 + \mathrm{j}\, b_3 & a_2 + \mathrm{j}\, b_4 & 0 & 0 \\ -a_2 + \mathrm{j}\, b_4 & a_1 - \mathrm{j}\, b_3 & 0 & 0 \\ 0 & 0 & a_3 + \mathrm{j}\, b_1 & a_4 + \mathrm{j}\, b_2 \\ 0 & 0 & -a_4 + \mathrm{j}\, b_2 & a_3 - \mathrm{j}\, b_1 \end{bmatrix}. \tag{5.3}$$

In this CIOD example, the real and imaginary parts are separately transmitted over M_1 and M_2 antennas, i.e., a_1 appears on the first two antennas only. Thus, full diversity gain cannot be achieved. The solution is to rotate the real and imaginary parts of the input symbols and then to map the rotated symbols to CIOD code matrices. This ensures that the real and imaginary parts of the input symbols are spread over all transmit antennas, leading to full symbol-wise diversity [19].

Nevertheless, not all signal rotations will result in the best error-rate performance. Khan and Rajan [92] use the coding gain [16] to minimize the worst-case PEP of code matrices, which may not be optimal for the overall code performance. In contrast, we investigate the performance of CIOD codes by deriving a tight union bound on SER. As a preliminary step, we derive a new simplified transmit-receive signal relation of CIOD codes, in which the equivalent channel can be shown explicitly.

5.1.3 Equivalent Channels and Maximum Likelihood Decoder

Since the mapping rule of the real and imaginary parts of symbols s_k are known, one can write explicitly the dispersion matrices of these symbols. For notational convenience, we reserve A and B for the dispersion matrices of OSTBC and use E and F for the dispersion matrices of CIOD codes; there are $K = 2\bar{K}$ pairs of such matrices E_k, F_k $(i = 1, 2, \ldots, K)$. Additionally, we write $A_i(\mathcal{O}_{M_j})$ or $B_i(\mathcal{O}_{M_j})$ to denote the dispersion matrices of OSTBC $\mathcal{O}_{M_j}$ $(j = 1, 2)$.

The matrices E_k and F_k can be explicitly written though they are quite lengthy. For example, the dispersion matrices of symbol s_1 are:

$$E_1 = \begin{bmatrix} A_1(\mathcal{O}_{M_1}) & \mathbf{0}_{T_1 \times M_2} \\ \mathbf{0}_{(n_1-1)T_1 \times M_1} & \mathbf{0}_{(n_1-1)T_1 \times M_2} \\ \mathbf{0}_{T_2 \times M_1} & \mathbf{0}_{T_2 \times M_2} \\ \mathbf{0}_{(n_2-1)T_2 \times M_1} & \mathbf{0}_{(n_2-1)T_2 \times M_2} \end{bmatrix}, \tag{5.4a}$$

$$F_1 = \begin{bmatrix} \mathbf{0}_{T_1\times M_1} & \mathbf{0}_{T_1\times M_2} \\ \mathbf{0}_{(n_1-1)T_1\times M_1} & \mathbf{0}_{(n_1-1)T_1\times M_2} \\ \mathbf{0}_{T_2\times M_1} & B_1(\mathcal{O}_{M_2}) \\ \mathbf{0}_{(n_2-1)T_2\times M_1} & \mathbf{0}_{(n_2-1)T_2\times M_2} \end{bmatrix}. \tag{5.4b}$$

We can write the CIOD codes using the dispersion form (2.4) as $\mathcal{C} = \sum_{k=1}^{K} (a_k E_k + b_k F_k)$, note that $K = 2\bar{K}$ and $\bar{K} = \mathrm{lcm}\{K_1, K_2\}$.

To simplify our analysis, we first consider the number of receive antennas is $N = 1$ and generalize for $N > 1$ later. The following derivation is similar to the steps to derive the decoder and equivalent channels of MDC-ABBA codes in Section 3.2.

Let the channel vector be $\boldsymbol{h} = \begin{bmatrix} h_1 & h_2 & \dots & h_M \end{bmatrix}^{\mathsf{T}}$, the receive vector be $\boldsymbol{y} = \begin{bmatrix} y_1 & y_2 & \dots & h_T \end{bmatrix}^{\mathsf{T}}$, the data vector $\boldsymbol{d} = \begin{bmatrix} a_1 & b_2 & a_2 & b_2 & \dots & a_K & b_K \end{bmatrix}^{\mathsf{T}}$, the additive noise vector be $\boldsymbol{w} = \begin{bmatrix} w_1 & w_2 & \dots & w_T \end{bmatrix}^{\mathsf{T}}$. Let C be a CIOD code matrix, the transmit-receive signals in (2.3) becomes

$$\begin{aligned} \boldsymbol{y} &= \sqrt{\rho} C \boldsymbol{h} + \boldsymbol{w} \\ &= \sqrt{\rho} \sum_{k=1}^{K} (a_k E_k \boldsymbol{h} + b_k F_k \boldsymbol{h}) + \boldsymbol{w} \\ &= \sqrt{\rho} \begin{bmatrix} E_1\boldsymbol{h} & F_1\boldsymbol{h} & E_2\boldsymbol{h} & F_2\boldsymbol{h} & \dots & E_K\boldsymbol{h} & F_K\boldsymbol{h} \end{bmatrix} \boldsymbol{d} + \boldsymbol{w}. \end{aligned} \tag{5.5}$$

In (5.4), the scalars κ_1 and κ_2 are not included for brevity. We can rewrite (5.5) equivalently as

$$\begin{bmatrix} \boldsymbol{y} \\ \boldsymbol{y}^* \end{bmatrix} = \sqrt{\rho} \begin{bmatrix} E_1\boldsymbol{h} & F_1\boldsymbol{h} & \dots & E_K\boldsymbol{h} & F_K\boldsymbol{h} \\ E_1^*\boldsymbol{h}^* & F_1^*\boldsymbol{h}^* & \dots & E_K^*\boldsymbol{h}^* & F_K^*\boldsymbol{h}^* \end{bmatrix} \boldsymbol{d} + \begin{bmatrix} \boldsymbol{w} \\ \boldsymbol{w}^* \end{bmatrix}. \tag{5.6}$$

Let $\bar{\mathcal{H}}_k = \begin{bmatrix} E_k\boldsymbol{h} & F_k\boldsymbol{h} \\ E_k^*\boldsymbol{h}^* & F_k^*\boldsymbol{h}^* \end{bmatrix}$ for $k = 1, 2, \dots, K$, it follows

$$\bar{\mathcal{H}}_k^{\dagger}\bar{\mathcal{H}}_k = \mathrm{diag}\left(\hat{h}_1, \hat{h}_2\right) \triangleq \hat{\mathcal{H}}_1, \quad \text{for } 1 \le k \le \bar{K}, \tag{5.7a}$$

$$\bar{\mathcal{H}}_k^{\dagger}\bar{\mathcal{H}}_k = \mathrm{diag}\left(\hat{h}_2, \hat{h}_1\right) \triangleq \hat{\mathcal{H}}_2, \quad \text{for } \bar{K} < k \le K, \tag{5.7b}$$

$$\bar{\mathcal{H}}_k^{\dagger}\bar{\mathcal{H}}_l = \mathbf{0}_{2\times 2}, \quad \text{for } k \ne l. \tag{5.7c}$$

where $\hat{h}_1 = 2\sum_{i=1}^{M_1} |h_i|^2, \hat{h}_2 = 2\sum_{i=1}^{M_2} |h_i|^2$.

Thus, if the two sides of (5.6) are multiplied by $\bar{\mathcal{H}}_k^{\dagger}$, one gets

$$\underbrace{\bar{\mathcal{H}}_k^{\dagger}\begin{bmatrix} \boldsymbol{y} \\ \boldsymbol{y}^* \end{bmatrix}}_{\bar{\boldsymbol{y}}_k} = \sqrt{\rho}\hat{\mathcal{H}}_p \underbrace{\begin{bmatrix} a_k \\ b_k \end{bmatrix}}_{d_k} + \underbrace{\bar{\mathcal{H}}_k^{\dagger}\begin{bmatrix} \boldsymbol{w} \\ \boldsymbol{w}^* \end{bmatrix}}_{\bar{\boldsymbol{w}}_k}. \tag{5.8}$$

where $p = 1$ if $1 \leq k \leq \bar{K}$ and $p = 2$ if $\bar{K} < k \leq K$.

The matrix $\bar{\mathcal{H}}_k^{\dagger}$ plays the role of the spatial signature of the data vector d_k. Since the data vectors d_k can be completely decoupled, (5.8) can be used for maximum likelihood detection. However, since the noise vector $\bar{\boldsymbol{w}}_k$ is colored with covariance matrix $\hat{\mathcal{H}}_p$, it needs to be whitened by a whitening matrix $\hat{\mathcal{H}}_p^{-1/2}$. After this whitening step, (5.8) becomes

$$\hat{\mathcal{H}}_p^{-1/2}\bar{\boldsymbol{y}}_k = \sqrt{\rho}\hat{\mathcal{H}}_p^{1/2}d_k + \hat{\mathcal{H}}_p^{-1/2}\bar{\boldsymbol{w}}_k. \tag{5.9}$$

We can conclude that the matrices $\mathcal{H}_1 = \hat{\mathcal{H}}_1^{1/2}$ and $\mathcal{H}_2 = \hat{\mathcal{H}}_2^{1/2}$ are the *equivalent channels* of CIOD codes.

The maximum likelihood solution of (5.9) is

$$\hat{d}_k = \arg\min_{d_k}(\rho d_k^{\mathsf{T}}\hat{\mathcal{H}}_p d_k - 2\sqrt{\rho}\Re(\bar{\boldsymbol{y}}_k^{\mathsf{T}})d_k). \tag{5.10}$$

The result in (5.10) can be generalized for multiple receive antennas. To this end, we include the scalars κ_1 and κ_2 for completeness. We can show that $\hat{h}_1 = 2\kappa_1 \sum_{j=1}^{N}\sum_{i=1}^{M_1}|h_{i,j}|^2$, $\hat{h}_2 = 2\kappa_2 \sum_{j=1}^{N}\sum_{i=1}^{M_2}|h_{i,j}|^2$, $\bar{\boldsymbol{y}}_k = \sum_{j=1}^{N}\bar{\mathcal{H}}_{k,n}^{\dagger}\begin{bmatrix}\boldsymbol{y}_n \\ \boldsymbol{y}_n^*\end{bmatrix}$, where $\boldsymbol{y}_n$ is the receive vector of nth antenna, $\bar{\mathcal{H}}_{k,n} = \begin{bmatrix}E_k\boldsymbol{h}_n & F_k\boldsymbol{h}_n \\ E_k^*\boldsymbol{h}_n^* & F_k^*\boldsymbol{h}_n^*\end{bmatrix}$, $\boldsymbol{h}_n$ is the nth column of the channel matrix H.

From (5.8), the decoding of the real symbols a_k and b_k can be decoupled. However, since the symbols a_k and b_k are not transmitted over M channels, full diversity cannot be achievable. Hence, we need to spread out these symbols over M channels by applying a real unitary rotation R_p as

$$R_p = \begin{bmatrix}\cos(\alpha_p) & \sin(\alpha_p) \\ \sin(\alpha_p) & -\cos(\alpha_p)\end{bmatrix}, \quad (p = 1, 2),$$

to the data vectors d_k [92, 125]. Including the rotation matrix to (5.9) and (5.10), we have

$$\hat{\mathcal{H}}_p^{-1/2}\bar{\boldsymbol{y}}_k = \sqrt{\rho}\hat{\mathcal{H}}_p^{1/2}R_p d_k + \hat{\mathcal{H}}_p^{-1/2}\bar{\boldsymbol{w}}_k, \tag{5.11}$$

and

$$\hat{d}_k = \arg\min_{d_k}(\rho d_k^{\mathsf{T}}R_p^{\mathsf{T}}\hat{\mathcal{H}}_p R_p d_k - 2\sqrt{\rho}\Re(\bar{\boldsymbol{y}}_k^{\mathsf{T}})R_p d_k). \tag{5.12}$$

Some interesting facts can be drawn from the newly proposed decoder of CIOD codes. First, akin to the decoding metric of OSTBC, the decoding metric (5.12) of CIOD codes

does not involve the dispersion matrices [62]. This fact reduces the decoding complexity compared with the one proposed in [92, eq. (84)], where the dispersion matrices of symbols are required. Second, with OSTBC, the MIMO channel is decoupled into single-input single-output (SISO) channels and the equivalent channel gain is the Frobenius norm of the MIMO channel. On the other hand, similar to the MDC-ABBA codes, the MIMO channel becomes 2×2 diagonal channels with CIOD codes; the two entries of the diagonal are simply Frobenius norms of the first M_1 and the other M_2 columns of the MIMO channel matrix, where respectively, the real and imaginary parts of the rotated signal are transmitted on.

In the next section, we will investigate the performance of CIOD codes with different types of constellations by exploiting this special structure of the equivalent channels.

5.1.4 Union bound on SER and Optimal Signal Designs

We first consider the data vectors $d_k = [a_k \; b_k]^\mathsf{T}$ for $1 \leq k \leq \bar{K}$. These data vectors are sent over the same equivalent channel $\hat{\mathcal{H}}_1^{1/2}$ and, therefore, they have the same error probability; we thus drop the subindex k for short. Let $d = [a \; b]^\mathsf{T}$ and $\hat{d} = [\hat{a} \; \hat{b}]^\mathsf{T}$ be the transmitted and the erroneous detected vectors, let $\delta_1 = a - \hat{a}$, $\delta_2 = b - \hat{b}$, $\Delta = [\delta_1 \; \delta_2]^\mathsf{T}$. From (5.11), the SPEP of the symbol pair d_k and $\hat{d}_k$ can be expressed by the Gaussian tail function as [32]

$$P(d \to \hat{d}|\hat{\mathcal{H}}_1) = Q\left(\sqrt{\frac{\rho|\hat{\mathcal{H}}_1 R_1 \Delta|^2}{4N_0}}\right) \tag{5.13}$$

where $N_0 = 1/2$ is the variance of the real part of the elements of the white noise vector $\hat{\mathcal{H}}_p^{-1/2}\bar{\boldsymbol{w}}$ in (5.11). Let

$$\begin{bmatrix}\beta_1 \\ \beta_2\end{bmatrix} = R_1\Delta = \begin{bmatrix}\cos(\alpha_1) & \sin(\alpha_1) \\ \sin(\alpha_1) & -\cos(\alpha_1)\end{bmatrix}\begin{bmatrix}\delta_1 \\ \delta_2\end{bmatrix}. \tag{5.14}$$

Using the Craig's formula [131] to derive the conditional SPEP in (5.13), one has

$$\begin{aligned} P(d \to \hat{d}|\hat{\mathcal{H}}_1) &= Q\left(\sqrt{\frac{\rho(\beta_1^2 h_1 + \beta_2^2 h_2)}{2}}\right) \\ &= \frac{1}{\pi}\int_0^{\pi/2} \exp\left(\frac{-\rho(\beta_1^2 h_1 + \beta_2^2 h_2)}{4\sin^2\theta}\right) d\theta \\ &= \frac{1}{\pi}\int_0^{\pi/2} \prod_{j=1}^{N}\left[\prod_{i=1}^{M_1}\exp\left(-\frac{\rho\kappa_1\beta_1^2|h_{i,j}|^2}{4\sin^2\theta}\right)\prod_{i=1}^{M_2}\exp\left(-\frac{\rho\kappa_2\beta_2^2|h_{i,j}|^2}{4\sin^2\theta}\right)\right] d\theta. \end{aligned} \tag{5.15}$$

We can apply a method based on the moment generating function (MGF) [132, 133] to obtain the unconditional SPEP in the following:

$$P_1(d \to \hat{d}) = \frac{1}{\pi} \int_0^{\pi/2} \left(1 + \frac{\rho\kappa_1\beta_1^2}{4\sin^2\theta}\right)^{-M_1N} \left(1 + \frac{\rho\kappa_2\beta_2^2}{4\sin^2\theta}\right)^{-M_2N} d\theta. \tag{5.16}$$

The exact SPEP of CIOD codes is quite similar to that of MDC-ABBA codes in (3.34). The difference is that the exponents of the term involving β_1 and β_2 are M_1N and M_2N, respectively, while the exponents of the term involving β_1 and β_2 are the same $MN/2$ with MDC-ABBA codes. Note that $M = M_1 + M_2$. We can further simplify (5.16) to avoid integration as we have done for MDC-ABBA codes. However, more details are omitted for purposes of brevity.

The SPEP in (5.16) is given for symbols s_k sent over the equivalent channel $\mathcal{H}_1$. For the symbols s_k $(\bar{K} < k \leq K)$ transmitted over the equivalent channel $\mathcal{H}_2$, the SPEP can be found similarly:

$$P_2(d \to \hat{d}) = \frac{1}{\pi} \int_0^{\pi/2} \left(1 + \frac{\rho\kappa_2\bar{\beta}_1^2}{4\sin^2\theta}\right)^{-M_2N} \left(1 + \frac{\rho\kappa_1\bar{\beta}_2^2}{4\sin^2\theta}\right)^{-M_1N} d\theta \tag{5.17}$$

where

$$\begin{bmatrix}\bar{\beta}_1 \\ \bar{\beta}_2\end{bmatrix} = \begin{bmatrix}\cos(\alpha_2) & \sin(\alpha_2) \\ \sin(\alpha_2) & -\cos(\alpha_2)\end{bmatrix} \begin{bmatrix}\delta_1 \\ \delta_2\end{bmatrix}. \tag{5.18}$$

Assume that d_i, d_j, d_m, d_n, $(i, j, m, n = 1, 2, \ldots, \Omega)$, are signals drawn from a constellation $\mathcal{S}$ of size Ω. From the SPEP expression (5.15) and (5.17), we can find the union bound on SER of CIOD codes with constellation $\mathcal{S}$ as

$$P_u(\mathcal{S}) = P_{u,1}(\mathcal{S}) + P_{u,2}(\mathcal{S}) \tag{5.19}$$

where

$$P_{u,1}(\mathcal{S}) = \frac{1}{\Omega} \sum_{i=1}^{\Omega-1} \sum_{j=i+1}^{\Omega} P(d_i \to d_j), \tag{5.20}$$

$$P_{u,2}(\mathcal{S}) = \frac{1}{\Omega} \sum_{m=1}^{\Omega-1} \sum_{n=i+1}^{\Omega} P(d_m \to d_n). \tag{5.21}$$

For a fixed SNR, the union bound $P_u(\mathcal{S})$ depends on the constellation $\mathcal{S}$ and the rotation angles α_1 and α_2. Thus, one can find the optimal values of α_1 and α_2 to minimize the union

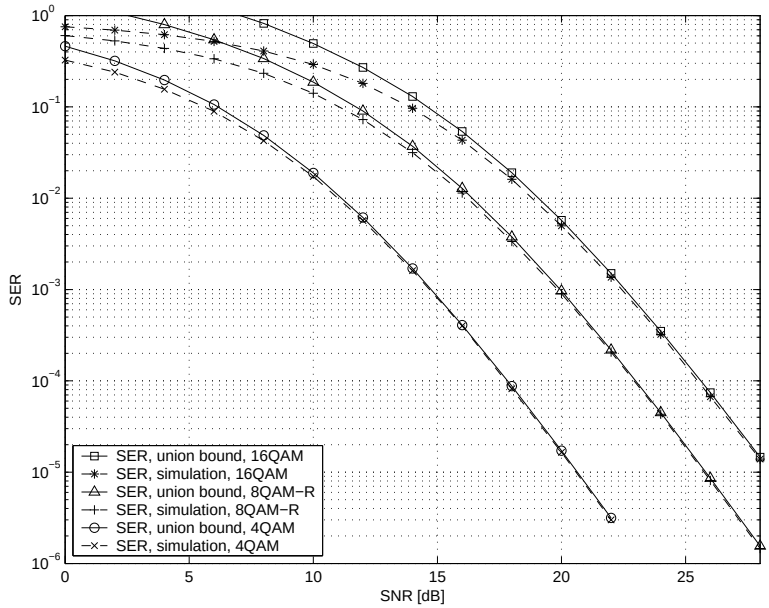

Figure 5.1: Comparison of the simulated SER and the union bound of a rate-one CIOD code for (4, 1) system and $M_1 = 2, M_2 = 2$.

bound on SER. Note that α_1 and α_2 can be optimized separately. We can run a computer search to find the optimal values of α_1 and α_2.

The run time for searching optimal values of α_1 and α_2 of a given constellation is only few minutes. However, we can further reduce the searching time by considering the following observation. In practice, $\mathcal{S}$ is usually symmetric via either horizontal or vertical axis of the Cartesian coordinate system. We can assume that $\mathcal{S}$ is symmetric via the vertical axis. If $\mathcal{S}$ is symmetric via the horizontal axis, we can always rotate the whole constellation an angle of $\pi/2$ to make it symmetric via the vertical axis.

Assume that $\alpha_2 = \pi/2 - \alpha_1$. For each pair of symbols $(d_i, d_j) = \big([a_i,\ b_i]^\mathsf{T}, [a_j,\ b_j]^\mathsf{T}\big)$, we can find one and only one pair $(d_m, d_n) = \big([a_i,\ -b_i]^\mathsf{T}, [a_j,\ -b_j]^\mathsf{T}\big)$ so that $P_1(d_i \rightarrow d_j) = P_2(d_m \rightarrow d_n)$. Therefore, $P_{u,1}(\mathcal{S}) = P_{u,2}(\mathcal{S})$; and if α_{opt} is the optimal value of α_1, then $\pi/2 - \alpha_{opt}$ is optimal for α_2. Hence, we just write the value of α_1 and imply that the value of $\alpha_2 = \pi/2 - \alpha_1$.

The union bound on SER is plotted in Fig. 5.1 for a CIOD code for $M = 4$ transmit antennas $(M_1, M_2) = (2, 2)$. For the three examined constellations (4QAM, 8QAM-R, and 16QAM), and $\alpha_1 = 31.7175^\circ$ [92], the union bound becomes tight when SER $< 10^{-1}$ and is less than 0.1 dB apart from the simulated SER at high SNR. Similar results can be found

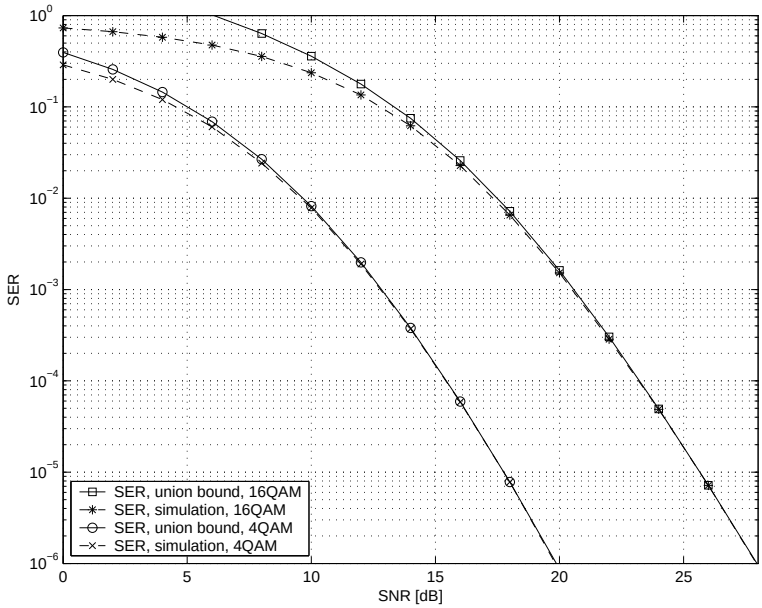

Figure 5.2: Comparison of the union bound and simulated SER of a CIOD code with rate of 6/7 symbol pcu for (6, 1) system and $M_1 = 2, M_2 = 4$.

for the case with $M = 6$, $M_1 = 2, M_2 = 4$ in Fig. 5.2; the union bound even converges with the simulated SER.

5.1.5 Numerical Examples

Since the union bound is very tight for SER < 10^{-2}, it can be used to optimize the values of rotation angles α_1 and α_1. The new optimal signal rotations for the popular constellations based on minimizing the SER union bound are summarized in Table 5.2. Only the optimal values α_{opt} of α_1 are listed, the optimal values of $\alpha_2 = \pi/2 - \alpha_{opt}$. The geometrical shapes of 8-ary constellations are sketched in Fig. 5.3. The best 8TRI in terms of minimum Euclidean distance (carved from the lattice of equilateral triangular) is selected [104].

Note that in Table 5.2, the α_{opt} varies with the number of antennas M_1 and M_2.

It is shown that CIOD codes perform better that OSTBC in [92]. We thus just compare the SER union bounds of CIOD code with new optimal signal designs in Fig. 5.4 for $(M_1, M_2) = (2, 4)$. Obviously, QAM signals yield the best performance compared with other constellations of the same size. On the other hand, TRI constellations have the best minimum Euclidean distance; however, their performance is inferior to that of QAM signals. This observation is also confirmed in Fig. 5.4, where the SER of CIOD codes for

Table 5.2: Optimal Rotation Angles of Popular Constellations

Signal	(2, 1)	(2, 2)	(2, 3)	(2, 4)	(3, 3)
4QAM	28.939°	30.417°	29.698°	29.003°	30.778°
4TRI	20.142°	13.883°	71.739°	68.687°	75.836°
8PSK	37.690°	39.216°	38.808°	38.534°	39.857°
8APSK	10.316°	11.528°	11.181°	11.000°	12.015°
8TRI	20.309°	45.000°	11.061°	9.430°	45.000°
8QAM-R	33.037°	31.834°	29.658°	28.626°	31.737°
8QAM-SR	12.234°	13.036°	12.925°	12.701°	13.173°
16PSK	3.485°	2.570°	2.832°	2.964°	2.200°
16TRI	19.236°	45.000°	47.116°	70.690°	45.000°
16QAM	31.436°	31.677°	31.557°	31.462°	31.704°

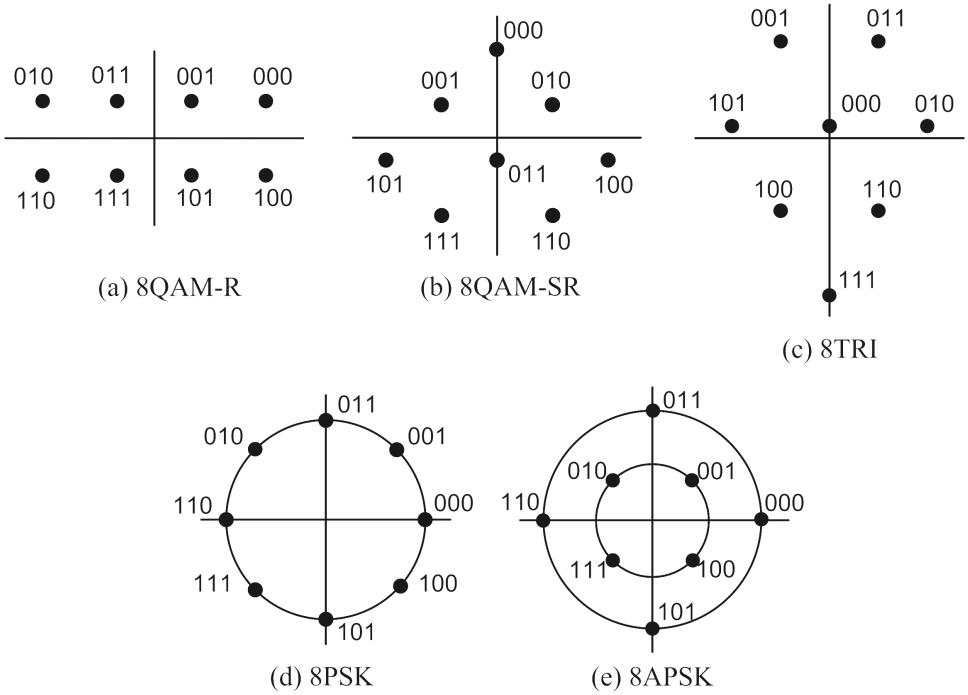

Figure 5.3: Geometrical shapes of 8-ary constellations.

$(M_1, M_2) = (3, 3)$ with various constellations is sketched.

Our newly proposed rotation angles are only slightly different from the optimal rotation angles for QAM in terms of coding gain derived in [92]. Therefore, the performance

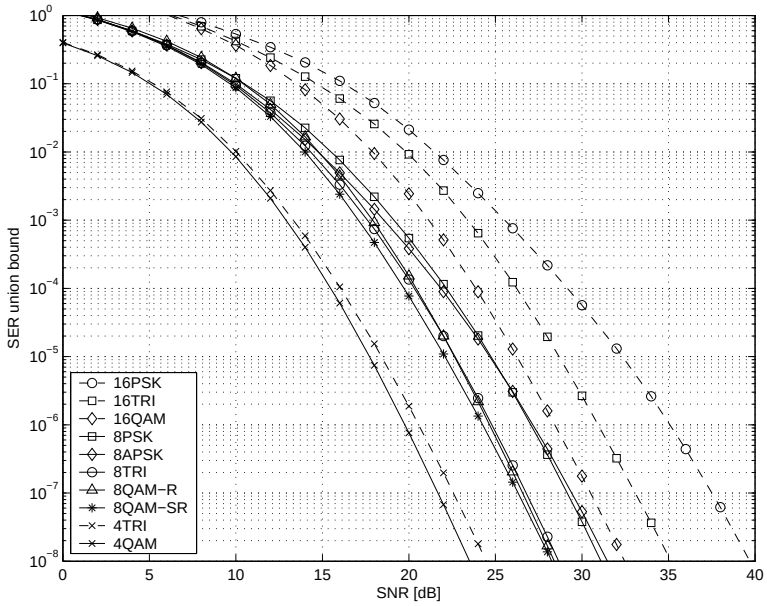

Figure 5.4: SER union bound a CIOD code with rate of 6/7 symbol pcu for (6, 1) system and $M_1 = 2, M_2 = 4$.

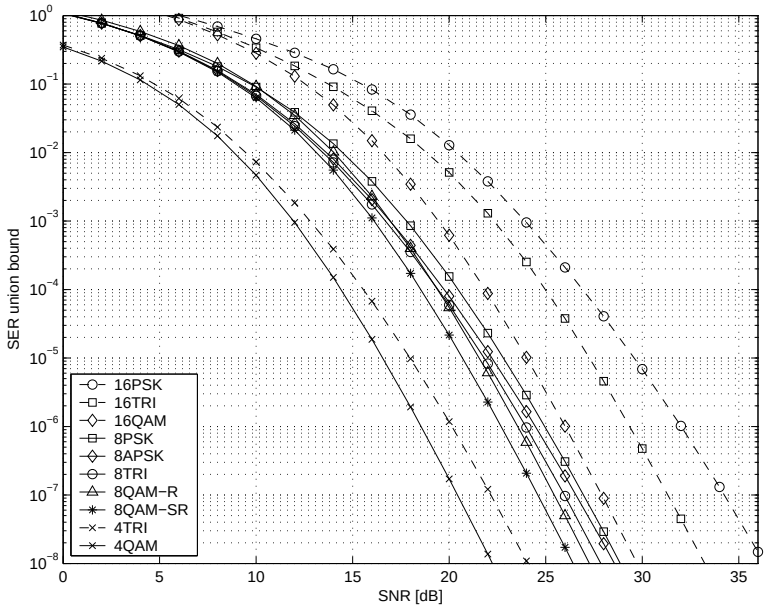

Figure 5.5: SER union bound a CIOD code with rate of 3/4 symbol pcu for (6, 1) system and $M_1 = 3, M_2 = 3$.

improvement is marginal, but note that [92] does not cover constellations other than QAM. Nevertheless, the exact PEP derivation is a useful tool to accurately analyze the performance of different constellations with signal rotations.

Note that we have used unitary rotations for the above analysis. This approach produces

good performance for signal constellations with even power of the real and imaginary parts. For the signal with bias powers of the real and imaginary parts, such as QAM-R, the non-unitary rotations may perform better. This approach works well for MDC-ABBA codes (see Section 3.5). In the next following, we will apply this method presented for MDC-ABBA codes to design the non-unitary rotation for CIOD codes with QAM-R by combining power allocation and signal rotation.

5.1.6 Optimal Signal Rotation with Power Allocation

For QAM-R, e.g. 8QAM-R in Fig. 5.3, the average powers of the real and imaginary parts of the signal points are different. We may change the power allocation to the real and imaginary parts of QAM-R signals to get better overall SER.

To change the power allocation, the real and imaginary of QAM-R signals are first multiplied by constants σ_1 and σ_2, respectively, then they are rotated by unitary matrix R_1, R_2. For example, let $\mathcal{S}$ be a constellation with signal set $\mathcal{S} = \{d \mid d = a + \mathrm{j}\, b, a, b \in \mathbb{R}\}$, the new constellation with new power allocation is $\bar{\mathcal{S}} = \{\bar{d} \mid \bar{d} = \sigma_1 a + \mathrm{j}\, \sigma_2 b; a, b \in \mathbb{R}\}$. The average energy of the constellation $\bar{\mathcal{S}}$ is kept the same as that of $\mathcal{S}$, i.e. unitary. For example, the 8QAM-R with signal points $\{(\pm 3 \pm \mathrm{j}, \pm 1 \pm \mathrm{j})/\sqrt{48}\}$ has constraint equation for coefficients σ_1 and σ_2 as $5\sigma_1^2 + \sigma_2^2 = 6$. Hence, if the value of σ_1 is given, the value of σ_2 is known explicitly.

We still use (5.15) to calculate the union bound on SER of CIOD codes with signal rotation and power re-allocation; (5.16) can be rewritten to include the effects of power re-allocation as

$$\begin{bmatrix} \beta_1 \\ \beta_2 \end{bmatrix} = \underbrace{\begin{bmatrix} \cos(\alpha_1) & \sin(\alpha_1) \\ \sin(\alpha_1) & -\cos(\alpha_1) \end{bmatrix} \begin{bmatrix} \sigma_1 & 0 \\ 0 & \sigma_2 \end{bmatrix}}_{\bar{R}_1} \begin{bmatrix} \delta_1 \\ \delta_2 \end{bmatrix}. \tag{5.22}$$

The total effect of signal rotation and power re-allocation is the non-unitary signal transform $\bar{R}_1$. Now the minimization of the union bound is based on two variables: σ_1 (or σ_2) and α_1. We run exhaustive computer search to find the optimal values of σ_1 and α_1. In fact, there is only single value of σ_1 so that the union bound is minimized; this value of σ_1 is the global solution of the union bound minimization. The optimal values of σ_1 and α_1 for 8QAM-R and 32QAM-R are provided in Table 5.3.

Table 5.3: Optimal Power Allocation and Signal Rotation for QAM-R

Constellation	σ_1	σ_2	α_{opt}
8QAM-R	0.9055	1.3784	$45.0°$
32QAM-R	0.8972	1.3487	$43.0°$

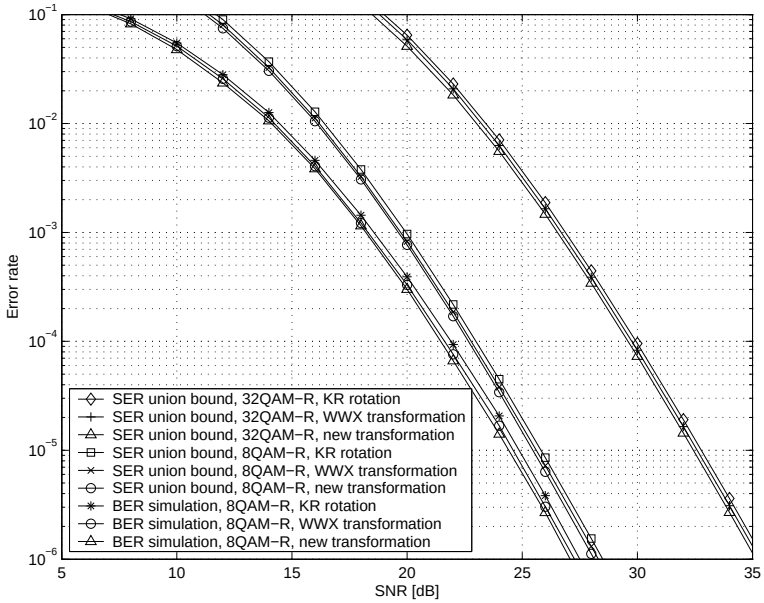

Figure 5.6: BER and union bound on SER of the rate-one CIOD code with rectangular 8QAM and 32QAM for (4, 1) system and $M_1 = 2, M_2 = 2$.

In Fig. 5.6, we compare the union bounds on SER of 8QAM-R and 32QAM-R using signal rotation of Khan-Rajan with $\alpha_1 = 31.7175°$ [92], signal transformation of Wang-Wang-Xia [125, Theorem 6], and our new signal transformation for CIOD codes with $M = 4$ $(M_1 = 2, M_2 = 2), N = 1$. At SER = 10^{-6}, our new signal transformation yields 0.2 dB and 0.4 dB gains compared with the signal designs of Wang-Wang-Xia and Khan-Rajan, respectively. The BER of 8QAM-R also confirms the improvement of our newly proposed transformation over the existing ones.

The success of the new signal design arises because the powers of the real and imaginary parts of QAM-R are significantly different. We found that for other constellations with more balanced powers of the real and imaginary parts, even though the new signal design method can improve the performance, the improvement is marginal.

To this point, we have extended the methodology, which has been used for MDC-ABBA

codes, to analyze CIOD codes. CIOD codes are single-symbol decodable. The main advantage of CIOD codes is the higher code rate compared with MDC-ABBA codes and OSTBC. Various open issues of CIOD codes have been addressed, including the equivalent channels, new maximum likelihood decoding method, performance analysis and optimal signal designs.

The next section will treat another class of STBC with 4-group decoding called 4-group QSTBC proposed by Yuen, Guan, and Tjhung [93]. We also follow the steps that help us in analyzing several low-complexity STBC. The key problem is how to derive the equivalent channel of 4-group QSTBC.

5.2 4-Group Quasi-Orthogonal STBC

5.2.1 Code Construction

The 4-group QSTBC is developed from MDC-QSTBC [120]. The real and imaginary parts of a complex symbol can be mapped to the same group. We thus use the general form of STBC in (2.4): $X = \sum_{k=1}^{K} (a_k A_k + b_k B_k)$ to study 4-group QSTBC; hence, Theorem 2.2 can be restated as follows.

Lemma 5.1. The necessary and sufficient conditions for a STBC in (2.4) becomes Γ-group decodable are

$$A_p^\dagger A_q + A_p^\dagger A_q = \mathbf{0}, \tag{5.23a}$$

$$B_p^\dagger B_q + B_p^\dagger B_q = \mathbf{0}, \tag{5.23b}$$

$$A_p^\dagger B_q + B_p^\dagger A_q = \mathbf{0}\,. \tag{5.23c}$$

$\forall p \in \Theta_i, \forall q \in \Theta_j, 1 \leq i \neq j \leq \Gamma$.

The sufficient condition so that a STBC is four-group decodable is found in [93].

Theorem 5.2 ([93])**.** Given a 4-group STBC for M transmit antennas with code length T and K sets of dispersion matrices $(A_k, B_k; 1 \leq k \leq K)$, A 4-group STBC with code length $2T$ for $2M$ transmit antennas, which consists of $2K$ sets of dispersion matrices denoted as

$(\bar{A}_i, \bar{B}_i), 1 \leq i \leq 2K$, can be constructed using the following mapping rules:

$$\bar{A}_{2k-1} = \begin{bmatrix} A_k & \mathbf{0} \\ \mathbf{0} & A_k \end{bmatrix}, \ \bar{A}_{2k} = \begin{bmatrix} B_k & \mathbf{0} \\ \mathbf{0} & B_k \end{bmatrix}, \ \bar{B}_{2k-1} = \begin{bmatrix} \mathbf{0} & A_k \\ A_k & \mathbf{0} \end{bmatrix}, \ \bar{B}_{2k} = \begin{bmatrix} \mathbf{0} & B_k \\ B_k & \mathbf{0} \end{bmatrix}. \tag{5.24}$$

The recursive construction of 4-group STBC specified in Theorem 5.2 suggests that we can start with the MDC-QSTBC for 4 transmit antennas proposed in [120] to construct 4-group STBC for 8, 16 transmit antennas and so on, because MDC-QSTBC is one of the STBC satisfying Lemma 5.1; the resulting STBC is thus called 4-group QSTBC. For practical interest, we will illustrate the encoding process of 4-group QSTBC for 8 transmit antennas from the MDC-QSTBC for 4 transmit antennas [120] in the following.

Note that MDC-QSTBC in [120] is actually equivalent to the ABBA codes [47, 125]. We can write the code matrix of MDC-QSTBC for 4 transmit antennas as

$$F_4 = \begin{bmatrix} a_1 + \mathrm{j}\, a_3 & a_2 + \mathrm{j}\, a_4 & b_1 + \mathrm{j}\, b_3 & b_2 + \mathrm{j}\, b_4 \\ -a_2 + \mathrm{j}\, a_4 & a_1 - \mathrm{j}\, a_3 & -b_2 + \mathrm{j}\, b_4 & b_1 - \mathrm{j}\, b_3 \\ b_1 + \mathrm{j}\, b_3 & b_2 + \mathrm{j}\, b_4 & a_1 + \mathrm{j}\, a_3 & a_2 + \mathrm{j}\, a_4 \\ -b_2 + \mathrm{j}\, b_4 & b_1 - \mathrm{j}\, b_3 & -a_2 + \mathrm{j}\, a_4 & a_1 - \mathrm{j}\, a_3 \end{bmatrix} = \begin{bmatrix} x_1 & x_2 & x_3 & x_4 \\ -x_2^* & x_1^* & -x_4^* & x_3^* \\ x_3 & x_4 & x_1 & x_2 \\ -x_4^* & x_3^* & -x_2^* & x_1^* \end{bmatrix}. \tag{5.25}$$

where $\mathrm{j}^2 = -1$, the intermediate variables $x_1 = a_1 + \mathrm{j}\, a_3, x_2 = a_2 + \mathrm{j}\, a_4, x_3 = b_1 + \mathrm{j}\, b_3$, and $x_4 = b_2 + \mathrm{j}\, b_4$ are used to highlight the ABBA structure of MDC-QSTBC codes [47, 120].

The four transmitted symbols $s_i = a_i + \mathrm{j}\, b_i, (i = 1, \ldots, 4)$ in the code matrix F_4 can be separated at the receiver for maximum likelihood detection. We now build the code matrix of 4-group QSTBC for 8 transmit antennas from F_4 using mapping rules in (5.24) below:

$$F_8 = \begin{bmatrix} a_1 + \mathrm{j}\, a_5 & a_3 + \mathrm{j}\, a_7 & a_2 + \mathrm{j}\, a_6 & a_4 + \mathrm{j}\, a_8 & \ldots \\ -a_3 + \mathrm{j}\, a_7 & a_1 - \mathrm{j}\, a_5 & -a_4 + \mathrm{j}\, a_8 & a_2 - \mathrm{j}\, a_6 & \ldots \\ a_2 + \mathrm{j}\, a_6 & a_4 + \mathrm{j}\, a_8 & a_1 + \mathrm{j}\, a_5 & a_3 + \mathrm{j}\, a_7 & \ldots \\ -a_4 + \mathrm{j}\, a_8 & a_2 - \mathrm{j}\, a_6 & -a_3 + \mathrm{j}\, a_7 & a_1 - \mathrm{j}\, a_5 & \ldots \\ b_1 + \mathrm{j}\, b_5 & b_3 + \mathrm{j}\, b_7 & b_2 + \mathrm{j}\, b_6 & b_4 + \mathrm{j}\, b_8 & \ldots \\ -b_3 + \mathrm{j}\, b_7 & b_1 - \mathrm{j}\, b_5 & -b_4 + \mathrm{j}\, b_8 & b_2 - \mathrm{j}\, b_6 & \ldots \\ b_2 + \mathrm{j}\, b_6 & b_4 + \mathrm{j}\, b_8 & b_1 + \mathrm{j}\, b_5 & b_3 + \mathrm{j}\, b_7 & \ldots \\ -b_4 + \mathrm{j}\, b_8 & b_2 - \mathrm{j}\, b_6 & -b_3 + \mathrm{j}\, b_7 & b_1 - \mathrm{j}\, b_5 & \ldots \end{bmatrix}$$

$$\begin{bmatrix} \ldots & b_1 + \mathrm{j}\, b_5 & b_3 + \mathrm{j}\, b_7 & b_2 + \mathrm{j}\, b_6 & b_4 + \mathrm{j}\, b_8 \\ \ldots & -b_3 + \mathrm{j}\, b_7 & b_1 - \mathrm{j}\, b_5 & -b_4 + \mathrm{j}\, b_8 & b_2 - \mathrm{j}\, b_6 \\ \ldots & b_2 + \mathrm{j}\, b_6 & b_4 + \mathrm{j}\, b_8 & b_1 + \mathrm{j}\, b_5 & b_3 + \mathrm{j}\, b_7 \\ \ldots & -b_4 + \mathrm{j}\, b_8 & b_2 - \mathrm{j}\, b_6 & -b_3 + \mathrm{j}\, b_7 & b_1 - \mathrm{j}\, b_5 \\ \ldots & a_1 + \mathrm{j}\, a_5 & a_3 + \mathrm{j}\, a_7 & a_2 + \mathrm{j}\, a_6 & a_4 + \mathrm{j}\, a_8 \\ \ldots & -a_3 + \mathrm{j}\, a_7 & a_1 - \mathrm{j}\, a_5 & -a_4 + \mathrm{j}\, a_8 & a_2 - \mathrm{j}\, a_6 \\ \ldots & a_2 + \mathrm{j}\, a_6 & a_4 + \mathrm{j}\, a_8 & a_1 + \mathrm{j}\, a_5 & a_3 + \mathrm{j}\, a_7 \\ \ldots & -a_4 + \mathrm{j}\, a_8 & a_2 - \mathrm{j}\, a_6 & -a_3 + \mathrm{j}\, a_7 & a_1 - \mathrm{j}\, a_5 \end{bmatrix}. \tag{5.26}$$

The code rate of 4-group QSTBC for 8 transmit antennas is one symbol pcu. In general, by construction, the rate of 4-group QSTBC for $2M$ transmit antennas is the same at the rate of MDC-QSTBC for M transmit antennas. Since the maximal rate of MDC-QSTBC is one symbol pcu [120], the maximal rate of 4-group QSTBC is also one symbol pcu and it is achievable for any number of transmit antennas. Since 4-group QSBTC is constructed for 2^m transmit antennas, if the number of transmit antennas is $M < 2^m$, then $(2^m - M)$ columns of the code matrix for 2^m transmit antennas can be deleted to obtain the code for M antennas. The resulting codes can be shown to achieve full-diversity [16, 96] if the mother code for 2^m antennas is full-diversity.

5.2.2 Decoding

We know that the symbols s_1, s_2, s_3, s_4 of F_4 can be separately detected. Therefore, from Theorem 5.2, the 4 groups of 8 symbols of F_8 can be detected independently. These 4 groups are $(s_1, s_2), (s_3, s_4), (s_5, s_6)$, and (s_7, s_8). We will present the decoding of 4-group QSTBC for 8 transmit antennas in details.

The decoding of 4-group QSTBC F_8 requires maximum likelihood search over 4 real-symbols [93]. It is desirable to alleviate this high complexity of maximum likelihood search by using a sphere decoder [107, 108]. To do so, we will derive an equivalent code and the equivalent channel of F_8.

The equivalent code of F_8 is obtained by column permutations for the code matrix of F_8 in (5.26): the order of columns is changed to (1, 3, 5, 7, 2, 4, 6, 8). This order of permutations is also applied for the rows of F_8. Let $x_1 = a_1 + \mathrm{j}\, a_5, x_2 = a_2 + \mathrm{j}\, a_6, x_3 = b_1 + \mathrm{j}\, b_5, x_4 = b_2 + \mathrm{j}\, b_6, x_5 = a_3 + \mathrm{j}\, a_7, x_6 = a_4 + \mathrm{j}\, a_8, x_7 = b_3 + \mathrm{j}\, b_7, x_8 = b_4 + \mathrm{j}\, b_8$ be the intermediate variables, we obtain a permutation-equivalent code of F_8 below

$$D = \begin{bmatrix} \mathcal{D}_1 & \mathcal{D}_2 \\ -\mathcal{D}_2^* & \mathcal{D}_1^* \end{bmatrix} \tag{5.27}$$

where

$$\mathcal{D}_1 = \begin{bmatrix} x_1 & x_2 & x_3 & x_4 \\ x_2 & x_1 & x_4 & x_3 \\ x_3 & x_4 & x_1 & x_2 \\ x_4 & x_3 & x_2 & x_1 \end{bmatrix}, \quad \mathcal{D}_2 = \begin{bmatrix} x_5 & x_6 & x_7 & x_8 \\ x_6 & x_5 & x_8 & x_7 \\ x_7 & x_8 & x_5 & x_6 \\ x_8 & x_7 & x_6 & x_5 \end{bmatrix}. \tag{5.28}$$

The sub-matrices $\mathcal{D}_1$ and $\mathcal{D}_2$ have a special form called *block-circulant matrix with circulant blocks* [64].

We next show how to decode the code D. For the sake of simplicity, we consider a single receive antenna. The generalization for multiple receive antennas is straightforward.

Assume that the transmit symbols are drawn from a constellation with unit average power. The transmit-receive signal model in (2.3) for the case of STBC D follows

$$\boldsymbol{y} = \sqrt{\frac{\rho}{8}} D\boldsymbol{h} + \boldsymbol{w}. \tag{5.29}$$

Let $\boldsymbol{x} = \begin{bmatrix} x_1 & x_2 & \dots & x_8 \end{bmatrix}^{\mathsf{T}}$, $\hat{\boldsymbol{y}} = \begin{bmatrix} y_1 & \dots & y_4 & y_5^* & \dots & y_8^* \end{bmatrix}^{\mathsf{T}}$, $\hat{\boldsymbol{w}} = \begin{bmatrix} w_1 & \dots & w_4 & w_5^* & \dots & w_8^* \end{bmatrix}^{\mathsf{T}}$, and

$$\mathcal{H}_1 = \begin{bmatrix} h_1 & h_2 & h_3 & h_4 \\ h_2 & h_1 & h_4 & h_3 \\ h_3 & h_4 & h_1 & h_2 \\ h_4 & h_3 & h_2 & h_1 \end{bmatrix}, \quad \mathcal{H}_2 = \begin{bmatrix} h_5 & h_6 & h_7 & h_8 \\ h_6 & h_5 & h_8 & h_7 \\ h_7 & h_8 & h_5 & h_6 \\ h_8 & h_7 & h_6 & h_5 \end{bmatrix}. \tag{5.30}$$

We have an equivalent expression of (5.29) as

$$\hat{\boldsymbol{y}} = \sqrt{\frac{\rho}{8}} \underbrace{\begin{bmatrix} \mathcal{H}_1 & \mathcal{H}_2 \\ \mathcal{H}_2^* & -\mathcal{H}_1^* \end{bmatrix}}_{\bar{\mathcal{H}}} \boldsymbol{x} + \hat{\boldsymbol{w}}. \tag{5.31}$$

Note that $\mathcal{H}_1$ and $\mathcal{H}_2$ are block-circulant matrices with circulant-blocks [64]. Thus, they are commutative and so do $\mathcal{H}_1^*$ and $\mathcal{H}_2^*$. We can multiply both sides of (5.31) with $\bar{\mathcal{H}}^\dagger$ to get

$$\underbrace{\bar{\mathcal{H}}^\dagger \hat{\boldsymbol{y}}}_{\bar{\boldsymbol{y}}} = \sqrt{\frac{\rho}{8}} \begin{bmatrix} \mathcal{H}_1^* \mathcal{H}_1 + \mathcal{H}_2^* \mathcal{H}_2 & \mathbf{0} \\ \mathbf{0} & \mathcal{H}_1^* \mathcal{H}_1 + \mathcal{H}_2^* \mathcal{H}_2 \end{bmatrix} \boldsymbol{x} + \underbrace{\bar{\mathcal{H}}^\dagger \hat{\boldsymbol{w}}}_{\bar{\boldsymbol{w}}}. \tag{5.32}$$

It is not hard to show that the noise elements of vector $\bar{\boldsymbol{w}}$ are correlated with covariance matrix $\bar{\mathcal{H}}^\dagger \bar{\mathcal{H}}$. Thus, this noise vector can be whitened by multiplying both sides of (5.32) with the matrix $(\bar{\mathcal{H}}^\dagger \bar{\mathcal{H}})^{-1/2}$. Let $\hat{\mathcal{H}} = \mathcal{H}_1^* \mathcal{H}_1 + \mathcal{H}_2^* \mathcal{H}_2$, (5.32) after the noise whitening step is equivalent to the following equations

$$\hat{\mathcal{H}}^{-1/2} \bar{\boldsymbol{y}}_1 = \sqrt{\tfrac{\rho}{8}} \hat{\mathcal{H}}^{1/2} \boldsymbol{x}_1 + \bar{\boldsymbol{w}}_1, \tag{5.33a}$$

$$\hat{\mathcal{H}}^{-1/2} \bar{\boldsymbol{y}}_2 = \sqrt{\tfrac{\rho}{8}} \hat{\mathcal{H}}^{1/2} \boldsymbol{x}_2 + \bar{\boldsymbol{w}}_2 \tag{5.33b}$$

where $\bar{\boldsymbol{y}}_1 = \begin{bmatrix} \bar{y}_1 & \bar{y}_2 & \bar{y}_3 & \bar{y}_4 \end{bmatrix}^{\mathsf{T}}$, $\bar{\boldsymbol{y}}_2 = \begin{bmatrix} \bar{y}_5 & \bar{y}_6 & \bar{y}_7 & \bar{y}_8 \end{bmatrix}^{\mathsf{T}}$, $\boldsymbol{x}_1 = \begin{bmatrix} x_1 & x_2 & x_3 & x_4 \end{bmatrix}^{\mathsf{T}}$, $\boldsymbol{x}_2 = \begin{bmatrix} x_5 & x_6 & x_7 & x_8 \end{bmatrix}^{\mathsf{T}}$. The noise vectors $\bar{\boldsymbol{w}}_1 = \hat{\mathcal{H}}^{-1/2} \begin{bmatrix} \bar{z}_1 & \bar{z}_2 & \bar{z}_3 & \bar{z}_4 \end{bmatrix}^{\mathsf{T}}$, $\bar{\boldsymbol{w}}_2 = \hat{\mathcal{H}}^{-1/2} \begin{bmatrix} \bar{z}_5 & \bar{z}_6 & \bar{z}_7 & \bar{z}_8 \end{bmatrix}^{\mathsf{T}}$ are uncorrelated and have elements $\sim \mathcal{CN}(0, 1)$.

At this point, the decoding of the 8 transmitted symbols in the code matrix D can be readily decoupled into 2 independent groups. However, since the code is a 4-group STBC, we can further decompose them into 4 groups in the following.

Denote the 2×2 (real) Fourier transform matrix by $\mathcal{F}_2 = \frac{1}{\sqrt{2}}\begin{bmatrix}1 & 1\\ 1 & -1\end{bmatrix}$. The block-circulant matrices $\mathcal{H}_1$ and $\mathcal{H}_2$ can be diagonalized by a (real) unitary matrix $T = \mathcal{F}_2 \otimes \mathcal{F}_2$ [64, Theorem 5.8.2, p. 185]. Note that $T^\dagger = T$, therefore, $\mathcal{H}_1 = T\Lambda_1 T$ and $\mathcal{H}_2 = T\Lambda_2 T$, where Λ_1 and Λ_2 are diagonal matrices, with eigenvalues of $\mathcal{H}_1$ and $\mathcal{H}_2$ in the main diagonal, respectively. Thus,

$$\hat{\mathcal{H}} = T(\Lambda_1^\dagger \Lambda_1 + \Lambda_2^\dagger \Lambda_2)T, \tag{5.34}$$

and also $\hat{\mathcal{H}}^{1/2} = T(\Lambda_1^\dagger \Lambda_1 + \Lambda_2^\dagger \Lambda_2)^{1/2}T$.

Since $\hat{\mathcal{H}}^{1/2}$ is a real matrix, (5.33) becomes

$$\hat{\mathcal{H}}^{-1/2}\Re(\bar{\boldsymbol{y}}_i) = \sqrt{\frac{\rho}{8}}\hat{\mathcal{H}}^{1/2}\Re(\boldsymbol{x}_i) + \Re(\bar{\boldsymbol{w}}_i), \qquad i = 1, 2, \tag{5.35a}$$

$$\hat{\mathcal{H}}^{-1/2}\Im(\bar{\boldsymbol{y}}_i) = \sqrt{\frac{\rho}{8}}\hat{\mathcal{H}}^{1/2}\Im(\boldsymbol{x}_i) + \Im(\bar{\boldsymbol{w}}_i), \qquad i = 1, 2. \tag{5.35b}$$

Note that $\Re(\boldsymbol{x}_1) = \begin{bmatrix}a_1 & a_2 & b_1 & b_2\end{bmatrix}^\mathsf{T} := \boldsymbol{d}_1$, i.e. $\Re(\boldsymbol{x}_1)$ is dependent on the complex symbols s_1 and s_2 only. Similarly, $\Re(\boldsymbol{x}_2), \Im(\boldsymbol{x}_1)$, and $\Im(\boldsymbol{x}_2)$ depend on $(s_3, s_4), (s_5, s_6)$, and (s_7, s_8), respectively.

From (5.35), the decoding of 8 transmitted complex symbols of STBC D reduces to the decoding of 4 groups, each with 4 real (or two complex) symbols. The maximum-likelihood solution of, for example, vector $\Re(\boldsymbol{x}_1)$, which consists of symbols s_1 and s_2, is:

$$\bar{\boldsymbol{d}}_1 = \arg\min_{\boldsymbol{d}_1}\left[\sqrt{\frac{\rho}{8}}\boldsymbol{d}_1^\mathsf{T}\hat{\mathcal{H}}\boldsymbol{d}_1 - 2\boldsymbol{d}_1^\mathsf{T}\Re(\bar{\boldsymbol{y}}_1)\right]. \tag{5.36}$$

Nevertheless, we can use a sphere decoder [108] to reduce the complexity of the maximum likelihood search (5.36). The matrix $\hat{\mathcal{H}}^{1/2}$ can be considered as the *equivalent channel* of the 4-group QSTBC D.

5.2.3 Performance Analysis

In (5.35), the four data vectors experience the same equivalent channel and the additive noise vectors have the same statistic; the PEP of the four vectors are the same. We only

need to consider the PEP of vectors $\boldsymbol{d}_1 = \Re(\boldsymbol{x}_1) = \begin{bmatrix} a_1 & a_2 & b_1 & b_2 \end{bmatrix}^{\mathsf{T}}$. For notational simplicity, the subindex 1 of $\boldsymbol{d}_1$ is dropped.

Additionally, we can introduce redundancy on the signal space by using a 4×4 real unitary rotation R to the data vector $\begin{bmatrix} a_1 & a_2 & b_1 & b_2 \end{bmatrix}^{\mathsf{T}}$ [138]. Thus, the data vector $\boldsymbol{d} = R \begin{bmatrix} a_1 & a_2 & b_1 & b_2 \end{bmatrix}^{\mathsf{T}}$. To keep the transmit power unchanged, the rotation matrix is assumed orthogonal, i.e. $R^{\mathsf{T}} R = \boldsymbol{I}$ [63].

From (5.35a), the PEP of the pair $\boldsymbol{d}$ and $\bar{\boldsymbol{d}}$ can be expressed by the Gaussian tail function as [32]

$$P(\boldsymbol{d} \to \bar{\boldsymbol{d}} | \hat{\mathcal{H}}) = Q\left(\sqrt{\frac{\rho}{8} \frac{|\hat{\mathcal{H}}^{1/2} R \boldsymbol{\delta}|^2}{4N_0}} \right) \tag{5.37}$$

where $N_0 = 1/2$ is the variance of the elements of the white noise vector $\Re(\boldsymbol{w}_1)$ in (5.35a), $\boldsymbol{\delta} = \boldsymbol{d} - \bar{\boldsymbol{d}}$. From (5.34), one has

$$P(\boldsymbol{d} \to \bar{\boldsymbol{d}} | \hat{\mathcal{H}}) = Q\left(\sqrt{\frac{\rho \left[\boldsymbol{\delta}^{\mathsf{T}} R^{\mathsf{T}} T^{\mathsf{T}} (\Lambda_1^{\dagger} \Lambda_1 + \Lambda_2^{\dagger} \Lambda_2) T R \boldsymbol{\delta} \right]}{16}} \right). \tag{5.38}$$

Let $\boldsymbol{\beta} = TR\boldsymbol{\delta}$. Remember that Λ_1 is a diagonal matrix with eigenvalues of $\mathcal{H}_1$ on the main diagonal. Let $\lambda_{i,j}$ $(i = 1, 2; j = 1, 2, 3, 4)$ be the eigenvalues of $\mathcal{H}_i$. Then $\Lambda_i = \operatorname{diag}(\lambda_{i,1}, \lambda_{i,2}, \lambda_{i,3}, \lambda_{i,4})$.

$$P(\boldsymbol{d} \to \bar{\boldsymbol{d}} | \hat{\mathcal{H}}) = Q\left(\sqrt{\frac{\rho (\sum_{i=1}^{2} \sum_{j=1}^{4} \beta_j^2 |\lambda_{i,j}|^2)}{16}} \right). \tag{5.39}$$

To derive a closed form of (5.38), we need to evaluate the distribution of $\lambda_{i,j}$. The eigenvectors of $\mathcal{H}_1$ is the columns of the matrix $T = \frac{1}{2} \mathcal{F}_2 \otimes \mathcal{F}_2$. Thus, the eigenvalues of $\mathcal{H}_1$ can be found to be

$$\begin{bmatrix} \lambda_{1,1} & \lambda_{1,2} & \lambda_{1,3} & \lambda_{1,4} \end{bmatrix}^{\mathsf{T}} = (\mathcal{F}_2 \otimes \mathcal{F}_2) \begin{bmatrix} h_1 & h_2 & h_3 & h_4 \end{bmatrix}^{\mathsf{T}}. \tag{5.40}$$

Since h_j $(j = 1, \ldots, 4)$ have distribution $\sim \mathcal{CN}(0, 1)$, thus, $\lambda_{1,j}$ $(j = 1, \ldots, 4)$ have distribution $\sim \mathcal{CN}(0, 4)$ and so do $\lambda_{2,j}$.

We now use the Craig's formular [131] to derive the conditional PEP in (5.39).

$$P(\boldsymbol{d} \to \bar{\boldsymbol{d}}|\hat{\mathcal{H}}) = Q\left(\sqrt{\frac{\rho(\sum_{i=1}^{2}\sum_{j=1}^{4}\beta_j^2|\lambda_{i,j}|^2)}{16}}\right)$$
$$= \frac{1}{\pi}\int_0^{\pi/2} \exp\left(\frac{-\rho(\sum_{i=1}^{2}\sum_{j=1}^{4}\beta_j^2|\lambda_{i,j}|^2)}{32\sin^2\alpha}\right) d\alpha. \quad (5.41)$$

We can apply a method based on the moment generating function (MGF) [132, 133] to obtain the unconditional PEP in the following:

$$P(\boldsymbol{d} \to \bar{\boldsymbol{d}}) = \frac{1}{\pi}\int_0^{\pi/2}\left[\prod_{i=1}^{4}\left(1+\frac{\rho\beta_i^2}{8\sin^2\alpha}\right)\right]^{-2} d\alpha. \quad (5.42)$$

Since there are four vectors to be decoded in each code matrix, the codeword PEP is therefore bounded by 4 times the PEP given in (5.42). Assume that there are σ possible vectors $\boldsymbol{d}$, the union bound on the frame error rate (FER) is

$$P_u = 4 \times \frac{2}{\sigma}\sum_{i=1}^{\sigma-1}\sum_{j=i+1}^{\sigma} P(\boldsymbol{d}^i \to \boldsymbol{d}^j). \quad (5.43)$$

We now examine the tightness of the union bound (5.43) compared with the simulated FER. Recall that the signal rotation R plays an important role on the decoding performance of 4-group QSTBC. In [93], the symbols s_1, s_3, s_5, s_7 are rotated by and angle γ_1, and the other symbols are rotated by an angle γ_2. This type of complex signal rotations is equivalent to the real signal rotation, denoted by R_{YGT}, below.

$$R_{YGT} = \begin{bmatrix} \cos\gamma_1 & \sin\gamma_1 & 0 & 0 \\ \sin\gamma_1 & -\cos\gamma_1 & 0 & 0 \\ 0 & 0 & \cos\gamma_2 & \sin\gamma_2 \\ 0 & 0 & \sin\gamma_2 & -\cos\gamma_2 \end{bmatrix}. \quad (5.44)$$

For this class of rotation matrices and 4QAM, the values $\gamma_1 = 7^\circ$ and $\gamma_2 = 23^\circ$ maximize the coding gain [16]. In Fig. 5.7, the FER of STBC D with the best-found rotation of the form in (5.44) is plotted for 16QAM. The union bound becomes tight at FER $< 10^{-2}$. Since a similar result was obtained with 4QAM, we omit the FER curve of 4QAM.

The tight union bound at medium and high SNR suggests that this bound can be used to optimize the signal rotation R. In the most general case, the 4×4 orthogonal matrix R has no less than 4 independent entries. Therefore, an exhaustive search becomes impractical.

To overcome this problem, we propose two search strategies with complexity reduction in the following.

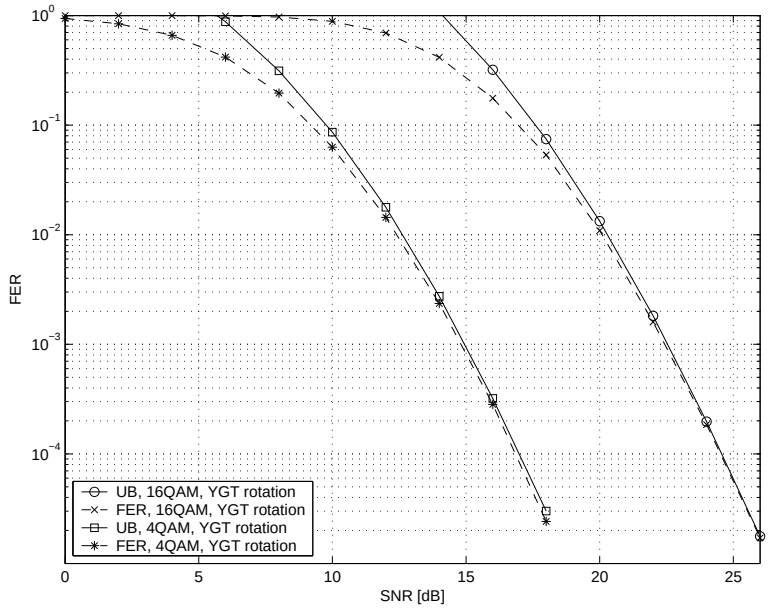

Figure 5.7: FER and union bound of 4-group QSTBC for (8, 1) system using the signal rotation in [93].

St1 Reducing number of independent variables of the rotation matrix R.

One class of the 4×4 real orthogonal matrix is given below:

$$R = \begin{bmatrix} o_1 & o_2 & o_3 & o_4 \\ -o_2 & o_1 & -o_4 & o_3 \\ -o_3 & o_4 & o_1 & -o_2 \\ -o_4 & -o_3 & o_2 & o_1 \end{bmatrix} \tag{5.45}$$

where $\sum_{i=1}^{4} o_i^2 = 1$ and entries o_i are real. Because of this normalization, there are only 3 independent variables out of 4 variables.

Another class of 4×4 orthogonal matrix is given in (5.44). This class has only two variables, we therefore would not expect further performance gain over the orthogonal family in (5.45).

St2 Optimizing R based on the asymptotic bound at high SNR. If $\beta_i \neq 0 \forall i = 1, 2, 3, 4$, then $1 + \frac{\rho\beta_i^2}{8\sin^2\alpha} \approx \frac{\rho\beta_i^2}{8\sin^2\alpha}$ at high SNR, the approximation of the exact PEP in (5.42) is

$$P(\boldsymbol{d} \to \bar{\boldsymbol{d}}) \approx \left(\frac{2^{24}\rho^{-8}}{\pi} \int_0^{\pi/2} (\sin\alpha)^{16} d\alpha \right) \prod_{i=1}^{4} |\beta_i|^{-4} = \frac{2^7\rho^{-8}16!}{8!8!} \prod_{i=1}^{4} |\beta_i|^{-4} \tag{5.46}$$

Using the asymptotic bound, the searching time is reduced tremendously, because no integration is required. We can also use the rotation given in (5.45) for the computer search. The values of o_i $(i = 1, 2, 3)$ are in the range $(-1, 1)$ and the increment is 0.005.

Similar to 4-group SAST codes, the asymptotic bound in (5.46) so that the PEP of 4-group QSTBC is heavily dependent on the product distance $\prod_{i=1}^{4} \beta_i$ (see, e.g. [138]). Recall that $\boldsymbol{\beta} = TR(\boldsymbol{d} - \bar{\boldsymbol{d}})$; we can consider the product matrix TR is a combined rotation matrix for data vector $\boldsymbol{d}$.

The exponent of SNR in (5.46) is -8. This indicates that the maximum diversity order of 4-group QSTBC is 8 and it is achievable if the product distance is non-zero for all possible data vectors. Furthermore, at high SNR, the asymptotic bound becomes very tight to the union bound and, therefore, very tight to the FER. Therefore, the larger the product distance, the lower FER can be obtained. This observation is very similar to the diversity-coding gain concept due to Tarokh *et al.* [16]. Thus, we can optimize the rotation by R so that the minimum product distance

$$d_{p,\min} = \min_{\forall \boldsymbol{d}^i, \boldsymbol{d}^j} \prod_{k=1}^{4} |\beta_k|, \qquad \text{where } \boldsymbol{\beta} = \left[TR(\boldsymbol{d}^i - \boldsymbol{d}^j)\right] \tag{5.47}$$

is non-zero and maximized.

Note that the searches for the best rotation matrix R based on the union bound (5.43) and the worst-case PEP (5.47) can be run independently. In addition, one can use the coding gain metric [16] to search for the matrix R [93]. The rotation matrix minimizing the union bound of FER should yield the lowest FER compared with the best rotation found by optimizing the worst-case PEP and coding gain. However, we have used the rotation matrices in (5.44) and (5.45) with a few independent variables to reduce the search complexity, the results may not as good as the case with the best rotation matrix in terms of optimizing the worst-case PEP.

If the complex signals are drawn from QAM, the (real) elements of $\boldsymbol{d}$ are in the set $\{\pm 1, \pm 3, \pm 5, \ldots\}$. The best known rotations for QAM in terms of maximizing the minimum product distance are provided in [139,140,142]; the rotation matrix for 4-dimensional vector is given in (4.27).

The FER and BER of 4-group QSTBC with 16QAM, using signal rotation in (4.27) and the best rotation in (5.44) (in terms of coding gain), are compared in Fig. 5.8. Clearly, the

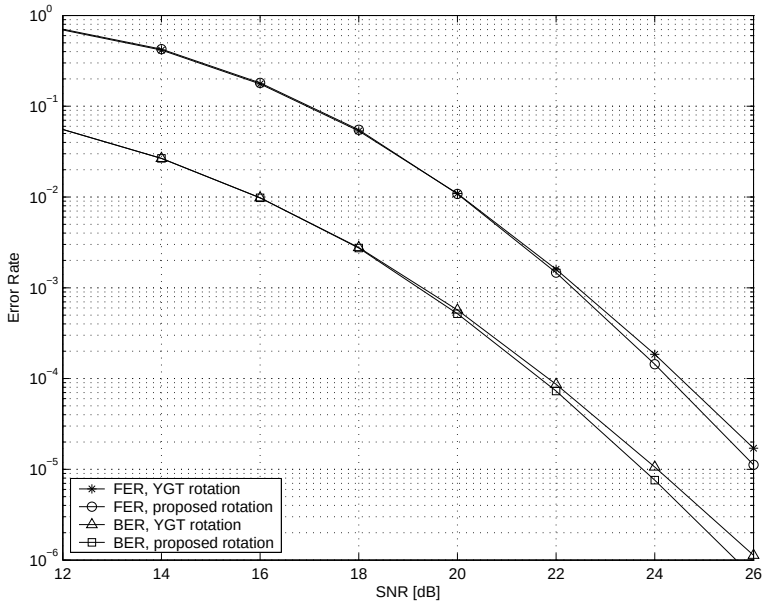

Figure 5.8: FER and BER of 4-group QSTBC with newly proposed rotation for (8, 1) system.

rotation in (5.44) performs better at high SNR.

We have compared performances of 4-group QSTBC with signal rotation in (4.27) and with the best rotations of the form (5.45) in terms of minimizing the union bound (5.43) and asymptotic bound (5.46). The rotation in (4.27) also yields the best performance. Thus, from now on, we use the rotation given in (4.27) for 4-group QSTBC.

Another application of the union bound on PEP is to compare the performance of 4-group QSTBC with different types of constellations. For example, we investigate the performance of 4-group QSTBC with 8QAM-R and 8QAM-S (see Fig. 4.2). The FER of 4-group QSTBC with these two constellations are also compared in Fig. 5.9. The union bounds for 8-ary constellations are very tight to the simulated FER when FER $< 10^{-2}$. We observe an SNR gain of 0.9 dB by using 8QAM-S instead of 8QAM-R. However, this improvement comes at the cost of complexity; we can use the sphere decoder to decode transmitted symbols from 8QAM-R, while maximum likelihood search must be used to decode signals from 8QAM-S.

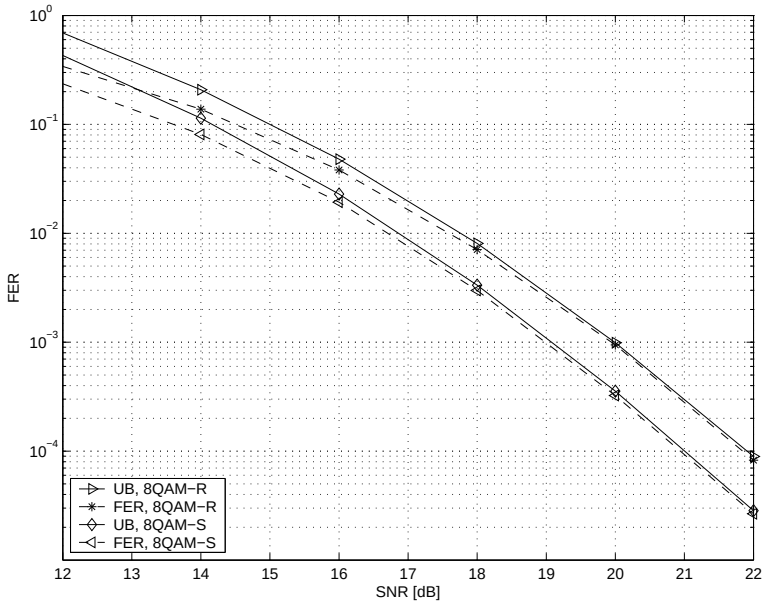

Figure 5.9: The union bound on FER of 4-group QSTBC using 8QAM-R and 8QAM-S rotated by the newly proposed rotation, (8, 1) system.

5.2.4 Summary

In this chapter, we have analyzed single-symbol decoding CIOD codes and 4-group QSTBC by applying the methods developed for OEST codes. The equivalent channels and new decoders of the two codes were derived. Optimal signal designs have been presented, based on the exact PEP and union bound. These results show that our approach for OEST codes is powerful for analyzing the performance of the existing STBC.

In the next chapter, design and performance of space-time codes in frequency selective fading channel are considered for MIMO-OFDM.

Chapter 6

Intercarrier Interference Self-Cancellation Space-Frequency Codes for MIMO-OFDM

In this chapter, the design of space-time codes in frequency-selective fading is considered. Since OFDM is robust against frequency-selective fading, it is used in current wireless systems and is under investigation for the future MIMO systems. In frequency-selective channels, the frequency diversity can be exploited so that the total diversity order becomes L_p times higher than that of a frequency-flat fading channel, where L_p is the channel order. This full spatial-frequency diversity can be extracted by combining OFDM with MIMO, and encoding the data symbols along the spatial and frequency dimensions. The resulting codes are called space-frequency codes. Since the performance of OFDM is sensitive to the intercarrier interference, which is caused by frequency offset, phase-noise, and time-varying channel, we will investigate the performance of space-frequency codes in the presence of intercarrier interference. Furthermore, a new encoding method will be proposed to effectively improve the performance of space-frequency codes when intercarrier interference is severe.

6.1 Introduction

The previous chapters focused on the low-decoding complexity STBC for flat-fading MIMO channels. In practice, because of the multipath propagation, the mobile wireless channels are frequency-selective. An OFDM front-end can be used to combat the frequency-

selective channels because OFDM converts the wideband frequency-selective channel into parallel frequency-flat channels. In order to exploit the frequency diversity, coding is performed across the subchannels or in the frequency dimension. Therefore, signal design for MIMO-OFDM can be regarded as space-frequency coding. Since the subchannels have different amplitudes and phases, the quasi-static assumption in space-time coding is no longer valid for space-frequency coding and low-complexity space-frequency code design is more difficult.

In OFDM systems, there are several inherent factors that could severely degrade the error rate performance of any space-frequency coding schemes. They are frequency offset, phase noise, fast time varying channels, to name a few. A residual frequency offset exists due to carrier synchronization mismatch and Doppler shift [85]. Residual frequency offset destroys subcarrier orthogonality, which generates inter-carrier interference and the BER increases consequently. The effect of such impairments on the conventional SISO (single input single output) OFDM has been widely investigated. For example, in [86], BER is calculated for uncoded SISO-OFDM systems with several modulation schemes. Several works have been done for MIMO-OFDM. The authors in [87], [88] provide BER expressions of MIMO-OFDM employing Alamouti's scheme [82]. The authors in [89] analyze the space-frequency code performance in different propagation settings, such as Rayleigh and Rician fading channels, and with spatial correlation at the transmitter and/or receiver. However, the impact of inter-carrier interference due to frequency offset on the pairwise error probability (PEP) performance of general space-frequency codes and whether the existing space-frequency code design criteria should be modified when inter-carrier interference exists have not been investigated. This important question will be addressed in this chapter.

We will analytically show that the conventional space-frequency code design criteria hold even with frequency offset. The performance loss is negligible if the normalized frequency offset is small. This loss, however, increases rapidly with the increasing normalized frequency offset and with SNR. When the normalized frequency offset is large, the dominance of inter-carrier interference noise power prevents the typical rapid decay of PEP with SNR and the PEP performance hits a floor.

Since inter-carrier interference can severely degrade the performance of OFDM, sev-

eral inter-carrier interference suppression methods are available (see [143], [144], [145] and references therein). For SISO-OFDM, the authors in [146], [147] propose an inter-carrier interference self-cancellation coding (or polynomial cancellation coding) method to mitigate inter-carrier interference (caused by frequency offset) effectively. By analyzing [146], [147] and [83], we derive a *new* class of space-frequency codes, named inter-carrier interference self-cancellation space-frequency (ISC-SF) codes, that provide a satisfactory trade-off among error correction ability, inter-carrier interference reduction and spectral efficiency. ISC-SF codes not only achieve the same diversity order (at least $2MN$) and coding gains as the corresponding space-frequency codes derived in [83] but also notably improve the performance of space-frequency codes with frequency offset. Although our primarily focus is the performance of ISC-SF codes with frequency offset, we demonstrate that ISC-SF codes also perform well when inter-carrier interference is caused by phase noise and time-varying channels. Due to the similar nature of inter-carrier interference caused by frequency offset, phase noise and time varying channels, we present the simulation results for frequency offset only.

6.2 MIMO-OFDM System Model

Consider a MIMO-OFDM system with M transmit and N receive antennas as illustrated in Fig. 1.4. The number of subcarriers in the OFDM modulators is K. The L_p-path quasi-static Rayleigh fading channel model is assumed for the link between transmit antenna m ($m = 1, ..., M$) and receive antenna n ($n = 1, ..., N$). The channel impulse response in the time domain is [6]

$$h_{m,n}(t, \tau) = \sum_{l=0}^{L_p-1} \alpha_{m,n}(t, l)\delta(\tau - \tau_l) \tag{6.1}$$

where τ_l is the channel delay of the lth path ($l = 0, ..., L_p - 1$) and $\delta(.)$ denotes Dirac's delta function. The coefficients $\alpha_{m,n}(t, l)$'s are complex channel gains of the lth path between transmit antenna m and receive antenna n. They are modeled as zero-mean complex Gaussian random variables (GRV's) with variance $\mathbb{E}\left[|\alpha_{m,n}(l)|^2\right] = \delta_l^2$. We assume the MIMO channel is spatially uncorrelated and remains constant for at least one OFDM symbol duration, but can vary randomly from symbol to symbol. Thus, the coefficients $\alpha_{m,n}(t, l)$ are independent variables and the time index t can be omitted. Without loss of generality,

the total power of L_p-path channels is normalized, so that $\sum_{l=0}^{L_p-1} \delta_l^2 = 1$. The frequency response of the channel between the transmit antenna m and the receive antenna n at subcarrier k is

$$H_{m,n}(k) = \sum_{l=0}^{L_p-1} \alpha_{m,n}(l)\ e^{-j2\pi k \Delta f \tau_l}\ , \quad j = \sqrt{-1} \tag{6.2}$$

where $\Delta f = 1/T_s$ is the subcarrier spacing and T_s is the OFDM symbol duration.

The transmitted symbols are distributed over M transmit antennas and K subcarriers of each OFDM modulator. Let $c_m(k)$ be the kth subcarrier being sent from transmit antenna m in one OFDM symbol duration. In the frequency domain, the transmitted symbols over M antennas can be represented in the matrix form as follows.

$$C = \begin{bmatrix} c_1(0) & c_2(0) & ... & c_M(0) \\ c_1(1) & c_2(1) & ... & c_M(1) \\ . & . & . & . \\ c_1(K-1) & c_2(K-1) & ... & c_M(K-1) \end{bmatrix}. \tag{6.3}$$

Before transmitting, the K symbols of each column in (6.3) are modulated by inverse discrete Fourier transform (IDFT) and cyclic prefix (CP) symbols are appended [148]. At the receiver side, the CP symbols are discarded to remove inter-block interference. The remaining K symbols are DFT demodulated to recover transmitted symbols in the frequency domain. Assume that received subcarriers are perfectly sampled and let the received signal at the receive antenna n be $y_n(k)$

$$y_n(k) = \sum_{m=1}^{M} c_m(k) H_{m,n}(k) + w_n(k)\ \ , k = 0, ..., K-1, \tag{6.4}$$

where $w_n(k)$'s are independent and identically distributed (i.i.d) noise samples, which are modeled as zero-mean complex GRV's. The transmit power from each antenna is normalized to 1, resulting a noise variance per dimension of $M/(2\rho)$ where ρ is the average SNR at each receive antenna.

The input-output relation of MIMO-OFDM systems can be described in several matrix forms. We adopt the approach in [83] to derive the PEP of space-frequency codes. For the zero frequency offset case, the received signal in (6.4) is presented in the vector form as

$$\mathbf{Y} = \mathbf{DH} + \mathbf{W} \tag{6.5}$$

where **Y** is the received signal vector that concatenates received signals of N receive antennas as

$$\mathbf{Y} = [\ y_1(0) \quad ... \quad y_1(K-1) \quad y_2(0) \quad ... \quad y_2(K-1) \quad y_N(0) \quad ... \quad y_N(K-1)\ ]^T, \tag{6.6}$$

and the channel vector H is of size $KMN \times 1$ is given by

$$\mathbf{H} = \left[\ H_{1,1}^T \quad ... \quad H_{M,1}^T \quad H_{1,2}^T \quad ... \quad H_{M,2}^T \quad ... \quad H_{1,N}^T \quad ... \quad H_{M,N}^T\ \right]^T \tag{6.7}$$

where

$$H_{m,n} = \left[\ H_{m,n}(0) \quad H_{m,n}(1) \quad ... \quad H_{m,n}(K-1)\ \right]^T. \tag{6.8}$$

The noise vector **W** is represented similarly to the received vector **Y** as

$$\mathbf{W} = [\ w_1(0) \quad ... \quad w_1(K-1) \quad w_2(0) \quad ... \quad w_2(K-1) \quad w_N(0) \quad ... \quad w_N(K-1)\ ]^T. \tag{6.9}$$

The data matrix **D** size $KM \times KMN$ represents the transmitted data in (6.3):

$$\mathbf{D} = \begin{bmatrix} D_1 & D_2 & \dots & D_M & 0 & 0 & \dots & 0 & \dots & 0 & 0 & \dots & 0 \\ 0 & 0 & \dots & 0 & D_1 & D_2 & \dots & D_M & \dots & 0 & 0 & \dots & 0 \\ \vdots & \vdots & \vdots & \vdots & \vdots & \vdots & \vdots & \vdots & \vdots & \vdots & \vdots & \vdots & \vdots \\ 0 & 0 & \dots & 0 & 0 & 0 & \dots & 0 & \dots & D_1 & D_2 & \dots & D_M \end{bmatrix}. \tag{6.10}$$

Each matrix D_m consists of coded symbols transmitted from antenna m

$$D_m = \mathrm{diag}\left[c_m(0), c_m(1), ..., c_m(K-1)\right]. \tag{6.11}$$

6.3 Model of MIMO-OFDM with Frequency Offset

We now extend the MIMO-OFDM system given in (6.5) for the non-zero frequency offset case. To subsume the frequency offset in (6.5), we first review the model of SISO systems with frequency offset that was described in [149].

There is always a frequency offset δf at the sampling points of received signal in frequency domain [149], [148]. In the SISO-OFDM system, the normalized frequency offset ε is defined by $\varepsilon = \delta f / \Delta f$. The normalized frequency offset is the same for all subcarriers of one OFDM symbol, but may vary from symbol to symbol. In the SISO systems, the received kth subcarrier is expressed as follows:

$$y(k) = \underbrace{S(0)H(k)c(k)}_{\text{desired signal}} + \underbrace{\sum_{p=0}^{K-1} \sum_{p \neq k} S(p-k)H(p)c(p)}_{\text{ICI}} + w(k) \tag{6.12}$$

Let $I(k)$ denotes inter-carrier interference from the other subcarriers to the received kth subcarrier:

$$I(k) = \sum_{p=0}^{K-1} \sum_{p \neq k} S(p-k) H(p) c(p) \,. \tag{6.13}$$

Coefficients $S(k)$ in (6.13) are expressed as:

$$S(k) = \frac{\sin\left[\pi\left(k+\varepsilon\right)\right]}{K \sin\left[\frac{\pi}{K}\left(k+\varepsilon\right)\right]} \exp\left[j\pi\left(1-\frac{1}{K}\right)\left(k+\varepsilon\right)\right] \,. \tag{6.14}$$

The coefficient $S(0)$ in (6.12) can be derived by substituting $k = 0$ in (6.14) to be

$$S(0) = \frac{\sin\left(\pi\varepsilon\right)}{K \sin\left(\frac{\pi}{K}\varepsilon\right)} \exp\left[j\pi\left(1-\frac{1}{K}\right)\varepsilon\right] \,. \tag{6.15}$$

Eqs. (6.12) and (6.15) show that due to the frequency offset, the amplitude of the desired subcarrier is attenuated and its phase is rotated. Furthermore, the inter-carrier interference from the other subcarriers can be considered as an additional noise. Hence, the SNR of the received signal is reduced.

We now generalize (6.12) for MIMO-OFDM systems and allow for distinct frequency offset's among different transmit/receive antennas pairs. Let the normalized frequency offset of the transmission link from transmit antenna m and receive antenna n be $\varepsilon_{m,n}$. For MIMO systems, the inter-carrier interference term $I_n(k)$ at subcarrier k of each receive antenna n is the superposition of M inter-carrier interference terms $I_{m,n}(k)$ caused by transmitted signals from transmit antennas m as

$$I_n(k) = \sum_{m=1}^{M} I_{m,n}(k) \tag{6.16}$$

where

$$I_{m,n}(k) = \sum_{p=0}^{K-1} \sum_{p \neq k} c_m(p) H_{m,n}(p) S_{m,n}(p-k) \tag{6.17}$$

and

$$S_{m,n}(k) = \frac{\sin\left[\pi\left(k+\varepsilon_{m,n}\right)\right]}{K \sin\left[\frac{\pi}{K}\left(k+\varepsilon_{m,n}\right)\right]} \exp\left[j\pi\left(1-\frac{1}{K}\right)\left(k+\varepsilon_{m,n}\right)\right] \tag{6.18}$$

$$S_{m,n}(0) = \frac{\sin\left(\pi\varepsilon_{m,n}\right)}{K \sin\left(\frac{\pi}{K}\varepsilon_{m,n}\right)} \exp\left[j\pi\left(1-\frac{1}{K}\right)\varepsilon_{m,n}\right] \,. \tag{6.19}$$

Eq. (6.12) becomes:

$$y_n(k) = \sum_{m=1}^{M} c_m(k) H_{m,n}(k)\, S_{m,n}(0) + I_n(k) + w_n(k) \,. \tag{6.20}$$

Note that $S_{m,n}(0)$ is a constant with respect to subcarrier index k. Hence, in (6.20) we can group $H_{m,n}(k)$ and $S_{m,n}(0)$ as:

$$\tilde{H}_{m,n}(k) = S_{m,n}(0)H_{m,n}(k)\,.$$

The equivalent form of (6.8) is

$$\tilde{H}_{m,n} = \left[\tilde{H}_{m,n}(0)\ \tilde{H}_{m,n}(1)...\ \tilde{H}_{m,n}(K-1)\right]^T\,. \tag{6.21}$$

Matrices $\tilde{H}_{m,n}$ are arranged into the matrix $\tilde{\mathbf{H}}$, which has exactly the same structure with the matrix $\mathbf{H}$ given in (6.7), but the matrix $\tilde{\mathbf{H}}$ accounts for the presence of frequency offset.

The equivalent noise at each received subcarrier is a sum of the inter-carrier interference noise and complex Gaussian thermal noise terms as

$$\tilde{z}_n(k) = I_n(k) + w_n(k)\,. \tag{6.22}$$

The MIMO-OFDM model with frequency offset is now written as

$$\mathbf{Y} = \mathbf{D}\tilde{\mathbf{H}} + \tilde{\mathbf{W}} \tag{6.23}$$

where $\mathbf{Y}$ is the received vector and the matrix $\mathbf{D}$ consists of transmitted symbols. They are described in (6.6) and (6.10) accordingly and rewritten in (6.23) without modification.

The matrix representations (6.5) and (6.23) are suitable for deriving the PEP performance of space-frequency codes. In the next section, the PEP upper bound of space-frequency codes without frequency offset based on (6.5) will be given. It is an asymptotic bound [150] and is tighter than the Chernoff bound [16] at high SNR. In the presence of frequency offset, the equivalent representation (6.23) will be used to derive the PEP performance (Section IV).

6.4 Design Criteria of Space-Frequency Codes

In the space-frequency encoding process, the source data is two-dimensionally encoded across the space (over multiple antennas) and frequency (over the subcarriers of OFDM symbols). A space-frequency codeword may occupy several OFDM symbols [77], [81]

or one OFDM symbol [67], [42], [83]. The maximal diversity order can be achieved by coding over the subcarriers of only one OFDM symbol [67], [83], whereas in [77], [81] the maximal diversity order is gained by coding over multiple OFDM symbols. That obviously causes higher coding and decoding delay. We adopt the approach in [83] for our analysis. In the following, we summarize the results of [83].

The input data symbols are divided into b-symbol source words and are parsed into blocks and mapped to space-frequency codewords as represented in (6.3). At the receiver, the maximum likelihood (ML) decoder selects a codeword E if its metric Me is minimum:

$$Me = \sum_{k=0}^{K-1} \sum_{n=1}^{N} \left| y_n(k) - \sum_{m=1}^{M} c_m(k) H_{m,n}(k) \right|^2 . \tag{6.24}$$

Assume perfect channel state information (CSI) is available at the receiver but not at the transmitter and perfect symbol timing. The PEP for a transmitted codeword C and erroneously decoded codeword E in a frequency-selective fading fading channel is upper bounded as [83]:

$$P(C \to E) \leq \begin{pmatrix} 2\Gamma N - 1 \\ \Gamma N \end{pmatrix} \left(\prod_{i=1}^{\Gamma} \lambda_i \right)^{-N} \rho^{-\Gamma N} \tag{6.25}$$

where Γ is the rank of the matrix Q which is defined as

$$Q \triangleq \Delta \circ R \tag{6.26}$$

and where $\circ$ denotes Hadamard product [63] and $\lambda_i (i = 1, ..., \Gamma)$ are non-zero eigenvalues of Q. The matrices Δ and R are as follows:

$$\Delta = (C - E)(C - E)^{\dagger} , \tag{6.27}$$

$$R = R_{m,n} = \mathbb{E}\left[H_{m,n} H_{m,n}^{\dagger} \right] = V \operatorname{diag}\left(\delta_0^2, \delta_1^2, ..., \delta_{L_p-1}^2 \right) V^{\dagger} \tag{6.28}$$

where

$$V = \begin{bmatrix} 1 & 1 & \dots & 1 \\ v^{\tau_0} & v^{\tau_1} & \dots & v^{\tau_{L_p-1}} \\ \vdots & \vdots & \vdots & \vdots \\ v^{(K-1)\tau_0} & v^{(K-1)\tau_1} & \dots & v^{(K-1)\tau_{L_p-1}} \end{bmatrix} \tag{6.29}$$

and $v = e^{-j2\pi\Delta f}$.

From (6.25), the space-frequency code design criteria can be stated as follows.

- Diversity criterion: The minimum rank of Q over all pairs of distinct codewords should be as large as possible.
- Product criterion: The minimum value of the product $\prod_{i=1}^{\Gamma} \lambda_i$ over all pairs of distinct codewords should be also maximized.

From (6.25), the diversity order of space-frequency codes is ΓN, maximum achievable diversity order is equal to $\min(L_p MN,\, KN)$.

6.5 Performance of Space-Frequency Codes with Frequency Offset

We continue the analysis with the two assumptions below:

- AS1: Residual normalized frequency offset's $\varepsilon_{m,n}$ are independent of the channel coefficients.
- AS2: The inter-carrier interference terms $I_{m,n}(k)$ in (6.16) and (6.17) are independent.

The coherent receiver first estimates the channel coefficients. Then the phase shift caused by frequency offset is compensated [149]. Thus, the residual frequency offset is somehow dependent on the channel estimation method. The AS1 is given to simplify our analysis. In practice, transmit data over multiple antennas are encoded. There may be a degree of correlation among the transmitted data streams and consequently, the inter-carrier interference noise terms $I_{m,n}(k)$ could be also correlated with respect to the subscript m. With AS2, all the inter-carrier interference noise at the receive antennas will have the same variance and zero mean. AS2 will be made clearer during the derivation below. Therefore, the ML detection in the presence of AWGN noise given in (6.24) holds.

To investigate the PEP of space-frequency codes with frequency offset using formula (6.25), the channel coefficients $\tilde{H}_{m,n}(k)$ in (6.21) should be complex GRVs. This requirement can be met if $S_{m,n}(0)$ is deterministic or normalized frequency offset is not a random variable (Case 1). In general case, $\varepsilon_{m,n}$ can be assumed to be i.i.d random variables in the range $[E_1,\, E_2]$, their values can be changed from OFDM symbol to symbol (Case 2).

However, the performance of space-frequency codes with fixed values of frequency offset is of greater interest since it provides a closer look at the performance of space-frequency codes at specific frequency offset values.

For analytical tractability, we further have the third assumption:

- AS3: normalized frequency offset $\varepsilon_{m,n}$ are constant and the same for all pair of indices (m, n): $\varepsilon_{m,n} = \varepsilon_0$.

If $|E_1| = |E_2| = |\varepsilon_0|$ (if the absolute value of random normalized frequency offset is not more than a fixed normalized frequency offset value), we expect that the PEP performance of Case 2 is more optimistic than that of the Case 1. Therefore, PEP obtained with AS3 is an upper bound of PEP with frequency offset. This assumption will be relaxed in our simulation study and thus more realistic performance evaluation is carried out by simulations. Our analytical results below, however, provide useful insight into the inter-carrier interference performance of space-frequency codes.

In OFDM systems, K is typically 64 or larger. Therefore, the central limit theorem can be applied to model the term $I_{m,n}(k)$ as a GRV [148]. The inter-carrier interference term $I_n(k)$ in (6.16) is a sum of M independent GRV's, it is also a GRV. The first two moments of the term $I_{m,n}(k)$ in (6.17) by Gaussian approximation are calculated as follows. Assume that coded symbols $c_m(p)$ have zero-mean (such as M-PAM, M-PSK, M-QAM signal constellations), then $\mathbb{E}\left[I_{m,n}(k)\right] = 0$.

The variance $\sigma^2_{I_{m,n}}$ of $I_{m,n}(k)$ in (6.17) is

$$\begin{aligned}
\sigma^2_{I_{m,n}} &= \mathbb{E}\left[|I_m(k)|^2\right] \\
&= \mathbb{E}\left[\left|\left(\sum_{p=0}^{K-1} c_m(p)H_{m,n}(p)S_{m,n}(p-k)\right) - c_m(k)H_{m,n}(k)S_{m,n}(0)\right|^2\right] \\
&= \mathbb{E}\left[\left|\left(\sum_{p=0}^{K-1} c_m(p)H_{m,n}(p)S_{m,n}(p-k)\right)\right|^2\right] - \mathbb{E}\left[|c_m(k)H_{m,n}(k)S_{m,n}(0)|^2\right] \\
&= \sum_{p=0}^{K-1} \mathbb{E}\left[|c_m(p)|^2\right]\mathbb{E}\left[|H_{m,n}(p)|^2\right]\mathbb{E}\left[|S_{m,n}(p-n)|^2\right] \\
&\quad - \mathbb{E}\left[|c_m(k)|^2\right]\mathbb{E}\left[|H_{m,n}(k)|^2\right]\mathbb{E}\left[|S_{m,n}(0)|^2\right] . \qquad (6.30)
\end{aligned}$$

In the last two rows of (6.30), the term $\mathbb{E}\left[|c_m(k)|^2\right]$ is the signal power, which is normalized to 1. The term $\mathbb{E}\left[|H_{m,n}(k)|^2\right]$ is the average of the channel power, and it is also

normalized to 1. Eq. (6.30) becomes

$$\sigma^2_{I_{m,n}} = \sum_{p=0}^{K-1} \mathbb{E}\left[|S(p-k)|^2\right] - S_0 \tag{6.31}$$

where $S_0 = \mathbb{E}\left[|S_{m,n}(0)|^2\right] = |S_{m,n}(0)|^2$. Note that the residual normalized frequency offset is usually small, $\varepsilon \leq 0.2$ [148], the number of subcarriers $K \geq 8$, hence $K\sin(\pi\varepsilon/K) \approx \pi\varepsilon$. Let $p(\varepsilon)$ be the probability density function (pdf) of $\varepsilon_{m,n}$. In the case of constant frequency offset, $p(\varepsilon) = 1$, S_0 can be evaluated as

$$S_0 = \left(\frac{\sin(\pi\varepsilon_0)}{\pi\varepsilon_0}\right)^2 = [\mathrm{sinc}(\varepsilon_0)]^2 \tag{6.32}$$

where $\mathrm{sinc}(x) = \frac{\sin(\pi x)}{\pi x}$.

It is found in [85] that the sum $\sum_{p=0}^{K-1} \mathbb{E}\left[|S(p-k)|^2\right] = 1$, hence

$$\sigma^2_{I_{m,n}} = 1 - S_0\,. \tag{6.33}$$

It is clear that $\sigma^2_{I_{m,n}}$ is independent of indices m and n, it is just dependent on the normalized frequency offset through S_0. With AS2, $I_n(k)$ is a complex GRV with zero-mean and variance $M(1-S_0)$. Therefore, the inter-carrier interference noise of MIMO-OFDM $\tilde{z}_n(k)$ given in (6.22) is also a zero-mean complex GRV with variance as

$$\sigma^2_z = M\left(1 - S_0 + 1/\rho\right). \tag{6.34}$$

Values of σ^2_z is identical for all receive antennas.

From (6.20), it is seen that the received signal power has a factor of S_0; hence the equivalent SNR at each receive antenna with frequency offset is

$$\tilde{\rho} = \frac{MS_0}{\sigma^2_z} = \left(\frac{S_0}{(1-S_0)\rho + 1}\right)\rho\,. \tag{6.35}$$

Using the MIMO-OFDM model developed in Section 6.3 and space-frequency code design criteria in Section 6.4, we derive PEP performance given in (6.25) with frequency offset in the following.

The correlation matrix defined in (6.28) for equivalent channel matrix $\tilde{H}_{m,n}$ given in (6.21) has a new form

$$\tilde{R} = \tilde{R}_{m,n} = \mathbb{E}\left[\tilde{H}_{m,n}(\tilde{H}_{m,n})^\dagger\right] = S_0\,\mathbb{E}\left[H_{m,n}H^\dagger_{m,n}\right] = S_0 R_{m,n}\,. \tag{6.36}$$

Hence, the matrix Q in (6.26) becomes matrix $\tilde{Q}$

$$\tilde{Q} = \Delta \circ \tilde{R}_{m,n} = S_0 \left(\Delta \circ R_{m,n}\right) = S_0 Q \,. \tag{6.37}$$

We can easily verify that:

- Matrices Q and $\tilde{Q}$ have the same rank Γ.
- If λ_i is an eigenvalue of Q then $\tilde{\lambda}_i = S_0 \lambda_i$ is an eigenvalue of $\tilde{Q}$.

Substitute $\tilde{\lambda} = S_0 \lambda_i$ and $\tilde{\rho}$ into (6.25), re-arrange the terms, the PEP expression with frequency offset is

$$P\left(C \to E\right) \leq L_0 \binom{2\Gamma N - 1}{\Gamma N} \left(\prod_{i=1}^{\Gamma} \lambda_i\right)^{-N} \rho^{-\Gamma N} \tag{6.38}$$

where

$$L_0 = \left(\frac{{S_0}^2}{\rho(1 - S_0) + 1}\right)^{-\Gamma N} . \tag{6.39}$$

Comparing (6.25) and (6.38), we discern that L_0 represents the PEP performance loss due to frequency offset. From (6.25), (6.38) and (6.39), we draw the following theoretical conclusions:

1. The design criteria for space-frequency codes without frequency offset is still valid in the case of frequency offset. The code design should maximize the diversity order and coding gain.

2. For the same transmit power, the higher the normalized frequency offset, the higher PEP performance loss. That is, at the same PEP, the higher normalized frequency offset, the further PEP curve shifted to the right.

3. The PEP curves will shift right if frequency offset is nonzero. However, with the same normalized frequency offset, the shift of PEP curves of lower diversity order systems is larger than the shift of PEP curves of the system with higher diversity order. This is due to the fact that given the same loss factor L_0, the SNR compensation for this loss is smaller for the codes with higher diversity order [c.f. (6.39)]. Thus, the higher diversity order systems are more robust to the effects of frequency offset.

4. If $\rho\left(1-S_0\right) \gg 1$ or at high transmit power and high value of frequency offset,

$$P\left(C \rightarrow E\right) \leq \binom{2\Gamma N-1}{\Gamma N}\left(\prod_{i=1}^{\Gamma}\lambda_i\right)^{-N} \times \left(\frac{{S_0}^2}{1-S_0}\right)^{-\Gamma N}. \tag{6.40}$$

The PEP is no longer inversely proportional with SNR and hits a floor.

These analytical results can be anticipated since the inter-carrier interference term is considered as an additional Gaussian noise. When frequency offset is small, the inter-carrier interference power is smaller than the power of thermal noise; thus, its impact on the performance of space-frequency codes is negligible. However, when the frequency offset is large, the inter-carrier interference noise dominates thermal noise. The inter-carrier interference power increases with desired signal power. Therefore, when SNR is large, inter-carrier interference causes the error floor as we have derived. Nevertheless, the analytical results reveal explicitly that when residual frequency offset is small, about 1%, the performance loss is almost negligible (cf. (6.39)).

To complete this section, we note that one can derive the ML receiver using (6.20) and (6.24), the same result as (6.38) can be obtained.

6.6 Inter-Carrier Interference Self-Cancellation Space-Frequency Codes

In Section IV, we have shown that if the normalized frequency offset is high, the PEP performance is limited by a floor level at high SNR. Thus, a space-frequency code which can mitigate the effects of high normalized frequency offset is desirable. We now relate space-frequency codes and polynomial cancellation coding (PCC). PCC is first proposed by authors in [146]. This idea is further analyzed in [147] from theory of finite differences.

We now summarize and analyze the main results of PCC in [146]. To mitigate the inter-carrier interference caused by frequency offset, one coded or uncoded data symbol modulates a group of r, where $r = 2, 3, 4, ...$, consecutive subcarriers. The optimum weighting coefficients for r subcarriers to minimize inter-carrier interference are the coefficients of the polynomial $(1-D)^{r-1}$. The code rate of PCC is $1/r$. The inter-carrier interference performance of this coding scheme increases with r at the cost of spectral efficiency. Simulation

results [146] show that this coding scheme with $r = 2$ (or code rate $1/2$) outperforms the system using rate $1/2$ convolutional code when normalized frequency offset is high (20%) but PCC performs poorly when normalized frequency offset is small or medium ($\leq 10\%$). The reason is that this code is particularly designed to minimize inter-carrier interference and hence may not be suitable for error correction purposes. To improve the performance of PCC, an outer error control code is required. The resultant concatenated code has lower rates as r increases. Thus, the smallest possible value of $r, r = 2$ is of practical interest.

Another result of [146] is the inter-carrier interference cancellation demodulation concept. For example, when $r = 2$ one data symbol x is sent over two subcarriers that satisfies: $c(k) = x$, $c(k+1) = -x$. This process is called inter-carrier interference cancellation modulation. The received signals $y(k)$ and $y(k+1)$ create a new signal for detection: $\bar{y}(k) = y(k) - y(k+1)$. This process is named interference cancellation demodulation. The combination of interference cancellation modulation and demodulation is called inter-carrier interference self-cancellation (ISC). The inter-carrier interference noise power of ISC is smaller than the original inter-carrier interference and inter-carrier interference of interference cancellation demodulation. Therefore, the ISC scheme is powerful against frequency offset. From a diversity point of view, using two values $y(k)$ and $y(k+1)$ to detect one transmitted symbol x could yield a diversity order of two. Since there is a strong correlation between adjacent subcarriers, however, the use of the two signals $y(k)$ and $y(k+1)$ may not, in fact, provide a diversity order of two. Our target is to maximize the diversity order of space-frequency codes. Thus, the interference cancellation modulation is our concern, but not the ISC scheme.

In sum, PCC is suitable for inter-carrier interference reduction. However, its error correction ability and spectral efficiency are low. Therefore, a low order PCC code with $r = 2$ concatenated with powerful error control codes would be a good trade-off solution. We next develop the idea of interference cancellation modulation to design a class of space-frequency codes that are robust to inter-carrier interference.

Su $et\,al.$ [83] show that the space-frequency code formed by repeating each row of a full diversity order space-time codeword r times ($1 \leq r \leq L_p$) achieves at least the diversity order $d = rMN$. This repetition obviously reduces the spectral efficiency; thus, we consider only $r = 2$.

Let the number of OFDM subcarriers $K = 2\hat{K}$. Suppose that the length of a space-frequency codeword equals to the number of subcarriers K. If the space-frequency codeword length is smaller than K, a zero-padding matrix can be used for the remaining subcarriers. A space-frequency codeword has the form

$$C_1 = \begin{bmatrix} c_1(0) & c_2(0) & ... & c_M(0) \\ c_1(0) & c_2(0) & ... & c_M(0) \\ . & . & ... & . \\ c_1(\hat{K}-1) & c_2(\hat{K}-1) & ... & c_M(\hat{K}-1) \\ c_1(\hat{K}-1) & c_2(\hat{K}-1) & ... & c_M(\hat{K}-1) \end{bmatrix}. \tag{6.41}$$

Applying the interference cancellation modulation scheme, for $r = 2$, this scheme is actually a repetition scheme but the repeated symbols are sign-reversed. In the case of MIMO-OFDM, the repeated rows are sign-reversed to form new ISC-SF codewords as

$$C_2 = \begin{bmatrix} c_1(0) & c_2(0) & ... & c_M(0) \\ -c_1(0) & -c_2(0) & ... & -c_M(0) \\ . & . & ... & . \\ c_1(\hat{K}-1) & c_2(\hat{K}-1) & ... & c_M(\hat{K}-1) \\ -c_1(\hat{K}-1) & -c_2(\hat{K}-1) & ... & -c_M(\hat{K}-1) \end{bmatrix}. \tag{6.42}$$

We call the space-frequency coding schemes given in (6.41) and (6.42) as SC1 and SC2 for short. We now prove that the new coding scheme SC2 yields the same coding gain and diversity order (at least $d = 2MN$) compared with SC1, but SC2 integrates inter-carrier interference self-cancellation capability.

Consider an entry $a_{i,j}$ of the matrix Δ_1 defined in (6.27) being created by space-frequency codewords (6.41). The entry $b_{i,j}$ of the matrix Δ_2 being created by space-frequency codewords in (6.42) is related with $a_{i,j}$ as

$$b_{ij} = \begin{cases} a_{ij}, & \text{if } (i+j) \text{ is even} \\ -a_{ij}, & \text{if } (i+j) \text{ is odd}. \end{cases}$$

Note that the size of Δ_1 and Δ_2 is $K \times K, K = 2\hat{K}$ and, in particular, they can be written as follows.

$$\Delta_1 = \begin{bmatrix} a_{11} & a_{12} & \cdots & a_{1K} \\ a_{21} & a_{22} & \cdots & a_{2K} \\ \vdots & \vdots & \ddots & \vdots \\ a_{K1} & a_{K2} & \cdots & a_{KK} \end{bmatrix},$$

$$\Delta_2 = \begin{bmatrix} b_{11} & b_{12} & \cdots & b_{1K} \\ b_{21} & b_{22} & \cdots & b_{2K} \\ \vdots & \vdots & \ddots & \vdots \\ b_{K1} & b_{K2} & \cdots & b_{KK} \end{bmatrix} = \begin{bmatrix} +a_{11} & -a_{12} & \cdots & -a_{1K} \\ -a_{21} & +a_{22} & \cdots & +a_{2K} \\ \vdots & \vdots & \ddots & \vdots \\ -a_{K1} & +a_{K2} & \cdots & +a_{KK} \end{bmatrix}.$$

The matrix R defined in (6.28) is the same for both SC1 and SC2. Therefore, comparing the signs of entries of $Q_1 = \Delta_1 \circ R$ and $Q_2 = \Delta_2 \circ R$ (defined in (6.26)), we can see that the signs of entries of Q_2 are changed in accordance with the sign changes of entries of Δ_2 compared to Δ_1. Thus, we have following relationship:

- If vector $X_1 = \begin{bmatrix} x_1 & x_2 & x_3 & x_4 & ... & x_{K-1} & x_K \end{bmatrix}$ is an eigenvector of $Q_1 = \Delta_1 \circ R$, then $X_2 = \begin{bmatrix} x_1 & -x_2 & x_3 & -x_4 & ... & x_{K-1} & -x_K \end{bmatrix}$ is an eigenvector of $Q_2 = \Delta_2 \circ R$ and vice verse, where (Q_1, Δ_1) and (Q_2, Δ_2) are sets of matrices associated with space-frequency codewords defined in (6.26) and (6.27) respectively.

- If λ is an eigenvalue of X_1, it is also an eigenvalue of X_2 and vice verse. The rank of Q_1 and Q_2 are the same, hence, space-frequency codes SC1 and SC2 have the same diversity order.

Thus, space-frequency codes constructed as in (6.41) and (6.42) have the same diversity order and coding gain.

We refer to SC2 codes as inter-carrier interference self-cancellation space-frequency codes or ISC-SF codes for short. The code rate of ISC-SF is $R_t/2$, where R_t is the code rate of the underlying ST code. Repetition the space-frequency codewords more than twice in combination with polynomial cancellation coding will gain additional diversity order and inter-carrier interference mitigation. However, the price paid for those improvements is the spectral efficiency reduction. Moreover, from the simulation results, we will see that the ISC-SF codes ($r = 2$) perform well compared with the codes without inter-carrier interference cancellation. The higher order PCC codes ($r > 2$) would not significantly improve inter-carrier interference reduction. Thus, analysis of the space-frequency schemes with higher repetition orders (i.e. lower rate) is not discussed further. The ISC-SF coding scheme (6.42) gives a satisfactory trade-off among error-control performance, inter-carrier interference reduction and spectral efficiency.

6.7 Phase Noise and Time Varying Channel

Channel variations and phase noise also produce inter-carrier interference. In Section II, we assume that the MIMO channels remain constant during one OFDM symbol. However, due to the relative movement of the transmitter and receiver, the channels may vary during one OFDM symbol. This variation causes inter-carrier interference and makes BER increase (see [151], [145] and references therein). For the description of phase noise and its effects, the readers may refer to the references [152], [143], [71].

In the following, we use continuous time model to show how inter-carrier interference is created by phase noise and time varying channels. Consider SISO-OFDM systems. The transmitted signal over a block including CP, is given by

$$s(t) = \sum_{k=0}^{K-1} c(k) e^{j2\pi k \Delta f t} \quad , -T_{cp} \leq t \leq T_s, \tag{6.43}$$

where T_{cp} is the length of CP. The duration of one OFDM symbol with CP is $T_b = T_{cp} + T_s$.

The signal at the input of the receiver is

$$\begin{aligned} r(t) = s(t) * h(t,\tau) &= \int_{-\infty}^{\infty} h(t,\tau) s(t-\tau) dt + w(t) \\ &= \sum_{k=0}^{K-1} \sum_{l=0}^{L_p-1} c(k) h(t,\tau_l) e^{-j2\pi k \Delta f \tau_l} e^{j2\pi k \Delta f t} + w(t)\,. \end{aligned} \tag{6.44}$$

where w(t) is an AWGN process with zero-mean and one-sided power spectral density is N_0. At the demodulator, the phase noise $\phi(t)$ between the carrier and the local oscillator is added to the phase of received signals. In the baseband representation, adding phase noise is equivalent to multiply $r(t)$ with $\theta(t) = e^{j\phi(t)}$.

If we consider the effect of frequency offset only as in Section II-B, let $\phi(t) = 0$ and $h(t,\tau)$ to be constant, one can derive $y(p)$ as in (6.12). In this section, we consider the inter-carrier interference due to phase noise and time varying channels. Thus, we let $\delta f = 0$ to simplify the expressions. The demodulated signal $y(p)$ is

$$y(p) = T_s^{-1} \sum_{k=0}^{K-1} \sum_{l=0}^{L_p-1} \left(c(k) e^{-j2\pi k \Delta f \tau_l} \int_0^{T_s} h(t,\tau_l) e^{j\phi(t)} e^{j2\pi (k-p) \Delta f t} dt \right) + w(p). \tag{6.45}$$

To consider the effect of time varying channels only, let $\phi(t) = 0$ in (6.45), we have

$$y(p) = \underbrace{\breve{H}(p)c(p)}_{\text{desired signal}} + \underbrace{\sum_{k=0,k\neq p}^{K-1} \breve{H}(p-k)c(k)}_{\text{ICI}} + w(p) \tag{6.46}$$

where

$$\breve{H}(i) = \sum_{l=0}^{L_p-1} \left(c(k)e^{-j2\pi k\Delta f\tau_l} \int_0^{T_s} h(t,\tau_l)e^{j2\pi(k-p)\Delta ft}dt \right). \tag{6.47}$$

The inter-carrier interference term in (6.46) can be approximated by a zero-mean GRV. Its power can be found in [153].

If we consider the effect of phase noise only, let $h(t,\tau)$ in (6.45) be constant, $y(p)$ becomes

$$y(p) = \underbrace{a(0)H(k)c(p)}_{\text{desired signal}} + \underbrace{\sum_{k=0,k\neq p}^{K-1} a(p-k)H(k)c(k)}_{\text{ICI}} + w(p) \tag{6.48}$$

where

$$a(i) = T_s^{-1} \int_0^{T_s} \theta(t)e^{-j2\pi i\Delta ft}dt\,, \qquad a(0) = T_s^{-1} \int_0^{T_s} \theta(t)dt\,. \tag{6.49}$$

Since $\breve{H}(i)$ in (6.47) is a non-GRV and $a(0)$ in (6.49) is non-constant, analyzing the PEP of space-frequency codes with phase noise and time varying channels becomes difficult. However, comparing Eqs. (6.46) and (6.48) with (6.13), one can see the inter-carrier interference contributions of subcarriers to one subcarrier due to time varying channels and phase noise are similar to the inter-carrier interference contribution due to frequency offset. Thus, ISC-SF codes with capability of cancelling inter-carrier interference should perform well compared with the space-frequency codes without this feature in cases of phase noise and time varying channels as discussed for the case of frequency offset.

6.8 Simulation Results and Discussion

We give simulation results to verify the theoretical analysis for space-frequency codes with frequency offset. We use two channel models: (1) a simple two-path channel with uniform power delay profile and time delay between the two paths is $5\mu s$ and (2) the six-path

COST207 typical urban channel model [6], a more realistic model. We use algebraic ST convolutional codes [42], [154] of code rate $1/2$ with generator polynomial $(5, 7)$ [32] without channel interleaver. The Viterbi decoder [154], [32] is employed. The similar simulation results are observed for both channel models. Thus, we present the simulations with six-path COST207 typical urban channel model for brevity.

6.8.1 Simulations with Constant Frequency Offset

We compare the performance of space-frequency codes for $1\%, 10\%$ and 20% normalized frequency offset. Fig. 6.1 illustrates PEP curves of two OFDM systems with 64 subcarriers and two transmit antennas. System 1 is equipped with one receive antenna and System 2 has two receive antennas, so that the diversity order of the two systems is at least $d = 2$ and $d = 4$, respectively. Using (6.32), for 1% normalized frequency offset, $S_0 = 0.9997$, $L_0 \approx 1$ in the SNR region of interest (≤ 30 dB). Therefore, theoretically the performance loss is not significant. Fig. 6.1 confirms this conclusion. If the normalized frequency offset is small, say 1%, the PEP curves almost overlap the PEP of the systems with no frequency offset. In case normalized frequency offset is 10%, the PEP curves of all systems are shifted to the right and less steep than the curves of PEP with 1% normalized frequency offset; this shift is larger for the system with smaller diversity order. For example, at $PEP = 10^{-3}$ the PEP curve of the system with $d = 2$ shifts right 1.4 dB, whereas it is 0.8 dB for the system with $d = 4$. The SNR needed to compensate the effect of frequency offset increases with normalized frequency offset. When normalized frequency offset is 20%, the PEP reduces slightly even if there are large increases in SNR. The PEP performance reaches a floor at an SNR of about 22 dB. This symptom is more serious for low diversity order systems, where the floor level is higher than that of higher diversity order systems.

6.8.2 Simulations with Inter-Carrier Interference Self-Cancellation Space-Frequency Codes

The performance of space-frequency coding schemes with and without inter-carrier interference self-cancellation (SC2 and SC1 accordingly) is illustrated in Fig. 6.2. The systems to be examined have 128 subcarriers, 2 transmit and 1 receive antennas. We can verify the results in Section 6.5 that when frequency offset is absent, SC1 and SC2 have the same

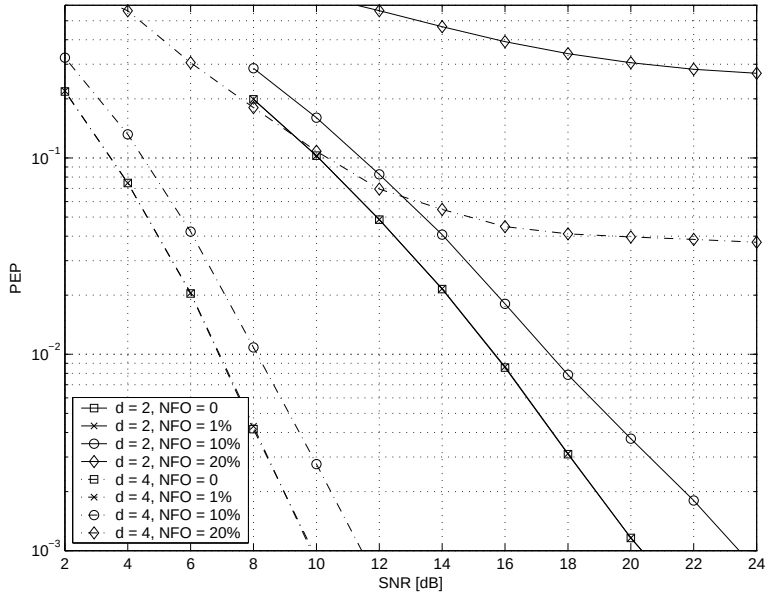

Figure 6.1: Performance of space-frequency codes with $K = 64$, constant frequency offset for the six-path COST207 typical urban channel model. NFO stands for normalized frequency offset.

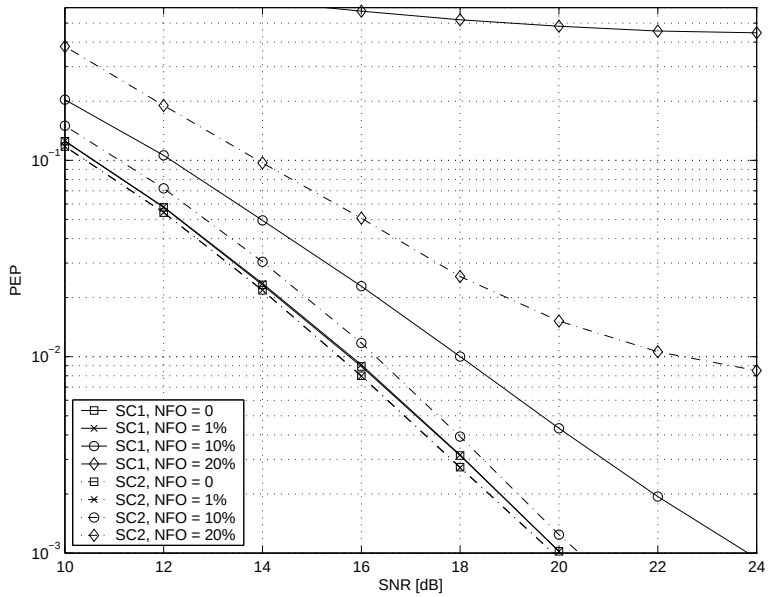

Figure 6.2: Performance of space-frequency codes with $K = 128, r = 2$, constant frequency offset, six-path COST207 channel model with and without inter-carrier interference self-cancellation.

diversity order. The difference between the coding gains of the two schemes is very small, less than 0.2 dB at the plotted SNR. This difference is expected to be zero at higher SNR region. Once again, the performance loss for 1% normalized frequency offset is negligible

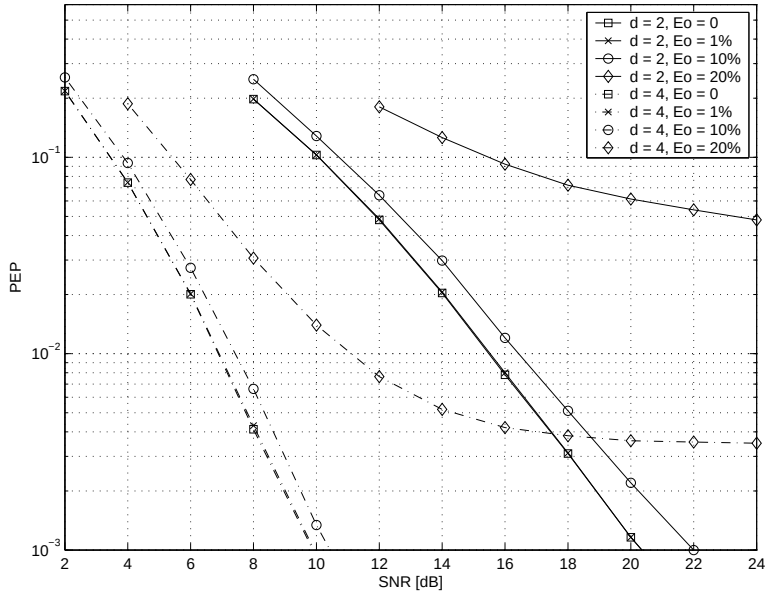

Figure 6.3: Performance of space-frequency codes with $K = 64$, uniformly distributed frequency offset and the six-path COST207 typical urban channel model.

for both SC1 and SC2. However, the improvement of SC2 over SC1 is remarkable when normalized frequency offset is 10% and 20%. For example, in Fig. 6.2 at $PEP = 10^{-3}$ and 10% normalized frequency offset, the performance loss of SC1 is about 3.7 dB, whereas the loss is about 0.5 dB with SC2. This improvement is significant in Fig. 6.2 where the loss of SC2 is only 0.5 dB. In addition, SC2 lowers the error floor level notably when normalized frequency offset is very high 20%.

6.8.3 Simulations with Variable Frequency Offset

In practice, the frequency offset values of receive signals at antenna n that were transmitted from antenna m can be different and they vary from symbol to symbol. We now provide simulation results for variable frequency offset. The distribution of normalized frequency offset values are assumed uniform over the range $[-E_0, E_0]$, where $|E_0|$ is the maximum normalized frequency offset. Similarly to the previous simulations, we will examine performance of the space-frequency codes for $|E_0| = 1\%, 10\%$ and 20%.

As discussed in Section IV, assumption AS3, the performance of space-frequency codes with variable frequency offset should be upper-bounded by the performance curves with the constant frequency offset. Fig. 6.3 presents performance of 64-subcarrier systems with one

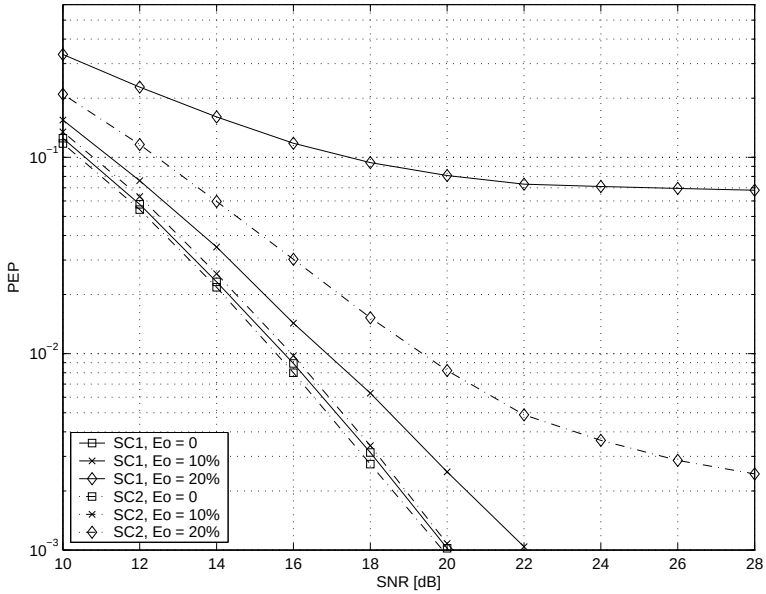

Figure 6.4: Performance of space-frequency codes with $K = 128, r = 2$, uniformly distributed frequency offset, six-path COST207 channel model with and without inter-carrier interference self-cancellation.

and two transmit antennas. The two systems have two transmit antennas. By examining Figs. 6.1 and 6.3, exactly the same observations can be made as with the constant frequency offset. The only difference between the constant and variable frequency offset cases is that in the latter case, the performance loss is always less than the loss of the former case, as expected. For example, comparing Figs. 6.1 and 6.3, for the system 1 ($d = 2$), 10% normalized frequency offset, at PEP = 10^{-3}, the loss is about 3 dB in case of constant frequency offset, while it is about 1.7 dB for the system with varying frequency offset.

Fig. 6.4 presents the performance of the space-frequency coding schemes SC1 and SC2 with variable frequency offset. Comparing with their performance that are given in Fig. 6.2 with fixed frequency offset, the loss for variable frequency offset is smaller.

6.9 Summary

We have analyzed the performance of space-frequency codes in the presence of frequency offset. A MIMO-OFDM model with frequency offset has been developed to analyze the PEP performance of space-frequency codes. Using the PEP upper bound for of space-frequency codes, we showed that the conventional code design criteria remain valid pro-

vided frequency offset is small. Inter-carrier interference is less severe for space-frequency codes with high diversity order. Therefore, diversity not only improves the performance of OFDM systems in the dispersive channels, but also makes the system robust to inter-carrier interference. Furthermore, we proposed a new class of space-frequency codes, ISC-SF codes with diversity order of at least $2MN$. ISC-SF codes are constructed from ST codes to mitigate inter-carrier interference caused by frequency offset, phase noise and time varying channels efficiently. This class of space-frequency codes permits a good trade-off among error correction capability, inter-carrier interference reduction and spectral efficiency. Our results suggest a new direction in the design of space-time/space-frequency codes capable of both error correction and inter-carrier interference reduction.

Chapter 7

Conclusion and Future Work

7.1 Conclusion

We have designed space-time codes for MIMO systems considering the practical constraints such as decoding complexity and system imperfections. While reduction in decoding complexity leads to power and manufacturing cost savings, mitigating the system imperfections is necessary to prevent possible transmission errors.

Low decoding complexity STBC have been considered in Chapters 2 to Chapter 5. The necessary and sufficient conditions for low decoding complexity STBC are proposed for quasi-static frequency-flat MIMO fading channels. To achieve low complexity, we have developed multi-group decodable STBC. For a fixed number of transmitted symbols encoded in a code matrix, an increase in the number of groups leads to lower decoding complexity.

We have proposed a new framework, OEST codes for low complexity STBC. The orthogonal designs are employed for constructing OEST codes, in which the indeterminates are substituted by circulant matrices and scalar product is replaced by Kronecker product. If the orthogonal designs have K indeterminates, the resulting OEST codes have K data vectors embedded in the K circulant matrices. At the receiver, these K data vectors can be detected separately with no interference from the other vectors. Hence, OEST codes are K-group STBC.

The main properties of OEST codes have been derived. We have shown that OEST codes can achieve full diversity with signal rotation. Optimal signal rotations that maximize the coding gain or minimize the union bound have been computed. The maximal mutual

information of OEST codes is shown to be equal to that of the underlying OSTBC. A general decoder of OEST codes has been developed.

Additionally, we have shown that OEST codes subsume OSTBC, QSTBC (ABBA codes), and circulant STBC. Therefore, many open problems of these codes can be solved in a systematic manner. Detailed analysis has been performed for ABBA codes. A new decoder is derived to facilitate single complex symbol decoding, i.e. minimal decoding complexity (MDC), a property has been known to be possessed by OSTBC only. Furthermore, the SER performance of MDC-ABBA codes is directly optimized. This approach is different from all the previous works, which optimize the code performance based on the worst-case codeword PEP. The combination of MDC-ABBA codes and various signal constellations is investigated. The results show that MDC-ABBA codes yield the best performance with QAM. We also considered antenna selection, a closed-loop method to improve the performance of MDC-ABBA codes. It is shown that MDC-ABBA codes can achieve full diversity even with limited feedback. Simulation results shown that MDC-ABBA codes perform better than OSTBC with the same decoding complexity. Thus MDC-ABBA codes are a potential replacement of OSTBC when there are more than 2 transmit antennas.

Importantly, the framework of OEST codes allows us to design a new STBC called SAST codes. SAST codes are constructed by the Alamouti code, thus they are 2-group decodable. SAST codes are of rate-one symbol pcu and they can nearly achieve the capacity of MISO channel. From extensive simulations, we find that SAST codes also perform better than other STBC having the same code rate, such as linear dispersion codes, DAST codes, LCP codes, and QSTBC.

We furthermore proposed a new encoding method so that the OEST codes become $2K$-group decodable, which was K-group decodable initially. The representative SAST codes have been analyzed in great detail. The new decoder for SAST codes has been derived for the new encoding method. This makes SAST codes 4-group decodable. The best signal transformations, in terms of coding gain, have been identified. They are the real rotation matrices proposed for square lattices. Since 4-group SAST codes have low complexity, are near-capacity achieving, and have good performance, 4-group SAST codes are suitable for downlink wireless channels, where the multiple transmit antennas are used to improve the diversity gain of the systems.

Another contribution of OEST framework is the general method to derive the decoder for low complexity STBC. This method is implemented into 3 sub-tasks: (1) to obtain the spatial signature of data vectors; (2) to derive the equivalent channels; and (3) to propose the simplified transmit-receive signal relations. This method has been successfully applied for other low-complexity STBC: CIOD codes and 4-group QSTBC. As a side product, we also derive the optimal signal designs for these two codes.

Chapters 2 to 5 deal with STBC in frequency-flat fading channels. However, frequency-selective channels are of interest too and OFDM is commonly employed to deal with such situations. We have studied the design of space-frequency codes for MIMO-OFDM systems with imperfections due to frequency offset. The design criteria of space-frequency codes have been revised when frequency offset exists. The results showed that the diversity gain of MIMO system may be totally lost when frequency offset is large, resulting in a irreducible error floor. We proposed a new space-frequency coding scheme to partially cancel the inter-carrier interference. The new coding scheme works well even when the frequency offset is 10%.

7.2 Future Work

7.2.1 Maximal Rate of Multi-Group Decodable STBC

We have derived the necessary and sufficient conditions so that a STBC is multi-group decodable. These conditions are given for a quasi-static fading channel, where the channel is constant during the transmission of a code matrix. However, given a specific number of groups $\Gamma > 1$, the maximal code rate that can be designed is still unknown. For example, the maximal code rate of OSTBC, a special case of single-symbol decodable, is known [44]; but the maximal rate of single-symbol decodable is not yet reported [92]. In another effort to search for high rate 2-group STBC, Yuen *et al.* [98] find a code of rate 5/4 for 4 antennas. Nevertheless, this rate is not shown to be maximal for 2-group STBC for 4 antennas. Thus in the direction of designing low complexity STBC, we have two main open problems.

1. What is the maximal rate of Γ-group STBC?

2. How to systematically construct Γ-group STBC with maximal code rate.

Another open problem is to design the low complexity space-frequency codes for MIMO-OFDM systems. Since the channels of subcarriers vary along the frequency axis, that means, the rows of space-frequency code matrix experience different channel gains. This fact opposes to the MIMO frequency-flat channels, where the rows of space-time code matrix experience the same channel gains. Therefore, the necessary and sufficient conditions so that a space-frequency code is multi-group decodable need to be revised. The design of low-complexity space-frequency codes becomes more difficult. Furthermore, the two open questions of designing low complexity STBC in quasi-static frequency-flat fading channels are the open problems of designing low complexity space-frequency codes in MIMO-OFDM.

7.2.2 Exploiting Channel State Information

We have pointed out that SAST codes are suitable for coherent MISO channels. SAST codes can also be used in MIMO systems where the code rate of one symbol pcu is acceptable. When some form of channel state information is available at the transmitter, one can derive the precoders to improve the performance of SAST codes. Several precoding methods have been proposed for OSTBC [155–159] and for QSTBC [19, 118, 119]. The combination of SAST codes (and also OEST codes in general) and precoding to exploit the channel state information can be investigated.

7.2.3 Combination with Error Control Coding in Multi-User Systems

We may investigate the combination of OEST codes with error control codes, which are employed by practical systems to correct transmission errors [41]. In Addition, modern error control codes, like turbo codes [160, 161] or low-density parity-check (LDPC) codes [162–164], require the soft output from the inner STBC for iterative decoding [165–167]. An OEST decoder that produces the soft output information may be developed. While this thesis has focused on point-to-point communications, adaptation of OEST codes and their subclasses, such as SAST codes and MDC-ABBA codes, in multi-user systems with error control codes can be investigated.

7.2.4 Applications of OEST Codes

We have designed OEST codes for coherent communications and for point-to-point links. However, OSTBC and QSTBC, two special cases of OEST codes are shown to be suitable for differential encoding and non-coherent detection [117, 168, 169]. Furthermore, OSTBC and QSTBC are recently investigated for relay cooperative communication protocols [170–172]. Therefore, the applications of OEST codes for non-coherent or cooperative communications, in general, can be further developed.

Appendix A

List of Publications

Journal papers

1. D. N. Đào and C. Tellambura, "Intercarrier interference self-cancellation space-frequency codes for MIMO-OFDM," *IEEE Transactions of Vehicular Technology*, vol. 54, pp. 1729 - 1738, Sep. 2005.

2. ——, "A general method to decode ABBA quasi-orthogonal space-time block codes," *IEEE Communications Letters*, vol. 10, pp. 713- 715, Oct. 2006.

3. ——, "A general combinatorial sphere decoder and its application," *IEEE Communications Letters*, vol. 10, pp. 810- 812, Dec. 2006.

4. ——, "Decoding, Performance Analysis, and Optimal Signal Designs for Coordinate Interleaved Orthogonal Designs," submitted to *IEEE Transactions on Wireless Communications*, Aug. 2006, accepted for publication, Nov. 2006, 13-page manuscript.

   Journal papers, under review

5. ——, "Semi-orthogonal space-time block codes," submitted to *IEEE Transaction of Information Theory*, Mar. 2005, 25-page manuscript.

6. ——, "Quasi-Orthogonal STBC with Minimum Decoding Complexity: Performance Analysis, Optimal Signal Designs, and Antenna Selection Diversity," submitted to *IEEE Transactions on Communications*, May 2006, 28-page manuscript.

7. D. N. Đào, Chau Yuen, Chintha Tellambura, Yong Liang Guan, and Tjeng Thiang Tjhung, "Four-group decodable space-time block codes," submitted to *IEEE Transactions on Signal Processing*, May 2006, 2nd round review, 12-page manuscript.

8. D. N. Đào and C. Tellambura, "Orthogonality-embedded space-time block codes," submitted to *European Transactions on Telecommunications*, Dec. 2006, 30-page manuscript.

Conference papers

1. D. N. Dao and C. Tellambura, "Performance of space-frequency codes in MIMO channels with frequency offset," in *Proc. 38th Asilomar Conf. on Signals, Systems, Computers*, Pacific Grove, USA, Nov. 2004, pp. 702 – 706.

2. D. N. Đào and C. Tellambura, "New Methods to Reduce Intercarrier Interference in OFDM Systems," in *Proc. 18th Canadian Conference on Electrical and Computer Engineering (CCECE '05)*, Saskatoon, Canada, May 2005.

3. ——, "On the design and performance of universal space-time codes in MIMO-OFDM," in *Proc. Canadian Workshop on Information Theory*, Montréal, Canada, June 2005.

4. ——, "Optimal rotations for quasi-orthogonal STBC with two-dimensional constellations," in *Proc. of IEEE Global Telecommunications Conference (Globecom) 2005*, St. Louis, USA, Nov./Dec. 2005, pp. 2317 – 2321.

5. ——, "Capacity-approaching semi-orthogonal space-time block codes," in *Proc. of IEEE Global Telecommunications Conference (Globecom) 2005*, St. Louis, USA, Nov./Dec. 2005, pp. 3305 – 3309.

6. ——, "On the Decoding, Performance Analysis, and Optimal Signal Designs of Space-Time Block Codes from Coordinate Interleaved Orthogonal Designs," *IEEE 2006 Communication Theory Workshop*, Puerto Rico, USA, May 2006.

7. ——, "A new class of space-time codes via orthogonal designs, circulant basis, and Kronecker product," in *Proc. of IEEE International Symposium on Information Theory (ISIT) 2006*, Seattle, USA, July 2006.

8. D. N. Đào, Chau Yuen, Chintha Tellambura, Yong Liang Guan, and Tjeng Thiang Tjhung, "On Decoding and Performance Optimizing of Four-Group Decodable Space-Time Block Codes," in *Proc. of International Conference on Communications and Electronics (ICCE), 2006*, Hanoi, Vietnam, Oct. 2006.

9. D. N. Đào and C. Tellambura, "On Space-Time Block Codes from Coordinate Interleaved Orthogonal Designs," in *Proc. of IEEE Military Communications Conference (MILCOM) 2006*, Washington, D.C., Oct. 2006.

10. ——, "On the decoding, mutual information, and antenna selection diversity for quasi-orthogonal STBC with minimum decoding complexity," in *Proc. of IEEE Global Telecommunications Conference (Globecom) 2006*, San Francisco, USA, Nov./Dec. 2006.

11. ——, "Performance analysis and optimal signal designs for minimum decoding complexity ABBA codes," in *Proc. of IEEE Global Telecommunications Conference (Globecom) 2006*, San Francisco, USA, Nov./Dec. 2006.

12. D. N. Đào, Chau Yuen, Chintha Tellambura, Yong Liang Guan, and Tjeng Thiang Tjhung, "A New Class of Four-Group Decodable Space-Time Block Codes," to appear in *Proc. of IEEE Wireless Communications Networking Conference (WCNC) 2007*, Hong Kong, Mar. 2007.

Bibliography

[1] T. S. Rappaport, A. Annamalai, R. M. Buehrer, and W. H. Tranter, "Wireless communications: Past events and a future perspective," *IEEE Commun. Mag.*, vol. 40, pp. 148–161, May 2002.

[2] S. N. Diggavi, N. Al-Dhahir, A. Stamoulis and A.R. Calderbank, "Great Expectations: The Value of Spatial Diversity in Wireless Networks," *Proc. IEEE,* vol. 92, pp. 219 – 270, Feb. 2004.

[3] H. Sampath, S. Talwar, J. Tellado, V. Erceg, and A. Paulraj, "A fourth-generation MIMO-OFDM broadband wireless system: design, performance, and field trial results," *IEEE Commun. Mag.*, vol. 40, pp. 143–149, Sep. 2002.

[4] A. Paulraj, D. A, Gore, R. Nabar, and H. Bolcskei, "An overview of MIMO communications - a key to gigabit wireless," *IEEE Proc.*, vol. 92, pp. 198 – 218, Feb. 2004.

[5] M. Gagnaire, "An overview of broad-band access technologies," *IEEE Proc.*, vol. 85, pp. 1958 – 1972, Dec. 1997.

[6] G. L. Stüber, *Principles of mobile communications*. Norwell, MA: Kluwer, 2nd. ed., 2001.

[7] A. J. Paulraj and T. Kailath, "Increasing capacity in wireless broadcast systems using distributed transmission/directional reception," U.S. Patent 5 345 599, 1994.

[8] I. E. Telatar, "Capacity of multiantenna gaussian channel," *Eur. Trans. Telecommun.*, vol. 10, pp. 585 – 595, Nov./Dec. 1999.

[9] G. J. Foschini, “Layered space-time architechture for wireless communication in fading environment when using multiple antennas,” *Bell Labs, Tech. J.*, vol. 1, pp. 41–59, Autumn 1996.

[10] I. E. Telatar, “Capacity of multi-antenna Gaussian channels,” tech. rep., Lucent Technologies, Bell Labs., Jun. 1995.

[11] G. J. Foschini and M. J. Gans, “On limits of wireless communication in a fading environment when using multiple antennas,” *Wireless Pers. Commun.*, vol. 6, pp. 311–335, Mar. 1998.

[12] P. W. Wolniansky, G. J. Foschini, G. D. Golden, and R. A. Valenzuela, “V-BLAST: an architecture for achieving very high data rates over the rich-scattering wireless channel,” in *Proc. Int. Symp. Signals, Systems, Electronics (ISSSE-98)*, (Pisa, Italy), pp. 295–300, Oct. 1998.

[13] G. J. Foschini, G. D. Golden, R. A. Valenzuela, and P. W. Wolniansky, “Simplified processing for wireless communication at high spectral efficiency,” *IEEE J. Select. Areas. Commun.*, vol. 17, pp. 1841–1852, Nov. 1999.

[14] G. J. Foschini, D. Chizhik, M. Gans, C. Papadias, and R. A.Valenzuela, “Analysis and performance of some basic spacetime architectures,” *IEEE J. Select. Areas. Commun.*, vol. 21, pp. 303–320, Apr. 2003.

[15] V. Tarokh, N. Seshadri, and A. R. Calderbank, “Space-time codes for high data rate wireless communications: Performance criterion and code construction,” in *Proc. IEEE Int. Conf. Communications (ICC)*, (Monréal, Canada), pp. 299–303, Jun. 1997.

[16] V. Tarokh, N. Seshadri, and A. R. Calderbank, “Space-time codes for high data rate wireless communication: Performance analysis and code construction,” *IEEE Trans. Inform. Theory*, vol. 44, pp. 744–765, Mar. 1998.

[17] J.-C. Guey, M. P. Fitz, M. R. Bell, and W.-Y. Kuo, “Signal design for transmitter diversity wireless communication systems over Rayleigh fading channels,” in *Proc. IEEE Vehicular Technology Conf. (VTC)*, pp. 136–140, Apr. 1996.

[18] J.-C. Guey, M. P. Fitz, M. R. Bell, and W.-Y. Kuo, "Signal design for transmitter diversity wireless communication systems over Rayleigh fading channels," *IEEE Trans. Commun.*, vol. 47, pp. 527–537, Apr. 1999.

[19] A. Hottinen, O. Tirkkonen, and R. Wichman, *Multi-Antenna Transceiver Techniques for 3G and Beyond*. West Sussex, UK: John Wiley & Sons, 2003.

[20] M. O. Damen, H. E. Gamal and N. C. Beaulieu, "Linear threaded algebraic space-time constellations," *IEEE Trans. Inform. Theory*, vol. 49, pp. 2372 – 2388, Oct. 2003.

[21] J. M. Wilson, "The next generation of wireless LAN emerges with 802.11n," *Technology@Intel Magazine*, pp. 1 – 8, Aug. 2004. [Online]. Available: http://www.intel.com/technology/magazine/communications/wi08041.pdf.

[22] S. Abraham, A. Meylan, and S. Nanda, "802.11n MAC design and system performance," in *Proc. IEEE Int. Conf. Communications (ICC)*, vol. 5, (Seoul, Korea), pp. 2957 – 2961, May 2005.

[23] S. Nanda, R. Walton, J. Ketchum, M. Wallace, and S. Howard, "A high-performance MIMO OFDM wireless LAN," *IEEE Commun. Mag.*, vol. 43, pp. 101 – 109, Feb. 2005.

[24] IEEE 802.16e-2005 Standard, "Air interface for fixed and mobile broadband wireless access systems - Amendment 2: Physical and medium access control layers for combined fixed and mobile operation in licensed bands and corrigendum 1," Feb. 2006.

[25] A. Ghosh, D. R. Wolter, J. G. Andrews, and R. Chen, "Broadband wireless access with WiMax/802.16: current performance benchmarks and future potential," *IEEE Commun. Mag.*, vol. 43, pp. 129 – 136, Feb. 2005.

[26] S. M. Alamouti, "A simple transmitter diversity scheme for wireless communication," *IEEE J. Select. Areas. Commun.*, vol. 16, pp. 1451–1458, Oct. 1998.

[27] M. Juntti, M. Vehkapera, J. Leinonen, V. Zexian, D. Tujkovic, S. Tsumura, and S. Hara, “MIMO MC-CDMA communications for future cellular systems,” *IEEE Commun. Mag.*, vol. 43, pp. 118 – 124, Feb. 2005.

[28] T. Zwick, C. Fischer, and W. Wiesbeck, “A stochastic multipath channel model including path directions for indoor environments,” *IEEE J. Select. Areas. Commun.*, vol. 20, pp. 1178 – 1192, Aug. 2002.

[29] J. P. Kermoal, L. Schumacher, K. I. Pedersen, P. E. Mogensen, and F. Frederiksen, “A stochastic MIMO radio channel model with experimental validation,” *IEEE J. Select. Areas. Commun.*, vol. 20, pp. 1211– 1226, Aug. 2002.

[30] D. Chizhik, J. Ling, P. Wolniansky, R. Valenzuela, N. Costa, and K. Huber, “Multiple-input-multiple-output measurements and modeling in Manhattan,” *IEEE J. Select. Areas. Commun.*, vol. 21, pp. 321– 331, Apr. 2002.

[31] H. Xu, D. Chizhik, H. Huang, and R. Valenzuela, “A generalized space-time multiple-input multiple-output (MIMO) channel model,” *IEEE Trans. Wirel. Commun.*, vol. 3, pp. 966 – 975, May 2004.

[32] J. G. Proakis, *Digital Communications*. New York: McGraw-Hill, 4th ed., 2001.

[33] B. Hassibi and B. M. Hochwald, “High-rate codes that are linear in space and time,” *IEEE Trans. Inform. Theory*, vol. 48, pp. 1804–1824, Jul. 2002.

[34] G. Taricco and E. Biglieri, “Exact pairwise error probability of space-time codes,” *IEEE Trans. Inform. Theory*, vol. 48, pp. 510 – 513, Feb. 2002.

[35] G. Taricco and E. Biglieri, “Correction to "exact pairwise error probability of space-time codes",” *IEEE Trans. Inform. Theory*, vol. 49, pp. 766 – 766, Mar. 2003.

[36] H.-F. Lu, Y. Wang, P. V. Kumar, and K. M. Chugg, “Remarks on space-time codes including a new lower bound and an improved code,” *IEEE Trans. Inform. Theory*, vol. 49, pp. 2752 – 2757, Oct. 2003.

[37] A. P. des Rosiers and P. H. Siegel, “On performance bounds for space-time codes on fading channels,” *IEEE Trans. Commun.*, vol. 52, pp. 1688 – 1697, Oct. 2004.

[38] J. Wang, X. Wang, and M. Madihian, "On the optimum design of space-time linear-dispersion codes," *IEEE Trans. Wirel. Commun.*, vol. 4, pp. 2928 – 2938, Nov. 2005.

[39] J. Wang and X. Wang, "Optimal linear space-time spreading for multiuser MIMO communications," *IEEE J. Select. Areas. Commun.*, vol. 24, pp. 113 – 120, Jan. 2006.

[40] V. Tarokh, H. Jafarkhani, and A. R. Calderbank, "Space-time block codes from orthogonal designs," *IEEE Trans. Inform. Theory*, vol. 45, pp. 1456–1466, Jul. 1999.

[41] S. Lin, D. J. Costello, *Error Control Coding*. NJ, USA: Prentice Hall, 2nd ed., 2004.

[42] H. El Gamal, A. R. Hammons, Jr., Y. Liu, M. P. Fitz and O. Y. Takeshita, "On the design of space-time and space-frequency codes for MIMO frequency-selective fading channels," *IEEE Trans. Inform. Theory*, vol. 49, pp. 2277 – 2292, Sep. 2003.

[43] B. Lu, G. Yue and X. Wang, "Performance analysis and design optimization of LDPC-coded MIMO OFDM systems," *IEEE Trans. Signal Processing*, vol. 52, pp. 348 – 361, Feb. 2004.

[44] X.-B. Liang, "Orthogonal designs with maximal rates," *IEEE Trans. Inform. Theory*, vol. 49, pp. 2468 – 2503, Oct. 2003.

[45] H. Wang and X.-G. Xia, "Upper bounds of rates of complex orthogonal space-time block codes," *IEEE Trans. Inform. Theory*, vol. 49, pp. 2788–2796, Oct. 2003.

[46] H. Jafarkhani, "A quasi-orthogonal space-time block code," *IEEE Trans. Commun.*, vol. 49, pp. 1–4, Jan. 2001.

[47] O. Tirkkonen, A. Boariu, and A. Hottinen, "Minimal nonorthogonality rate 1 space-time block code for 3+ Tx antennas," in *Proc. IEEE 6th Int. Symp. Spread-Spectrum Techniques and Applications (ISSSTA 2000)*, (Parsippany, NJ, USA), pp. 429–432, Sep. 2000.

[48] C. B. Papadias and G. J. Foschini, "Capacity-approaching space-time codes for systems employing four transmitter antennas," *IEEE Trans. Inform. Theory*, vol. 49, pp. 726–732, Mar. 2003.

[49] M. O. Damen, K. Abed-Meraim and J. -C. Belfiore, “Diagonal algebraic space-time block codes,” *IEEE Trans. Inform. Theory*, vol. 48, pp. 628 – 636, Mar. 2002.

[50] M. O. Damen, H. E. Gamal, and N. C. Beaulieu, “Systematic construction of full diversity algebraic constellations,” *IEEE Trans. Inform. Theory*, vol. 49, pp. 3344 – 3349, Dec. 2003.

[51] Y. Xin, Z. Wang, and G. B. Giannakis, “Space-time diversity systems based on linear constellation precoding,” *IEEE Trans. Wirel. Commun.*, vol. 2, pp. 294 – 309, Mar. 2003.

[52] B. A. Sethuraman, B. S. Rajan, and V. Shashidhar, “Full-diversity, high rate space-time block codes from division algebras,” *IEEE Trans. Inform. Theory*, vol. 49, pp. 2596–2616, Oct. 2003.

[53] G. Wang, H. Liao, H. Wang, and X. -G. Xia, “Systematic and optimal cyclotomic lattices and diagonal space-time block code designs,” *IEEE Trans. Inform. Theory*, vol. 50, pp. 3348 – 3360, Dec. 2004.

[54] D. Wang and X.-G. Xia, “Optimal diversity product rotations for quasi-orthogonal STBC with MPSK Symbols,” *IEEE Commun. Lett.*, vol. 9, pp. 420 – 422, May 2005.

[55] R. T. Derryberry, S. D. Gray, D. M. Ionescu, G. Mandyam, and B. Raghothaman, “Transmit diversity in 3G CDMA systems,” *IEEE Commun. Mag.*, vol. 40, pp. 68–75, Apr. 2002.

[56] S. Parker, M. Sandell, M. S. Yee, Y. Sun, M. Ismail, P. Strauch, and J. McGeehan, “Space-time codes for future WLANs: principles, practice, and performance,” *IEEE Commun. Mag.*, vol. 42, pp. 96–103, Dec. 2004.

[57] H. Yang, “A road to future broadband wireless access: MIMO-OFDM-Based air interface,” *IEEE Commun. Mag.*, vol. 43, pp. 53– 60, Jan. 2005.

[58] H. El Gamal and M. O. Damen, “Universal space-time coding,” *IEEE Trans. Inform. Theory*, vol. 49, pp. 1097 – 1119, May 2003.

[59] O. Tirkkonen and A. Hottinen, "Square-matrix embeddable space-time block codes for complex signal constellations," *IEEE Trans. Inform. Theory*, vol. 48, pp. 384 – 395, Feb. 2002.

[60] A. V. Geramita and J. Seberry, *Orthogonal Designs, Quadratic Forms and Hadamard Matrices*, vol. 43 of *Lecture Notes in Pure and Applied Mathematics*. New York: Marcel Dekker, 1979.

[61] W. Su and X.-G. Xia, "Signal constellations for quasi-orthogonal space-time block codes with full diversity," *IEEE Trans. Inform. Theory*, vol. 50, pp. 2331 – 2347, Oct. 2004.

[62] X. Li, T. Luo, G. Yue, and C. Yin, "A squaring method to simplify the decoding of orthogonal space-time block codes," *IEEE Trans. Commun.*, vol. 49, pp. 1700–1703, Oct. 2001.

[63] R. A. Horn and C. R. Johnson, *Matrix Analysis*. Cambridge, U.K.: Cambridge Univ. Press, 1985.

[64] P. J. Davis, *Circulant Matrices*. New York: Wiley, 1st ed., 1979.

[65] N. Jacobson, *Finite-Dimensional Division Algebras Over Fields New York*. Springer-Verlag, 1996.

[66] B. Lu and X. Wang, "Space-time code design in OFDM systems," in *Proc. IEEE GLOBECOM*, (San Francisco, USA), pp. 1000 – 1004, Nov. 2000.

[67] H. Bölcskei and A. J. Paulraj, "Space-frequency coded broadband OFDM systems," in *Proc. IEEE Wireless Communications Networking Conf. (WCNC)*, vol. 1, (Chicago, USA), pp. 1 – 6, Sep. 2000.

[68] R. W. Chang and R. A. Gibby, "A theoretical study of performance of an orthogonal multiplexing data transmission scheme," *IEEE Trans. Commun.*, vol. 16, pp. 529 – 540, Aug. 1968.

[69] S. B. Weinstein and P. M. Ebert, “Data transmission by frequency-division multiplexing using the discrete Fourier transform,” *IEEE Trans. Commun. Technol.*, vol. Com-19, pp. 628 – 634, Oct. 1971.

[70] L. J. Cimini, “Analysis and simulation of a digital mobile channel using orthogonal frequency division multiplexing,” *IEEE Trans. Commun.*, vol. COM-33, pp. 665–675, Jul. 1985.

[71] R. van Nee and R. Prasad, *OFDM for Wireless Multimedia Communications*. MA, USA: Artech House, Inc., 2000.

[72] L. Hanzo, W. Webb, and T. Keller, *Single- and multi-carrier quadrature amplitude modulation : principles and applications for personal communications, WLANs and broadcasting*. New York: Wiley, 2000.

[73] H. Sampath, S. Talwar, J. Tellado, V. Erceg, and A. Paulraj, “A fourth-generation MIMO-OFDM broadband wireless system: Design, performance, and field trial results,” *IEEE Commun. Mag.*, vol. 40, pp. 143 – 149, Sep. 2002.

[74] G. L. Stüber, J. R. Barry, S. W. McLaughlin, Ye Li, M. A. Ingram, and T. G. Pratt, “Broadband MIMO-OFDM wireless communications,” *IEEE Proc.*, vol. 92, pp. 271 – 294, Feb. 2004.

[75] X. -H. Yu, G. Chen, M. Chen, and X. Gao, “The FuTURE Project in China,” *IEEE Commun. Mag.*, vol. 43, pp. 70 – 75, Jan. 2001.

[76] M. Qin and R. Blum, “Properties of space-time codes for frequency-selective channels,” *IEEE Trans. Signal Processing*, vol. 52, pp. 694 – 702, Mar. 2004.

[77] Z. Liu, Y. Xin and G.B. Giannakis, “Space-time-frequency coded OFDM over frequency-selective fading channels,” *IEEE Trans. Signal Processing*, vol. 50, pp. 2465 – 2476, Oct. 2002.

[78] H. E. Gamal and A. R. Hammons, Jr., “On the design of algebraic space-time codes for MIMO block-fading channels,” *IEEE Trans. Inform. Theory*, vol. 49, pp. 151 – 163, Jan. 2003.

[79] X. Ma and G.B. Giannakis, "Full-diversity full-rate complex-field space-time coding," *IEEE Trans. Signal Processing*, vol. 51, pp. 2917 – 2930, Nov. 2003.

[80] Z. Wang and G. B. Giannakis, "Complex-field coding for OFDM over fading wireless channels," *IEEE Trans. Inform. Theory*, vol. 49, pp. 707 – 720, Mar. 2003.

[81] Yi Gong and K. B. Letaief, "An efficient space-frequency coded OFDM system for broadband wireless communications," *IEEE Trans. Commun.*, vol. 51, pp. 2019 – 2029, Dec. 2003.

[82] S. Alamouti, "A simple transmit diversity technique for wireless communications," *IEEE J. Select. Areas. Commun.*, vol. 16, pp. 1451 – 1458, Oct. 1998.

[83] W. Su, Z. Safar, M. Olfat and K. J. R. Liu, "Obtaining full-diversity space-frequency codes from space-time codes via mapping," *IEEE Trans. Signal Processing*, vol. 51, pp. 2905 – 2916, Nov. 2003.

[84] S. Verdu, *Multiuser Detection*. New York, NY: Cambridge Univ. Press, 1st ed., 1998.

[85] T. Pollet, M. V. Bladel and M. Moeneclaey, "BER sensitivity of OFDM systems to carrier frequency offset and wiener phase noise," *IEEE Trans. Commun.*, vol. 43, pp. 191–193, Feb./Mar./Apr. 1995.

[86] K. Sathananthan and C. Tellambura, "Probability of error calculation of OFDM systems with frequency offset," *IEEE Trans. Commun.*, vol. 49, pp. 1884 – 1888, Nov. 2001.

[87] H.-K. Song, S.-J. Kang, M.-J. Kim and Y.-H. You, "Error performance analysis of STBC-OFDM systems with parameter imbalances," *IEEE Trans. Broadcast.*, vol. 50, pp. 76 – 82, Mar. 2004.

[88] R. Narasimhan, "Performance of diversity schemes for OFDM systems with frequency offset, phase noise, and channel estimation errors," *IEEE Trans. Commun.*, vol. 50, pp. 1561 – 1565, Oct. 2002.

[89] H. Bölcskei, M. Borgmann and A. J. Paulraj, "Impact of the propagation environment on the performance of space-frequency coded MIMO-OFDM," *IEEE J. Select. Areas. Commun.*, vol. 21, pp. 427 – 439, Apr. 2003.

[90] M. Z. A. Khan and B. S. Rajan, "Space-time block codes from co-ordinate interleaved orthogonal designs," in *Proc. IEEE Int. Symp. on Information Theory (ISIT)*, (Lausanne, Switzerland), p. 275, Jun./Jul. 2002.

[91] M. Z. A. Khan and B. S. Rajan, and M. H. Lee, "Rectangular co-ordinate interleaved orthogonal designs," in *Proc. IEEE GLOBECOM*, vol. 4, (San Francisco, USA), pp. 2004 – 2009, Dec. 2003.

[92] M. Z. A. Khan and B. S. Rajan, "Single-symbol maximum likelihood decodable linear STBCs," *IEEE Trans. Inform. Theory*, vol. 52, pp. 2062 – 2091, May 2006.

[93] C. Yuen, Y. L. Guan, and T. T. Tjhung, "A class of four-group quasi-orthogonal space-time block code achieving full rate and full diversity for any number of antennas," in *Proc. IEEE Personal, Indoor and Mobile Radio Communications Symp. (PIMRC)*, (Berlin, Germany), pp. 92 – 96, Sep. 2005.

[94] G. D. Golden, G. J. Foschini, R. A. Valenzuela, and P. W. Wolniansky, "Detection algorithm and initial laboratory results using the V-BLAST space-time communication architecture," *IEE Elect. Lett.*, vol. 35, pp. 14–15, Jan. 1999.

[95] R. A. Horn and C. R. Johnson, *Topics in Matrix Analysis*. Cambridge, U.K.: Cambridge Univ. Press, 1991.

[96] N. Sharma and C. B. Papadias, "Full-rate full-diversity linear quasi-orthogonal space-time codes for any number of transmit antennas," *EURASIP Journal on Applied Sign. Processing*, vol. 9, pp. 1246–1256, Aug. 2004.

[97] C. Yuen, Y. L. Guan and T. T. Tjhung, "Full-rate full-diversity STBC with constellation rotation," in *Proc. IEEE Vehicular Technology Conf. (VTC)*, (Jeju, South Korea), pp. 296 – 300, Apr. 2003.

[98] C. Yuen, Y. L. Guan, and T. T. Tjhung, "On the search for high-rate quasi-orthogonal space-time block code," *International Journal of Wireless Information Network (IJWIN)*, to appear. [Online] Available: dx.doi.org/10.1007/s10776-006-0033-2.

[99] L. Xian and H. Liu, "Rate-one space-time block codes with full diversity," *IEEE Trans. Commun.*, vol. 53, pp. 1986 – 1990, Dec. 2005.

[100] D. N. Đào and C. Tellambura, "Capacity-approaching semi-orthogonal space-time block codes," in *Proc. IEEE GLOBECOM*, (St. Louis, MO, USA), Nov./Dec. 2005.

[101] M. Rupp, C. Mecklenbrauker, and G. Gritsch, "High diversity with simple space time block-codes and linear receivers," in *Proc. IEEE GLOBECOM*, (San Francisco, USA), pp. 302 – 306, Dec. 2003.

[102] G. Ganesan and P. Stoica, "Space-time block codes: A maximum SNR approach," *IEEE Trans. Inform. Theory*, vol. 47, pp. 1650–1656, Jan. 2001.

[103] D. A. Marcus, *Number fields*. New York: Springer-Verlag, 1977.

[104] G. J. Foschini, R. D. Gitlin, and S. B. Weinstein, "Optimization of two-dimensional signal constellations in the presence of Gaussian noise," *IEEE Trans. Commun.*, vol. 22, pp. 28–38, Jan. 1974.

[105] D. N. Đào and C. Tellambura, "Optimal rotations for quasi-orthogonal STBC with two-dimensional constellations," in *Proc. IEEE GLOBECOM*, (St. Louis, USA), Nov./Dec. 2005.

[106] K. Lu, S. Fu, and X.-G. Xia, "Closed-form designs of complex orthogonal space-time block codes of rates (k+1)/(2k) for 2k-1 or 2k transmit antennas," *IEEE Trans. Inform. Theory*, vol. 51, pp. 4340 – 4347, Dec. 2005.

[107] E. Agrell, T. Eriksson, A. Vardy, and K. Zeger, "Closest point search in lattices," *IEEE Trans. Inform. Theory*, vol. 48, pp. 2201 – 2214, Aug. 2002.

[108] M. O. Damen, H. El Gamal and G. Caire, "On maximum-likelihood detection and the search for the closest lattice point," *IEEE Trans. Inform. Theory*, vol. 49, pp. 2389 – 2402, Oct. 2003.

[109] M. O. Damen and N. C. Beaulieu, "On diagonal algebraic space-time block codes," *IEEE Trans. Commun.*, vol. 51, pp. 911 – 919, Jun. 2003.

[110] W. C. Jakes, *Microwave Mobile Communications*. New York: IEEE Press, 1994.

[111] C. Xu and K.S. Kwak, "On Decoding Algorithm and Performance of Space-Time Block Codes," *IEEE Trans. Wirel. Commun.*, vol. 4, pp. 825 – 829, May 2005.

[112] H. Zhang and T. A. Gulliver, "Capacity and error probability analysis for orthogonal space-time block codes over fading channels," *IEEE Trans. Wirel. Commun.*, vol. 4, pp. 808 – 819, Mar. 2005.

[113] D. Tse and P. Viswanath, *Fundamentals of Wireless Communication*. Cambridge, UK: Cambridge University Press, 2005.

[114] L. Zheng and D. N. C. Tse, "Diversity and multiplexing: a fundamental tradeoff in multiple-antenna channels," *IEEE Trans. Inform. Theory*, vol. 49, pp. 1073 – 1096, May 2003.

[115] H. Yao and G. W. Wornell, "Structured space-time block codes with optimal diversity-multiplexing tradeoff and minimum delay," in *Proc. IEEE GLOBECOM*, (San Francisco, USA), pp. 1941 – 1945, Dec. 2003.

[116] U. Fincke and M. Pohst, "Improved methods for calculating vectors of short length in a lattice, including a complexity analysis," *Math. Comput.*, vol. 44, pp. 463 – 471, Apr. 1985.

[117] Y. Zhu and H. Jafarkhani, "Differential modulation based on quasi-orthogonal codes," *IEEE Trans. Wirel. Commun.*, vol. 4, pp. 3005 – 3017, Nov. 2005.

[118] L. Liu and H. Jafarkhani, "Application of quasi-orthogonal space-time block codes in beamforming," *IEEE Trans. Signal Processing*, vol. 53, pp. 54 – 63, Jan. 2005.

[119] M. Vu and A. Paulraj, "Optimal linear precoders for MIMO wireless correlated channels with nonzero mean in space-time coded systems," *IEEE Trans. Signal Processing*, vol. 54, pp. 2318 – 2332, Jun. 2006.

[120] C. Yuen, Y. L. Guan, and T. T. Tjhung, "Quasi-orthogonal STBC with minimum decoding complexity," *IEEE Trans. Wirel. Commun.*, vol. 4, pp. 2089 – 2094, Sep. 2005.

[121] S. Rouquette, S. Merigeault, and K. Gosse, "Orthogonal full diversity space-time block coding based on transmit channel state information for 4 Tx antennas," in *Proc. IEEE Int. Conf. Communications (ICC)*, vol. 1, (New York, USA), pp. 558–562, Apr. 2002.

[122] C. Toker, S. Lambotharan, and J. A. Chambers, "Closed-loop quasi-orthogonal STBCs and their performance in multipath fading environments and when combined with turbo codes," *IEEE Trans. Wirel. Commun.*, vol. 3, pp. 1890 – 1896, Nov. 2004.

[123] J. K. Milleth, K. Giridhar, and D. Jalihal, "Closed-loop transmit diversity schemes for five and six transmit antennas," *IEEE Signal Processing Lett.*, vol. 12, pp. 130 – 133, Feb. 2005.

[124] N. Sharma and C. B. Papadias, "Reduced-complexity ML decoding of rate 6/8 and rate 1 linear complex space-time codes for up to eight transmit antennas with phase feedback," *IEEE Signal Processing Lett.*, vol. 12, pp. 565 – 568, Aug. 2005.

[125] H. Wang, D. Wang, and X.-G. Xia, "On Optimal Quasi-Orthogonal Space-Time Block Codes with Minimum Decoding Complexity," *IEEE Trans. Inform. Theory*, Submitted on June 9, 2004. Its short version is published in *Proc. IEEE Int. Symp. on Information Theory* (ISIT), Adelaide, Australia, Sep. 2005.

[126] G. D. Forney Jr., R. G. Gallager, G. R. Lang, F. M. Longstaff, and S. U. Qureshi, "Efficient modulation for band-limited channels," *IEEE J. Select. Areas. Commun.*, vol. 2, pp. 632–647, Sep. 1984.

[127] L. He and H. Ge, "Fast maximum likelihood decoding of quasi-orthogonal codes," in *Thirty-Seventh Asilomar Conference on Signals, Systems and Computers (Asilomar)*, vol. 1, (Pacific Grove, CA, USA), pp. 1022 – 1026, Nov. 2003.

[128] C. Yuen, Y. L. Guan, and T.T. Tjhung, "Decoding of quasiorthogonal space-time block code with noise whitening," in *Proc. IEEE Personal, Indoor and Mobile Radio*

Communications Symp. (PIMRC), vol. 3, (Beijing, China), pp. 2166 – 2170, Sep. 2003.

[129] M.-T. Le, V.-S. Pham, L. Mai, and G. Yoon, "Low-complexity maximum-likelihood decoder for four-transmit-antenna quasi-orthogonal space-time block code," *IEEE Trans. Commun.*, vol. 53, pp. 1817 – 1821, Nov. 2005.

[130] D. J. Love and R. W. Heath, Jr., "Diversity performance of precoded orthogonal space-time block codes using limited feedback," *IEEE Commun. Lett.*, vol. 8, pp. 305 – 307, May 2004.

[131] J. W. Craig, "A new, simple and exact result for calculating the probability of error for two-dimensional signal constellations," in *Proc. IEEE Military Communications Conf. (MILCOM)*, (Boston, USA), pp. 25.5.1 – 25.5.5, Nov. 1991.

[132] C. Tellambura, A. J. Mueller and V. K. Bhargava, "Analysis of M-ary phase-shift keying with diversity reception for land-mobile satellite channels," *IEEE Trans. Veh. Technol.*, vol. 46, pp. 910–922, Nov. 1997.

[133] M. K. Simon and M.-S. Alouini, *Digital Communication over Fading Channels*. New York: Wiley, 1 ed., 2000.

[134] X. N. Zeng and A. Ghrayeb, "Performance bounds for space-time block codes with receive antenna selection," *IEEE Trans. Inform. Theory*, vol. 50, pp. 2130–2137, Sep. 2004.

[135] D. Gore and A. Paulraj, "MIMO antenna subset selection with space-time coding," *IEEE Trans. Signal Processing*, vol. 50, pp. 2580 – 2588, Oct. 2002.

[136] D. J. Love, "On the probability of error of antenna-subset selection with space-time block codes," *IEEE Trans. Commun.*, vol. 53, pp. 1799 – 1803, Nov. 2005.

[137] H. Kan and H. Shen, "A counterexample for the open problem on the minimal delays of orthogonal designs with maximal rates," *IEEE Trans. Inform. Theory*, vol. 51, pp. 355– 359, Jan. 2005.

[138] J. Boutros and E. Viterbo, "Signal space diversity: A power and bandwidth efficient diversity technique for the Rayleigh fading channel," *IEEE Trans. Inform. Theory*, vol. 44, pp. 1453 – 1467, Jul. 1998.

[139] E. Bayer-Fluckiger, F. Oggier, and E. Viterbo, "New algebraic constructions of rotated Z^n-lattice constellations for the Rayleigh fading channel," *IEEE Trans. Inform. Theory*, vol. 50, pp. 702 – 714, Apr. 2004.

[140] F. Oggier and E. Viterbo Full Diversity Rotations. [Online]. Available: www1.tlc.polito.it/∼viterbo/rotations/rotations.html.

[141] C. Yuen, Y. L. Guan, and T. T. Tjhung, "Optimizing quasi-orthogonal STBC through group-constrained linear transformation," in *Proc. IEEE GLOBECOM*, vol. 1, (Dallas, USA), pp. 550 – 554, Nov./Dec. 2004.

[142] E. Bayer-Fluckiger, F. Oggier, and E. Viterbo, "Algebraic lattice constellations: bounds on performance," *IEEE Trans. Inform. Theory*, vol. 52, pp. 319 – 327, Jan. 2006.

[143] L. Piazzo and P. Mandarini, "Analysis of phase noise effects in OFDM modems," *IEEE Trans. Commun.*, vol. 50, pp. 1696 – 1705, Oct. 2002.

[144] J. Armstrong, "Analysis of new and existing methods of reducing intercarrier interference due to carrier frequency offset in OFDM," *IEEE Trans. Commun.*, vol. 47, pp. 365 – 369, Mar. 1999.

[145] X. Cai and G. B. Giannakis, "Bounding performance and suppressing intercarrier interference in wireless mobile OFDM," *IEEE Trans. Commun.*, vol. 51, pp. 2047 – 2056, Dec. 2003.

[146] Y. Zhao and S. Häggman, "Intercarrier interference self-cancellation scheme for OFDM mobile communication systems," *IEEE Trans. Commun.*, vol. 49, pp. 1185–1191, Jul. 2001.

[147] K. A. Seaton and J. Armstrong, "Polynomial cancellation coding and finite differences," *IEEE Trans. Inform. Theory*, vol. 46, pp. 311–313, Jan. 2000.

[148] T. Keller and L. Hanzo, "Adaptive multicarrier modulation: A convenient framework for time-frequency processing in wireless communications," *IEEE Proc.*, vol. 88, pp. 611 – 640, May 2000.

[149] P. H. Moose, "A technique for orthogonal frequency division multiplexing frequency offset correction," *IEEE Trans. Commun.*, vol. 42, pp. 2908–2914, Oct. 1994.

[150] S. Siwamogsatham, M. P. Fitz and J. H. Grimm, "A new view of performance analysis of transmit diversity schemes in correlated Rayleigh fading," *IEEE Trans. Inform. Theory*, vol. 48, pp. 950 – 956, Apr. 2002.

[151] M. Russell and G. L. Stüber, "Interchannel interference analysis of OFDM in a mobile environment," in *Proc. IEEE Vehicular Technology Conf. (VTC)*, (Chicago, USA), pp. 820–824, Jul. 1995.

[152] P. Robertson and S. Kaiser, "Analysis of the effect of phase-noise in orthogonal frequency division multiplex (OFDM) systems," in *Proc. IEEE Int. Conf. Communications (ICC)*, (Seattle, USA), pp. 1652 – 1657, Jun. 1995.

[153] Y. Li and L. J. Cimini, Jr., "Bounds on the interchannel interference of OFDM in time-varying impairments," *IEEE Trans. Commun.*, vol. 49, pp. 401 – 404, March 2001.

[154] A. R. Hammons, Jr., and H. El Gamal, "On the theory of space-time codes for PSK modulation," *IEEE Trans. Inform. Theory*, vol. 46, pp. 524 – 542, Mar. 2000.

[155] G. Jöngren, M. Skoglund, and B. Ottersten, "Combining beamforming with orthogonal space-time block coding," *IEEE Trans. Inform. Theory*, vol. 48, pp. 611 – 627, Mar. 2002.

[156] S. Zhou and G. B. Giannakis, "Optimal transmitter eigen-beamforming and space-time block coding based on channel mean feedback," *IEEE Trans. Signal Processing*, vol. 50, pp. 2599 – 2613, Oct. 2002.

[157] S. Zhou and G. B. Giannakis, "Optimal transmitter eigen-beamforming and space-time block coding based on channel correlations," *IEEE Trans. Inform. Theory*, vol. 49, pp. 1673 – 1690, Jul. 2003.

[158] D. J. Love and R. W. Heath Jr., "Limited feedback unitary precoding for orthogonal space-time block codes," *IEEE Trans. Signal Processing*, vol. 53, pp. 64 – 73, Jan. 2005.

[159] A. Hjorungnes, D. Gesbert, and J. Akhtar, "Precoding of space-time block coded signals for joint transmit-receive correlated MIMO channels," *IEEE Trans. Wirel. Commun.*, vol. 5, pp. 492 – 497, Mar. 2006.

[160] C. Berrou, A. Glavieux, and P. Thitimajshima, "Near Shannon limit error-correcting coding and decoding: Turbo-codes," in *Proc. IEEE Int. Conf. Communications (ICC)*, vol. 2, (Geneva, Switzerland), pp. 1064 –1070, May 1993.

[161] C. Berrou and A. Glavieux, "Near optimum error correcting coding and decoding: Turbo-codes," *IEEE Trans. Commun.*, vol. 44, pp. 1261 – 1271, Oct. 1996.

[162] R. G. Gallager, "Low-density parity-check codes," *IRE Trans. Inf. Theory*, vol. IT-8, pp. 21 – 28, Jan. 1962.

[163] D. J. C. MacKay and R. M. Neal, "Near Shannon limit performance of low-density parity-check codes," *IEE Elect. Lett.*, vol. 32, pp. 1645 – 1646, Aug. 1996.

[164] D. J. C. MacKay, "Good error-correcting codes based on very sparse matrices," *IEEE Trans. Inform. Theory*, vol. 45, pp. 399 – 431, Mar. 1999.

[165] L. Bahl, J. Cocke, F. Jelinek, and J. Raviv, "Optimal decoding of linear codes for minimizing symbol error rate," *IEEE Trans. Inform. Theory*, vol. 20, pp. 284 – 287, Mar. 1974.

[166] S. ten Brink, "Convergence of iterative decoding," *IEE Elect. Lett.*, vol. 35, pp. 806 – 808, May 1999.

[167] S. ten Brink, "Convergence behavior of iteratively decoded parallel concatenated codes," *IEEE Trans. Commun.*, vol. 49, pp. 1727 – 1737, Oct. 2001.

[168] V. Tarokh and H. Jafarkhani, "A differential detection scheme for transmit diversity," *IEEE J. Select. Areas. Commun.*, vol. 18, pp. 1169 – 1174, July 2000.

[169] H. Jafarkhani and V. Tarokh, "Multiple transmit antenna differential detection from generalized orthogonal designs," *IEEE Trans. Inform. Theory*, vol. 47, pp. 2626–2631, Sept. 2001.

[170] A. Sendonaris, E. Erkip, and B. Aazhang, "User cooperation diversity - Part I: System description," *IEEE Trans. Commun.*, vol. 51, pp. 1927–1938, Nov. 2003.

[171] A. Sendonaris, E. Erkip, and B. Aazhang, "User cooperation diversity - Part II: Implementation aspects and performance analysis," *IEEE Trans. Commun.*, vol. 51, pp. 1939–1948, Nov. 2003.

[172] Y. Jing and H. Jafarkhani, "Using orthogonal and quasi-orthogonal designs in wireless relay networks," in *Proc. IEEE GLOBECOM*, San Francisco, California, USA, Nov./Dec. 2006.